

**Novel Ligands for the Recovery of Copper *via* Solvent
Extraction**

Lucy C. Emeleus



Doctor of Philosophy

University of Edinburgh

December 1999



Preface and Declaration

Since graduating from the University of Hull in 1996 with a BSc. (Hons) degree in Chemistry with German, the author has been engaged in a programme of full time research under the supervision of Professor P.A. Tasker and Dr. D.J. White at the University of Edinburgh and Dr. D. Cupertino and Mr. J. Campbell at Avecia (Blackley, Manchester).

No part of the work referred to in this thesis has been submitted in support of an application for another degree or qualification from this or any other university or other institute of learning.

Abstract

This thesis is concerned with the development of solvent extractants for copper, which could be used in existing processes to recover the metal by hydrometallurgical methods. Current, successful copper extractants are based on 2-hydroxybenzaldehyde oxime and are synthesised from alkyl phenol precursors. The success of phenolic oximes as copper extractants is attributed to their ability to form a hydrogen-bonded, pseudomacrocyclic of an ideal geometry to complex copper(II). These structural features have been utilised in the design of second generation copper extractants.

Chapter one of the thesis introduces the technology behind extractive metallurgy and focuses on the chemistry involved in solvent extraction. In chapter two, studies performed to clarify the mode of action of phenolic oximes in a solvent extraction system are discussed, and it is concluded that extractant association, and therefore extractive capability, is both solvent and concentration dependent.

In an attempt to move away from the use of alkyl phenol precursors in the synthesis of new extractants, ligands based on 3-methyl-1-phenyl-5-pyrazolone have been synthesised and their solvent extraction properties assessed. Chapter three describes two classes of pyrazolone-based extractants. 4-Acyl-3-methyl-1-phenyl-5-pyrazolones have been shown to extract and strip copper well, whilst the oxime derivatives studied are too strong to be used in conventional circuits because copper cannot be efficiently stripped using process strength sulphuric acid. The copper complexes formed by these pyrazolone oxime ligands are shown to have similar pseudomacrocyclic structures to their phenolic oxime analogues.

In chapter four, the solvent extraction properties of ligands based on 3-(2-hydroxyphenyl)-pyrazole are discussed. 1-H-5-alkyl-3-(2-hydroxyphenyl)-pyrazoles have been shown to have a copper loading strength similar to that of commercial phenolic oximes, but protonate during stripping with strong acid. Ester-functionalised forms of this type of ligand have, however, been found to load and strip copper without becoming protonated

on prolonged contact with acid, and could therefore be considered as candidate second generation extractants.

Finally, in chapter five, the synthesis and solvent extraction properties of the 4-aryazo-5-pyrazolones are described. These ligands are found to be weak solvent extractants in comparison with phenolic oximes, but are applicable to processes, which involve ammoniacal leaching of copper ores. The background to these processes is described and the characteristics that make these extractants suitable are investigated and discussed.

Acknowledgements

I would like to thank my supervisors, Prof. Peter Tasker and Dr. David White, for all their help and support throughout my PhD. In addition, the knowledge and help of Dr. Domenico Cupertino, Mr. John Campbell and Mrs. Sue Owens at Avecia has been invaluable. I would also like to thank current and ex-Tasker group members, in particular Dr. Jeremy Holmes and Mr. Andrew Smith, for an enjoyable three years.

I am extremely grateful to Dr. David Reed, Mr. John Millar and Mr. Wes Kerr for their NMR work, and to Dr. Ian Sadler for helpful discussions. I thank Mr. Alan Taylor and Mr. Harry Mackenzie for all the mass spectrometry they have done for me, and also Dr. Ian Atkinson for help with the ESMS. Thanks also go to Dr. Lorna Eades for C/H/N analyses. I am very grateful to Dr. Matt Davidson for his cryoscopic expertise and to Dr. Lesley Yellowlees and Mr. Ken McNamara for their help with the electrochemistry. In addition I would like to thank Dr. Michael Charlton and Dr. David Buttar at Avecia for the theoretical calculations they have done as part of this project. I am indebted to Dr. Simon Parsons and Dr. Steve Harris for X-ray structural analysis of my compounds.

I would like to thank Mr. Derek Thorp and Dr. Hamish McNab for their help concerning my work on diazopyrazolones and Dr. George Tennant for his help with the synthesis of pyrazolone oximes. Last, but not least, thanks go to Avecia for the funding of this project.

On a more personal note, thank you Mum and Dad for all the help, support and encouragement you have given me not just during my time here in Edinburgh but always. Finally, Iain, thank you for keeping me (relatively) sane these past months you're definitely the best result of all !!

Contents

Preface and Declaration	i
Abstract	ii
Acknowledgements	iv
Contents	v
Abbreviations	xii
Thesis Format	xvi
Index of Compounds	xvi
Chapter 1 : Introduction	1
1.1 The History of Copper	3
1.2 The Uses of Copper	5
1.3 Copper Processing Technologies	5
1.3.1 Pyrometallurgy	6
1.3.2 Hydrometallurgy	10
1.3.2.1 Nineteenth Century	10
1.3.2.2 Early Twentieth Century	11
1.3.2.3 Late Twentieth Century	11
1.3.2.4 The Process	12
1.3.2.5 Advantages over Pyrometallurgy	15
1.3.3 New Sulphate Technologies	16
1.3.3.1 Chloride Leaching Processes	16
1.3.3.2 Ammoniacal Leaching Processes	17
1.3.3.3 Bioleaching	18
1.4 Criteria for the Design of a Copper Solvent Extractant	19
1.4.1 Assessing the Strength of a Solvent Extractant	20
1.5 Current Copper Solvent Extractants	21
1.6 The Need for a New Type of Copper Extractant	23
1.6.1 Toxicological Concerns	23
1.6.2 Environmental Concerns	25
1.7 Objectives in Designing New Copper Extractants	26

1.7.1	Copper Coordination Chemistry	26
1.7.2	Copper in Biology	27
1.7.3	Target Molecules	28
1.8	References for Chapter 1	31
Chapter 2	: Extractant Preorganisation	34
2.1	Introduction	36
2.1.1	Current Copper Extractants	36
2.1.2	The Macrocyclic Effect	37
2.2	Evidence for Extractant Preorganisation	39
2.2.1	X-Ray Crystallography	39
2.2.2	Infrared Spectroscopy	42
2.2.2.1	Calculation of Association Constants	47
2.2.3	Proton Nuclear Magnetic Resonance Spectroscopy	50
2.2.3.1	Solvent Effects	50
2.2.3.2	Concentration Effects	52
2.2.3.3	Nuclear Overhauser Effect Experiments	54
2.2.4	Molecular Weight Determinations	57
2.2.5	Electrospray Mass Spectrometry	58
2.2.6	Theoretical Calculations	62
2.3	Conclusions	66
2.4	Experimental	67
2.4.1	Instrumentation	67
2.4.2	Solvent and Reagent Pretreatment	67
2.4.3	Synthesis	68
2.4.4	Molecular Weight Determination : Cryoscopic Method	70
2.4.5	Electrospray Mass Spectrometry : Experimental Conditions	71
2.5	References for Chapter 2	73
Chapter 3	: Acyl Pyrazolones and Pyrazolone Oximes	76
3.1	Introduction	80
3.1.1	Acyl Pyrazolones	80

3.1.1.2	Tautomerism of Acyl Pyrazolones	82
3.1.2	Pyrazolone Oximes	83
3.1.2.1	Tautomerism of Pyrazolone Oximes	84
3.2	Synthesis of Acyl Pyrazolones, Pyrazolone Oximes and their Metal Complexes	85
3.2.1	Acyl Pyrazolones	85
3.2.1.1	Free Ligands	86
3.2.1.2	Metal Complexes	87
3.2.2	Pyrazolone Oximes	88
3.2.2.1	Free Ligands	89
3.2.2.2	Metal Complexes	91
3.3	Characterisation of Acyl Pyrazolones, Pyrazolone Oximes and their Metal Complexes	92
3.3.1	IR Spectroscopy	92
3.3.1.1	Acyl Pyrazolones	92
3.3.1.2	Pyrazolone Oximes	93
3.3.2	NMR Spectroscopy	94
3.3.2.1	Acyl Pyrazolones	94
3.3.2.2	Pyrazolone Oximes	94
3.3.3	Mass Spectrometry	95
3.3.3.1	Acyl Pyrazolones	95
3.3.3.2	Pyrazolone Oximes	95
3.4	Solvent Extraction from Sulphate Media	96
3.4.1	Load and Strip Characteristics	99
3.4.2	Selectivity for Copper(II) over Iron(III)	100
3.5	X-ray Crystallography	102
3.5.1	Acyl Pyrazolones	102
3.5.1.1	Free Ligands	102
3.5.1.1.1	Tautomerism	102
3.5.1.1.2	Hydrogen Bonding	106
3.5.1.2	Metal Complexes	107
3.5.1.2.1	Mesomerism	109

3.5.1.2.2	Metal to Donor Atom Bond Lengths	111
3.5.1.2.3	Bite Angles and Dihedral Angles between Coordination Planes	115
3.5.1.2.4	Bite Distances	118
3.5.1.2.5	Dihedral Angles in the Coordinated Ligands	121
3.5.2	Pyrazolone Oximes	123
3.5.2.1	Free Ligands	123
3.5.2.2	Metal Complexes	126
3.5.2.2.1	Mesomerism	127
3.5.2.2.2	Hydrogen Bonding	128
3.5.2.2.3	Metal to Donor Atom Bond Lengths	132
3.5.2.2.4	Bite Angles and Bite Distances	134
3.5.2.2.5	Dihedral Angles	136
3.5.2.2.6	Differences between the structures of metal complexes of P50-type oxime and pyrazolone oxime ligands	137
3.6	Conclusions	138
3.7	Experimental	140
3.7.1	Instrumentation	140
3.7.2	Solvent Reagent and Pretreatment	140
3.7.3	Synthesis of Starting Pyrazolones	141
3.7.4	Acylpyrazolones	141
3.7.4.1	Synthesis of Ligands	141
3.7.4.2	Synthesis of Metal Complexes	148
3.7.5	Pyrazolone Oximes	149
3.7.5.1	Synthesis of Ligands	149
3.7.5.2	Synthesis of Metal Complexes	154
3.7.6	Solvent Extraction Experiments from Sulphate Media	157
3.7.6.1	Using Acylpyrazolones	159
3.7.6.2	Using Pyrazolone Oximes	160
3.7.7	X-ray Crystallography	161
3.8	References for Chapter 3	164

Chapter 4 : 3-(2-Hydroxyphenyl)-pyrazoles	169
4.1 Introduction	171
4.2 Synthesis of 3-(2-hydroxyphenyl)-pyrazoles and their Metal Complexes	172
4.2.1 Free Ligands	172
4.2.2 Metal Complexes	174
4.3 Characterisation	175
4.3.1 Free Ligands	175
4.3.2 Metal Complexes	177
4.4 Solvent Extraction from Sulphate Media	177
4.5 X-Ray Crystallography	179
4.5.1 Free Ligands	180
4.5.2 Metal Complexes	184
4.6 Conclusions	190
4.7 Experimental	191
4.7.1 Instrumentation	191
4.7.2 Solvent and Reagent Pretreatment	191
4.7.3 Synthesis of Precursors	192
4.7.4 Synthesis of 1-H-3-(2-Hydroxyphenyl)-pyrazole	194
4.7.5 Synthesis of Metal Complexes	195
4.7.6 Solvent Extraction Experiments	196
4.7.7 X-Ray Crystallography	196
4.8 References for Chapter 4	198
Chapter 5 : Diazopyrazolones	200
5.1 Introduction	203
5.1.1 The Escondida Process	203
5.1.1.1 Background to the Process	203
5.1.1.2 The Process	204
5.1.1.3 Advantages of an Ammoniacal Leach over an Acid Leach	205
5.1.1.4 Current Reagents	206
5.1.1.5 The Requirements of a Solvent Extractant	208

5.1.1.6	Diazopyrazolones	208
5.2	Synthesis of Diazopyrazolones and their Metal Complexes	209
5.2.1	Ligands	209
5.2.2	Metal Complexes	210
5.2.3	Stability of Diazopyrazolone Ligands	211
5.3	Characterisation of Diazopyrazolones and their Metal Complexes	211
5.3.1	IR Spectroscopy	211
5.3.2	NMR Spectroscopy	212
5.3.2.1	Free Ligands	212
5.3.2.2	Metal Complexes	216
5.3.3	Mass Spectrometry	218
5.3.4	Electrochemistry	219
5.4	Solvent Extraction using Diazopyrazolones	220
5.4.1	From Sulphate Media	220
5.4.2	From Ammoniacal Media	226
5.5	X-ray Crystallography of Diazopyrazolones and their Metal Complexes	229
5.5.1	Bonding	230
5.5.1.1	In the Free Ligands : Tautomerism	230
5.5.1.2	In the Metal Complexes : Mesomerism	232
5.5.2	General Trends in the Structures of the Metal Complexes, 8-12	234
5.5.2.1	Metal to Donor Atom Bond Lengths	234
5.5.2.2	Bite Angles and Bite Distances	235
5.5.2.3	Torsion Angles and Dihedral Angles	237
5.5.3	Comparison of the two Copper(II) Structures, 8 and 12	238
5.5.4	The Zinc(II) Complex, 9	242
5.5.5	The Cobalt(III) Complex, 10	243
5.5.6	The Nickel(II) Complex, 11	245
5.6	Conclusions	246
5.7	Experimental	247
5.7.1	Instrumentation	247

5.7.2 Solvent Reagent and Pretreatment	247
5.7.3 Synthesis of Starting Pyrazolones	248
5.7.4 Synthesis of the Ligands	248
5.7.5 Synthesis of the Metal Complexes	253
5.7.6 Solvent Extraction Experiments	256
5.7.6.1 From Sulphate Media	256
5.7.6.2 From Ammoniacal Media	259
5.7.6.3 Stability Tests on Diazopyrazolone Ligands	261
5.7.7 X-ray Crystallography	262
5.8 References for Chapter 5	264
Chapter 6 : Conclusions and Future Work	268

Abbreviations

A	amp
Å	Angstrom
AM1	Austin Model 1
Ar	aryl
arb.	arbitrary
B.M.	Bohr magneton
br	broad (spectroscopy)
BSSE	basis-set superposition error
c	cents
°C	degree Centigrade
ca.	<i>circa</i> (approximately)
calc.	calculated
cf.	<i>compare</i> (compared with)
Ch.	chapter
cm ⁻¹	wavenumber (IR)
cyclen	tetra-azacyclododecane
d	doublet (NMR)
δ	chemical shift (NMR)
DCM	dichloromethane
DMF	dimethylformamide
DMSO	dimethylsulphoxide
E	energy; entgegen (isomerism)
E°	standard electrode potential
Eds.	editor(s)
EI	electron impact (MS)
en	ethylenediamine
ESI	electrospray ionisation (MS)
<i>et al.</i>	<i>et alli</i> (and others)
eV	electron volt
FAB	fast atom bombardment (MS)
<i>fac</i>	facial (coordination geometry)

g	gram
G	Gibbs free energy
g l ⁻¹	gram per litre (also gpl and g/l)
h	hour
H	heat / enthalpy
ICP-AES	inductively coupled plasma optical emission spectrometry
IR	infrared
J	coupling constant (NMR)
K _a	association constant
kcal mol ⁻¹	kilocalorie per mole
kT	kilo tonne
kV	kilo volt
l mol ⁻¹	litre per mole
m	medium (spectroscopy); multiplet (NMR)
M	molar
μA	milliamp
<i>mer</i>	meridional (coordination geometry)
mg	milligram
min	minute
ml	millimetre
μl min ⁻¹	microlitre per minute
mM	millimolar
μm	micromolar
mmol	millimole
MS	mass spectrometry
<i>m/z</i>	molecular ion (MS)
n	normal (alkyl chain)
NMR	nuclear magnetic resonance
NOE	nuclear overhauser effect (NMR)
obs.	observed
pK _a	-log ₁₀ K _a

pp.	inclusive pages
ppm	parts per million
q	quartet (NMR)
RT	room temperature
s	singlet (NMR); strong (IR)
t	triplet (NMR)
T	temperature
trien	triethylenediamine
Vol.	volume
vs.	<i>versus</i>
w	weak (IR)
wt %	weight percent
Z	zusammen (isomerism)
\$	dollar
Δ	change in
v	wavenumber (IR)

Abbreviations of Journal Titles

<i>Acta. Chem. Scand.</i>	Acta Chemica Scandinavica
<i>Acta Cryst.</i>	Acta Crystallographica
<i>Aust. J. Chem.</i>	Australian Journal of Chemistry
<i>Canadian J. Chem.</i>	Canadian Journal of Chemistry
<i>Chem. Abstr.</i>	Chemical Abstracts
<i>Chem. Phys. Lett.</i>	Chemical Physics Letters
<i>Chin. Sci. Bull.</i>	Chinese Science Bulletin
<i>Coord. Chem. Rev.</i>	Coordination Chemistry Reviews
<i>Croatica Chem. Acta</i>	Croatica Chemica Acta
<i>Cryst. Struct. Commun.</i>	Crystal Structure Communications
<i>Environ. Sci. Technol.</i>	Environmental Science and Technology
<i>Inorg. Chem.</i>	Inorganic Chemistry
<i>J. Am. Chem. Soc.</i>	Journal of the American Chemical Society
<i>J. Appl. Cryst.</i>	Journal of Applied Crystallography

<i>J. Biol. Chem.</i>	Journal of Biological Chemistry
<i>J. Chem. Inf. Comput. Sci.</i>	Journal of Chemical Information and Computing Science
<i>J. Chem. Phys.</i>	Journal of Chemical Physics
<i>J. Chem. Soc. Chem. Comm.</i>	Journal of the Chemical Society : Chemical Communications
<i>J. Chem. Soc. Dalton Trans.</i>	Journal of the Chemical Society : Dalton Transactions
<i>J. Chem. Soc. Faraday Trans.</i>	Journal of the Chemical Society : Faraday Transactions
<i>J. Chem. Soc. Perkin Trans. 1 / 2</i>	Journal of the Chemical Society : Perkin Transactions 1 / 2
<i>J. Comput. Chem.</i>	Journal of Computational Chemistry
<i>J. Coord. Chem.</i>	Journal of Coordination Chemistry
<i>J. Crystallogr. Spectrosc. Res.</i>	Journal of Crystallographic and Spectroscopic Research
<i>J. Hetero. Chem.</i>	Journal of Heterocyclic Chemistry
<i>J. Indian Chem. Soc.</i>	Journal of the Indian Chemical Society
<i>J. Inorg. Biochem.</i>	Journal of Inorganic Biochemistry
<i>J. Inorg. Chem.</i>	Journal of Inorganic Chemistry
<i>J. Inorg. Nucl. Chem.</i>	Journal of Inorganic and Nuclear Chemistry
<i>J. Mater. Chem.</i>	Journal of Materials Chemistry
<i>J. Org. Chem.</i>	Journal of Organic Chemistry
<i>J. Organomet. Chem.</i>	Journal of Organometallic Chemistry
<i>J. Phys. Chem.</i>	Journal of Physical Chemistry
<i>J. Radioanal. Chem.</i>	Journal of Radioanalytical Chemistry
<i>Koord. Khim.</i>	Koordinatsionnaya Khimiya
<i>Pol. J. Chem.</i>	Polish Journal of Chemistry
<i>Spectrochim. Acta</i>	Spectrochimica Acta
<i>Synth. Comm.</i>	Synthetic Communications
<i>Synth. React. Inorg. Met.-Org. Chem.</i>	Synthesis and Reactivity in Inorganic and Metal-Organic Chemistry
<i>Z. Anorg. Allg. Chemie</i>	Zeitschrift für Anorganische und Allgemeine Chemie

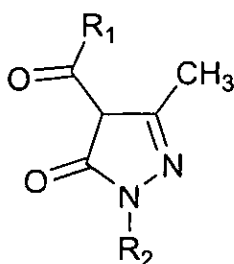
Thesis Format

Each chapter in this thesis is written as a separate entity, such that the numbering of compounds, figures, tables and references is individual to each chapter. The compound numbering for chapters 3-5 is summarised in the following section.

Index of Compounds

Chapter 3

(i) 4-Acyl-3-methyl-1-R₂-5-pyrazolones



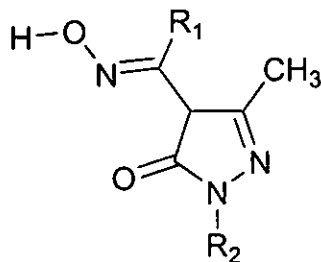
Ligands	R ₁	R ₂
1	Ph	Ph
2	Me	Ph
3	H	Ph
4	Ph	t-Bu
5	4-n-octylphenyl	Ph
6	4-n-heptylphenyl	Ph

Metal Complexes

7	[Cu(1-H) ₂] ^a
8	[Zn(1-H) ₂] ^b
9	Co(1-H) ₂ .H ₂ O.MeOH ^a
10	Ni(1-H) ₂ .H ₂ O.MeOH ^a
11	[Cu(4-H) ₂ (MeOH) ₂] ^b

(ii) 4-Acyl-3-methyl-1-R₂-5-pyrazolone Oximes

Nomenclature : R₁ = H : aldoxime; R₁ = alkyl, aryl : ketoxime

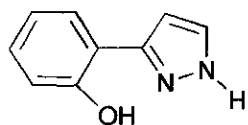


Ligands	R ₁	R ₂
12	Ph	Ph
13	Me	Ph
14	H	Ph
15	4-n-octylphenyl	Ph
16	4-n-heptylphenyl	Ph

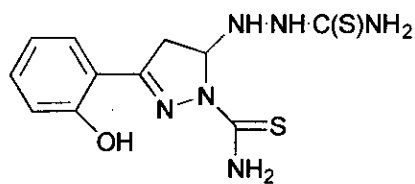
Metal Complexes

17	[Cu(12-H) ₂ (DMF) ₂] ^b
18	[Zn(12-H) ₂ (DMF) ₂] ^b
19	[Ni(12-H) ₂ (DMF) ₂] ^b
20	[Co(12) ₂ (MeOH) ₂](NO ₃) ₂ ^b
21	Cu(13-H) ₂ ^a
22	Cu(14-H) ₂ ^a
23	Zn(14-H) ₂ · ³ / ₄ H ₂ O ^a
24	Co(14-H) ₂ ·2 ¹ / ₂ H ₂ O ^a
25	Ni(14-H) ₂ ·2 ¹ / ₂ H ₂ O ^a
26	Cu(15-H) ₂

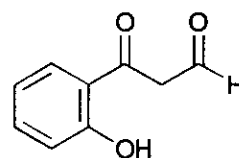
Chapter 4 : 3-(2-Hydroxyphenyl)-pyrazoles



1



2



3

Precursors

2 : 3-(2-hydroxyphenyl)-1-thiocarbamyl-5-thiosemicarbazide-2-pyrazoline

3 : 2-Hydroxy- ω -formylacetophenone

Ligands

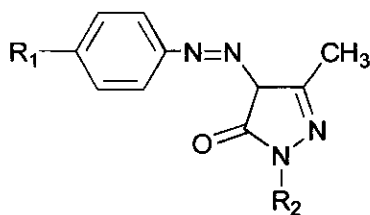
1 : 1-H-3-(2-hydroxyphenyl)-pyrazole

Complexes

4 : Cu(1-H)₂

5 : Ni(1-H)₂

Chapter 5 : 4-Arylazo-3-methyl-1-R₂-5-pyrazolones



Ligands

1

R₁

t-Bu

R₂

Ph

2

H

Ph

3

t-Bu

H

4

t-Bu

Me

5

t-Bu

t-Bu

6

s-Bu

t-Bu

7

nonyl

t-Bu

Metal Complexes

8	$[\text{Cu}(1\text{-H})_2]^b$
9	$[\text{Zn}(1\text{-H})_2]^b$
10	$[\text{Co}(1\text{-H})_3] \cdot 3\text{MeOH}^b$
11	$[\text{Ni}(1\text{-H})_2 \cdot (\text{MeOH})_2] \cdot 2\text{MeOH}^b$
12	$[\text{Cu}(2\text{-H})_2]^a$
13	$[\text{Cu}(5\text{-H})_2]^a$
14	$[\text{Cu}(6\text{-H})_2]^a$
15	$[\text{Cu}(7\text{-H})_2]^a$

Notes

- ^a Formula consistent with C/H/N analytical data
- ^b Formula confirmed by X-ray crystallography

Chapter 1 : Introduction

Contents	Page
1.1 The History of Copper	3
1.2 The Uses of Copper	5
1.3 Copper Processing Technologies	5
1.3.1 Pyrometallurgy	6
1.3.2 Hydrometallurgy	10
1.3.2.1 Nineteenth Century	10
1.3.2.2 Early Twentieth Century	11
1.3.2.3 Late Twentieth Century	11
1.3.2.4 The Process	12
1.3.2.5 Advantages over Pyrometallurgy	15
1.3.3 New Sulphate Technologies	16
1.3.3.1 Chloride Leaching Processes	16
1.3.3.2 Ammoniacal Leaching Processes	17
1.3.3.3 Bioleaching	18
1.4 Criteria for the Design of a Copper Solvent Extractant	19
1.4.1 Assessing the Strength of a Solvent Extractant	20
1.5 Current Copper Solvent Extractants	21
1.6 The Need for a New Type of Copper Extractant	23
1.6.1 Toxicological Concerns	23
1.6.2 Environmental Concerns	25
1.7 Objectives in Designing New Copper Extractants	26
1.7.1 Copper Coordination Chemistry	26
1.7.2 Copper in Biology	27
1.7.3 Target Molecules	28
1.8 References for Chapter 1	31

This thesis is concerned with the development of new solvent extractants for copper, which could be used in processes to recover the metal by hydrometallurgical methods. This chapter describes the historical development of copper production and the design requirements for solvent extractants, which could be used to recover copper from acid sulphate media.

1.1 The History of Copper¹

Copper has played an important rôle in the development of civilisation for over 10 000 years. The earliest evidence for the use of copper is a brooch, dating back to 8 500 B.C., which was found in Iraq. The Greeks (ca. 800 - 400 B.C.) used copper for coinage and from ca. 300 B.C. onwards the Romans exploited the large copper deposits in Spain and Cyprus, for both military and civilian purposes. The chemical symbol "Cu" is in fact derived from "aes Cyprium", which is Latin meaning "metal of Cyprus". Worldwide copper production over the centuries can be followed very accurately through the study of the copper content of Greenland ice cores using atomic absorption spectrometry². Results from such studies reveal a significant decrease in the observed copper levels coinciding directly with the decline of the Roman empire around 200 A.D. and a peak between the 10th and 12th centuries corresponding to widespread copper production in China during this period, which has been estimated at approximately 13 000 metric tonnes *per annum*. Worldwide copper production did not increase again until the Middle Ages when smelters were operating in Germany, Sweden and Wales. In fact a smelter located in Swansea (Wales) used techniques similar to those found in modern smelters, based on successive oxidations and reductions to eliminate sulphur.

Modern-scale copper production did not begin until the late nineteenth century (ca. 1865) when the Calumet and Hecla Company based on the Keweenaw Peninsula in Michigan became the world's largest single copper producer with an annual output of approximately 6 200 metric tonnes.

Unusually, this area is still being mined today, (although the majority of copper produced is in fact reclaimed) in contrast to the majority of ore deposits mined during this period, which are now exhausted. The Rio Tinto mines in Spain and subsequently the Anaconda Copper Company in Montana soon exceeded Calumet and Hecla in terms of copper production. Anaconda was producing over 50 000 metric tonnes of copper a year by 1890 . It should be noted that up until this point only mining of high-grade copper ores ($\geq 10\%$) was carried out and that recovery of copper from low-grade ores ($\leq 2\%$) only became feasible in the twentieth century. The first concentration methods (flotation) were applied in the mining of the vast, low-grade, porphyry deposits (large bodies of rock containing widely dispersed grains of copper minerals; copper content $\approx 1\%$) at Bingham Canyon in Utah during the 1930s.

Today, over 11 million metric tonnes of copper are produced annually worldwide³, of which over one fifth is recovered *via* hydrometallurgical solvent extraction processing. The majority of copper recovery is carried out in the U.S.A., Africa (Zambia, Zaire), Russia, Australasia and South America (Chile, Peru), with approximately 30 % of worldwide production occurring in Chile. Worldwide copper production in 1998, specifying the quantities recovered by solvent extraction, is summarised in table 1.

Area	Total Copper produced / kT	Copper produced by solvent extraction / kT
Africa	564	75
Asia	1261	40
Latin America	5737	1582
North America	2579	583
Oceania	970	89
Western Europe	358	8
World Total	11469	2377

Table 1 : Worldwide copper production in 1998

The rapid expansion of worldwide copper production in the twentieth century is illustrated by the fact that, despite its 10 000 year history, over three quarters of all copper ever consumed has been produced since the Second World War.

1.2 The Uses of Copper

Copper owes its vast array of applications to its physicochemical properties of malleability, conductivity and ease of alloy formation. The majority of copper produced today is used in construction, for example, in the U.S.A. as water piping (40 %), and in the electrical and electronics industries (25 %). Transportation and related equipment account for a further 15 % of all copper produced, while 10 % is used in the production of industrial machinery. Copper alloys, such as those formed with zinc (brass) and chromium, are not only decorative but are also extremely resistant to corrosion, and such consumer and other general products account for the remaining 10 % of annual copper production⁴.

Copper is the 26th most prolific element in the earth's crust with an abundance of ca. 50 g per tonne. There are over 200 known copper minerals, of which only 20 are important as copper ores or semi-precious stones such as malachite and turquoise. The principal copper minerals are sulphides, such as chalcocite (Cu_2S), bornite (Cu_5FeS_4 / Cu_3FeS_3) and chalcopyrite (CuFeS_2), of which over 40 % of the world's total reserves are found in the U.S.A. and Chile.

1.3 Copper Processing Technologies

There are two methods employed in the recovery of copper from its ores, pyrometallurgy and hydrometallurgy. Various pyrometallurgical methods have been used since ca. 9 000 B.C. to recover copper from sulphidic ores

such as chalcocite (Cu_2S), chalcopyrite (CuFeS_2) and covellite (CuS). In contrast, copper hydrometallurgy is a twentieth century development.

1.3.1 Pyrometallurgy^{1,5}

Pyrometallurgy involves the use of heat to extract metals from their ores. Since the 1940s, technological progress in primary smelting has changed the face of the pyrometallurgical copper processing industry. This has been driven not only by economic but, more importantly, environmental demands. Not only has “flash smelting” (a smelting method, in which the ore is heated for a fixed length of time rather than continuously) found acceptance as a commercially viable process for the recovery of copper from ores with low iron and sulphur content, but increased attention has also been paid to the development of improved, traditional, oxygen smelting technologies for the direct production of copper from chalcopyrite (CuFeS_2) reserves. Pyrometallurgical systems are still responsible for the majority (around 80 %) of worldwide copper production, however they are unlikely to have a place in any ideal copper recovery methodology of the future.

The pyrometallurgical recovery of copper is a complicated process based on a series of three key steps, concentration (2), roasting (4) and electrolytic refining (9), as described in figure 1.

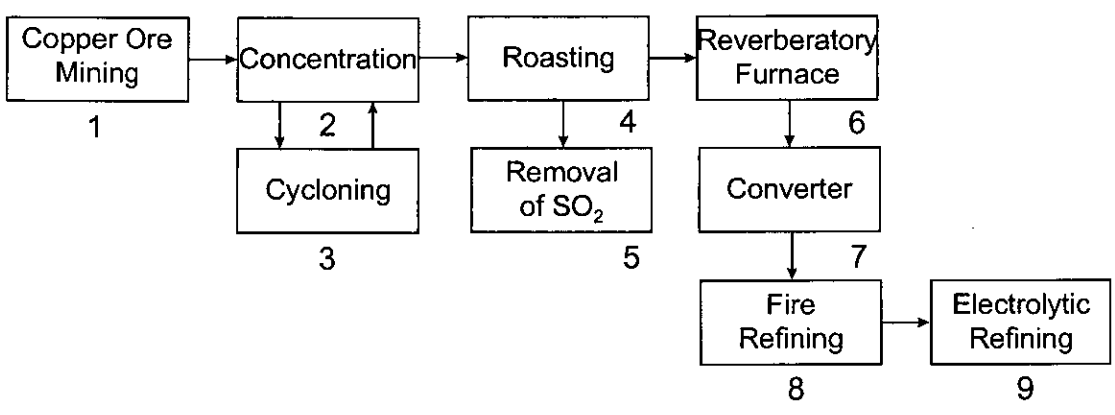


Figure 1 : Schematic representation of the pyrometallurgical recovery of copper

1. Copper Ore Mining

Copper ore is recovered from either surface or underground mines. The ore is removed from underground mines by the construction of tunnels or shafts, while ore from surface mines is recovered by removing the overburden (waste on top of the ore) to expose the ore below.

2. Concentration

The copper ore is initially concentrated by a series of crushing, grinding and flotation steps in order for the resulting copper feed to be of sufficient concentration to facilitate efficient smelting. Typically, copper ores can contain as little as 1 % copper, which needs to be increased to 20-30 % in the smelter feed. Crushing and grinding reduce the size of the ore particles to facilitate efficient flotation. The slurry produced passes into the flotation tanks where it is aerated. Air bubbles stick to the copper mineral particles causing them to float to the surface and form a froth, which passes on to the next stage of the process. Reagents such as oils or long chain alcohols are added to assist froth formation. Additionally, chemicals such as dithiophosphonates are added to aid flotation of the copper minerals while lime is added to control the pH of the process and depress, for example, any pyrite (FeS_2) in the slurry.

3. Cycloning

More copper minerals are recovered from the flotation tailings by cycloning. If the ore contains a large concentration of clay slimes, the tailings are normally cycloned to remove these impurities before being returned to the flotation tanks. This step is known to improve the efficiency of copper recovery by as much as 3 % and involves the separation of the larger copper ore particles from the grains of impurities which form the slimes.

4. Roasting

The copper feed is subsequently passed through the roaster where part of the sulphur present is converted to sulphur dioxide (Equation 1) at a temperature of between 500 - 850 °C depending on the specific roasting process. Water is also removed from the feed at this stage. The sulphur

dioxide produced is, in turn, converted into sulphuric acid (Step 5; equation 2).

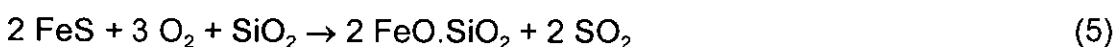


6. Reverberatory Furnace

The resulting "calcine feed" (crude feed) is then passed into a reverberatory furnace where the remaining copper(I) sulphide forms a molten "matte" with the iron(II) sulphide present. Heat produced by burners at one end of the furnace is re-radiated by the furnace roof, providing very efficient heating, hence the name "reverberatory furnace".

7. Converter

Iron silicates and oxides form a separate layer and are removed by flotation, and the matte continues on into the converter where it is transformed into "blister copper" *via* air oxidation at high temperature (ca. 600 °C) as described by equations 3 - 8. More slag (iron silicate waste) and sulphur are removed in the converter and the blister copper then enters the refining stage of the process.



8. Fire Refining

Despite the continual removal of impurities during the concentration and smelting stages, blister copper still contains high levels of sulphur, oxygen and other impurities, which result in uneven anode surfaces and must be

removed before the copper can be cast into fire-refined ingots. Sulphur and oxygen are removed *via* a process known as “gas poling”, which uses natural gas to reduce copper(I) in copper(I) sulphide and copper(I) oxide to copper(0), and subsequently oxidises the sulphide to sulphur dioxide, venting off the gases produced. The main reactions involved in fire refining are described in equations 9 - 11.



9. Electrolytic Refining

Electrolytic refining produces copper intended for use in the electrical and electronics industries. Nickel and selenium, for example, are not removed during fire refining and for these applications must be removed by electrolytic refining. Anodes produced from blister copper are dissolved electrolytically in acidic copper sulphate (Equation 12) and copper of at least 99.97 % purity is deposited on the thin, stainless steel starter cathodes in the electrolytic cell (Equation 13). Anodic impurities form a slime at the bottom of the electrolytic cell, which contains valuable by-products such as silver, gold, selenium and tellurium. These metals are recovered in a separate refining process. The pure copper is finally cast into various forms and sold.



Although pyrometallurgy produces good quality copper it has many disadvantages, primarily high energy consumption, the production of large amounts of solid and gaseous waste and, as a result, high running costs. The large energy consumption is due in part to the necessity to concentrate the feeds before smelting and also to the fact that copper is effectively reduced twice from copper(II) to copper(0) during the pyrometallurgical

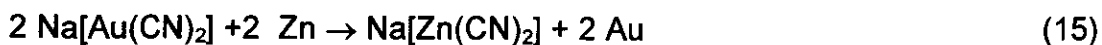
recovery and refining stages of the process. In addition, dusts contaminated with arsenic, antimony, bismuth, mercury and other harmful elements are often produced at a smelter site, illustrating the environmental concerns associated with this method of copper recovery⁶.

1.3.2 Hydrometallurgy

Hydrometallurgical processing is increasingly preferred to pyrometallurgy as an environmentally sound and economically viable alternative for the recovery of copper from all grades of ore. For copper recovery using hydrometallurgy, solvent extraction is the most commonly used technology to facilitate the selective transfer of the desired metal to an aqueous solution, which is then electrolysed (electrowon)⁷. The alternative technique for the selective removal of copper from leach solutions is cementation. This involves the displacement of copper(II) from the leach solution using de-tinned, scrap iron and relies on the fact that iron has a more positive electrode potential (Fe/Fe^{2+} $E^\ominus +0.447$ eV) than copper (Cu/Cu^{2+} $E^\ominus -0.342$ eV). The iron therefore passes into solution and precipitates metallic copper. The main drawback with this method of copper recovery is that the product, "cement copper", often contains iron and must undergo electrodeposition to produce a marketable product⁸.

1.3.2.1 Developments of the Nineteenth Century

During the late nineteenth century, two pioneering hydrometallurgical processes were developed⁸. The cyanidation process for the recovery of gold from its ores was patented by John Stewart MacArthur in 1887, although the chemistry of the process was known as early as the 1780s. In this process, an aerated, powdered mineral slurry, which typically contains approximately 10 ppm of gold, is treated with sodium cyanide solution (Equation 14). The resulting filtrate is then treated with zinc chips to precipitate impure gold in a cementation process (Equation 15) similar to the one described above. Roasting of the impure gold followed by melting produces gold of 80 - 90 % purity.



Around the same time, Karl Josef Bayer developed the “Bauxite” process for the preparation of pure aluminium oxide (Al_2O_3). This process, which involves the leaching of bauxite ($\text{AlO}_x(\text{OH})_{3-2x}$; $0 < x < 1$) with sodium hydroxide (Equation 16) to give aluminate, and the subsequent calcining of the aluminium trihydroxide produced from hydrolysis (Equation 17) to yield pure aluminium oxide, was originally designed to meet the needs of the textiles industry. It was only after the development of the electrolytic aluminium process that Bayer realised the potential application of his system to metallurgy.



1.3.2.2 Developments of the early Twentieth Century

During the 1940s solvent extraction was used in the Manhattan Project, to extract uranium, and later other politically important and high-value metals such as plutonium and thorium, for use in atomic weapons¹. It was not until the 1960s, however, that it was applied to the recovery of copper, a relatively inexpensive metal.

1.3.2.3 Developments of the late Twentieth Century

In 1968 the first commercial plant for the recovery of copper by solvent extraction was set up in Miami, Arizona, and by the early 1990s there were more than thirty large-scale, copper solvent extraction plants in operation worldwide⁹. An idealised flowsheet for the recovery of copper from an oxidic ore in an integrated leach / solvent extraction / electrowinning circuit is shown in figure 2.

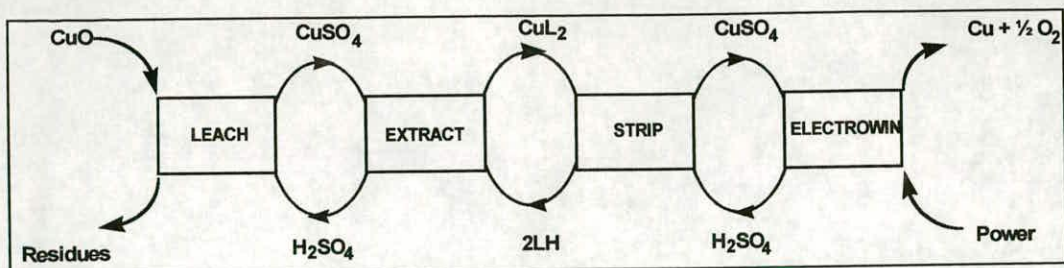


Figure 2 : An idealised flowsheet for the recovery of copper *via* solvent extraction

1.3.2.4 The Process

Figure 3 shows a diagram of a copper solvent extraction plant showing the main stages of the process. In reality, more than one leach and one strip stage is incorporated into the circuit along with intermittent washing stages to maintain good phase separation.

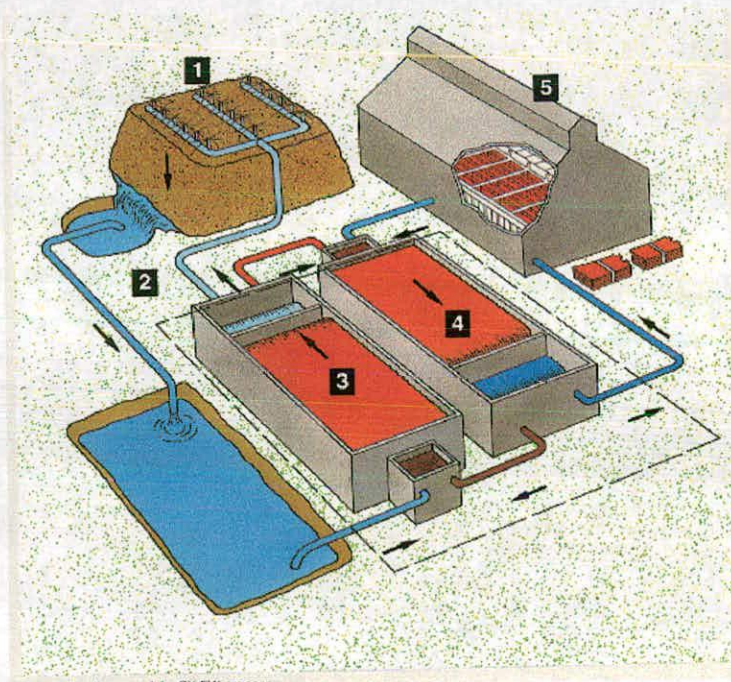
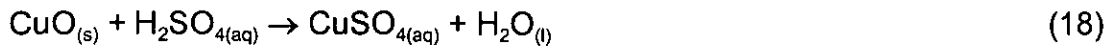


Figure 3 : Diagram of a solvent extraction plant

1. & 2. Leaching and Storage

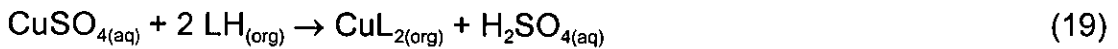
Initially, copper is leached (Equation 18) out of a “pad” of oxidic ore using sulphuric acid to form a “leach solution” of impure copper sulphate.



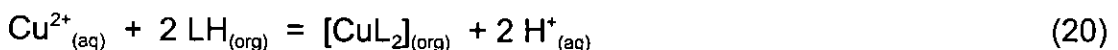
It is often not financially viable to employ ore grinding or agitation techniques during leaching to maximise the acid - ore contact and so heap leaching is employed as a low cost alternative. This can be problematic, however, as although the kinetics of copper mineral dissolution are fast, seepage of the acid through the heap leach pad to the underlying ore is slow and dependent on grain size and packing characteristics. In practice, therefore, the height of the heap is limited and often pre-mixing of the ore with concentrated acid occurs before the heap is constructed in order to speed up the leaching process¹⁰. The resulting "pregnant leach solution" typically contains approximately 10 gl⁻¹ copper and a comparable concentration of iron(III).

3. Extraction

In the extraction step, the aqueous leach solution is contacted with an organic (kerosene) phase containing an organic reagent, the "solvent extractant" (Equation 19).



This extractant selectively transfers copper from the aqueous phase into the organic phase *via* the formation of a neutral copper complex. The protons displaced on formation of this complex are released to the aqueous phase regenerating sulphuric acid, which is then recycled into the initial leaching process. The solvent extraction of copper operates around a "pH-swing" equilibrium between the extract and strip stages of the process⁸ (Equation 20).



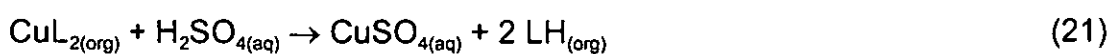
It is clear from the equilibrium constant, defined by equation 20a, that the more protons in the system the less $[\text{CuL}_2]_{(\text{org})}$ can be present .

$$K_{\text{ex}} = \frac{[\text{CuL}_2][\text{H}^+]^2}{[\text{Cu}^{2+}][\text{LH}]^2} \quad (20a)$$

The ligand acts as an organic acid releasing protons to the aqueous phase in order to facilitate formation of the copper complex and efficient copper extraction to the organic phase occurs at pH values of greater than 1. This type of “pH-swing” extraction process is therefore well-suited to acidic sulphate leach processes such as the one described.

4. Stripping

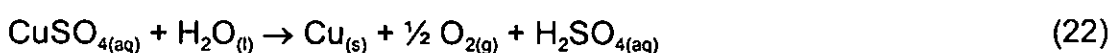
The organic phase loaded with the copper complex passes on to the stripping step where it is contacted with sulphuric acid of a higher concentration, typically 180 gl^{-1} (1.84 M) sulphuric acid. Copper is removed from the organic phase to form a copper sulphate solution of high concentration and purity (Equation 21).



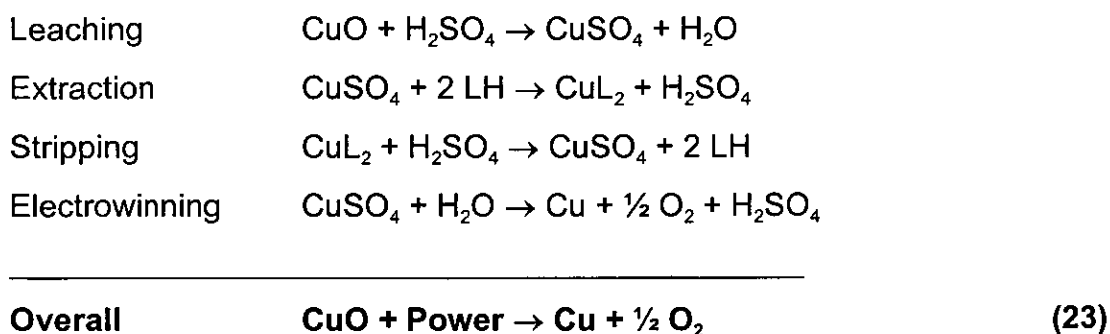
Again transfer of protons occurs to reprotonate the ligand, which is subsequently recycled back into the extraction step.

5. Electrowinning

Finally, the copper sulphate solution passes into the tankhouse where it undergoes electrowinning (Equation 22). This can deposit as much as 60 gl^{-1} of copper with 99.99 % purity per cycle of the electrolyte, with the acid generated being recycled to the stripping step.



In the leach / solvent extraction / electrowinning circuit the overall mass balance (Equation 23) illustrates how effective the process is. In an idealised circuit, copper oxide and power are consumed, and copper and oxygen are produced.



1.3.2.5 Advantages of Hydrometallurgy over Pyrometallurgy

1. The operational temperature of a solvent extraction plant is typically 40 °C, which is easily attained with minimal energy input in the majority of plant locations, for example Chile or Zambia. In fact the only substantial energy input is during the electrowinning stage.
2. The amount of waste generated by a solvent extraction plant is also minimal in comparison with that produced by smelting. The main contaminants in the circuit are iron impurities in the ore, however the efficiency of the system is maintained as, although a significant amount of iron is dissolved up into the leach solution, it builds up to such levels that it precipitates on the heap leach pad. Additionally, the selectivity of the extractant for copper over iron ensures that any iron present in the leach solution is not transferred across the extraction circuit.
3. Precious metals, such as gold and silver, and “by-product metals”, such as zinc, cobalt and nickel, can be recovered in separate solvent extraction stages integrated into the overall copper recovery circuit⁶.
4. Hydrometallurgical copper recovery does not produce sulphur dioxide.
5. Fossil fuels are not required to heat the process, hence emissions associated with the burning of fossil fuels are not an issue.

One of the major reasons for the growth of solvent extraction technology for copper recovery is the overall economics of the process. Costings are very dependent on the price of energy, particularly electrical power, and the accessibility of the ores. The costs of copper produced by pyrometallurgy and hydrometallurgy have been quoted as approximately \$1 and 35c per pound of copper respectively³.

1.3.3 New Sulphate Solvent Extraction Technologies

In order to facilitate the treatment of a wider range of copper ores, hydrometallurgical systems are now being developed, which incorporate leaching using ammoniacal ($\text{NH}_3 / \text{NH}_4^+$), chloride ($\text{FeCl}_3 / \text{NaCl}$) solutions or micro-organisms⁶.

1.3.3.1 Chloride Leaching Processes

In the early 1980s, ICI developed a solvent extractant, CLX50, for the extraction of copper from solutions of high chloride concentration. The active component of CLX50 is an ester derivative of pyridine, while related reagents contain amide derivatives (Figure 4).

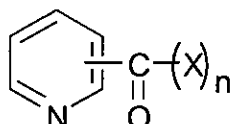


Figure 4 : Structure of CLX50 and its derivatives
 $\text{X} = \text{OR}_1, \text{NR}_2\text{R}_3; \text{R}_1, \text{R}_2, \text{R}_3 = \text{alkyl}$

The ester or amide functionalities reduce the basicity of the pyridine nitrogen thus avoiding the formation of hydrochlorides and the transport of HCl by the reagent as $[\text{LH}]\text{Cl}$, or of iron(III) by an iron pair mechanism involving $[\text{LH}][\text{FeCl}_4]^{12}$. Chloride leaching processes are, however, still much less well developed for reasons, which are summarised as follows.

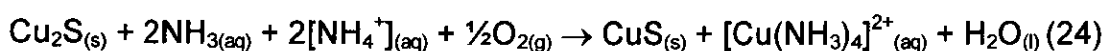
1. Chloride leaching chemistry is non-specific, which means that not only copper but also zinc, lead and silver will dissolve into the leach solution.

2. It has been shown to be very difficult to remove silver, selenium and tellurium from copper chloride solutions and these metals tend to readily co-deposit with copper.
3. Chloride solutions are much more corrosive than the standard sulphate solutions used in the majority of solvent extraction plants.
4. Chlorine produced at the anode during electrolytic refining must be recovered, unlike the oxygen produced in sulphate circuits, which can be vented directly into the atmosphere.

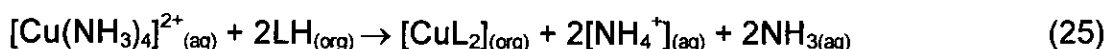
Despite these drawbacks, it is still thought to be possible to develop a viable chloride process and a substantial amount of work is continuing in this area^{13,14,15}

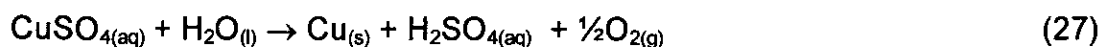
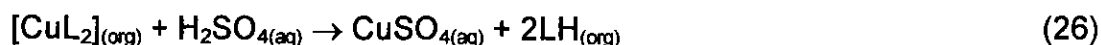
1.3.3.2 Ammoniacal Leaching Processes

The leaching of copper sulphide ores using ammonia was first proposed by a Frenchman, Balzac, in 1903. At that time, however, ammonia was an expensive reagent and only became affordable with the development of the Haber process some ten years later⁸. Since the 1970s a large number of copper recovery processes using ammoniacal leaching have been patented¹⁶, the most well developed of which is the Escondida process¹¹. The leaching process is described in equation 24.



This process produces two copper streams, an enriched copper ore, covellite (CuS), which is treated in a conventional smelter, and an aqueous solution of copper ammine complexes, which undergoes solvent extraction, stripping and electrowinning in the conventional manner, as described in equations 25, 26 and 27.

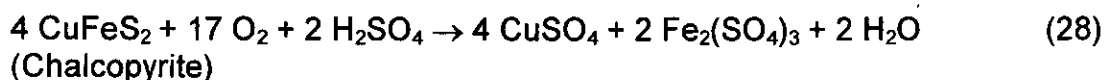




The limitations of the Escondida process are based on the choice of solvent extractant. Work carried out to try to improve this process is discussed in chapter 5.

1.3.3.3 Bioleaching

With the continuing demand for more environmentally friendly and less expensive technology, bioleaching is playing an increasing role in metal recovery processes, particularly for copper, uranium and gold. It is estimated that over 15 % of the copper produced in Chile each year is leached using microbes¹⁷. As a result of microbial metabolism, insoluble metal sulphides and, to a lesser extent oxides, are converted to soluble sulphates as described in equations 28 and 29¹⁸.



The bioleaching of high grade ores is usually carried out on a heap leach pad, as previously described. Low grade ores and process waste dumps can be leached *in situ*, however, which reduces the overall cost of the metal recovery process. It should be noted that although the microbes used have a high tolerance of heavy metals and harsh, acidic conditions (note the incorporation of sulphuric acid in equation 28), their action is inhibited by traces of solvent extractant in the aqueous phase recycled to the leach pad after extraction¹⁷. In order to avoid this problem, an additional scrubbing step is added to the circuit. Bioleaching will continue to increase in industrial importance, particularly due to its successful application in the treatment of very low grade ores and waste materials.

1.4 Criteria for the Design of a Copper Solvent Extractant

The key to an efficient solvent extraction circuit is identifying a reagent whose copper extraction and stripping chemistry fits the chemical parameters defined by the leaching and electrowinning stages of the overall process. Good load and strip characteristics represent only one aspect of a successful solvent extractant, however, as there are other essential criteria to be met⁹.

A good copper extractant must :

- extract and strip copper under the conditions determined by the leaching and electrowinning stages of solvent extraction. For example, in an acid sulphate circuit the pH of the leach solution is approximately 2, therefore the extractant is required to load copper efficiently below this pH. Additionally it should allow efficient stripping of the copper using tankhouse electrolyte (pH 0).
- extract copper selectively over other species which may be present in the leach solution. A sulphate leach feed typically contains high ($\leq 10 \text{ g l}^{-1}$) concentrations of iron and lower concentrations of other transition metals, such as cobalt and nickel, as well as high concentrations of alkali and alkaline earth metal salts. A typical plant feed contains 10 g l^{-1} copper, $1\text{-}10 \text{ g l}^{-1}$ iron, 1 g l^{-1} calcium, 1 g l^{-1} zinc, 30 ppm molybdenum, 2-10 ppm aluminium, 30 ppm cobalt and 30 ppm nickel at a pH of ca. 2-2.5.
- have good load and strip kinetics. The extractant should remove copper rapidly and efficiently from the aqueous phase into the organic phase, but also be able to release it quickly during the stripping stage of the process.
- be chemically stable to the often severe conditions of the solvent extraction plant and its surroundings. Solvent extraction plants are often situated in hot climates, so the extractant must be stable to heat and light. Additionally, it should also be stable to other chemicals used in the circuit such as concentrated acids or bases.

- be soluble in the organic, kerosene-type solvents employed in solvent extraction circuits in both the free ligand and copper complex forms.
- be cheap and easy to synthesise, thus keeping production costs to a minimum.
- have good separation and phase disengagement properties to avoid entrainment of the free ligand or copper complex in the aqueous phase.
- be safe to use, thus minimising the risk in operating a solvent extraction plant.

Preferably, a successful, new copper extractant should fit the requirements of *existing* solvent extraction circuits thus minimising investment required in a new plant.

1.4.1 Assessing the “Strength” of a Solvent Extractant

The pH of the leach solution in an acid sulphate circuit is approximately 2, therefore a solvent extractant is required to load copper efficiently below this pH, as already stated. A convenient way of assessing the strength of an extractant is to determine its $\text{pH}_{1/2}$ value. This is the pH value at which half of the total copper present has been loaded into the organic phase, ie: where D , the distribution coefficient (Equation 30), is equal to 1.

$$D = \frac{[\text{Cu}_{(\text{org})}]}{[\text{Cu}_{(\text{aq})}]} \quad (30)$$

$[\text{Cu}_{(\text{org})}]$ and $[\text{Cu}_{(\text{aq})}]$ are the concentrations of copper in the organic and aqueous phases respectively. The $\text{pH}_{1/2}$ value of a solvent extractant is usually determined by plotting a graph of pH vs. % copper loaded into the organic phase. These graphs are called S-curves because of their characteristic shape. The S-curves for the extraction of a range of metals using 2-hydroxy-5-nonylbenzaldehyde oxime (“P50”) are presented in figure 5.

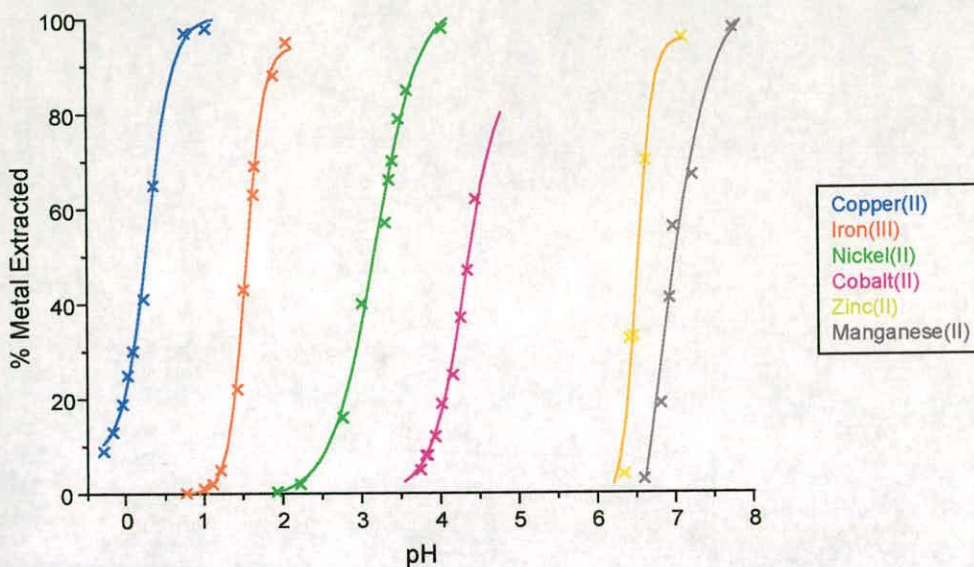


Figure 5 : S-curves for the extraction of a range of metals using P50 in kerosene

Typical $pH_{1/2}$ values for the extraction of copper(II) using hydroxyoximes vary between 0-2 pH units and are dependent on the system conditions, eg: ionic strength, choice of solvent and ratio of extractant to metal present¹².

1.5 Current Copper Extractants

The only ligands, which have met all of the design criteria for a successful copper extractant to date, are those containing the hydroxyphenyl oxime functionality (Figure 6)^{8,12}.

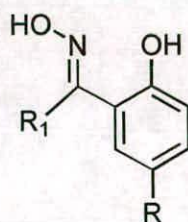


Figure 6 : The hydroxyphenyl oxime functionality
 R = alkyl ; R₁ = H (aldoximes), alkyl, aryl (ketoximes)

Initially, ketoximes were exclusively used in the solvent extraction of copper from acidic sulphate leach solutions but they have since been largely

replaced by aldoximes, which have a greater extractive strength. In practice this type of extractant is slightly too strong to permit efficient stripping of the copper back into the aqueous phase using conventional electrolytes and must be used in conjunction with a “modifier”¹⁹, usually a long chain alcohol or an ester of a long chain carboxylic acid, to promote stripping. Avecia's current copper extractant, P50 (Figure 6 : R = C₉H₁₉, R = H), is based on the oxime of salicylaldehyde, a simple and inexpensive precursor. It is a monobasic ligand, deprotonating at the phenolic hydrogen to form a neutral 2:1 ligand : metal complex with a high stability constant. A typical value for Log β₂ is 21.5. β₂ is the overall stability constant as described by equations 31-33¹².



$$K_1 K_2 = \beta_2 = \frac{[\text{CuL}]^+ [\text{H}^+]}{[\text{Cu}^{2+}] [\text{LH}]} \times \frac{[\text{CuL}_2] [\text{H}^+]}{[\text{CuL}]^+ [\text{LH}]} = \frac{[\text{CuL}_2] [\text{H}^+]^2}{[\text{Cu}^{2+}] [\text{LH}]^2} \quad (33)$$

An interesting feature of the chemistry of P50 is its ability to form a hydrogen-bonded, preorganised dimer in non-polar, organic solvents. This “pseudomacrocyclic” structure is assumed to possess some of the properties associated with macrocycles themselves thus promoting solvent extraction (Figure 7). The disposition of N and O donors in the free ligand dimer is very similar to that needed in the copper complex so little conformational reorganisation of the ligand is required on complexation. Such ligand systems have been referred to as preorganised.

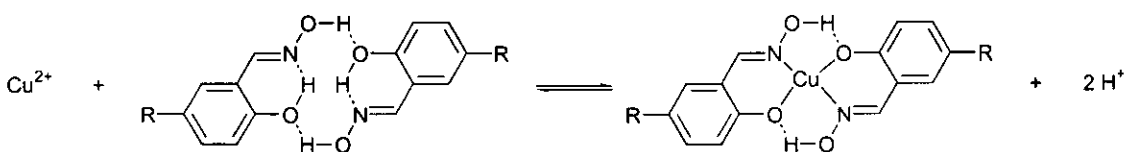


Figure 7 : Complexation of copper(II) by a P50 “pseudomacrocyclic”

Evidence for the behaviour of hydroxyphenyl oximes in solution will be discussed in chapter 2.

1.6 The Need for a New Type of Copper Extractant

1.6.1 Toxicological Concerns

The ability of alkyl phenols, the precursors of P50-type oxime extractants, to mimic the behaviour of oestrogens is of current concern, and as such the use of these chemicals may well become restricted in the near future. Alkyl phenols have been banned in Switzerland and are restricted in Germany. It is however, important to distinguish between hormone mimicking chemicals, such as alkyl phenols and their ethoxylate derivatives (Figure 8), which are widely used as non-ionic surfactants in detergents and emulsifiers and as additives in plastics, and classical toxins, such as carcinogens and neurotoxins. To this end the term “endocrine disrupting chemical” (EDC) is employed²⁰.

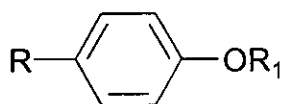


Figure 8 : 4-Alkyl phenols : R = alkyl; R₁ = H, $-(\text{C}_2\text{H}_4\text{-O})_n\text{-C}_2\text{H}_5$

By definition, an EDC is a chemical which can affect the level of hormones in the blood and the action of these hormones, thus having the potential to affect hormone production, release, transport and metabolism. This can ultimately lead, for example, to the disruption of subsequent receptor binding action. It is well documented that the most potent oestrogenic chemicals are those containing a phenolic group. This is understandable on consideration of the structure of the body's natural oestrogen, oestradiol-17 β (E₂) (Figure 9). However, other non phenol-containing chemicals are also known to be oestrogenic, the most documented example being the pesticide 1,1,1-

trichloro-2,2-bis(*o,p'*-chlorophenyl)ethane, more commonly known as DDT (Figure 10)^{21,22}.

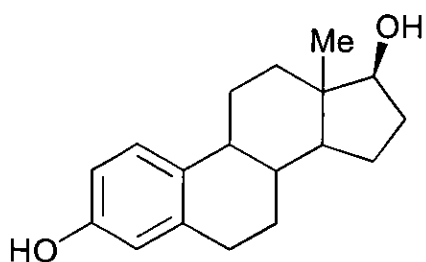


Figure 9 : Oestradiol-17 β (E₂)

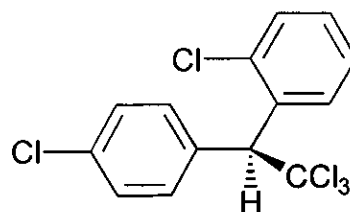


Figure 10 : *o,p'*-DDT

Alkyl phenols have been found to interact directly with the human oestrogen receptor (hER) in an identical manner to oestradiol-17 β and have therefore been the subject of an extensive structure / activity study²³. The test used in this study consists of the incubation of the alkyl phenol with a genetically engineered yeast strain in a medium containing a chromogenic substrate. The yeast genome is modified such that interaction with an oestrogen will ultimately induce a colour change in the medium so that oestrogenic activity can be monitored spectrophotometrically²⁴.

The results of this study show that the size of the alkyl substituent and type of branching, as well as its position on the phenyl ring are important factors affecting the oestrogenicity of alkyl phenols. Oestrogenicity increases with increasing number of carbon atoms in the alkyl group up to C₈, after which it levels out. Alkyl phenols with tertiary alkyl substituents are significantly more active than their straight chain or branched counterparts. It was also found that the oestrogenic activity of the alkyl phenol depends on the position of the alkyl group on the phenyl ring, and was found to increase in the order *ortho* < *meta* < *para*. Thus 4-*t*-butyl-phenol was the most potent alkyl phenol tested, however, it should be noted that it was still found to be approximately 1000 times less oestrogenic than the natural oestrogen, oestradiol-17 β . In summary, this study has shown that although alkyl phenols are oestrogenic, they are significantly less active than natural oestrogens and as such these

particularly as *in vivo* behaviour is likely to be different from that observed *in vitro*.

1.6.2 Environmental Concerns

The environmental problems associated with the pyrometallurgical recovery of copper have been extensively documented. These problems are dominated by the production of sulphur dioxide during smelting and the seepage of copper and other harmful elements, such as arsenic and lead, into the surrounding environment, the effects of which can be directly monitored, for example, by the study of fish populations in nearby rivers²⁵. The use of hydrometallurgy obviously removes such risks associated with smelting but introduces other potential pollutants in the form of the chemicals used in the solvent extraction circuit. The on-site leakage of phenolic oxime extractants has been modelled from the results of column leach tests, a type of laboratory test often used to model heap and dump leaching, which were carried out on ore samples from the U.S.A. using radio-labelled P50²⁶. These tests have shown that a slow, perceptible leakage of P50 is observed particularly at low pH, which would have implications for the long term management of plant sites. The fact that P50 has also been found to be non-biodegradable makes this an important issue. Additionally the biodegradability of compounds can be limited if they inhibit the action of the micro-organisms, which are actually responsible for their degradation. Alkyl phenols are an example of such compounds and work carried out by Razo-Flores *et al.*²⁷ has shown that even at sub-toxic concentrations alkyl phenols are non-biodegradable. Obviously this has implications for the use of alkyl phenols not only in the production of P50-type oximes but also as modifiers in the solvent extraction process.

In view of these concerns over the toxicity and biodegradability of phenolic oximes and their precursors, a search for new extractants, which perform equally well in terms of metal extraction but are environmentally friendlier, was undertaken.

1.7 Objectives in Designing New Copper Extractants

As P50 is such a successful copper extractant, in designing its replacement one approach would be to mimic its chemistry as closely as possible. In this way it may be possible to reproduce its extractive strength and selectivity, whilst moving away from the use of alkyl phenol precursors.

1.7.1 Copper(II) Coordination Chemistry²⁸

Copper(II) is the most common oxidation state for copper. Copper(I) readily oxidises to copper(II) and disproportionates to copper(II) and copper(0). The majority of copper(II) complexes are both air and moisture stable, which makes them easy to synthesise and study. The copper hexa-aquo ion, $[\text{Cu}(\text{H}_2\text{O})_6]^{2+}$, is extremely stable in aqueous solution, leading to an extensive copper(II) aqueous chemistry. Additionally the main coordination numbers of copper(II) complexes are four, five and six, but seven and eight are also known, resulting in a large number of known copper(II) X-ray structures. Four-coordinate copper(II) complexes are either distorted tetrahedral or square planar. Five-coordinate complexes can be either square pyramidal, which is distorted within the square plane, or trigonal bipyramidal, which is distorted towards a square pyramidal geometry. Six-coordinate copper(II) complexes have tetragonally distorted octahedral geometries, either displaying compression along the z-axis due to stabilisation of the $d_{x^2-y^2}$ orbital, or elongation along the z-axis due to stabilisation of the d_{z^2} orbital²⁹.

Recent literature surveys of mononuclear copper(II) tetra- and pentacoordinated compounds³⁰ and hexa-, hepta- and octacoordinated compounds³¹ have shown that in all cases the most common ligands, whether mono- or multidentate, are nitrogen and oxygen donating. This is expected as the copper(II) ion is classified as a borderline hard acid³² and is therefore expected to preferentially bind with hard bases such as nitrogen and oxygen, and, to a lesser extent, sulphur and chlorine³³.

1.7.2 Copper in Biology

Copper is one of the most abundant metals in the human body and also occurs widely in nature. There are therefore many copper-containing proteins, whose coordination spheres can be studied with a view to designing new copper solvent extractants. Selected copper proteins along with their functions and donor atom sets are presented in table 2^{34,35,36}.

Function	Protein	Donor Atom Set ^a
Electron Transfer	Azurin	N ₂ S ₂ O
	Plastocyanin	N ₂ S ₂
	Stellacyanin	N ₂ S ₂
Dioxygen Transport	Hemocyanin (deoxy)	N ₃
Oxidase O ₂ → H ₂ O	Laccase	N ₂ S ₂
	Ascorbate Oxidase	N ₂ S ₂ /N ₃ O/N ₂ O
O ₂ → H ₂ O ₂	Amine Oxidase ^b	N ₃ O
	Galactose Oxidase	N ₃ O
Copper Mono-oxygenase	Tyrosinase	N ₂ O
Copper Dioxygenase	Quercetinase	N ₃ O
Other	Superoxide Dismutase ^c	N ₄
	Cytochrome c Oxidase ^d	N ₂ S ₂

Table 2 : Copper-containing Proteins

^a Nitrogen donor atoms come from histidines, sulphur donor atoms from methionine, glutamine or cysteine and oxygen donor atoms from water or OH⁻.

^b contains pyridoxal phosphate as well as copper

^c contains zinc as well as copper

^d contains heme as well as copper

In addition to proteins containing copper bound to nitrogen and oxygen donor atoms, there are a number of "blue copper proteins" containing Cu - S bonds, which suggests that copper also forms stable compounds with sulphur donors³⁶. Several ligands containing sulphur donor atoms have been

been tested as possible solvent extractants for copper, however they bind so strongly that concentrated hydrochloric acid is required to strip the metal back into the aqueous phase³⁷. This strength of binding is thought to be due to increased π -donation attributable to the sulphur atoms. Additionally, the well known reduction of copper(II) to copper(I) by sulphur donors is observed²⁸.

1.7.3 Target Molecules

From these observations it seemed sensible to preserve the nitrogen-oxygen donor atom set provided for copper by P50. With this in mind, it is possible to rewrite the P50 structure schematically (Figure 11).

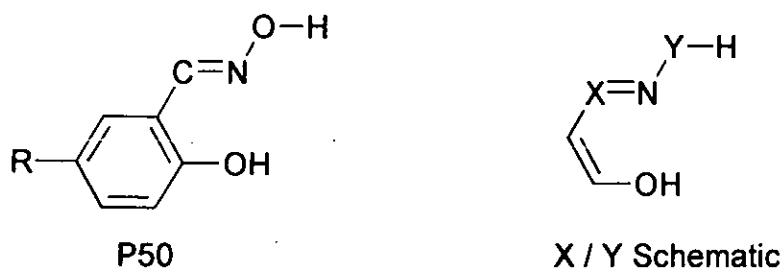


Figure 11 : Schematic representation of the P50 structure

A study of the Cambridge Crystallographic Data Centre (CCDC) database³⁸ led to a set of suitable target molecules being compiled. This search revealed 11 structures of molecules and 20 structures of metal complexes containing the 2-hydroxybenzaldehyde oxime fragment (Figure 11 : R = H), but only a handful of other structures containing the hydroxyoxime chelating fragment (Figure 11 : X = C; Y = O). The results of the search are summarised in table 3.

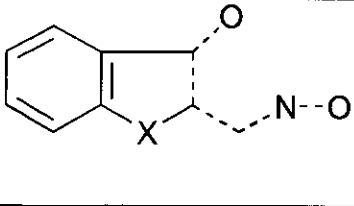
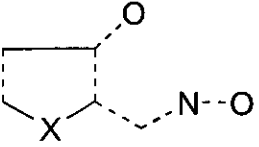
Fragment	X	CCDC Code
	O	DIRRUR CEXDEO
	S	no structures
	N	no structures
	O	NUFRUB
	S	no structures
	N	HIBYAS HIBYAS10

Table 3 : Results of CCDC search for P50 schematic fragment
 Note : - - - denotes "any" type of bond

Additionally other compounds, for which no structures could be found in the CCDC database, were proposed on the basis of X/Y permutations of figure 11 and these are presented in figure 12.

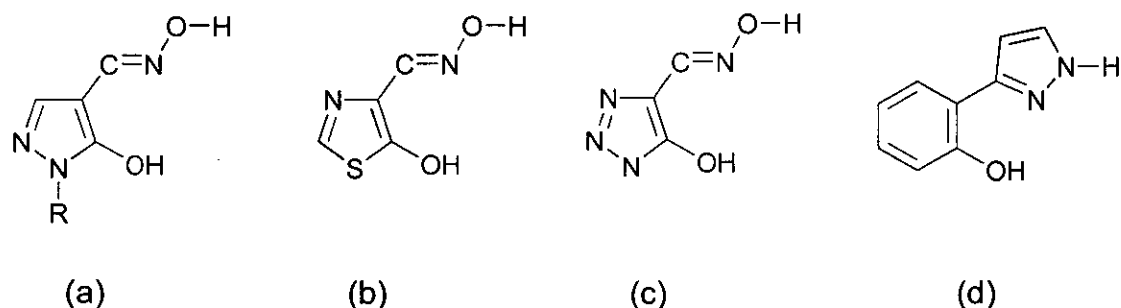


Figure 12 : Additional compounds containing the P50 schematic fragment

From this set of target molecules, the pyrazolone oximes (Figure 12 : a) were chosen as a logical starting point for further study due to previous investigation of the solvent extraction properties of the related 4-acyl derivatives³⁹ and chemistry involving the pyrazolone oximes will be discussed in chapter 3. The coordination chemistry and solvent extraction properties of 3-(2-hydroxyphenyl)-pyrazoles (Figure 12 : d) were also investigated and will be discussed in chapter 4. Additionally, a related set of compounds, the

diazopyrazolones (Figure 13), were chosen for further study as potential solvent extractants for copper from ammoniacal media and this work will be discussed in chapter 5.

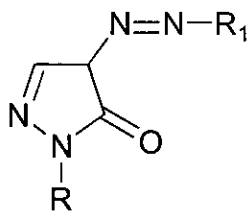


Figure 13 : Structure of a diazopyrazolone

1.8 References for Chapter 1

- 1 *Kirk-Othmer Encyclopædia of Chemical Technology*, Eds. M. Grayson and D. Eckroth, Wiley, New York, 3rd Edition, 1978, **6**, pp. 819-868
- 2 S. Hong, J.P. Candelone, C.C. Patterson and C.F. Boutron, *Science*, 1996, **272**, 246-249
- 3 Personal Communication : AVECIA Mining Chemicals Business, 1998
- 4 <http://www.copper.org>
- 5 *Handbook of Extractive Metallurgy*, Ed. F. Habashi, Wiley-VCH, Weinheim (Germany), 1997, Vols. II & III
- 6 D. Dreisinger, *The Hydrometallurgical Treatment of Copper Concentrates : Recent Developments*. Personal Communication
- 7 Zeneca Specialties : Acorga Mining Chemicals, *Extracting the Maximum* (Trade Literature), Blackley, Manchester, U.K.
- 8 F. Habashi, *A Textbook of Hydrometallurgy*, Imprimerie D'Édition Marquis Limité, Quebec, 1993, ch. 21, pp. 408-497
- 9 G.A. Kordosky, *Journal of the Minerals, Metals and Materials Society*, 1992, **44** (5), 40-45
- 10 R.W. Bartlett, *Metallurgical and Materials Transactions B*, 1997, **28B**, 529-545
- 11 *Proceedings of "The Paul Queneau International Symposium on Extractive Hydrometallurgy of Copper, Nickel and Cobalt"* , Vol. 1 : Fundamental Aspects, Eds. R.G. Reddy & R.N. Weizenbach, The Minerals, Metals and Materials Society, Warrendale (U.S.A.) , 1993, pp. 881-910
- 12 J. Szymanowski, "*Hydroxyoximes and Copper Hydrometallurgy*", CRC Press, London, 1993, pp. 67-74
- 13 C. Bouvier, G. Cote, R. Cierpiszewski and J. Szymanowski, *Solvent Extraction and Ion Exchange*, 1998, **16**(6), 1465-1492
- 14 O. Herreros, R. Quiroz, E. Manzano, C. Bou and J. Viñals, *Hydrometallurgy*, 1998, **49**, 87-101

- 15 G.L. Pashkov, N.P. Bezrukova, V.N. Volk, I.Y. Fleitlich, N.I. Pavlenko, G.E. Selutin and E.D. Korniyets, *Solvent Extraction and Ion Exchange*, 1991, **9**(4), 549-567
- 16 IBM Intellectual Property Network; www.patents.ibm.com
- 17 K. Bosecker, *FEMS Microbiology Reviews*, 1997, **20**, 591-604
- 18 D.E. Rawlings and S. Silver, *Biotechnology*, 1995, **13**, 773-778
- 19 J. Szymanowski, *Critical Reviews in Analytical Chemistry*, 1995, **25**(3), 143-194
- 20 <http://www.aperc.org>
- 21 T.E. Wiese and W.R. Kelce, *Chemistry and Industry*, 1997, **16**, 648-653
- 22 *Chemistry and Industry*, 1999, **12**, 451
- 23 E.J. Routledge and J.P. Sumpter, *J. Biol. Chem.*, 1997, **272**(6), 3280-3288
- 24 E.J. Routledge and J.P. Sumpter, *Environmental Toxicology and Chemistry*, 1996, **15**(3), 241-248
- 25 J.N. Moore and S.N. Luoma, *Environ. Sci. Technol.*, 1990, **24**(9), 1278-1285
- 26 Avecia Internal Report
- 27 E. Razo-Flores, B. Donlon, J. Field and G. Lettinga, *Water Science and Technology*, 1996, **33**(3), 47-57
- 28 *Comprehensive Coordination Chemistry*, Eds. G. Wilkinson, R.D. Gillard and J.A. McCleverty, Pergamon Press, Oxford, 1987, Vol. 5, pp. 533-774
- 29 M.J. Winter, *d-Block Chemistry*, Oxford University Press, Oxford, 1994
- 30 R.G. Pearson, *Inorg. Chem.*, 1988, **27**, 734-740
- 31 *The Encyclopædia of Inorganic Chemistry*, Ed. R.B. King, Wiley, Chichester (U.K.), 1994, Vol. 2, pp. 829 - 840
- 32 M. Melnik, M. Kabesova, M. Dunaj-Jurco and C.E. Holloway, *J. Coord. Chem.*, 1997, **41**(1-2), 35-182

- 33 M. Melnik, M. Kabesova, L. Macaskova and C.E. Holloway, *J. Coord. Chem.*, 1998, **45**(1-4), 31-145
- 34 F.A. Cotton and G. Wilkinson, *Advanced Inorganic Chemistry*, Wiley, New York, 5th Edition, 1988, pp. 1363-1369
- 35 W. Kaim and B. Schwederski, *Bioinorganic Chemistry : Inorganic Elements in the Chemistry of Life*, Wiley, New York, 1998
- 36 S.J. Lippard and J.M. Berg, *Principles of Bioinorganic Chemistry*, University Science Books, Mill Valley (U.S.A.), 1994
- 37 Avecia Internal Report
- 38 D.A. Fletcher, R.F. McMeeking and D.J. Parkin, *J. Chem. Inf. Comput. Sci.*, 1996, **36**, 746-749
- 39 Y.A. Zolotov and N.M. Kuzmin, *Extraction of Metals with Acylpyrazolones*, Nauka, Moscow , 1977; *Chem. Abstr.* 89 : B81023X

Chapter 2 : Extractant Preorganisation

Contents	Page
2.1 Introduction	36
2.1.1 Current Copper Extractants	36
2.1.2 The Macrocyclic Effect	37
2.2 Evidence for Extractant Preorganisation	39
2.2.1 X-Ray Crystallography	39
2.2.2 Infrared Spectroscopy	42
2.2.2.1 Calculation of Association Constants	47
2.2.3 Proton Nuclear Magnetic Resonance Spectroscopy	50
2.2.3.1 Solvent Effects	50
2.2.3.2 Concentration Effects	52
2.2.3.3 Nuclear Overhauser Effect Experiments	54
2.2.4 Molecular Weight Determinations	57
2.2.5 Electrospray Mass Spectrometry	58
2.2.6 Theoretical Calculations	62
2.3 Conclusions	66
2.4 Experimental	67
2.4.1 Instrumentation	67
2.4.2 Solvent and Reagent Pretreatment	67
2.4.3 Synthesis	68
2.4.4 Molecular Weight Determination : Cryoscopic Method	70
2.4.5 Electrospray Mass Spectrometry : Experimental Conditions	71
2.5 References for Chapter 2	73

2.1 Introduction

2.1.1 Current Copper Extractants

Current, commercially successful copper extractants are those containing the hydroxyphenyl oxime functionality, such as P50 (Figure 1), which is marketed by Avecia. However just why these molecules are such good copper extractants, ie: their mode of action, is not well understood.

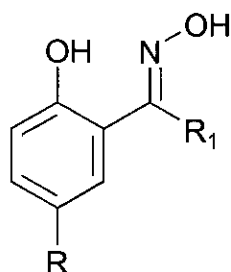


Figure 1 : P50-type oximes; R = H, alkyl; R₁ = H, alkyl, aryl

It has been proposed that P50 forms a hydrogen-bonded, preorganised dimer (Figure 2) in non-polar, organic solvents, and that this "pseudomacrocyclic" structure might possess some of the properties associated with macrocycles, therefore promoting metal ion complexation (Figure 3).

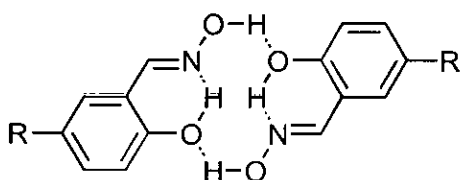


Figure 2 : Ligand dimer

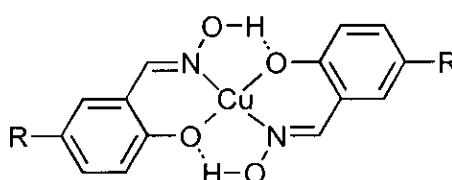
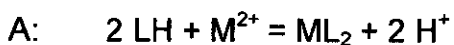


Figure 3 : Copper complex

There are two possible equilibria to consider here, A, involving the complexation of the metal ion by two, separate ligands, and B, involving the complexation of the metal ion by a preorganised ligand dimer, as shown below.



The equilibrium constant for each case is obviously dependent on the ratio of free ligand to “ligand dimer” present in the system, and as such this will affect the thermodynamics of the system and therefore the overall efficiency of extraction of the metal ion into the organic phase.

2.1.2 The Macrocyclic Effect

Consideration of the “macrocyclic effect”, which describes the observation that macrocyclic ligands form much more stable metal complexes than their straight-chain counterparts¹, is important here in an attempt to understand the potential role of the dimeric oxime “pseudomacrocyclic” (Figure 2) in a metal extraction system. Figure 4 describes the energy terms involved in the complexation of a metal (M) with ligand(s) (L) in a single phase system (water in this case).

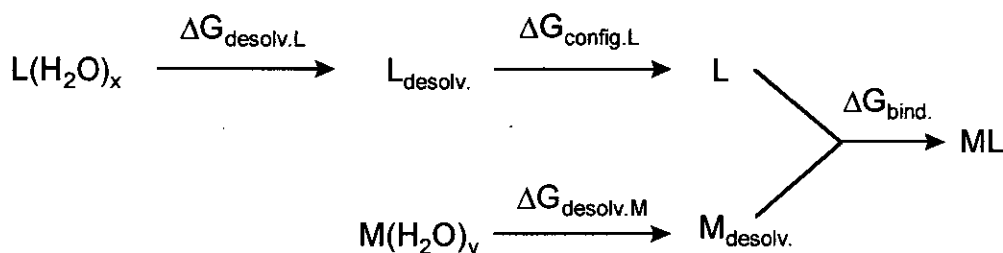
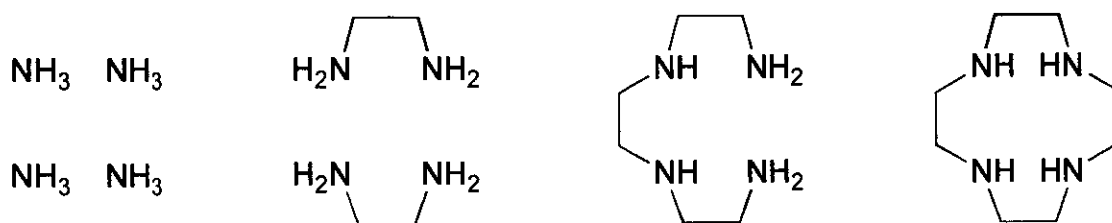


Figure 4 : Metal-ligand complexation energy terms

It is clear that the overall free energy of complex formation, ΔG_{ML} , is dependent on the four energy terms described in Figure 4. However, there has been some controversy as to whether enthalpic or entropic terms predominate in the ease of complex formation¹. It is clear from consideration of Figure 4, that the less free energy required to desolvate the ligand and to change its conformation in order to present a donor set of the geometry required by the metal ion, the more favourable the free energy of complex formation. The highly preorganised donor set in a macrocycle means that

relatively little free energy is required to change the donor set conformation to match the requirements of the metal ion. In addition, the macrocyclic ligand will be considerably less solvated than the straight chain ligands. In contrast, a significant entropy loss will be needed to preorganise the donor atoms in a bis-bidentate ligand system and donor-donor repulsion enthalpies will also have to be overcome. In the "intermediate" case of a linear, tetradentate ligand there will be a smaller entropic loss on organisation of the donor atoms for metal ion complexation, however, donor-donor repulsion on configuration change may be an issue, and the ligand will still be more highly solvated than the macrocycle. As a consequence, it is expected that ΔG_{ML} will become increasingly favourable in forming analogous complexes of bis-bidentate, linear tetradentate and macrocyclic complexes. This is very well illustrated by formation of the comparable ammine and amine copper complexes^{2,3} shown in Figure 5.

Ligands :



Complex formed :



Overall Stability Constant :



Figure 5 : Effects of increasing the preorganisation of nitrogen donor ligands in the complexation of a copper(II) ion

Note : For each of these four complexes, four coordinated water molecules have been replaced. This involves four stepwise equilibria for [Cu(NH₃)₄]²⁺, hence $K_1K_2K_3K_4 = \beta_4$, whereas for [Cu(cyclen)]²⁺ only one equilibrium is involved, hence $K_1 = \beta_1$.

It is important to note, however, that a significant negative effect on ease of complex formation will be observed if the macrocycle forces a change in coordination geometry on the metal ion, with which it is uncomfortable⁴. The key to favourable complexation of transition metal ions is to fit the size of the macrocyclic cavity as closely as possible to that of the metal ion itself. In a metal extraction system, the inner coordination sphere of the metal ion will be initially occupied by water molecules, however, ligand solvation is more complicated as it is dependent on the type of organic diluent in use (% aromatics vs. % aliphatics). It is well known that variations in solvent system affect the efficiency of an SX circuit⁵, for example solvent – ligand interactions are not possible in aliphatic hydrocarbon solvents such as heptane, and will also be minimised in polar solvent systems if, as is proposed here, the ligand is preorganised, i.e. all possible hydrogen-bond functionalities are already “occupied”.

Overall we can conclude that initial formation of a “pseudomacrocycle” will enhance the *thermodynamics* of metal extraction, and it is clear that such pseudomacrocyclic effects influence both ligand behaviour and complex formation. It is ligand behaviour which is of primary interest here and a review of the work previously done in this area and recent work carried out in our laboratory to try to ascertain the extent to which P50-type oxime ligands behave either as pseudomacrocyclic or bis-bidentate ligand systems in metal extraction systems will be discussed in this chapter.

2.2 Evidence for Extractant Preorganisation

2.2.1 X-Ray Crystallography

Although it is perhaps misleading to use solid state evidence to predict the behaviour of molecules in solution, the solid state structures will give some indication of stable intermolecular interactions. It must be noted that in addition to these, crystal packing forces absent in solution may play an important role in determining the observed structure. The seven, fully reported X-ray structures⁶ of phenolic oximes are all dominated by hydrogen-

bond interactions. Structures are also reported for the four compounds, in which R = nonyl and R₁ = H, R = methyl and R₁ = nonyl, R = methyl and R₁ = ethyl, R = methyl and R₁ = methyl (R and R₁ refer to figure 1), but the information files do not contain any three dimensional or packing information, only the space groups and structural parameters⁷.

The seven, full, X-ray structures fall into two classes, dimeric (Figure 6) and polymeric (Figure 7). Preorganised, dimeric motifs are only observed for aldoximes, in which R is hydrogen⁸ or chlorine⁹. The introduction of groups which remove planarity in the molecule, such as alkyl or alkoxy groups, appears to stop efficient packing of dimeric units resulting instead in the formation of polymeric arrays¹⁰⁻¹³.

There are several factors which may be important in determining which of the structural motifs is observed. It is likely that a fine balance between hydrogen bonds and crystal packing forces may determine which modification is seen, ie: the more planar the molecule, the more likely it is to form dimers, as already observed.

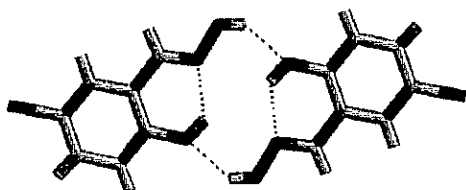


Figure 6 : P50-type dimer

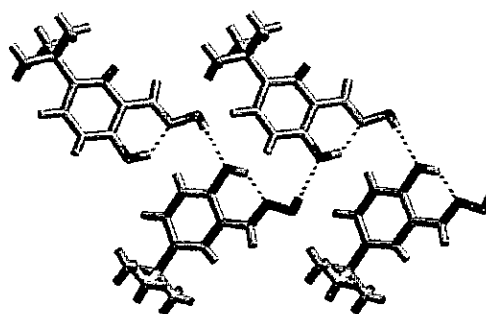
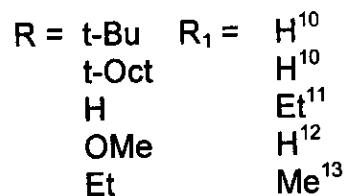


Figure 7 : P50-type oligomer



It is sometimes useful to compare the structures of closely related molecules when trying to build up an overall picture of the general trends associated with structural features of a series of compounds. It is important to

remember, however, that often only very slight chemical modifications can have a significant effect on molecular structure¹⁴. However, comparison of salicylaldoxime type molecules with the closely related N-acetylsalicylamide¹⁵ shows that this molecule does form discrete, hydrogen-bonded dimers in the solid state (Figure 8), and it is interesting to note that this molecule also has a single atom, a proton, in the 5-position of the phenyl ring as is true of the two other “dimer-forming” molecules discussed here.

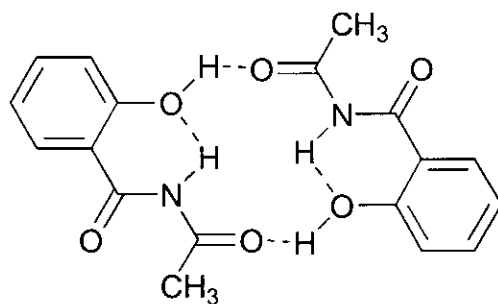


Figure 8 : Hydrogen-bonded dimer of N-acetylsalicylamide
The lengths of the intra- and intermolecular hydrogen bonds are 1.88Å and 1.77Å respectively.

“Practical measures” such as choice of solvent and solution concentration will also play a role. As will be shown later (Section 2.2.4), the association number of hydroxyphenyl oximes in solution is highly solvent dependent. Solvents of recrystallisation are, however, not reported for several of the systems discussed above and it is therefore difficult to draw conclusions on the solvent effect, particularly as, for example, both dimeric and polymeric structures have been recrystallised from ethanol. Similarly, solution concentration is an important factor, as although it is likely that the predominant species in solution will be the one to crystallise, this will change with variations in concentration¹⁶. It is also, of course, very rare that single crystal X-ray diffraction is accompanied by a powder diffraction experiment in order to ascertain that the chosen crystal is representative of the bulk material¹⁴. Solid state observations are still important, however, as they outline possibilities of what *could* be present in solution.

2.2.2 Infrared Spectroscopy (IR)

As infrared spectroscopy has been the most widely used technique in the study of secondary bonding interactions involving 2-hydroxyphenyl oximes¹⁷⁻²⁰, it was the first technique employed in this investigation into extractant preorganisation. The IR spectra of 2-hydroxyphenyl oximes display three characteristic absorptions in the fingerprint hydroxyl region (ca. 3000-4000 cm^{-1}), which, in solution, are sufficiently resolved to be confidently assigned. These absorptions are due to the free oximic hydroxyl group, the intermolecularly hydrogen-bonded oximic hydroxyl group and the intramolecularly hydrogen-bonded phenolic group, and are found at ca. 3600 cm^{-1} , ca. 3400 cm^{-1} and ca. 3200 cm^{-1} respectively. This order reflects the relative bond strengths of these three types of OH bond. The stronger the hydrogen bond, the longer and considerably weaker the O-H bond. In practice this leads to a lowering of the vibrational energy of the bond and a broadening of the absorption band, ie: strongly hydrogen-bonded OH groups are observed at lower ν in the IR spectrum²¹. Part of the IR spectrum of a 0.05 M solution of 2-hydroxy-5-*tert*-butylbenzaldehyde oxime (Figure 1 : R = *t*-Bu, R₁ = H) in heptane is presented in figure 9.

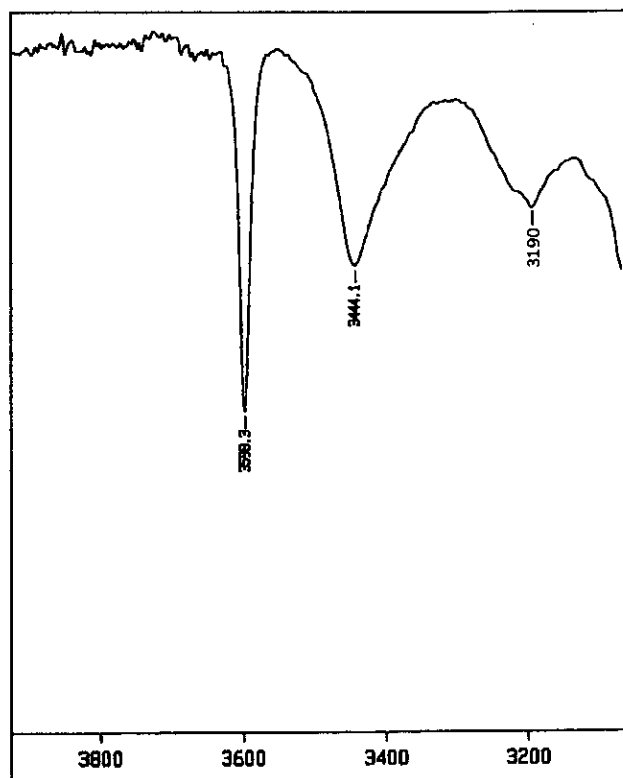


Figure 9 : IR Spectrum of 2-hydroxy-5-*tert*-butylbenzaldehyde in heptane;
Scale : cm^{-1}

The first evidence for extractant association was reported by Laskorin *et al.*¹⁷, who carried out a series of solid and solution IR experiments on 2-hydroxy-5-*tert*-butylacetophenone oxime (Figure 1 : $R = t\text{-Bu}$, $R_1 = \text{Me}$). The solid phase spectrum (KBr disc) shows only a broad band at 3250-3350 cm^{-1} . This is conventionally assigned to intermolecularly hydrogen-bonded oximic hydroxyl groups and it is assumed that the band associated with the intramolecularly hydrogen-bonded phenolic groups, usually observed at *ca.* 3200 cm^{-1} , is masked by this absorption. In tetrachloromethane solution, however, bands associated with monomeric oxime molecules increase in intensity (free NOH at *ca.* 3600 cm^{-1} and phen-OH at *ca.* 3200 cm^{-1}) as concentration decreases, until at concentrations of ≤ 0.002 M the band assigned to the intermolecularly hydrogen-bonded oximic hydroxyl group is no longer seen. This is also the case when a 0.025 M solution is heated to 70 °C, suggesting a predominance of oxime monomers at low concentration and high temperature, as would be predicted.

Similar work carried out in our laboratory on solutions of 2-hydroxy-5-*tert*-butylbenzaldehyde oxime (Figure 1 : R = *t*-Bu, R₁ = H) in chloroform at room temperature gave comparable results, which are presented (in cm⁻¹) in table 1. Again, as concentration decreases the three major absorptions become individually detectable.

Sample	Free NOH	H-bonded NOH	H-bonded phen-OH
KBr Disc	-	3345.2 (s)	3345.2 (masked)
0.1 M sol'n	3574.7(m)	3300 ± 200 (broad)	3300 ± 200 (broad)
0.001 M sol'n	3586.8(m)	3420.7 (m)	3214.3 (w)

Table 1 : IR results for 2-hydroxy-5-*tert*-butylbenzaldehyde oxime (in cm⁻¹)

The X-ray structures of this type of aldoxime^{10,12} are polymeric, which is in agreement with this solid state IR data as no monomeric OH band is seen in the fingerprint region. A similar IR spectrum for ketoximes would therefore be predicted, as their solid state structures are also polymeric^{11,13}. It should be noted, however, that the solid state IR spectrum of 2-hydroxybenzaldehyde oxime (Figure 1 : R = R₁ = H) only shows a broad band at *ca.* 3380 cm⁻¹. The X-ray structure⁸ of this molecule shows it to be dimeric, which underlines the fact that IR spectroscopy cannot be used to distinguish between dimeric and polymeric oxime forms.

Stepniak-Biniakiewicz¹⁸ has carried out extensive IR studies of 2-hydroxy-5-alkylbenzaldehyde oximes (Figure 1 : R = *t*-C₈H₁₇ or *n*-C₁₂H₂₅, R₁ = H) in heptane, tetrachloromethane and also mixtures of xylene and heptane. The spectra of the oximes in pure heptane at 20 °C show a sharp band at 3580cm⁻¹ assignable to the monomeric oxime, a band at 3420 cm⁻¹ of the associated species and a band at 3220 cm⁻¹ of the phenolic group, as before. Tetrachloromethane has a bathochromic effect of approximately 5 cm⁻¹ on these bands. A dependence of the relative intensities of the three absorptions on the concentrations of the sample solutions is not evident from these data, as the concentration range is small (*ca.* 0.005-0.01 M). However, an interesting comparison between these spectra and that of a

0.01 M solution of the *ortho*-substituted oxime, 2-hydroxy-3,5-ditert-butyl benzaldehyde oxime (Figure 10), in heptane can be made. The latter shows a strong band assignable to the monomeric oxime but only a very weak band assignable to an associated species. This observation suggests that the bulk of the *ortho* substituent is preventing association from occurring.

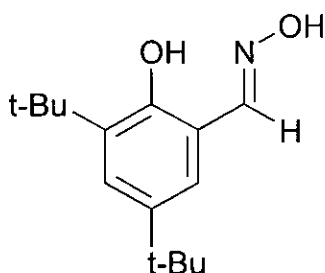


Figure 10 : 2-Hydroxy-3,5-ditert-butyl benzaldehyde oxime

More interesting are the results of a study of the behaviour of 2-hydroxy-5-*tert*-octylbenzaldehyde oxime (Figure 11 : $R = t\text{-C}_8\text{H}_{17}$, $R_1 = \text{H}$) in mixed diluent systems (Table 2). The spectra were run at 20 °C and the sample concentrations were ca. 0.01 M.

Xylene : Heptane Ratio	Free NOH 3560 cm⁻¹	H-bonded NOH 3480 cm⁻¹	phen-OH 3200 cm⁻¹
1 : 0	-	strong	weak
4 : 1	-	strong	weak
1 : 1	weak	strong	weak
1 : 9	strong	medium	weak

Table 2 : IR results for 2-hydroxy-5-*tert*-octylbenzaldehyde oxime in a mixed diluent system

These results show that in predominantly aliphatic solvent systems bands associated with both monomeric and intermolecularly hydrogen-bonded oximes are observed and any association here must be due for the most part to self-association. In aromatic solvent systems the monomeric oxime band

is not observed, which suggests that the oxime is associating either with itself or with the solvent. Solvent interaction could indeed occur due to the weak hydrogen bond acceptance of the aromatic ring of the xylene (NOH--- π) and evidence for a solute-solvent interaction has, in fact, been reported by Dalton *et al.*¹⁹, who observe an IR band associated with interaction between the phenolic OH group of P50 and the solvent, toluene. Such a band is not seen in the spectrum of an equivalent sample of P50 in heptane. Hosking and Rice²⁰ have investigated the behaviour of the Shell extractant SME 529 (Figure 1 : R = C₉H₁₉, R₁ = Me) in toluene and n-dodecane. Interestingly the results of this study in toluene differ from those of Stepniak-Biniakiewicz¹⁸ in xylene, in that over a concentration range of 0.0125 - 0.10 M the monomeric oxime band predominates and the associated oxime band is minimal in all cases. This suggests that solvent interaction is not occurring in toluene. In n-dodecane, however, the associated species predominates over a similar concentration range (0.025 - 0.10 M) indicating that self-association must be occurring in this case (NB: temperature not given, assumed to be room temperature).

It is important to remember that while salicylaloximes and acetophenone oximes exist almost exclusively in their E isomeric forms (Figure 11 : R = alkyl, H; R₁ = H, Me), benzophenone oximes occur in both the E and the non-complexing Z (Figure 12 : R = H, alkyl; R₁ = Ph) forms. While both isomers are able to form associated dimeric species, evidence for higher associates of the Z form has also been recorded. This may be due to the unshared pair of electrons on the oximic nitrogen being more basic as electron density is pulled away from it by the formation of the intramolecular hydrogen bond involving the oximic hydroxyl group and the phenolic oxygen atom²².

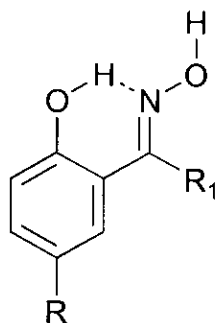


Figure 11 : E-isomer

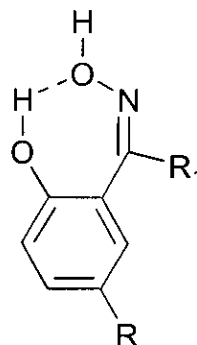


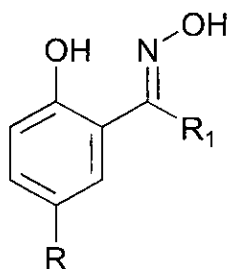
Figure 12 : Z-isomer

Szymanowski²² reports that while the solid state spectrum of 2-hydroxy-5-methyl-benzophenone oxime (Figure 12 : R = methyl, R₁ = phenyl) shows bands at 3260, 3220 and 3180 cm⁻¹ associated with the intermolecularly hydrogen-bonded oxime OH, these bands are replaced by a band at 3267 cm⁻¹ and a shoulder at 3215 cm⁻¹, which are assigned to an oxime trimer (lower energy) and dimer respectively. Early IR work on the formation of dimers and trimers by cycloalkanone oximes was reported by Geiseler and Fruwert²³ in 1960 and, more recently, Szymanowski *et al.*²⁴ have proposed both dimer and trimer formation by the Henkel reagent LIX 65N (Active component : Figure 12 : R = nonyl, R₁ = phenyl) from their studies on the interfacial tension in solvent extraction systems. Their work also states that the rate of metal extraction will decrease if aromatic solvents (or equally aromatic modifiers such as alkyl phenols) are used, due to the ability of the solvent molecules to penetrate the layer of adsorbed oxime molecules at the organic:aqueous interface thus decreasing the interfacial concentration of extractant molecules. This is an example of another solvent effect on the rate of metal extraction, which in this case is unrelated to extractant association but may have great practical implications²⁵.

2.2.2.1 Calculation of Association Constants

Several workers¹⁷⁻¹⁹ have used IR techniques to calculate association and dimerisation constants of 2-hydroxyphenyl oximes in solution. Their results are summarised in table 3, the values quoted having been calculated from the ratio of intensities of the relevant IR bands.

These results are based on the assumption that the **only** associated species present in solution are dimers, which is now known to be inaccurate (Section 2.2.4). Several general observations can still be made from these results. Although the values vary quite significantly, $K_{\text{dimerisation}}$ is highest in aliphatic solvent systems such as heptane and lowest in aromatic systems such as toluene, as would be predicted. Additionally, dimer formation is unfavourable for the sterically hindered 2-hydroxy-3,5-di-*tert*-butylbenzaldehyde oxime¹⁸.



Reference	Oxime		Solvent	$K_{\text{dim}} / \text{Imol}^{-1}$	$-\Delta G_{\text{dim}} / \text{kcal mol}^{-1}$	$-\Delta H_{\text{dim}} / \text{kcal mol}^{-1}$
	R	R ₁				
19 ^a	nonyl	H	Hexane	117	2.85	-
			Toluene	11.5	1.46	-
18 ^b	H	H	Heptane	28.5	-	1.16
	n-Bu	H	Heptane	27.1	-	1.68
	<i>t</i> -Bu	H	Heptane CCl ₄	30.5 9.5	-	1.86
	<i>t</i> -Octyl	H	Heptane	35.0	-	2.01
	n-Dodecyl	H	Heptane	41.2	-	1.94
	<i>o</i> -substd: both <i>t</i> -Bu	H	Heptane	7.6	-	-
17 ^a	<i>t</i> -Bu [OMe at 2]	CH ₃	CCl ₄	42.29	2.14	5.06
	<i>t</i> -Bu	CH ₃	CCl ₄	12.36	1.67	4.66
	<i>t</i> -Bu	Ph	CCl ₄	50.77	2.37	4.28

Table 3 : Thermodynamic data and dimerisation constants calculated from solution IR data of P50-type oximes

^a No values for temperature or concentration given

^b T = 20°C; Concentration = 0.01 M

The results of Laskorin *et al.*¹⁷ for the non-polar solvent, tetrachloromethane, are higher than those for toluene, but dimerisation in this type of solvent is still not thought to be as favourable as in hydrocarbon diluents, and discrepancies in these results are likely to be due to errors and variation in the methods of determination. Stepniak-Biniakiewicz¹⁸ has found that the dimerisation constants of *para*-alkyl hydroxyphenyl oximes in heptane solution are dependent on the length and structure of the alkyl chain, with calculated values increasing slightly with increasing alkyl chain length, and branched chain derivatives having higher dimerisation constants than their straight chain equivalents. The dimerisation constant determined by Dalton *et al.*¹⁹ for P50 in hexane is however much higher than that of its n-dodecyl equivalent, but this may again be due to variations in experimental technique. Such discrepancies are also likely to be due to variations in water content of each of the systems studied as this will disrupt the hydrogen-bonding capabilities of the oxime molecules. It is important to note that these dimerisation constants are still relatively low in comparison with, for example, those of dialkyl phosphonic acid derivatives²⁶, which can be as high as 10^4 . The values for the Gibbs free energies of dimerisation ($-\Delta G_{\text{dim}}$) remain fairly constant, again being highest for P50 in hexane. The values of the enthalpy of dimer formation ($-\Delta H_{\text{dim}}$) are more variable. All values reported for solutions in tetrachloromethane are higher than those in hydrocarbon solvents. There is no obvious explanation for this and some care must be taken in evaluating all these data as, as already stated, these methods are approximate and are based on the assumption that only dimerisation and not higher oligomerisation occurs. Overall these results suggest that dimerisation is, as expected, much more favourable in non-polar solvents than in aromatic solvent systems.

In conclusion, these IR studies provide evidence for self-association of oximes in non-polar, aliphatic solvents, but the nature of the associated species present and the mean aggregation numbers cannot be determined.

2.2.3 Proton Nuclear Magnetic Resonance Spectroscopy (^1H NMR)

NMR has been extensively used to study the self-association of biological molecules, such as the nucleobase, uridine²⁷ (Figure 13), and the anti-tumour drug, actinomycin D^{28,29} (Figure 14), in order to clarify their modes of action.

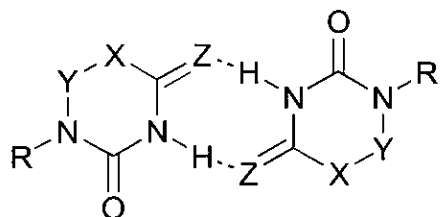


Figure 13 : Uridine derivatives
X-Y = $-\text{CH}=\text{CH}-$, $-\text{CH}_2-\text{O}-$; Z = O, S

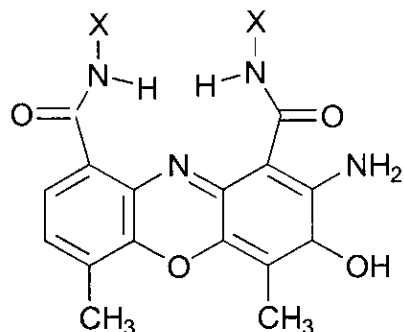


Figure 14 : Actinomycin D
X = pentalactone ring

Hosking and Rice²⁰ have carried out NMR experiments on solutions of aromatic *ortho*-hydroxyoximes in various solvents at various concentrations and observed both solvent and concentration dependent variations in the frequencies of both the phenolic and oximic proton resonances. They did not observe any NMR evidence for "a specific dimeric species", however, and so NMR has never been used to study the association of P50-type extractants.

2.2.3.1 Solvent Effects

The ^1H NMR work carried out initially focused on investigating the solvent-dependent behaviour of hydroxyoximes in solution. Although differences had already been observed using IR, it was hoped that ^1H NMR might be able to clarify these observations. The results of the study of the solvent-dependent behaviour of 2-hydroxy-5-*tert*-butylbenzaldehyde oxime (Figure 1 : R = *t*-Bu, R₁ = H), are presented in figure 15 as a plot of chemical shift (in ppm) *versus* the dielectric constant of the solvent. The spectra were acquired at room temperature and the concentrations of the solutions were ca. 0.12 M.

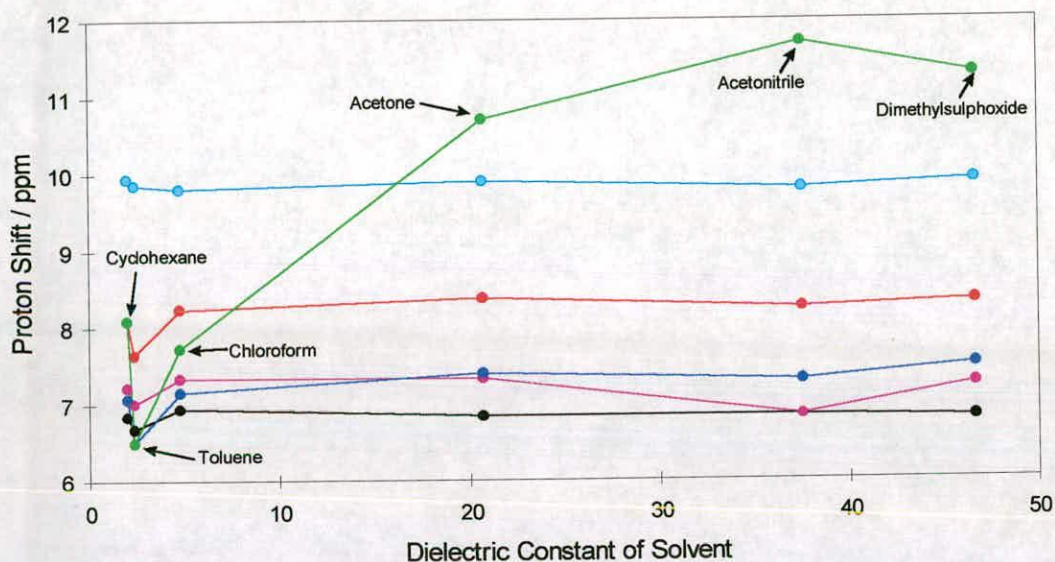
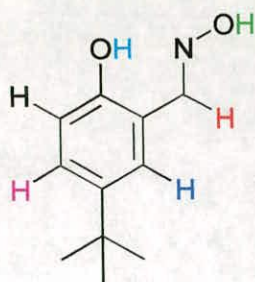


Figure 15 : Results of an NMR study of the solvent-dependent behaviour of 2-hydroxy-5-*tert*-butylbenzaldehyde oxime

The results show that while the alkyl, aromatic, aldehydic and phenolic protons are essentially unaffected by change in polarity of the solvent, the oximic proton is, and from the variation in its chemical shift value, three distinct types of solvent-dependent behaviour can be identified, if we assume that increased hydrogen-bonding leads to deshielding of the proton and a shift to lower field (ie: larger δ -value). It might be expected that donor solvents such as acetone, acetonitrile and dimethylsulphoxide will hydrogen-bond to the oxime and result in high chemical shift values of ca. 10.5-11.5 ppm. Conversely, it is probable that cyclohexane does not interact with the oxime function. In this solvent, however, self association will be favourable, giving a chemical shift value of approximately 8 ppm. Chloroform is a only a weak hydrogen bond acceptor in comparison with polar solvents such as acetone. The oximic shift of ca. 7.5 ppm could reflect a combination of a

weak interaction with the chloroform and some self-association. Finally toluene, which is also a weak hydrogen bond acceptor, gives the lowest chemical shift value of *ca.* 6.5 ppm and the oxime molecules are assumed to be completely non-associated, although weak π -interaction of the tolyl ring with the oximic proton is theoretically possible. Careful drying of the NMR solvents to remove trace water, which might interact with the phenolic oximes, did not alter the spectra.

2.2.3.2 Concentration Effects

Having defined the influence of solvent type on the behaviour of 2-hydroxyphenyl oximes in solution, the effect of concentration change was also studied using ^1H NMR. Spectra were acquired for (i) 2-hydroxybenzaldehyde oxime, (ii) its 5-*tert*-butyl derivative and (iii) the unsubstituted benzaldehyde oxime (Figure 16) in non-polar solvents. The sample concentrations for each oxime were 0.001, 0.01, and 0.1 M. Figures 17-19 show plots of the variation in proton shift of protons 1-5 with varying concentration in each of the three solvents, chloroform (Figure 17), toluene (Figure 18) and cyclohexane (Figure 19).

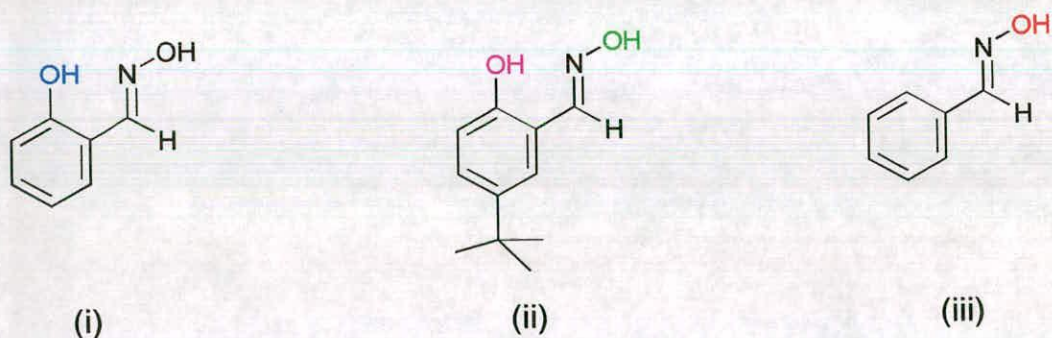


Figure 16 : Benzaldehyde oxime (iii) and derivatives

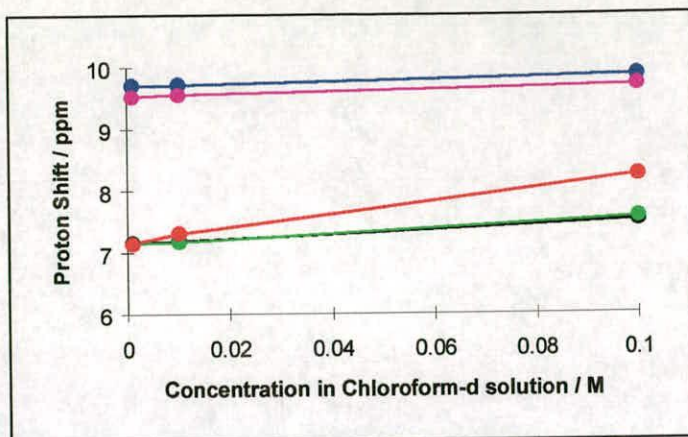


Figure 17 : Behaviour in chloroform-d

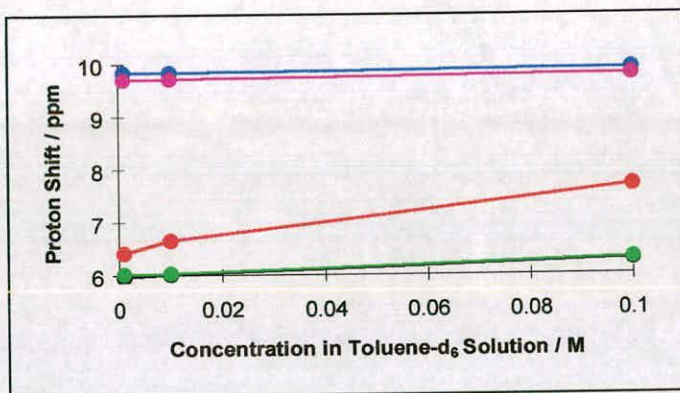


Figure 18 : Behaviour in toluene-d₆

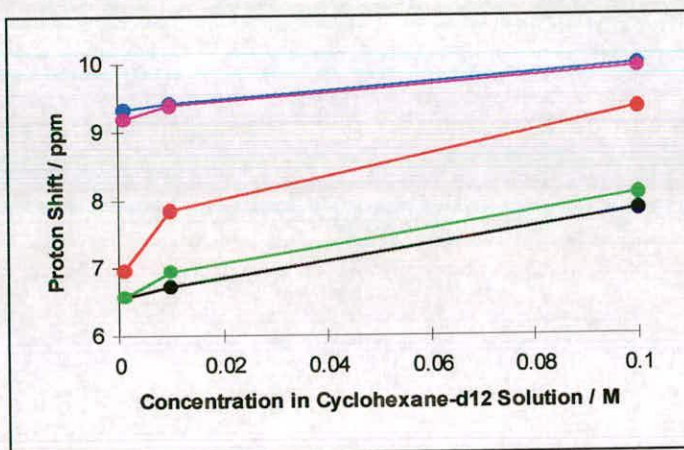


Figure 19 : Behaviour in cyclohexane-d₁₂

In all cases, the oximic proton shows greater chemical shift variations than the phenolic proton suggesting that it is the more labile. Additionally, the highest shift values are obtained for the oximic proton of the unsubstituted

benzaldehyde oxime, which is perhaps unexpected, as it might be expected that the oximic protons in 2-hydroxyphenyl oximes would be more labile due to the withdrawal of electron density *via* formation of the intramolecular hydrogen bond. The reasons for this observation are unclear, but it does suggest that the hydroxyl substituent in 2-hydroxyphenyl oximes may exert an “intramolecular” stabilising effect on the oximic proton, thus decreasing its lability in some way. Additionally, benzaldehyde oxime is the more “open” system, thus there are more opportunities for association to occur.

2.2.3.3 Nuclear Overhauser Effect (NOE) Experiments

In an attempt to gain evidence for dimerisation of 2-hydroxyphenyl oximes in non-polar solvents, nuclear overhauser effect (NOE) experiments were carried out on 2-hydroxy-5-*tert*-butylbenzaldehyde oxime (Figure 1 : R = *t*-Bu, R₁ = Me) in deuterated chloroform and cyclohexane. The spectra were acquired at room temperature and samples concentrations were 0.37 M and 0.1 M respectively. It was hoped that if the 2-hydroxyphenyl oxime was present as a dimer then a positive enhancement of the *ortho*-aromatic proton due to the oximic proton would be seen (Figure 20). This technique has previously been used by Corbin and Zimmerman³⁰ to determine the presence of hydrogen-bonded dimers in solutions of urea derivatives in deuterated toluene and chloroform at room temperature. In this experiment the sample concentrations were extremely low ranging from 10 μ M to 40 mM.

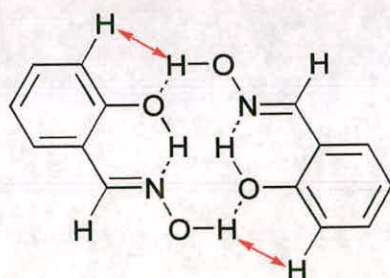


Figure 20 : NOE interactions in a dimer of a 2-hydroxyphenyl oxime

In chloroform, irradiation of the oximic proton peak led to the simultaneous and equivalent irradiation of the phenolic proton peak indicating that fast exchange takes place between these two protons. It is feasible that the negligible amount of water present in the chloroform may have acted as a catalyst in this exchange mechanism. Cooling the sample to $-60\text{ }^{\circ}\text{C}$ in an attempt to slow this exchange process did not alter the results of the experiment. Repeating the experiment in carefully dried cyclohexane (water undetectable by NMR) gave similar results, which, while not wholly unambiguous, suggests that self-exchange must have been occurring between the two protons in this case. It was therefore impossible to confirm or disprove the presence of oxime dimers in solutions of either chloroform or cyclohexane using this technique. The spectra obtained from the NOE experiments carried out in chloroform are presented in figure 21.

Like IR, therefore, the NMR experiments gave qualitative evidence for the self-association of 2-hydroxyphenyl oximes, but the results could not be interpreted in terms of aggregation number or allow any measurement of equilibria constants for association.

NOE experiment in chloroform-d

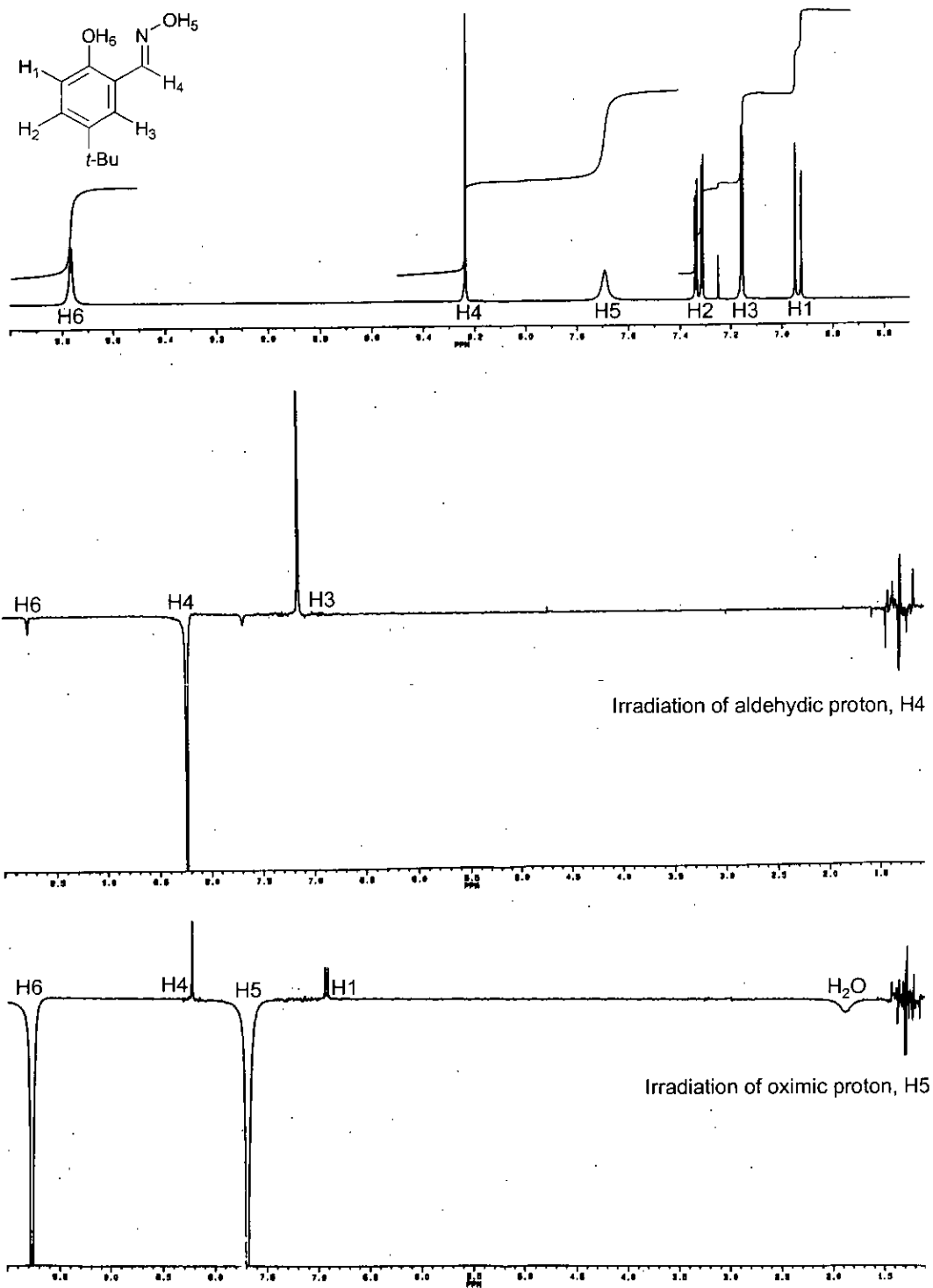


Figure 21 : NOE spectra of 2-hydroxy-5-*tert*-butylbenzaldehyde oxime in chloroform.

NB : The full spectrum and NOE spectra are plotted on different scales.

2.2.4 Molecular Weight Determinations

In recent years, several reports³¹⁻³⁶ on the determination of molecular weights of 2-hydroxyphenyl oximes in solution using both cryoscopy and osmometry have been published. The results of molecular weight determinations (both cryoscopic and osmometric) carried out on P50-type oximes by Hosking and Rice²⁰ (Figure 1 : R = C₉H₁₉, R₁ = H; Solvents : cyclohexane and benzene), Komazawa *et al.*³¹ (Figure 1 : R = C₉H₁₉, R₁ = Ph; Solvents : n-heptane and benzene) and in this study (Figure 1 : R = R₁ = H; Solvent : benzene) are combined in Figure 22. The work done as part of this study was carried out in collaboration with Dr. M.G. Davidson at the University of Durham³². As in the NMR and IR experiments, these results identify distinct, solvent-dependent differences in the behaviour of 2-hydroxyphenyl oximes in solution. They suggest that in aromatic solvents such as benzene the majority of oxime molecules are monomeric and an aggregation number of only ~1.4 is achieved in a 0.8 M solution. It must be remembered that the value obtained from molecular weight determinations is only an average of all species present in solution, meaning that whilst dimers or higher oligomers are obviously present in benzene, they are by no means the predominant species. In contrast, mean aggregation numbers of more than 2 are reported for solutions of 2-hydroxyphenyl oximes in aliphatic solvent systems, suggesting that not only dimers but higher oligomers are formed in solvents such as heptane and cyclohexane.

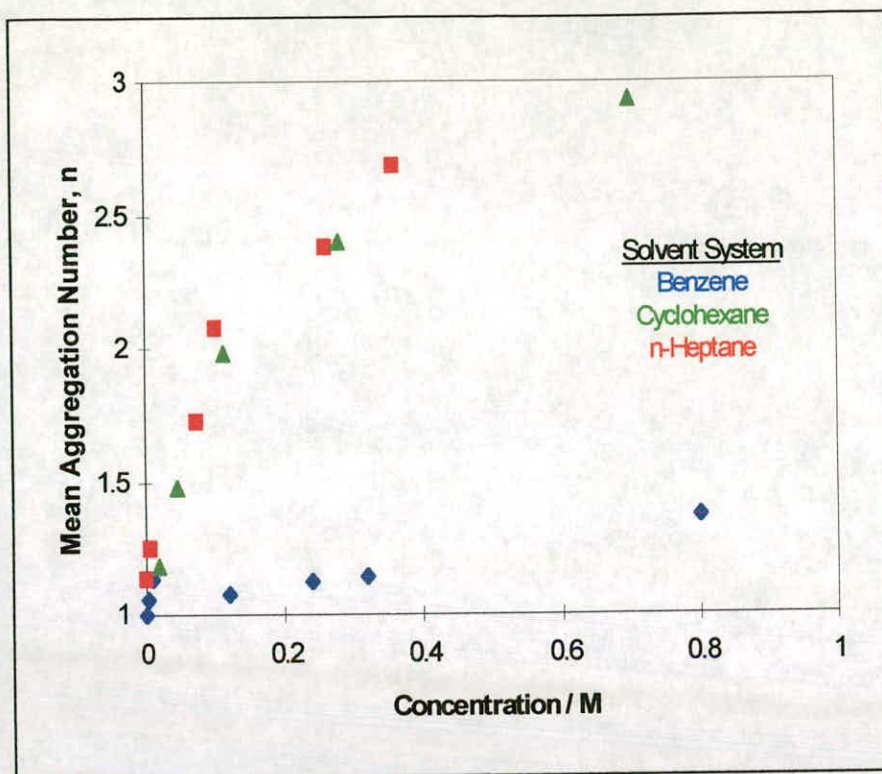


Figure 22 : Molecular weight determinations for P50-type oximes

Interestingly, Stepniak-Biniakiewicz and Symanowski³⁵ note that although the results of their cryoscopic studies of a range of hydroxyoximes in benzene suggest the presence of an equilibrium between monomers and dimers, somewhat higher association is also observed for oximes with branched alkyl R substituents, which agrees with the solid state observations of polymeric arrays for this type of oxime.

2.4.5 Electrospray Mass Spectrometry (ESMS)

Electrospray mass spectrometry (ESMS) has been increasingly used as a tool to study associated species in solution, for example proteins, oligonucleotides and, more recently, supramolecular, hydrogen-bonded assemblies^{36,37}. Interactions of the $\pi - \pi$ type have also been observed using ESMS³⁸. Such studies are possible because of the relatively mild ionisation conditions employed in ESMS in comparison with other MS techniques, such

as FAB and EI. Experiments were carried out on 10^{-5} M solutions of P50-type oximes in methanol.

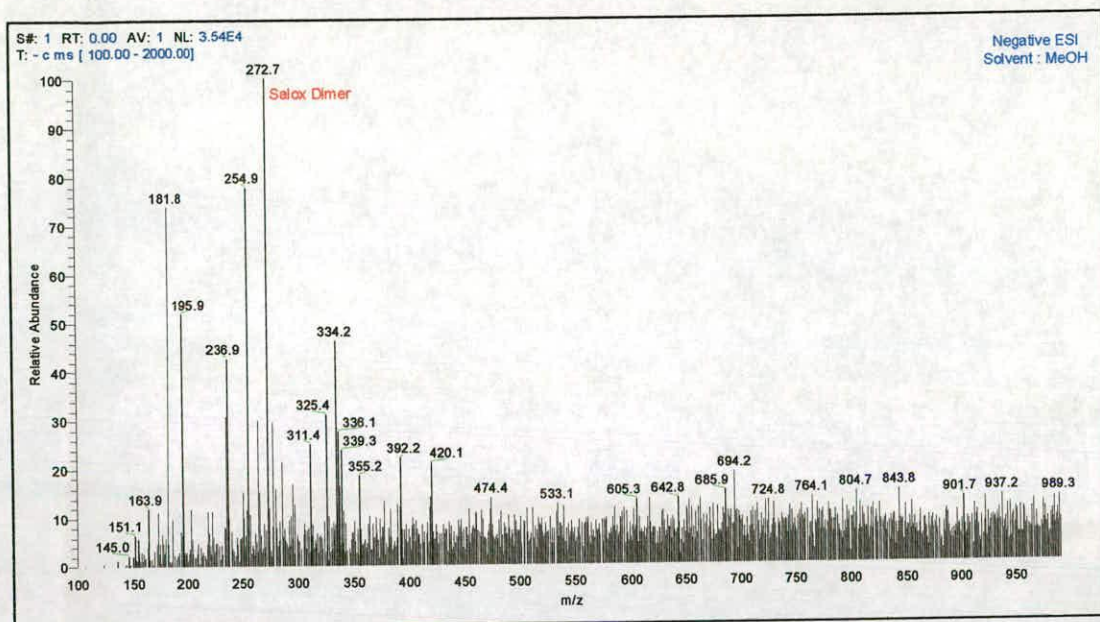


Figure 23 : ESMS of 2-hydroxybenzaldehyde oxime
(The Salox Monomer is observed in the low mass range at 136 - negative ESI)

The choice of methanol as solvent reflects its suitability, in terms of ease of spray formation and sensitivity of results, for this type of experiment, although NMR results indicate that it may not promote the self-association of P50-type oximes, rather the formation of solvent-oxime adducts. By virtue of the technique, however, the ratio of molecule to solvent is extremely high at the point of entry into the electrospray chamber as the solvent molecules evaporate from the analyte solution to leave free gas-phase ions³⁹. This also means that the "concentration of solution" at the point of analysis will be considerably greater than 10^{-5} M. The spectra of 2-hydroxybenzaldehyde oxime (Figure 23), its 5-*tert*-butyl derivative (Figure 24) and P50 itself (Figure 25) show peaks corresponding to both monomeric and dimeric species indicating that such species are stable in the gas phase. The relative peak intensities of dimer to monomer, the latter of which were 100 % in all spectra, in the spectra of 5-*t*-butyl-2-hydroxybenzaldehyde oxime (Figure 24) and P50 (Figure 25) are 52% and 28% respectively. This suggests that P50 may not form dimers as readily as its *tert*-butyl equivalent,

however, reliable data cannot be reliably obtained from this technique. Additionally, the spectrum of 2-methoxy-benzaldehyde oxime showed no peaks attributable to dimers or higher oligomers, which would be expected due to the bulk of the methyl group blocking hydrogen bonding to the methoxy oxygen atom.

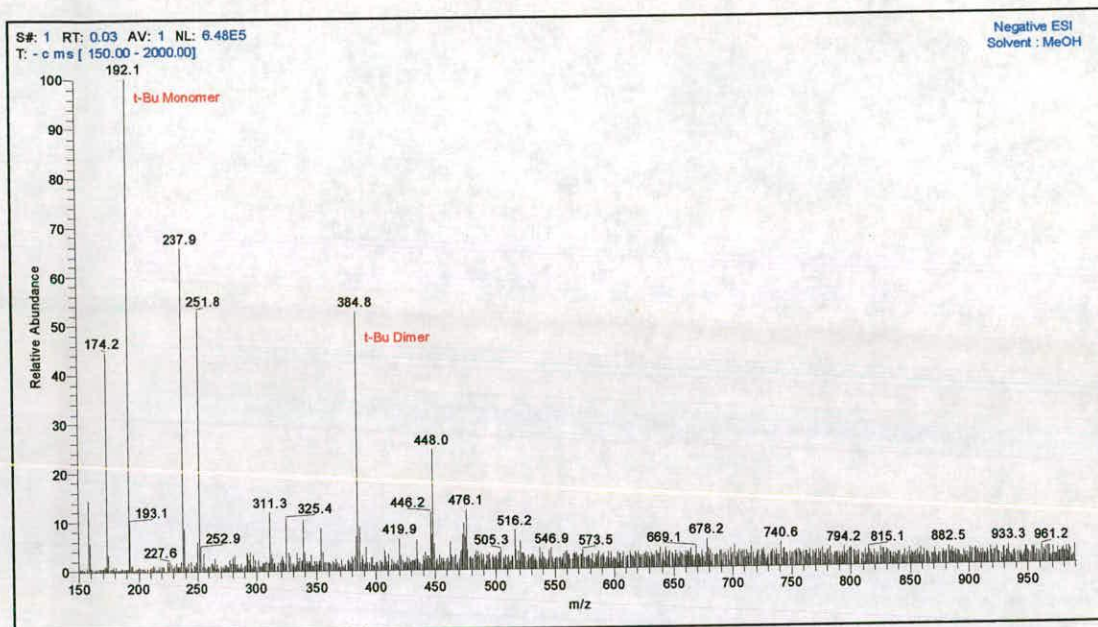


Figure 24 : ESMS of 2-hydroxy-5-*tert*-butylbenzaldehyde oxime

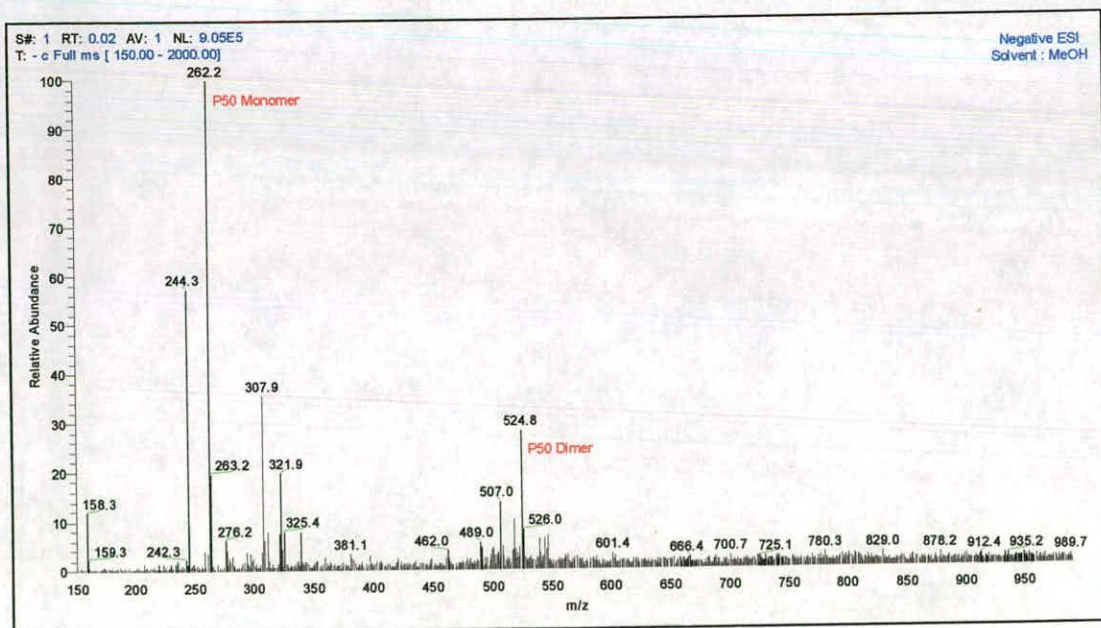


Figure 25 : ESMS of P50

The formation of the dimeric pseudomacrocycles can also be studied using a combination of different, monomeric phenolic oximes. The spectrum of a 1:1 mixture of P50 and 2-hydroxy-5-*tert*-butylbenzaldehyde oxime is presented in figure 26. Peaks assignable not only to the pure monomeric and dimeric species (Relative intensities : *t*-Bu monomer 6%, dimer 4%; P50 monomer 100%, dimer 60%) but also to the “P50 / *tert*-butyl associate” (Relative intensity 13%) are observed, which confirms that mixed dimers of 2-hydroxyphenyl oximes can also exist as stable gas phase species. The relative peak intensities in this spectrum could also be interpreted to suggest that P50 forms dimers much more readily than the *tert*-butyl derivative, disagreeing with previous observations, and additionally that the mixed dimer also forms preferentially over the pure *tert*-butyl dimer.

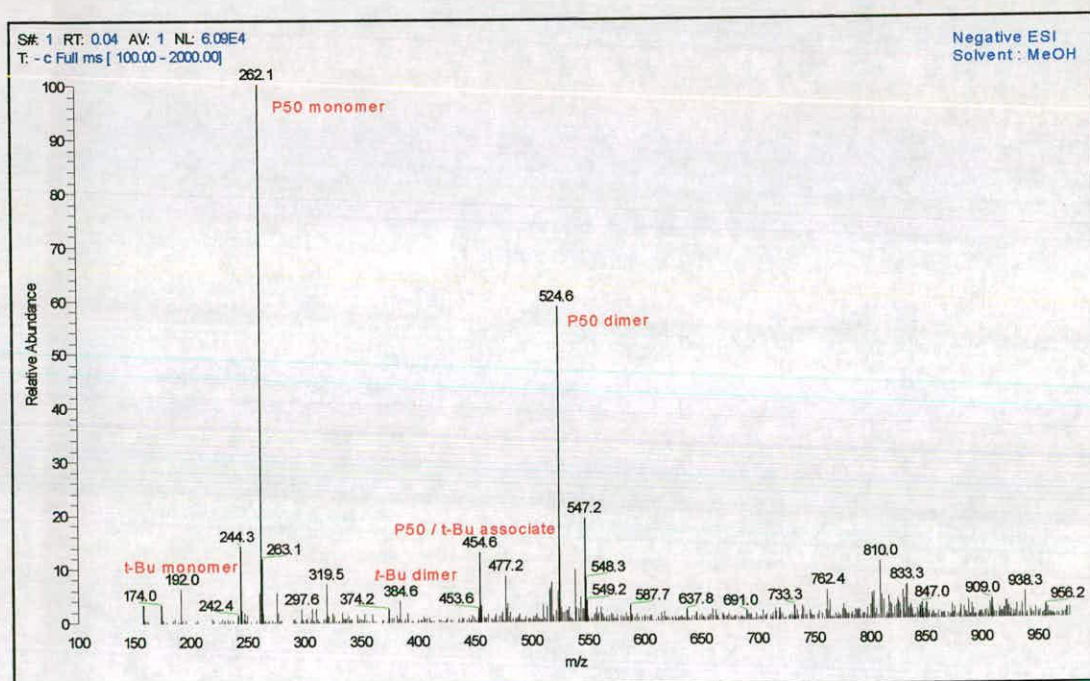


Figure 26 : ESMS of a mixture of P50 and its *tert*-butyl derivative

Additionally, ESMS analysis of a 1:1 mixture of 2-hydroxy-5-*tert*-butylbenzaldehyde oxime and the modifier 4-nonylphenol did not provide evidence for the breaking up of oxime dimers by the modifier, as might be expected. It is important to remember, however, that care is needed in the

interpretation of electrospray mass spectrometry results as the species analysed are in the gas phase are generated by evaporation of analyte solutions. They may therefore only represent the species present at the surface of the remaining droplet, which may well be different to that present in the “bulk” droplet.

2.2.6 Theoretical Calculations

Ab initio and semi-empirical (Hartree Fock) calculations were performed on 2-hydroxybenzaldehyde oxime (Figure 1 : R = R₁ = H) to compare the enthalpies of formation of the monomeric and dimeric species in various solvents and in the gas phase. The calculations were carried out by Dr. Michael Charlton of Avecia (Manchester). Results are presented in table 4.

Conditions	Monomer	Dimer	Dimerisation	Solvation Energy	
	$\Delta H_f / \text{kcal mol}^{-1}$	$\Delta H_f / \text{kcal mol}^{-1}$	$E^a / \text{kcal mol}^{-1}$	$\Delta H_{\text{sol}}^b / \text{kcal mol}^{-1}$ Monomer	Dimer
Ab initio	-	-	- 5.95	-	-
Gas phase	- 18.8	- 43.1	- 5.5	-	-
Hexane	- 26.8	- 57.3	- 3.7	- 8.0	- 14.2
Benzene	- 26.9	- 58.0	- 4.2	- 8.1	- 14.9
Water	- 31.3	- 59.1	+ 3.5	- 12.5	- 16.0

Table 4 : Results of theoretical calculations performed on 2-hydroxybenzaldehyde oxime

Note : *Ab initio* calculations were performed using the basis set 6-31G* and corrected for BSSE. The dimer structure is in an unsymmetrical, chair conformation; Semi-empirical energies were optimised with AM1⁴⁰. Solvation calculations were performed using AMSOL⁴¹ incorporating the SMx models of Cramer and Truhlar for water⁴² and hydrocarbons⁴³ as required.

^a Dimerisation energies were calculated from $\{\Delta H_{\text{dimer}} - 2(\Delta H_{\text{monomer}})\}$

^b Solvation energies were calculated from $\{\Delta H_f^{\text{Solvent}} - \Delta H_f^{\text{Gas Phase}}\}$ for both monomer and dimer individually

These results show that dimer formation is predicted to be favoured over the monomer in the gas phase and in organic solvents. The oxime does not dimerise in water, as would be expected. Additionally, solvation of the

monomer is found to be much more favourable in water than in either hexane or benzene, which is also expected, as solvent - oxime interactions are much more prevalent in water. The solvation of the dimer is also found to be slightly more favourable in water than in non-polar solvents.

Curiously, the very similar ΔH_f values for dimerisation calculated for hexane and benzene, and the more favourable solvation value for the dimer in benzene, in comparison with that for heptane, do not agree at all with the molecular weight determination data discussed previously. Such molecular weight determinations have shown that dimer formation is highly disfavoured in benzene, whereas not only dimers but higher oligomers will readily form in aliphatic solvents such as hexane.

Simperler and Mikenda⁴⁴ have characterised intramolecular hydrogen-bonding in 2-hydroxybenzaldimines (Figure 27), including 2-hydroxybenzaldehyde oxime (R = OH), using spectroscopic (gas phase IR) and quantum mechanical data. Their methodology is based on earlier work carried out on related 2-hydroxybenzoyl compounds⁴⁵. Unfortunately their experiments were performed at concentrations purposefully low enough to ensure the absence of any intermolecular associations effects, which are of primary interest here.

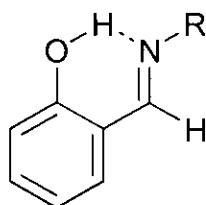


Figure 27 : 2-Hydroxybenzaldimines

(i) R = H, CH₃, C₆H₅, CHO, (CO)CH₃; (ii) R = NH₂, NHC₆H₅, OH, OCH₃

However, they draw some interesting conclusions regarding the strength of the intramolecular hydrogen bond, which is represented by the distance $r(\text{O}-\text{H})$, and, in fact, correlate this very well with the distances $r(\text{H}\cdots\text{N})$ and $r(\text{O}\cdots\text{N})$. The group of compounds under study can also be split conveniently into two sub-groups, (i) and (ii) (Figure 27). Compounds (i) have electron-donating carbon or hydrogen R substituents and therefore have stronger

intramolecular hydrogen bonds than compounds (ii), which have electron-withdrawing oxygen or nitrogen R substituents, which weaken the electron density around the imino nitrogen and thus the intramolecular hydrogen bond. The electronegativity of such R substituents does, of course, play an important role in the formation of intermolecular hydrogen bonds to other, eg: oxime, molecules, and as such this work may have implications for the ease of dimer/oligomer formation depending on (a) the R substituent and (b) the strength of the intramolecular bond.

Komasawa *et al.*³¹ have estimated $K_{\text{dimerisation}}$ for LIX65N (Figure 1 : R = nonyl, R₁ = phenyl) in both toluene and n-heptane from values obtained for the aqueous solubilities of the oxime. Values from plots of $[\text{LH}_{\text{aq}}]$ versus $[\text{LH}_{\text{org}}]$ have been fed into a curve fitting programme to fit the following equations (1, 2) relating the organic to aqueous (O:A) distribution constant, K_{dist} , to the dimerisation constant, K_{dim} .

$$[\text{LH}_{(\text{org})}] = \frac{[\text{LH}_{(\text{aq})}]}{K_{\text{dist}}} \times \frac{(1 + 2K_{\text{dim}}[\text{LH}_{(\text{aq})}])}{K_{\text{dist}}} \quad (1) \text{ gives}$$

$$[\text{LH}_{(\text{org})}] = \frac{[\text{LH}_{(\text{aq})}]}{K_{\text{dist}}} + \frac{2K_{\text{dim}}[\text{LH}_{(\text{aq})}]^2}{(K_{\text{dist}})^2} \quad (2)$$

The values obtained for K_{dim} are 120 and 3 l mol⁻¹ for n-heptane and toluene respectively, again illustrating that dimerisation is much more favourable in aliphatic solvent systems. It should be noted that for simplicity only dimerisation and not higher oligomerisation was considered in this work.

Whewell and Hughes⁴⁶ have developed and evaluated three theoretical models for the extraction of copper(II) from sulphate by LIX64N (Figure 1 : R = nonyl, R₁ = phenyl plus 5,8-diethyl-n-hydroxydecan-6-oxime) in the solvent Escaid 100 (80% aliphatics, 20% aromatics). The three models are based on equations for the formation of an oxime dimer, a tetramer and a "series", ie: a range of higher oligomers, and mass balance equations, and have been tested against "real" solvent extraction data. Interestingly they find that the

tetramer and series models describe the real data much better than the dimer model, this work again stressing the importance of extractant aggregation in commercial systems.

Finally, Russell and Rickel⁴⁷ have developed solvent extraction mathematical models, which, like those of Whewell and Hughes, are based on both mass action and mass balance equations specific to each extractant. They have also tried to fit experimental data to these theoretical models of the extraction of copper(II) from sulphate using LIX84 (Figure 1 : R = nonyl, R₁ = methyl), PT5050 (Figure 1 : R = nonyl, R₁ = H plus tridecanol as modifier) and P5100 (Figure 1 : nonyl, R₁ = H plus nonyl phenol as modifier). The results are presented in table 5.

Extractant & Solvent System	Extraction Equilibrium Constant	$K_{dim} / \text{Imol}^{-1}$	"Modifier - Extractant Associate" Formation Constant / Imol^{-1}
LIX84 / Kermac	145	65	-
LIX84 / Solvesso	ca. 14.5	ca. 13	-
PT5050 / Kermac	53	-	-
P5100 / Kermac	400	3.7	5.8

Table 5 : Results of extraction models incorporating LIX84, PT5050 and P5100

Note : Kermac = Kermac 470B, a solvent containing 85-90% aliphatics and 10-15 % aromatics
 Solvesso = Solvesso 100, a solvent containing 99% aromatics and 1% aliphatics

These results are interpreted by the authors to indicate that PT5050 behaves as a monomer, LIX84 behaves as a mixture of monomer and dimer and P5100 behaves as a mixture of monomer, dimer and extractant-modifier associate. The modifier in P5100, nonyl phenol, can associate with the oxime *via* both intermolecular hydrogen-bonding and π -interaction of the phenyl rings. It is also interesting to note that the use of LIX84 in an aromatic solvent reduces the extraction capability of the oxime by ca. 90% and that oxime dimerisation is also reduced by ca. 80%, in comparison with

LIX84 in an aliphatic solvent. These observations agree very well with the results discussed previously.

This work has shown that theoretical calculations can be used to estimate the behaviour of P50-type solvent extractants in solution, and, for the most part, that theoretical extraction models agree with “real” data.

2.3 Conclusions

The work presented in this chapter has provided evidence for the self association of 2-hydroxyphenyl oximes in solution as observed in the IR and NMR spectra of P50-type compounds. However the associated species cannot be identified as dimer, trimer, oligomer or solvent-oxime adducts. Electrospray mass spectrometry confirms that 2-hydroxyphenyl oximes form dimeric species, which are stable in the gas phase, but such a technique cannot provide reliable evidence for dimerisation, or indeed any type of association, in solution.

Molecular weight determination techniques such as cryoscopy and osmometry give quantitative information on the self association of oximes in solution. This is found to be both solvent and concentration dependent, with dimerisation occurring in aliphatic solvent systems at concentrations of approximately 0.1 M. At higher concentrations oligomerisation occurs in aliphatic solvents. In contrast, however, dimerisation never predominates in aromatic solvent systems.

NMR analyses also identify distinct solvent dependent differences in the behaviour of 2-hydroxyphenyl oximes in solution. In polar solvents, solvent-oxime adducts will form, whereas in aliphatic non-polar solvents the oximes associate preferentially with themselves. In aromatic, non-polar solvents, evidence for dimerisation is not seen, although some evidence for solvent association is.

These results are of considerable industrial relevance as they suggest that the choice of diluent used in a solvent extraction process may significantly

affect the operating performance of the plant. The observation that diluent type influences the *kinetics* of the process was made by Price and Tumilty in 1975³, who stated that as the extraction reaction occurs at the solvent / water interface, it must be a diluent-dependent process. As the concentration of extractant at the interface will be higher in a diluent, which solvates the ligand only weakly, it follows that aliphatic solvent systems should promote faster extraction kinetics. However, as solubility is a problem at high copper loadings, a mixture of aliphatic and aromatic solvents is preferentially employed to give the copper complex the sufficient solubility required for efficient extraction. If dimer formation does favour the *thermodynamics* of solvent extraction, as has been assumed, then these results show that the use of an aliphatic diluent will maximise the potential of the solvent extraction plant.

2.4 Experimental

2.4.1 Instrumentation

Melting points were determined with a Gallenkamp apparatus and are uncorrected. Elemental analysis was performed on a Perkin Elmer 2400 elemental analyser. IR spectra were obtained on a Perkin Elmer Paragon 1000 FT-IR spectrometer as potassium bromide discs or as liquid thin films. ¹H and ¹³C NMR spectra were run on Bruker WP200 and AC250 spectrometers. NOE experiments were run on a Bruker WH360 spectrometer. Chemical shifts (δ) are reported in parts per million (ppm) relative to residual solvent protons as internal standards. Electron impact (EI) mass spectra were obtained either on a Finnigan MAT4600 quadrupole spectrometer or on a Kratos MS50TC spectrometer. Electrospray (ES) mass spectra were obtained on a Thermoquest LCQ spectrometer.

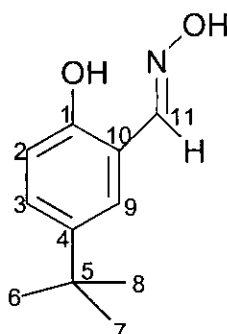
2.4.2 Solvent and Reagent Pretreatment

All reagents were commercially available (Aldrich, Acros), with the exception of 2-hydroxy-5-*tert*-butylbenzaldehyde oxime and 2-methoxybenzaldehyde

oxime, which were prepared following literature methods^{48,49} as described below. Solvents used for analytical purposes (NMR, IR, MS) were of spectroscopic grade. Deuterated solvents for use in ¹H NMR and NOE experiments were degased (N₂), dried over 4 Å sieves and stored under nitrogen. All other reagents and solvents were used as received.

2.4.3 Synthesis

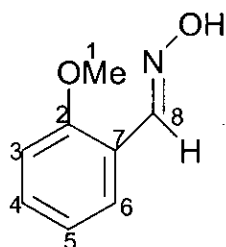
2-Hydroxy-5-*tert*-butylbenzaldehyde oxime⁴⁸



7.4 wt % magnesium methoxide (in methanol) solution (442 ml, 0.31 mol) was mixed with toluene (63 ml). 4-*tert*-butyl phenol (75.12 g, 0.50 mol) was added to the mixture, which was then heated under reflux for 1 h. The brown solution was diluted with toluene (300 ml) and the methanol / toluene azeotrope subsequently removed by fractional distillation until the temperature at the still head rose to 95 °C. Toluene (63 ml) was added to mobilise the resulting pale brown suspension, to which was added a slurry of paraformaldehyde (46.92 g, 1.56 mol) in toluene (100 ml) over 1 h with the continuous removal of volatiles from the reaction medium *via* distillation. Stirring was continued at 95 °C for a further 30 min, after which time the reaction mixture was cooled to 55 °C and treated with a solution of hydroxylamine sulphate (49.24 g, 0.30 mol) in water (150 ml). This solution was added over a period of 30 min with vigorous stirring. Stirring at 55 °C was continued for 1 h, the reaction medium subsequently cooled to room temperature and the purple organic layer separated and washed with 7 %

sulphuric acid (240 ml) and water (2 x 185 ml). The solvent was removed from the resulting pale yellow organic phase using a rotary evaporator to leave a very pale yellow crystalline solid (65.19 g). The oily brown residue from the filtrate was taken up in hexane (50 ml) to yield more product (5.8316 g). Total yield 71.0216 g, 73.49 %. m.p. 115 - 117 °C (Found C, 68.77; H, 7.83; N, 7.15; C₁₁H₁₅NO₂ requires C, 68.36; H, 7.84; N, 7.15 %); IR (cm⁻¹, KBr Disc) : ν 3358.4s & 2971.1s (OH), 2868.8w (CH), 1589.3w (C=N), 1497.5s (C=C), 100.38s (C-O), 715.9 (Ar CH); ¹H NMR (CDCl₃, 200 MHz) : δ 1.29 (s, 9H, H-6,7,8), 6.61 - 6.94 (d, J_{ortho} 8.61 Hz, 1H, H-2), 7.15 - 7.16 (d, J_{meta} 2.48 Hz, 1H, H-9), 7.30 - 7.34 (dd, J_{ortho} 8.63 Hz, J_{meta} 2.49 Hz, 1H, H-3), 7.81 (br s, 1H, NOH), 8.23 (s, 1H, H-11), 9.80 (s, 1H, OH); ¹³C NMR CDCl₃, 63 MHz) : δ 31.25 (C-6,7,8), 33.86 (C-5), 115.58 (C-4), 116.07 (C-2), 127.18 (C-9), 128.40 (C-3), 142.53 (C-10), 153.15 (C-11), 154.45 (C-1); EIMS *m/z* 193 (58.8 %, LH), 178 (100.0 %, LH - CH₃), 160 (31.5 %, LH - NOH), 132 (30.3 %, LH - OH - CHNOH), 77 (11.5 %, Ph).

2-Methoxy benzaldehyde oxime⁴⁹



Hydroxylamine hydrochloride (1.362 g, 0.01 mol) and potassium hydroxide (0.730 g, 0.011 mol) were dissolved up in hot ethanol (20 ml and 20 ml respectively). The alkaline solution was added to the hydroxylamine solution to liberate free hydroxylamine with the precipitation of potassium chloride. The reaction was maximised by standing in an ice bath for 10 min. The resulting colourless suspension was filtered into a yellow solution of 2-methoxybenzaldehyde (1.362 g, 0.01 mol) in ethanol (50 ml) and the reaction medium was then heated under reflux for 3 hour. Some solvent was removed using a rotary evaporator to leave a brown viscous solution, which

precipitated a cream coloured powder on standing (0.908 g). The crude product was recrystallised from hot ethanol (20 ml) to yield feathery pale yellow microcrystals (0.503 g, 33.27 %). m.p. 97 °C (Found, C, 63.60; H, 6.10; N, 9.07; C₈H₉NO₂ requires C, 63.55; H, 6.01; N, 9.27 %); IR (cm⁻¹, KBr Disc) : ν 3161.8m (OH), 1629.7w (C=N), 1600.1s & 1578.4w & 1495.6s (Ar C=C), 1026.8s (C-O), 752.9s (Ar CH); ¹H NMR (CDCl₃, 200 MHz) : δ 3.86 (s, 3H, H-1), 6.89 - 7.00 (m, 2H, H-3,5), 7.31 - 7.39 (t(dqd), J_{ortho} 7.85 Hz, J_{meta} 1.76 Hz, 1H, H-4), 7.61 - 7.65 (dd, J_{ortho} 7.64 Hz, J_{meta} 1.77 Hz, 1H, H-6), 8.47 (s, 1H, H-8), 9.70 (br s, 1H, OH); ¹³C NMR (CDCl₃, 63 MHz) : δ 55.33 (C-1), 110.98 (C-5), 120.34 (C-7), 120.58 (C-4), 127.52 (C-3), 131.01 (C-6), 157.45 (C-2); EIMS *m/z* 151 (47.5 %, LH), 134 (41.9 %, LH - OH), 120 (54.5 %, LH - NOH), 107 (35.7 %, LH - CHNOH).

2.4.4 Molecular Weight Determination : Cryoscopic Method

Molecular weight determinations for 2-hydroxybenzaldehyde oxime in benzene were carried out as described in the literature^{32,50}. The results are presented in table 6.

Sample	Mass / g	Solution Concentration / M	Reading / °	Average Reading / ± 0.004 °	$\Delta T / \pm 0.008$ °
Benzene	28.37	-	1.110 1.112 1.112	1.111	-
Salox	0.4878	0.12	1.726 1.725 1.730	1.727	0.616
Salox	1.0024	0.24	2.285 2.290	2.288	1.177

Table 6 : Cryoscopic data for 2-hydroxybenzaldehyde oxime in benzene

Note: The readings refer to those taken from the Beckmann thermometer (arbitrary scale); The errors are estimated, not calculated

The actual molecular weight (M_r) of the species in solution was then calculated using equation 3.

$$M_r = \frac{5300 \times w_s}{w_B \times \Delta T} \quad (3)$$

where w_s is the mass of the solute and w_B is the mass of the benzene. M_r was found to be 148 ± 2 and 159 ± 2 for the 0.012 and 0.24 M solutions respectively. The degree of association, n , was subsequently calculated using equation 4, and was found to be 1.08 ± 0.02 and 1.16 ± 0.02 respectively.

$$\text{Degree of Association} = \text{Actual } M_r \div \text{Theoretical } M_r \quad (4)$$

2.4.5 Electrospray Mass Spectrometry : Experimental Conditions

The concentrations of the sample solutions were 1×10^{-6} M. The sample run conditions are presented in tables 7 - 14.

Table 7 : 2-Hydroxybenzaldehyde oxime; Low mass range; Spectrum tuned on 136.1

Flow Rate / μmin^{-1}	Sheath Gas, arb.	Aux. Gas, arb.	Spray Voltage / kV	Capillary Temp./ $^{\circ}\text{C}$	Capillary Volt. / V
10	80	18	4	100	-47
Tube Lens off / V	Octapole 1 / V	Lens Voltage / V	Octapole 2 / V	Octapole RF / A	Spray Current / μA
0	3	18	5	120	0.10

Table 8 : 2-Hydroxybenzaldehyde oxime; High mass range; Spectrum tuned on 272.9

Flow Rate / μmin^{-1}	Sheath Gas, arb.	Aux. Gas, arb.	Spray Voltage / kV	Capillary Temp./ $^{\circ}\text{C}$	Capillary Volt. / V
10	80	18	4	100	-4
Tube Lens off / V	Octapole 1 / V	Lens Voltage / V	Octapole 2 / V	Octapole RF / A	Spray Current / μA
20	2.75	14.0	6.50 / 3.50	400	0.10

Table 9 : 2-Hydroxy-5-*tert*-butylbenzaldehyde oxime; Spectrum tuned on 385.0

Flow Rate / μmin^{-1}	Sheath Gas, arb.	Aux. Gas, arb.	Spray Voltage / kV	Capillary Temp./ $^{\circ}\text{C}$	Capillary Volt. / V
10	80	18	4	100	-4
Tube Lens off / V	Octapole 1 / V	Lens Voltage / V	Octapole 2 / V	Octapole RF / A	Spray Current / μA
20	3	18	6	400	0.19

Table 10 : P50; Spectrum tuned on 525.0

Flow Rate / μlmin^{-1}	Sheath Gas, arb.	Aux. Gas, arb.	Spray Voltage / kV	Capillary Temp./ $^{\circ}\text{C}$	Capillary Volt. / V
10	80	18	4	100	-4
Tube Lens off / V	Octapole 1 / V	Lens Voltage / V	Octapole 2 / V	Octapole RF / A	Spray Current / μA
10	4	16	6	400	0.19

Table 11 : P50 / *t*-Bu Mixture; Spectrum tuned on 262.1

Flow Rate / μlmin^{-1}	Sheath Gas, arb.	Aux. Gas, arb.	Spray Voltage / kV	Capillary Temp./ $^{\circ}\text{C}$	Capillary Volt. / V
10	30	9	4	100	-3.2
Tube Lens off / V	Octapole 1 / V	Lens Voltage / V	Octapole 2 / V	Octapole RF / A	Spray Current / μA
20	5	35	11	400	0.05

Table 12 : 2-Methoxybenzaldehyde oxime; Low mass range; Spectrum tuned on 152.1

Flow Rate / μlmin^{-1}	Sheath Gas, arb.	Aux. Gas, arb.	Spray Voltage / kV	Capillary Temp./ $^{\circ}\text{C}$	Capillary Volt. / V
10	50	0	5.5	150	3
Tube Lens off / V	Octapole 1 / V	Lens Voltage / V	Octapole 2 / V	Octapole RF / A	Spray Current / μA
50	-3.25	-16	-5.5	-	0.19

Table 13 : Nonylphenol / *t*-Bu Mixture; Spectrum tuned on 194.1

Flow Rate / μlmin^{-1}	Sheath Gas, arb.	Aux. Gas, arb.	Spray Voltage / kV	Capillary Temp./ $^{\circ}\text{C}$	Capillary Volt. / V
10	70	5	5	150	21
Tube Lens off / V	Octapole 1 / V	Lens Voltage / V	Octapole 2 / V	Octapole RF / A	Spray Current / μA
35	-3.5	-42	-7.5	400	0.34

2.5 References for Chapter 2

- 1 L.F. Lindoy, *The Chemistry of Macrocyclic Ligand Complexes*, Cambridge University Press, Cambridge, 1989
- 2 A. Anichini, L. Fabbrizzi, P. Paoletti and R.M. Clay, *J. Chem. Soc. Dalton Trans.*, 1978, 577-583
- 3 *Critical Stability Constants*, Vol. 2, Eds. R.M. Smith and A.E. Martell, Plenum Press, New York, 1976
- 4 G.F. Smith and D.W. Margerum, *J. Chem. Soc. Chem. Comm.*, 1975, 807-808
- 5 R. Price and J.A. Tumilty, *Hydrometallurgy - Institute of Chemical Engineers Symposium Series*, 1975, **42**, 18.1-18.8
- 6 D.A. Fletcher, R.F. McMeeking and D.J. Parkin, *J. Chem. Inf. Comput. Sci.*, 1996, **36**, 746-749. Version 5.18 of the CCDC
- 7 A. Koziol and Z. Kosturkiewicz, *Pol. J. Chem.*, 1979, **53**, 1393-1395
- 8 C.E. Pfluger and R.L. Harlow, *Acta Cryst.*, 1973, **B29**, 2608-2609
- 9 S.H. Simonsen, C.E. Pfluger and C.M. Thompson, *Acta Cryst.*, 1964, **14**, 269-272
- 10 J.M. Thorpe, PhD Thesis, University of Manchester, 1992
- 11 J.K Maurin, *Acta Cryst.*, 1994, **C50**, 1357-1359
- 12 C.E. Pfluger, M.T. Pfluger and E.B. Brackett, *Acta Cryst.*, 1978, **B34**, 1017-1019
- 13 A. Koziol and Z. Kosturkiewicz, *Pol. J. Chem.*, 1984, **58**, 569-575
- 14 C.B. Aakeröy, *Acta Cryst.*, 1997, **B53**, 569-586
- 15 K. Vyas, V. Mohan Rao and H. Manohar, *Acta Cryst.*, 1987, **C43**, 1201-1204
- 16 D.J. White and P.A. Tasker (in press : *Coord. Chem. Rev.*)
- 17 B.N. Laskorin, V.V. Yaksin, V.S. Ul'yanov and A.M. Mirokin, *Proceedings of the International Solvent Extraction Conference*, 1974, **2**, 1775-1790
- 18 D. Stepniak-Biniakiewicz, *Pol. J. Chem.*, 1987, **61**, 433-441

- 19 R.F. Dalton, F. Hauxwell and J.A. Tumilty, *Chemistry and Industry*, 1976, 181-184
- 20 J.W. Hosking and N.M. Rice, *Hydrometallurgy*, 1978, **3**, 217-231
- 21 D.H. Williams and I. Fleming, *Spectroscopic Methods in Organic Chemistry*, McGraw-Hill, Maidenhead (U.K), 5th Edition, 1995, pp. 41
- 22 J. Szymanowski, *Hydroxyoximes and Copper Hydrometallurgy*, CRC Press, London, 1993, pp. 136-137
- 23 G. Geiseler and J. Fruwert, *Zeitschrift für Physikalische Chemie Neue Folge*, 1960, **26**, 111-113
- 24 J. Szymanowski, K. Prochaska and K. Alejski, *Hydrometallurgy*, 1990, **25**, 329-348
- 25 R. Barhoum, K. Prochaska and J. Szymanowski, *Journal of Colloid and Interface Science*, 1998, **204**, 394-397
- 26 M.B. Bogacki, *Solvent Extraction and Ion Exchange*, 1997, **15**(5), 731-755
- 27 A. Dunger, H.H. Limbach and K. Weisz, *Chemistry : A European Journal*, 1998, **4** (4), 621-628
- 28 D.B. Davies, L.N. Dymant and A.N. Veselkov, *J. Chem. Soc. Faraday Trans.*, 1996, **92** (3), 383-390
- 29 A.N. Veselkov, L.N. Dymant, S.F. Baranovskii, P.A. Bolotin, O.S. Zav'yalova, D.A. Veselkov, H. Parkes and D. Davies, *Journal of Structural Chemistry*, 1995, **36** (1), 69-75
- 30 P.S. Corbin and S.C. Zimmerman, *J. Am. Chem. Soc.*, 1998, **120**, 9710-9711
- 31 I. Komasaawa, T. Otake and A. Yamada, *Journal of Chemical Engineering of Japan*, 1980, **13** (2), 130-136
- 32 M.G. Davidson, R. Snaith, D. Stalke and D.S. Wright, *J. Org. Chem.*, 1993, **58**, 2810-2816
- 33 M. Cox, C.G. Hirons and D.S. Flett, *ISEC-Liege 1*, 1980, Paper 80-118
- 34 J.S. Preston and Z.B. Luklinska, *J. Inorg. Nucl. Chem.*, 1980, **42**, 431-439

- 35 D. Stepniak-Biniakiewicz and J. Syzmanowski, *Hydrometallurgy*, 1981, **7**, 299-313
- 36 K.C. Russell, E. Leize, A. Van Dorsselaer and J.M. Lehn, *Angewandte Chemie (International Edition)*, 1995, **34** (2), 209-213
- 37 C.A. Schalley, R.K. Castellano, M.S. Brody, D.M. Rudkevich, G. Siuzdak and J. Rebek Jr., *J. Am. Chem. Soc.*, 1999, **121**, 4568-4579
- 38 E. Ishow, A. Gourdon and J.P. Launay, *J. Chem. Soc. Chem. Comm.*, 1998, 1909-1910
- 39 J.B. Fenn, M. Mann, C.K. Meng, S.F. Wong and C.M. Whitehouse, *Mass Spectrometry Reviews*, 1990, **9**, 37-70
- 40 M. J. S. Dewar, E. G. Zoebisch, E. F. Healy and J. J. P. Stewart, *J. Am. Chem. Soc.*, 1985, **107**(13), 3902-3909
- 41 AMSOL5.4, QCPE program 606. Quantum Chemistry Program Exchange (QCPE), Creative Arts Building 181, Indiana University, Bloomington, Indiana 47405
- 42 SM2.1, D. A. Liotard, G. D. Hawkins, G. C. Lynch, C. J. Cramer and D. G. Truhlar, *J. Comput. Chem.*, 1995, **16**(4), 422-440
- 43 SM4, D. J. Giesen, C. J. Cramer, and D. G. Truhlar, *J. Phys. Chem.*, 1995, **99**(18), 7137-7146
- 44 A. Simperler and W. Mikenda, *Monatshefte für Chemie*, 1997, **128**, 969-980
- 45 H. Lampert, W. Mikenda and A. Karpfen, *J. Phys. Chem.*, 1996, **100**, 7418-7425
- 46 R.J. Whewell and M.A. Hughes, *Hydrometallurgy*, 1979, **4**, 125-140
- 47 J.H. Russell and R.L. Rickel, *Solvent Extraction and Ion Exchange*, 1990, **8**(6), 855-873
- 48 R. Aldred, R. Johnston, D. Levin and J. Neilan, *J. Chem. Soc. Perkin Trans. 1*, 1994, 1823-1831
- 49 J. March, *Advanced Organic Chemistry*, Wiley, New York, 3rd Edition, 1985, pp. 805-806
- 50 Shoemaker, Garland and Nibler, *Experiments in Physical Chemistry*, McGraw-Hill, London, 5th Edition, 1989, pp 185-205

Chapter 3 : Acyl Pyrazolones and Pyrazolone Oximes

Contents	Page
3.1 Introduction	80
3.1.1 Acyl Pyrazolones	80
3.1.1.2 Tautomerism of Acyl Pyrazolones	82
3.1.2 Pyrazolone Oximes	83
3.1.2.1 Tautomerism of Pyrazolone Oximes	84
3.2 Synthesis of Acyl Pyrazolones, Pyrazolone Oximes and their Metal Complexes	85
3.2.1 Acyl Pyrazolones	85
3.2.1.1 Free Ligands	86
3.2.1.2 Metal Complexes	87
3.2.2 Pyrazolone Oximes	88
3.2.2.1 Free Ligands	89
3.2.2.2 Metal Complexes	91
3.3 Characterisation of Acyl Pyrazolones, Pyrazolone Oximes and their Metal Complexes	92
3.3.1 IR Spectroscopy	92
3.3.1.1 Acyl Pyrazolones	92
3.3.1.2 Pyrazolone Oximes	93
3.3.2 NMR Spectroscopy	94
3.3.2.1 Acyl Pyrazolones	94
3.3.2.2 Pyrazolone Oximes	94
3.3.3 Mass Spectrometry	95
3.3.3.1 Acyl Pyrazolones	95
3.3.3.2 Pyrazolone Oximes	95
3.4 Solvent Extraction from Sulphate Media	96
3.4.1 Load and Strip Characteristics	99
3.4.2 Selectivity for Copper(II) over Iron(III)	100
3.5 X-ray Crystallography	102
3.5.1 Acyl Pyrazolones	102
3.5.1.1 Free Ligands	102

3.5.1.1.1	Tautomerism	102
3.5.1.1.2	Hydrogen Bonding	106
3.5.1.2	Metal Complexes	107
3.5.1.2.1	Mesomerism	109
3.5.1.2.2	Metal to Donor Atom Bond Lengths	111
3.5.1.2.3	Bite Angles and Dihedral Angles between Coordination Planes	115
3.5.1.2.4	Bite Distances	118
3.5.1.2.5	Dihedral Angles in the Coordinated Ligands	121
3.5.2	Pyrazolone Oximes	123
3.5.2.1	Free Ligands	123
3.5.2.2	Metal Complexes	126
3.5.2.2.1	Mesomerism	127
3.5.2.2.2	Hydrogen Bonding	128
3.5.2.2.3	Metal to Donor Atom Bond Lengths	132
3.5.2.2.4	Bite Angles and Bite Distances	134
3.5.2.2.5	Dihedral Angles	136
3.5.2.2.6	Differences between the structures of metal complexes of P50-type oxime and pyrazolone oxime ligands	137
3.6	Conclusions	138
3.7	Experimental	140
3.7.1	Instrumentation	140
3.7.2	Solvent Reagent and Pretreatment	140
3.7.3	Synthesis of Starting Pyrazolones	141
3.7.4	Acylpyrazolones	141
3.7.4.1	Synthesis of Ligands	141
3.7.4.2	Synthesis of Metal Complexes	148
3.7.5	Pyrazolone Oximes	149
3.7.5.1	Synthesis of Ligands	149
3.7.5.2	Synthesis of Metal Complexes	154
3.7.6	Solvent Extraction Experiments from Sulphate Media	157
3.7.6.1	Using Acylpyrazolones	159

3.7.6.2 Using Pyrazolone Oximes	160
3.7.7 X-ray Crystallography	161
3.8 References for Chapter 3	164

3.1 Introduction

3.1.1 Acyl Pyrazolones

The chemistry of acyl pyrazolones (Figure 1) and their metal complexes has been the subject of considerable study¹. The diverse applications of related β -diketones and their metal complexes, for example as NMR shift reagents², in laser technology³ and in the field of metal separation, have attracted extensive research. However, of these potential applications, only the metal separation capabilities of acyl pyrazolones have been extensively investigated⁴. Additionally, the fungicidal activity of metal complexes of acyl pyrazolones has been trialled⁵, further illustrating the potential and versatility of this class of compound.

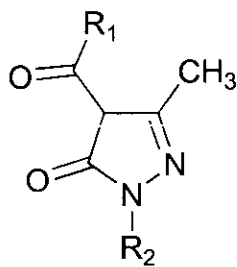


Figure 1 : Acyl pyrazolones; $R_1 = \text{H, alkyl, aryl}$; $R_2 = \text{alkyl, aryl}$

Solvent extraction from acidic media using acyl pyrazolones has been applied to an extremely diverse range of metal ions. Data on the extraction of transition metal ions such as iron(II), iron(III), cobalt(II), nickel(II), copper(II), zinc(II) and cadmium(II) using conventional acyl pyrazolones⁶⁻¹¹ (Figure 1) as well as that of copper(II) using bridged acyl pyrazolones^{12,13} (Figure 2) are extensive. Additionally the synergistic extraction of copper(II)⁸ and alkaline earth metals¹⁴, such as magnesium(II), calcium(II), barium(II) and strontium(II), using acyl pyrazolones in conjunction with phosphine oxides has been investigated.

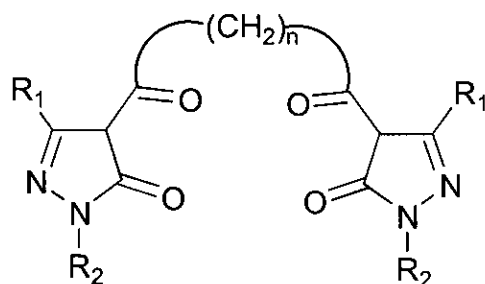


Figure 2 : Bridged acyl pyrazolone ligands

Acyl pyrazolones have, however, been considered too weak for use as copper extractants and so more recently the greatest impetus in this field has been put into the development of the extraction of lanthanides and actinides. The extraction of lanthanides has been achieved using either acyl pyrazolones alone^{11,15} or synergistically in conjunction with, for example, crown ethers¹⁶. Additionally, the synergistic extraction of plutonium(VI), as the plutonyl ion (PuO_2)⁺, using acyl pyrazolones and substituted trialkyl phosphates may have real implications to the nuclear industry¹⁷.

The versatility of acyl pyrazolones as chelators for a wide range of metal ions is further illustrated by the ca. 50 structures of metal complexes of these ligands in the Cambridge Crystallographic Database (CCDC)¹⁸. This group of structures represents the chelation of some 18 different metal ions as illustrated in figure 3. The X-ray crystallography of acyl pyrazolones will be further discussed in section 3.5.1.

H																		He
Li	Be											B	C	N	O	F		Ne
Na	Mg											Al	Si	P	S	Cl		Ar
K	Ca	Sc	Ti	V	Cr	Mn	Fe	Co	Ni	Cu	Zn	Ga	Ge	As	Se	Br		Kr
Rb	Sr	Y	Zr	Nb	Mo	Tc	Ru	Rh	Pd	Ag	Cd	In	Sn	Sb	Te	I		Xe
Cs	La	La	Hf	Ta	W	Re	Os	Ir	Pt	Au	Hg	Tl	Pb	Bi	Po	At		Rn
Fr	Ra	Ac																
			Ce	Pr	Nd	Pm	Sm	Eu	Gd	Tb	Dy	Ho	Er	Tm	Yb	Lu		
			Th	Pa	U	Np	Pu	Am	Cm	Bk	Cf	Es	Fm	Md	No	Lr		

Figure 3 : Periodic table showing metals for which crystal structures of complexes with acyl pyrazolone ligands are known

3.1.1.2 Tautomerism of Acyl Pyrazolones

There are four possible tautomers of acyl pyrazolones, which are shown in figure 4.

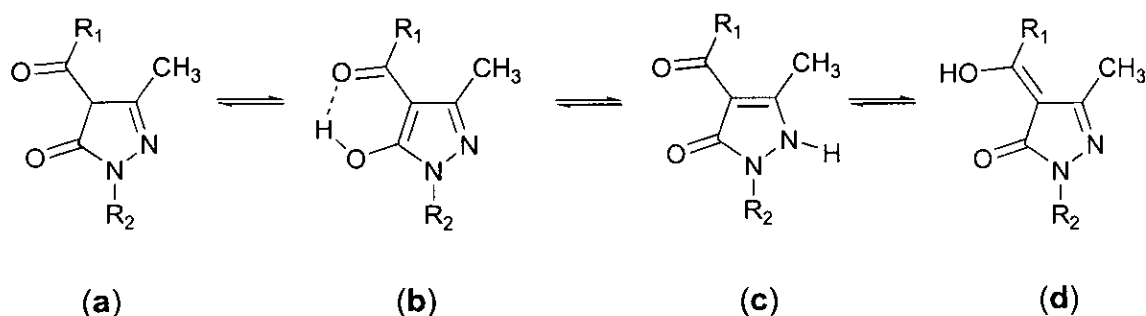


Figure 4 : Tautomers of acyl pyrazolones; NB: There are two possible structural conformers for tautomer **d**.

Of these four tautomers, examples of X-ray structures of only **(a)**¹⁹, **(b)**^{20,21} and **(c)**^{21,22} are known. Tautomer **(b)** is stabilised by intramolecular hydrogen bonding between the OH and carbonyl group, while **(c)** is stabilised by weaker intermolecular hydrogen bonding between the NH and carbonyl group at the 5 position of the pyrazolone ring of adjacent molecules. It is therefore expected that tautomer **(b)** will be more stable in solution and this is supported by IR and NMR solution studies in chloroform²³, which have shown that 3-methyl-4-benzoyl-1-phenyl-5-pyrazolone ($R_1 = R_2 = \text{phenyl}$) exists principally as tautomer **(b)** with a minor contribution from **(c)**²². Additionally, it has been proposed that different tautomers can be identified from their colour in the solid state²⁴. However both solid and solution IR and Raman spectroscopic data show this methodology is unreliable²⁰, with variations in colour more likely to be due to the presence of impurities in the products. IR and NMR data for acyl pyrazolones will be further discussed in sections 3.3.1.1 and 3.3.2.1.

Solid state IR and X-ray crystallography has shown that chelation to a metal ion occurs through the two oxygen atoms and that the ligand adopts the expected enolic **(b)** tautomeric form on complexation. The tautomeric form of the free ligand is not thought to effect the ease of metal ion complexation,

however, as the electron rearrangement required after initial deprotonation of the ligand is a low energy process.

3.1.2 Pyrazolone Oximes

Pyrazolones with an oxime group attached directly to the heterocyclic ring (Figure 5 : a) were synthesised by Knorr in the late nineteenth century²⁵.

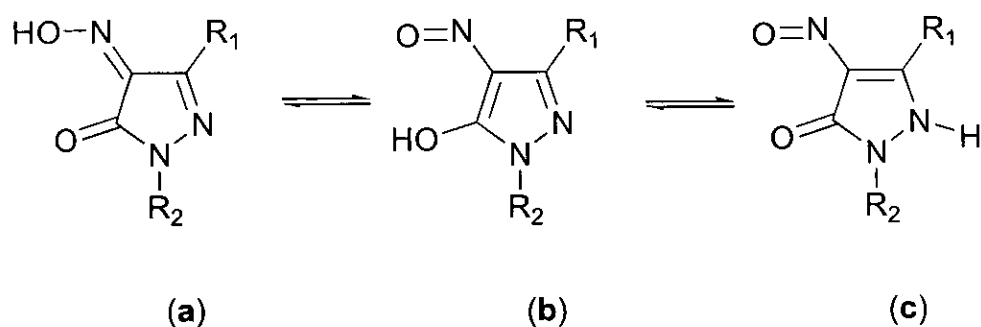


Figure 5 : Tautomeric forms of 1,3-disubstituted-4-oximino-5-pyrazolones
 ... R₁ = alkyl, R₂ = alkyl, aryl ...

The coordination chemistry of these ligands with a range of metal ions, in particular alkaline earth metal such as calcium(II) and magnesium(II), and their use as analytical reagents for both qualitative and quantitative determination of these metals have been well studied²⁶⁻²⁸. Formation constants for the copper(II) complexes of this type of oxime have been determined at *ca.* 5-10, and this low range may reflect the fact that on complexation *via* the oxime nitrogen and the oxygen at the 5-position of the ring, a strained 5-membered chelate ring is formed. Another limitation of these ligands is that deprotonation of the ligand must occur in order to form neutral complexes and, because of the monoprotic nature of the chelating site, there can be no opportunity for inter-ligand hydrogen bonds to form in the metal complexes as in those of P50-type oximes, which is thought to significantly enhance the stability of such complexes (Section 1.5).

A more stable 6-membered chelate ring and the retention of the oxime OH group on metal ion complexation can be achieved by the use of oxime derivatives of 4-acyl-5-pyrazolones shown in figure 6.

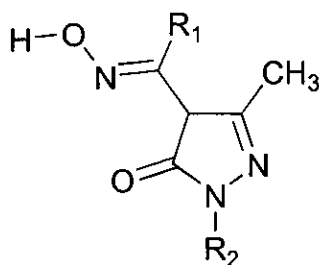


Figure 6 : 4-Acyl-3-methyl-1- R_2 -5-pyrazolone oximes
 R_1 = alkyl, aryl (Ketoximes), H (Aldoximes); R_2 = alkyl, aryl

The synthesis of these ligands was first reported in 1959²⁹, since when only a handful of papers reporting their coordination chemistry have been published³⁰⁻³³. Interestingly, the potential use of pyrazolone oximes as metal extractants was alluded to in 1986³² but no subsequent work has been reported. IR data for pyrazolone oxime complexes have indicated that the oxime OH is indeed retained on coordination to a metal ion, which means that intramolecular hydrogen bonding could occur, and that coordination occurs *via* the nitrogen and oxygen atoms as shown in figure 7. Additionally, all complexes reported are octahedral and of the general formula $ML_2(H_2O)_2$, in which the two water molecules occupy axial coordination sites, apart from those of iron(III) and chromium(III), which have the general formula ML_3 .

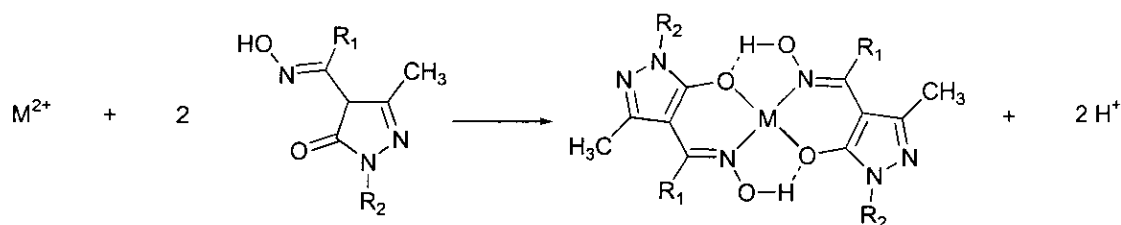


Figure 7 : Complexation of a metal(II) ion by pyrazolone oximes showing the proposed intramolecular hydrogen bonding involving the oxime OH group

3.1.2.1 Tautomerism of Pyrazolone Oximes

Like acyl pyrazolones, pyrazolone oximes can also form a number of tautomers, which are presented in figure 8.

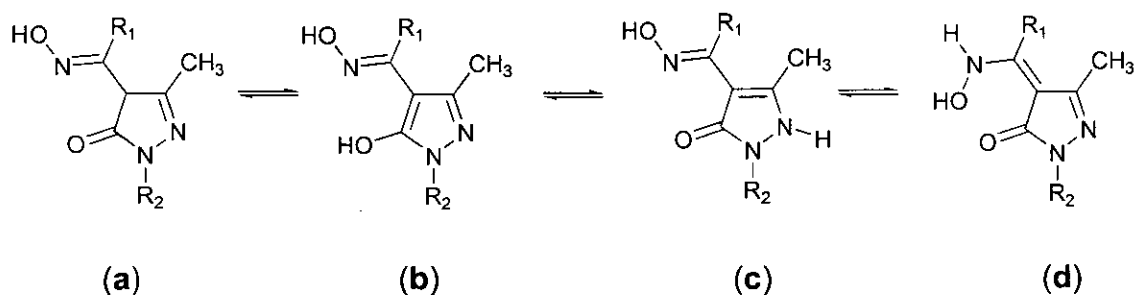


Figure 8 : Tautomeric forms of pyrazolone oximes. NB: there are two structural conformers for tautomer **d**.

Structural data in the literature for the free ligands is sparse, with solid state IR spectra generally being assigned to either tautomer **(a)** or **(b)**. From IR data for metal complexes, it is concluded that tautomer **(b)** is the form adopted by the ligand on complexation following deprotonation of the OH at the 5-position of the ring. IR and NMR data for pyrazolone oximes will be fully discussed in sections 3.3.1.2 and 3.3.2.2. There are no known X-ray structures of either free ligands or metal complexes of pyrazolone oximes or related ligands¹⁸. X-ray crystallography of pyrazolone oximes will be discussed in section 3.5.2.

3.2 Synthesis of Acyl Pyrazolones, Pyrazolone Oximes and their Metal Complexes

3.2.1 Acyl Pyrazolones

The acyl pyrazolone ligands (Figure 9) and metal complexes prepared in this project are summarised in table 1.

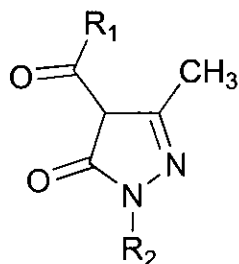


Figure 9 : Acyl pyrazolones; $R_1 = \text{H, alkyl, aryl}$; $R_2 = \text{alkyl, aryl}$

Ligands	R ₁	R ₂	Metal Complexes	
1	Ph	Ph	7	[Cu(1-H) ₂] ^a
2	Me	Ph	8	[Zn(1-H) ₂] ^b
3	H	Ph	9	Co(1-H) ₂ .H ₂ O.MeOH ^a
4	Ph	t-Bu	10	Ni(1-H) ₂ .H ₂ O.MeOH ^a
5	4-n-octylphenyl	Ph	11	[Cu(4-H) ₂ (MeOH) ₂] ^b
6	4-n-heptylphenyl	Ph		

Table 1 : Acyl pyrazolone ligands and metal complexes

^a Formula consistent with C/H/N analytical data

^b Formula confirmed by X-ray crystallography

3.2.1.1 Free Ligands

Acyl pyrazolones **1**, **5** and **6** were synthesised in good yield *via* the Claisen-type condensation reaction involving one equivalent of the appropriate acyl chloride with one equivalent of the appropriate starting pyrazolone according to the method of Jensen³⁴. The reaction scheme is shown in figure 10.

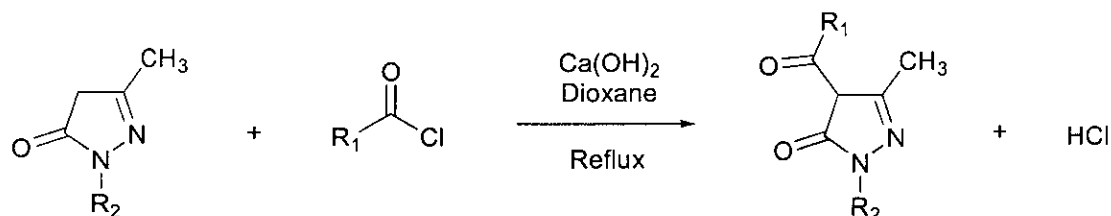


Figure 10 : Synthesis of acyl pyrazolones **1**, **5** and **6**

Attempts to prepare ligand **4** using this method resulted in an impure product, which was subsequently purified *via* the formation of the solid copper complex **11**, recrystallising and stripping of this complex using 7 M sulphuric acid to yield the free ligand in acceptable yield.

The attempted synthesis of ligand **2** using the method of Jensen was unsuccessful and so a similar literature method^{35,36} using sodium carbonate and tetrahydrofuran was employed. This reaction resulted in a poor yield

(ca. 20 %), which was not improved on repetition. Ligand **3** was prepared in good yield *via* a classical Vilsmeier-Haack type formylation reaction of the starting pyrazolone using phosphoryl chloride and dimethylformamide³⁷. The reaction scheme is shown in figure 11.

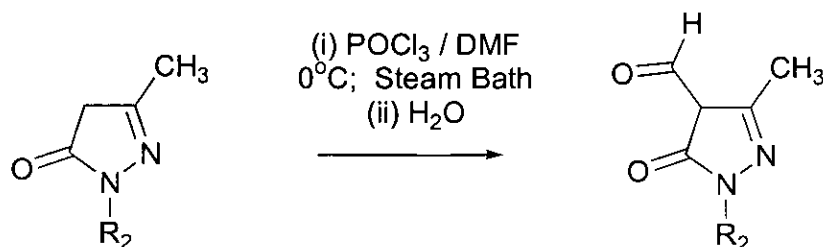


Figure 11 : Synthesis of 4-formyl-5-pyrazolones

It should be noted that the ligand was not purified due to previous difficulties encountered with the formation of a dimeric, intermolecular condensation product on recrystallisation, as shown in figure 12³⁷.

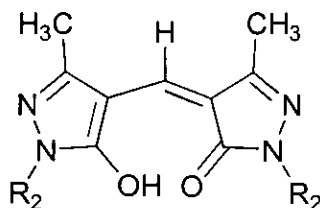


Figure 12 : Intermolecular condensation product of 4-formyl-5-pyrazolones

3.2.1.2 Metal Complexes

Metal complexes of acyl pyrazolone ligands were synthesised by the standard method of reaction of two equivalents of the appropriate ligand with one equivalent of the appropriate divalent metal acetate³⁸. The acetate in the reaction medium removes the protons liberated by the ligand to form acetic acid. The reaction scheme is shown in figure 13.

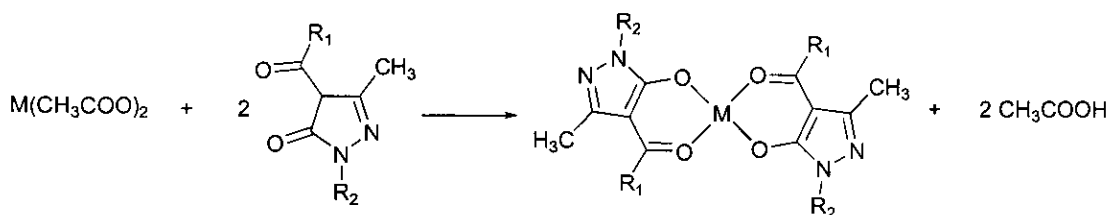


Figure 13 : Synthesis of metal complexes of acyl pyrazolones

The copper(II) complex **11** was isolated during the purification of the free ligand **4** as already discussed (Section 3.2.1.1).

3.2.2 Pyrazolone Oximes

The free pyrazolone oxime ligands (Figure 14) and metal complexes prepared are summarised in table 2.

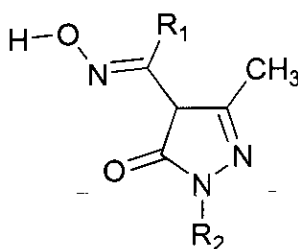


Figure 14 : Pyrazolone oximes; R₁ = alkyl, aryl, H; R₂ = alkyl, aryl

Ligands	R ₁	R ₂	Metal Complexes	
12	Ph	Ph	17	[Cu(12 -H) ₂ (DMF) ₂] ^b
13	Me	Ph	18	[Zn(12 -H) ₂ (DMF) ₂] ^b
14	H	Ph	19	[Ni(12 -H) ₂ (DMF) ₂] ^b
15	4-n-octylphenyl	Ph	20	[Co(12) ₂ (MeOH) ₂](NO ₃) ₂ ^b
16	4-n-heptylphenyl	Ph	21	Cu(13 -H) ₂ ^a
			22	Cu(14 -H) ₂ ^a
			23	Zn(14 -H) ₂ · ³ / ₄ H ₂ O ^a
			24	Co(14 -H) ₂ ·2½H ₂ O ^a
			25	Ni(14 -H) ₂ ·2½H ₂ O ^a
			26	Cu(15 -H) ₂

Table 2 : Pyrazolone oxime ligands and metal complexes

^a Formula consistent with C/H/N analytical data

^b Formula confirmed by X-ray crystallography

3.2.2.1 Free Ligands

The pyrazolone oxime ligands **12-14** were prepared in good yield by the conventional method of reaction of the appropriate acyl pyrazolone with hydroxylamine hydrochloride in alcohol³⁹. The reaction scheme is shown in figure 15.

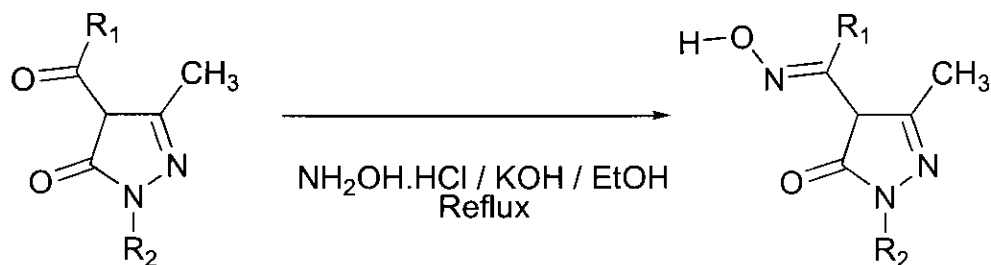


Figure 15 : Synthesis of pyrazolone oximes **12-14**

The solubility of ligand **12** was very low and could not be determined by ¹H NMR techniques (<< 0.1 M), rendering the ligand unsuitable for use in solvent extraction experiments. In an attempt to synthesise more soluble ligands, the oximation of acyl pyrazolones such as **4** (R₁ = Ph, R₂ = *t*-Bu) was undertaken, as it was thought that the R₂ alkyl substituent would reduce the planarity of the ligand thus increasing its solubility in hydrocarbon solvents. Oximation of 4-benzoyl-1-*t*-butyl-3-methyl-pyrazolone *via* the conventional method³⁹ was unsuccessful. So too were subsequent attempts, in which the ratio of reagents, the reaction temperature or time were varied. The attempted isolation of an oxime product from impure (NMR) reaction mixtures *via* complexation and subsequent acid stripping resulted in the recovery of the starting acyl pyrazolone. It was concluded that such N-*t*-butyl substituted products, if successfully synthesised, might well be inherently unstable to acid, rendering them useless in existing solvent extraction circuits. Consequently the synthesis of pyrazolones **5** and **6** containing acyl groups with lengthy n-alkyl units was undertaken to positively enhance the

solubility of the resulting oxime ligands, whilst retaining the acid stability of previous N-aromatic derivatives.

The attempted synthesis of the n-octyl substituted ligand **15** using the conventional oximation method³⁹ was also unsuccessful and again variation in reagent ratio, reaction temperature and time was undertaken but with no success. The pH-rate profiles of this type of condensation reaction display maxima at weakly acidic pH values of approximately 4 and are indicative of a two step reaction mechanism⁴⁰. The mechanism is illustrated in figure 16.

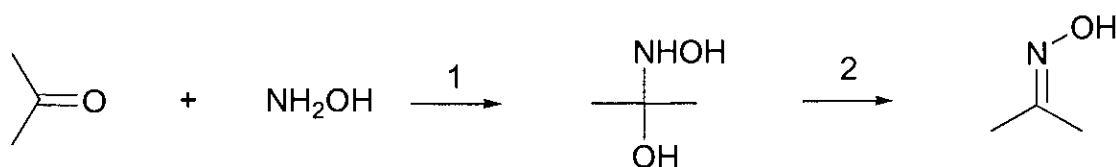


Figure 16 : General mechanism of an oximation reaction

It is thought that at pH < 4 the concentration of protonated $[\text{NH}_3\text{OH}]^+$, which cannot attack the carbonyl, increases such that step 1 becomes the rate limiting step. At pH > 4, step 2 is the rate determining step, as dehydration of the intermediate carbinolamine is acid-catalysed^{41,42}. Therefore a slightly acidic pH value is optimum for efficient reaction. Interestingly, pH-dependent rates of reactions of aromatic carbonyl compounds with hydroxylamine have not been widely observed⁴³, however it could still play an important role in determining the success of oximations of aromatic-substituted acyl pyrazolones. Additionally, although removal of water from the reaction medium is not deemed necessary for successful oximations⁴⁴, under equilibrium conditions such a condensation reaction will be favoured by removal of water.

A method was devised, in which oximation was carried out under anhydrous conditions and at room temperature⁴⁵, by which both **15** and **16** were prepared in good yield. The reaction scheme is shown in figure 17. It should be noted that although the pH of the reaction was not controlled, it was found to be approximately 6. The solubility of ligand **15** in toluene was found to be

ca. 0.8 M using ^1H NMR techniques, which is suitable for solvent extraction experiments.

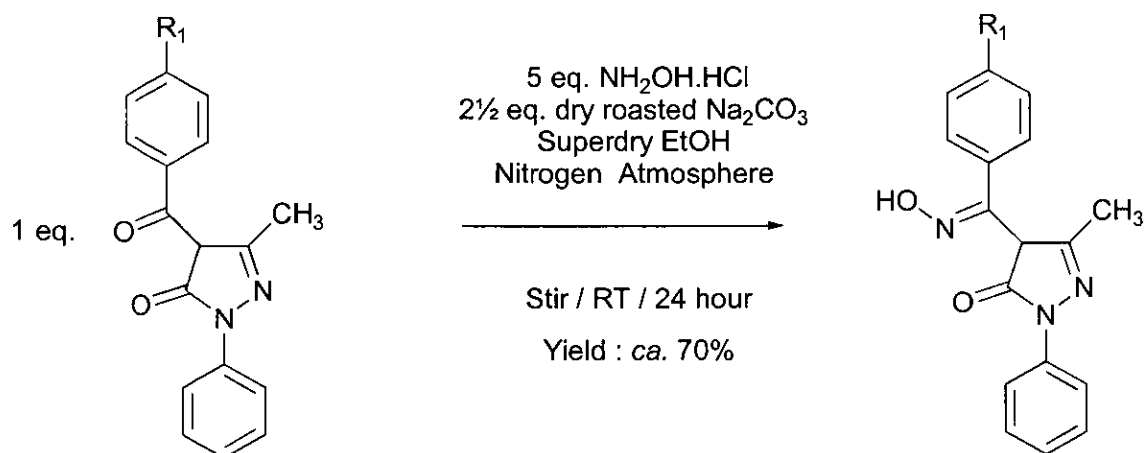


Figure 17 : Synthesis of pyrazolone oximes **15** ($\text{R}_1 = \text{n-octyl}$) and **16** ($\text{R}_1 = \text{n-heptyl}$)

3.2.2.2 Metal Complexes

Metal complexes of pyrazolone oxime ligands were synthesised by the reaction of two equivalents of the appropriate ligand with one equivalent of the appropriate divalent metal salt³⁸. It is interesting to consider the effect of using different starting metal salts on the formation of complexes of ligand **12**, as shown in figure 18.

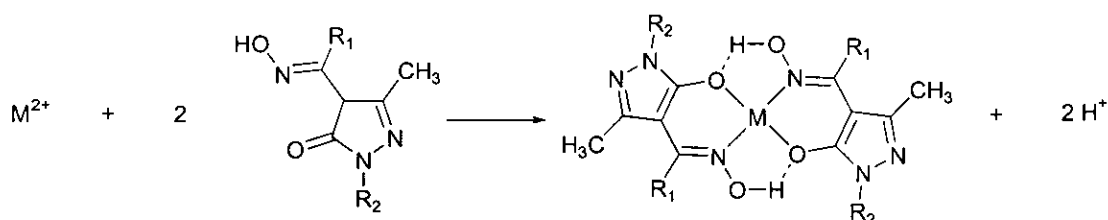


Figure 18 : Synthesis of metal complexes of pyrazolone oximes

The neutral copper(II) and zinc(II) complexes were readily prepared from acetate precursors. The protons liberated in the reaction medium produce acetic acid on reaction with the basic acetate anions. Likewise, the neutral nickel(II) complex, **19**, was prepared from the chloride salt, forming

hydrochloric acid. When cobalt(II) nitrate was used to prepare complexes of ligand **12**, a dicationic complex was obtained as the nitrate salt, $[\text{Co}(\mathbf{12})_2(\text{MeOH})_2](\text{NO}_3)_2$. An X-ray structure of this complex (see below : Figure 37) shows that the protons liberated from the chelating portion of the ligand are in this case transferred to the pyrazolone ring nitrogen (N2). This implies that nitrate is not as strong a base as the pyrazolone ring nitrogen (N2), thus the protons are bound by N2 instead of forming nitric acid. This observation indicates that the basic nitrogen atoms in the pyrazolone units could lead to the transfer of acid from the stripping section of a solvent extraction circuit.

3.3 Characterisation of Acyl Pyrazolones, Pyrazolone Oximes and their Metal Complexes

3.3.1 IR Spectroscopy

3.3.1.1 Acyl Pyrazolones

The solid state IR spectra of ligands **1-4** and **6** all display bands, which can be assigned to the keto/enol tautomer (Figure 4 : **b**) of the acyl pyrazolone ligands. Bands attributed to the pyrazolone ring (C=N, C=C) are observed between ca. 1500-1600 cm^{-1} and the C=O stretch is observed between 1600-1670 cm^{-1} , while the band assigned to the OH stretch is broad and varies between 2500-3000 cm^{-1} . These variations in the wavenumbers of both the C=O and OH stretches are assumed to be affected by the varying strength of the hydrogen bonding within the molecule. Additionally, bands assignable to the out-of-plane bending mode of aryl C-H bonds are observed at ca. 700-800 cm^{-1} . Literature data for such keto/enol tautomeric forms^{1,23,24} are very similar to those reported here. The bands at 2500-3000 cm^{-1} in ligands **1-4** and **6** are assigned to OH rather than NH as the literature spectrum for the NH tautomer (Figure 4 : **c**) of **1** displays a slightly sharper band at 3300 cm^{-1} indicative of an NH stretch¹.

The solid state IR spectra of the metal complexes **7-11** all display bands assignable to the carbonyl stretch at ca. 1600-1610 cm^{-1} , which has been

slightly lowered in energy on complexation. Bands attributable to OH disappear on complexation indicating that it is occurring *via* deprotonation of the OH at the 5-position of the pyrazolone ring. Additionally, bands at between 1360 and 1380 cm^{-1} can be assigned to the stretching mode of the enolic C-O bond⁵. Broad OH bands at 3250-3500 cm^{-1} seen in the spectra of complexes **8-11** are indicative of coordinated methanol molecules.

3.3.1.2 Pyrazolone Oximes

The solid state IR spectra of ligands **12-16** all show broad bands at between 3000-3500 cm^{-1} , which are assigned to $\nu(\text{OH})$ of both the oxime OH and the enolic OH, in agreement with the literature³⁰⁻³³. Additional, broad, $\nu(\text{OH})$ bands at *ca.* 2500-2700 cm^{-1} in the spectra of **15** and **16** indicate the presence of strongly intramolecularly hydrogen bonded hydroxyl groups in these ligands. Bands assignable to the C-H stretch at *ca.* 2700-2900 cm^{-1} and the bending mode at 700-800 cm^{-1} are also consistently observed. The region between 1500-1650 cm^{-1} is the most interesting in the spectra of the pyrazolone oximes as in general three bands at variable wavelengths are observed, the lowest of which is conventionally assigned to the C=C stretch³⁰⁻³³. The other two bands could theoretically be due to C=O or C=N and are consistently assigned as $\text{C}=\text{N}_{\text{oxime}}$ and $\text{C}=\text{N}_{\text{ring}}$ in the literature^{30,31}. It should be noted, however, that $\text{C}=\text{N}_{\text{oxime}}$ stretches, if observed at all are generally weak⁴⁶, and these assignments are probably incorrect, as the solid state structure of **12** shows a different tautomeric form (**d**) as discussed in section 3.5.2.1.

The spectra of the metal complexes **17-26**, all show a broad band at 3300 cm^{-1} , which is attributed, for the most part, to the OH_{oxime} bond, which remains in tact on complexation. Bands attributable to C=N at *ca.* 1600 cm^{-1} in all spectra and, additionally, bands at *ca.* 1000 cm^{-1} , which are assigned to $\nu(\text{N-O})$ from comparison of the literature data, are observed in the spectra of **17**, **18** and **20**³⁰⁻³³.

3.3.2 NMR Spectroscopy

3.3.2.1 Acyl Pyrazolones

The ^1H NMR spectra of ligands **1-6** all display a broad peak at between 8.5-12.0 ppm assignable to the hydroxyl proton of the keto/enol tautomer (Figure 4 : **b**). Additionally, none of these spectra show a peak which could be assigned to a proton at the 4-position of the pyrazolone ring thus precluding the diketone tautomer (Figure 4 : **a**). This is in agreement with the literature^{5,23}.

^{13}C NMR data provide supporting evidence for the keto/enol tautomer being the dominant form of this type of ligand. The carbonyl carbon peak occurs at 181-194 ppm while the enolic carbon peak occurs at 157-162 ppm. These data are in good agreement with the literature^{5,23}. The ^1H NMR spectrum of the zinc complex, **8**, showed no peaks assignable to a hydroxyl proton indicating that complexation had occurred *via* deprotonation of the enolic OH of the free ligand.

3.3.2.2 Pyrazolone Oximes

The ^1H NMR spectra of the pyrazolone oximes, in particular those of **12-14**, are much less well defined than those of their acyl precursors. This suggests that proton exchange might be occurring on the NMR timescale, but lowering the acquisition temperature of the spectrum of **12** did not improve its clarity. Such lack of definition may also be indicative of oligomerisation of the oxime molecules. It is interesting to note that the spectra of **15** and **16** are much clearer, which, in turn, may be due to the lower propensity of such bulky molecules to oligomerise. Peaks assignable to either one or two hydroxyl protons are observed in all the spectra apart from that of **14**, in which no such peaks are seen. The reason for this is unclear, but is likely to be due to solvent exchange on the NMR timescale. The most interesting peaks to consider in the ^{13}C NMR spectra of ligands **12-16** are those of the oxime carbon and the carbon at the 5-position of the pyrazolone ring. The carbon in the ring is assigned as the peak closest to 160 ppm in all the spectra apart

from that of **12**, in which it occurs at 147.55 ppm but is poorly resolved. This assignment is made from comparison of the equivalent peaks in the spectra of the acyl precursors. The oxime carbon signals vary significantly between 138-178 ppm and are assumed to reflect both the varying strengths of the intermolecular hydrogen bonds of the different ligands, which will directly effect the electron density distribution within the ligand. Neither ^1H nor ^{13}C NMR data provided any evidence for the existence of a proton at the 4-position of the pyrazolone ring, indicating that pyrazolone oxime ligands do not exist as their ketone tautomers in solution.

3.3.3 Mass Spectrometry

3.3.3.1 Acyl Pyrazolones

The EI mass spectra of ligands **1-6** all show peaks assignable to the free ligands and also to expected fragmentations of, for example, the substituents on the pyrazolone nitrogen and the acyl group. The electrospray (ES) mass spectrum of **6** showed a peak attributable to the free ligand, but no peaks associated with higher oligomers. The FAB mass spectra of complexes **7-11** all show the expected peaks for ML_2 species. In addition, the spectra of **8, 9** and **11** show peaks assignable to the oligomeric species M_2L_3 . These species are assumed to have been formed in the mass spectrometer as C/H/N data does not suggest the presence of such species in the bulk samples.

3.3.3.2 Pyrazolone Oximes

The EI mass spectra of ligands **12-14** and the FAB mass spectra of ligands **15** and **16** all show peaks assignable to the free ligand and fragmentations expected for this type of substituted pyrazolone. As in the spectra of their acyl precursors, there are peaks assignable to fragmentation at the pyrazolone nitrogen and 4-position substituents. Additionally, minor peaks assignable to dimeric, $(\text{LH})_2$ species are observed in the FAB mass spectra of ligands **15** and **16**. Although these species must have formed in the mass

spectrometer, they are perhaps still indicative of the inclination of this type of compound to dimerise. The electrospray (ES) mass spectrum of ligand **16** (Figure 19) provides additional evidence for this, showing peaks assignable to both the free ligand and a dimeric species. Peaks attributable to higher oligomers were not observed. Additionally, the ESMS analysis of a 1:1 mixture of **16** and the modifier nonylphenol did not give any evidence for the breaking up of oxime dimers by the modifier, as might be expected.

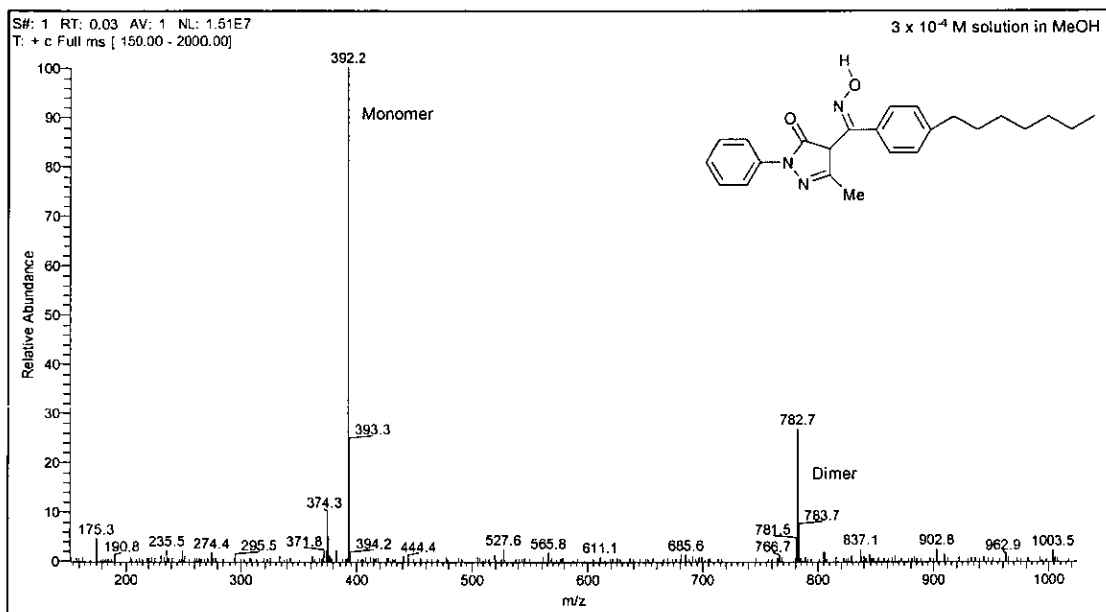


Figure 19 : ESMS of pyrazolone oxime **16**

The FAB mass spectra of complexes **17-20** and **22-26** all show the expected ML_2 peaks and only the spectrum of **26** shows peaks assignable to higher oligomers such as M_2L_3 , M_3L and M_2L . The spectrum of the copper(II) complex of the acetyl pyrazolone oxime ligand, **13**, does not have the expected CuL_2 peak but instead the parent ion is assigned as $(CuL_2 - 2CH_3)$, which may be indicative of the instability of this acetyl ligand.

3.4 Solvent Extraction from Sulphate Media

The solvent extraction of copper(II) using acyl pyrazolones has been well studied^{7-9,12,13}. The literature values for the $pH_{1/2}$ of various mono- and bis-acyl

pyrazolones are presented in table 3. The $pH_{1/2}$ -values for mono- and bis-pyrazolones are similar and generally fall within the range 1.2 - 2.0 pH units, with variations of the values for a specific ligand usually due to the use of different solvent systems, the effects of which are discussed in chapter 2. The data suggest that $pH_{1/2}$ -values for a ligand determined in chloroform or benzene will be much lower in kerosene⁸.

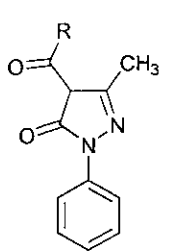
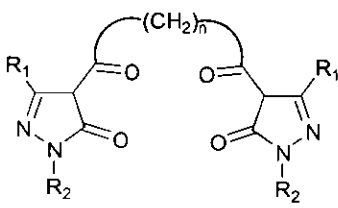
Ligand	Substituent	Solvent System	$pH_{1/2}$ -value
	R = phenyl ⁸	Kerosene	2.0
	R = <i>p</i> -NO ₂ Ph ⁷	CHCl ₃	1.9
	R = <i>n</i> -C ₇ H ₁₅ ⁷	Kerosene	1.8
	R = <i>iso</i> -C ₇ H ₁₅ ⁷	Kerosene	2.0
	R = <i>n</i> -C ₈ H ₁₇ ^{8,12}	Kerosene	1.5
		Benzene	1.9
		CHCl ₃	2.1
	C ₂ H ₄ Cl ₂	2.7	
	n = 7 ¹³	CHCl ₃ / C ₂ H ₄ Cl ₂	1.6
	n = 8 ¹²	CHCl ₃	1.2
	n = 8 ¹³	CHCl ₃	1.6
	n = 10 ¹³	CHCl ₃	1.4
	n = 12 ¹³	CHCl ₃	1.5

Table 3 : Literature data for the solvent extraction of copper(II) using acyl pyrazolones

Additionally, the bis-pyrazolones were found to be slightly stronger extractants than their mono-pyrazolone counterparts, despite being slightly weaker acids¹³. This is due to the fact that the overall equilibrium constant, K_e , is dependent not only on the acidity of the ligand, but also its relative affinity for binding copper(II) ions *versus* protons, as described in equations 1-8. The pK_a -value of 3-methyl-1-phenyl-4-benzoyl-5-pyrazolone (R = phenyl) is 3.8⁸, whereas the pK_a -values of the C_n-linked bis-pyrazolones (n = 1-9) increase with increasing n, and are found to be ≥ 4 ¹³.

conventional strip acid. On the basis of extractive strength, the acyl pyrazolone would therefore seem to be the better replacement for P50. However its O_2^- donor atom set might introduce problems due to a lack of selectivity for copper(II) over iron(III) as already mentioned. The selectivity of these ligands will be discussed in section 3.4.2.

The S-curves for copper(II) extraction using acyl pyrazolone **6** and pyrazolone oxime **15** in toluene are presented in figure 20.

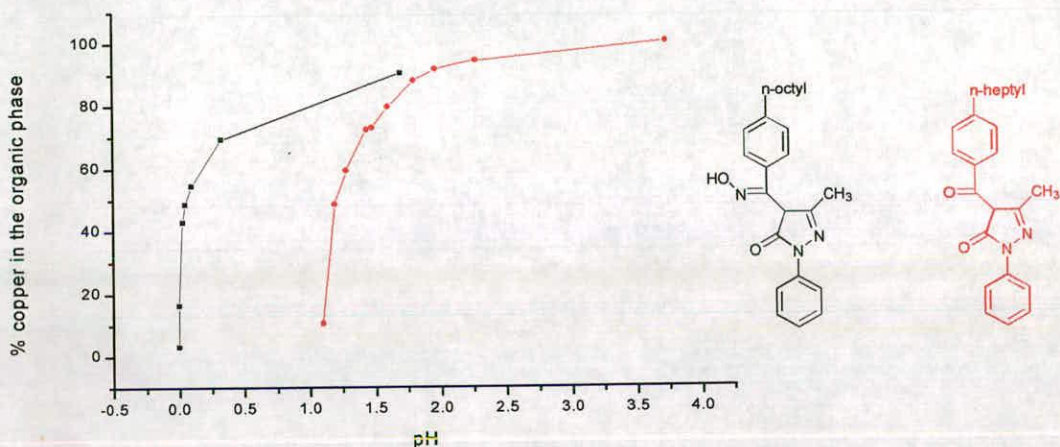


Figure 20 : S-curves for the extraction of copper(II) using ligands **6** and **15**

The $pH_{1/2}$ values for **6** and **15** were found to be approximately 1.2 and 0.1 respectively, confirming that while the pyrazolone oximes are perhaps too strong to be used as replacement extractants for P50, the acyl pyrazolones are not so weak that they could not be considered as copper extractants for use in existing acid leach solvent extraction circuits.

3.4.2 Selectivity for Copper(II) over Iron(III)

The selectivity data for copper(II) over iron(III) of P50, the acyl pyrazolone **5** and the pyrazolone oxime **15** in dichloromethane are presented in table 5.

These initial results indicate that while P50 is the most selective ligand for copper(II) over iron(III), acyl pyrazolones are still significantly more selective than pyrazolone oximes. In addition, despite its O_2^- donor atom set, **5** is

acid leach solvent extraction circuit. Additionally, the metal complexes have limited solubility in the type of hydrocarbon solvent used in solvent extraction circuits, which would explain the use of solvent systems such as chloroform and kerosene solutions of very low concentration in these experiments.

3.4.1 Load and Strip Characteristics

The copper(II) load and strip characteristics of P50 (2-hydroxy-5-nonylbenzaldehyde oxime), the acyl pyrazolone **5** and the pyrazolone oxime **16** in dichloromethane are presented in table 4. These results were obtained from screening tests established by Avecia to compare the loading, stripping and selectivity (Table 5) characteristics of new extractants with those of P50 oxime. The choice of dichloromethane as solvent avoids the need to prepare alkyl-substituted versions of the candidate ligands for use in this preliminary screen.

Test	Aqueous Contact Sol'n	Cu _{org} / gl ⁻¹		
		P50	Acyl 5	Oxime 16
Load	5.00 gl ⁻¹ Cu; pH 2	1.28	1.20	1.60
Strip	45.0 gl ⁻¹ Cu / 125 gl ⁻¹ H ₂ SO ₄	0.18	0.044	1.65

Table 4 : Load and strip characteristics of **5**, **16** and P50.

Test conditions : 0.05 M ligand solution in DCM; O:A ratio 1:1; Equilibration time : 1 h at room temperature.

These results show that although the acyl pyrazolone is a slightly weaker copper extractant than P50, which loads copper to 80 % in this test, it is still comparable to P50 with a loading capacity of 75 %. These loading capacities are based on the formation of CuL₂ from a 0.05 M ligand solution. More importantly, copper can be stripped from the acyl pyrazolone much more efficiently on contact with conventional strip acid. Conversely, the pyrazolone oxime is a much stronger extractant than P50, loading to 100 % in this test (again based on the formation of CuL₂ from a 0.05 M ligand solution), and is, in fact, so strong that it is impossible to strip using

found to be a poor ligand for iron(III) and only loads to approximately 10 % on contact with 5 gl⁻¹ iron(III) assuming FeL₃ formation from a 0.05 M ligand solution. Surprisingly, the pyrazolone oxime is not nearly as selective for copper(II) over iron(III) and also loads iron(III) very well from an aqueous feed containing 5 gl⁻¹ iron(III), despite its less favourable NO donor atom set. Assuming FeL₃ formation, the load value of 705 ppm represents 75 % loading of the ligand.

Test	Aqueous Contact Sol'n	P50		Acyl 5		Oxime 16	
		Cu _{org} gl ⁻¹	Fe _{org} ppm	Cu _{org} gl ⁻¹	Fe _{org} ppm	Cu _{org} gl ⁻¹	Fe _{org} ppm
Selectivity	5.00 gl ⁻¹ Cu / 5.00 gl ⁻¹ Fe	1.42	<1	1.35	12	1.67	88
Iron Load	5.00 gl ⁻¹ Fe	-	69	-	87	-	705

Table 5 : Selectivity data for P50, 5 and 16

Test conditions : 0.05 M ligand solution in DCM; O:A ratio 1:1; Equilibration time : 1 h at room temperature.

The results of additional tests to monitor changes in selectivity for copper(II) over iron(III) of acyl pyrazolone 6 and pyrazolone oxime 15 in toluene with time are presented as a histogram in figure 21.

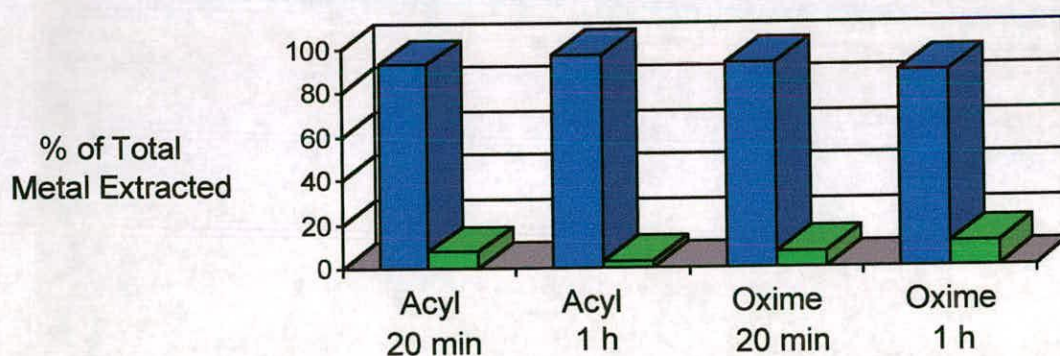


Figure 21 : Changes in the selectivity of 6 and 15 for copper(II) over iron(III) with time

These results show that over time the selectivity of acyl pyrazolone **6** for copper(II) over iron(III) seems to improve, whereas that of pyrazolone oxime **15** is diminished. The selectivity of the acyl pyrazolone increases from 12 : 1 to 35 : 1, while that of the oxime decreases from 14 : 1 to 8 : 1.

In summary, pyrazolone oximes have been found to be too strong to be used as solvent extractants for copper(II) but do show acceptable selectivity for copper(II) over iron(III). The acyl pyrazolones, however, were found to extract and strip copper(II) efficiently and in addition show surprisingly high selectivity for copper(II) over iron(III).

3.5 X-Ray Crystallography

3.5.1 Acyl Pyrazolones

The Cambridge Crystallographic Database (CCDC)¹⁸ (Search performed : September 1999) contains over 50 structures of metal complexes of acyl pyrazolones and related ligands. In addition there are 10 structures of acyl pyrazolones and structurally related free ligands. This large number of structures may be explained by the fact that all but two⁴⁷ of them contain ligands with N-phenyl substituted pyrazolone rings. This is thought to enhance the planarity of the ligand unit thus increasing opportunities for π -stacking in the crystal packing and ultimately therefore the crystallinity of the compound.

3.5.1.1 Free Ligands

3.5.1.1.1 Tautomerism

There are four possible tautomeric forms of acyl pyrazolones, as already mentioned (Section 3.1.1.2, figure 4). The solution structures of these ligands have been investigated using IR and NMR (Sections 3.3.1.1 and 3.3.2.1) and have been found to exist in at least two tautomeric forms (Figure 4 : **a** and **b**), as is common for heterocyclic compounds⁴⁸. However, it is far less common for potentially tautomeric compounds to exist in more than one

tautomeric form in the solid state, a phenomenon known as desmotropy⁴⁷. As the starting pyrazolone, 3-methyl-1-phenyl-5-pyrazolone, is found to exist in two tautomeric forms in the solid state⁴⁹, it is assumed that this possibility will also exist for 4-substituted pyrazolones, such as the acyl pyrazolones, and this is indeed observed.

Of the seven directly related acyl pyrazolones reported, four structures are of the tautomeric forms **a**¹⁹, **b**^{21,22} and **c**^{21,22} of ligand **1** (4-benzoyl-3-methyl-1-phenyl-5-pyrazolone), two are of the tautomeric forms **b** and **c** of 4-cinnamoyl-1,3-dimethyl-5-pyrazolone⁴⁷ and one is of tautomer **b** of 4-butanoyl-3-methyl-1-phenyl-5-pyrazolone²⁰. These tautomeric forms were assigned on the basis of determined hydrogen atom positions. The three compounds are presented in their conventional diketone tautomeric forms along with the relevant CCDC codes for each tautomer (**a-c**) observed in the solid state in figure 22.

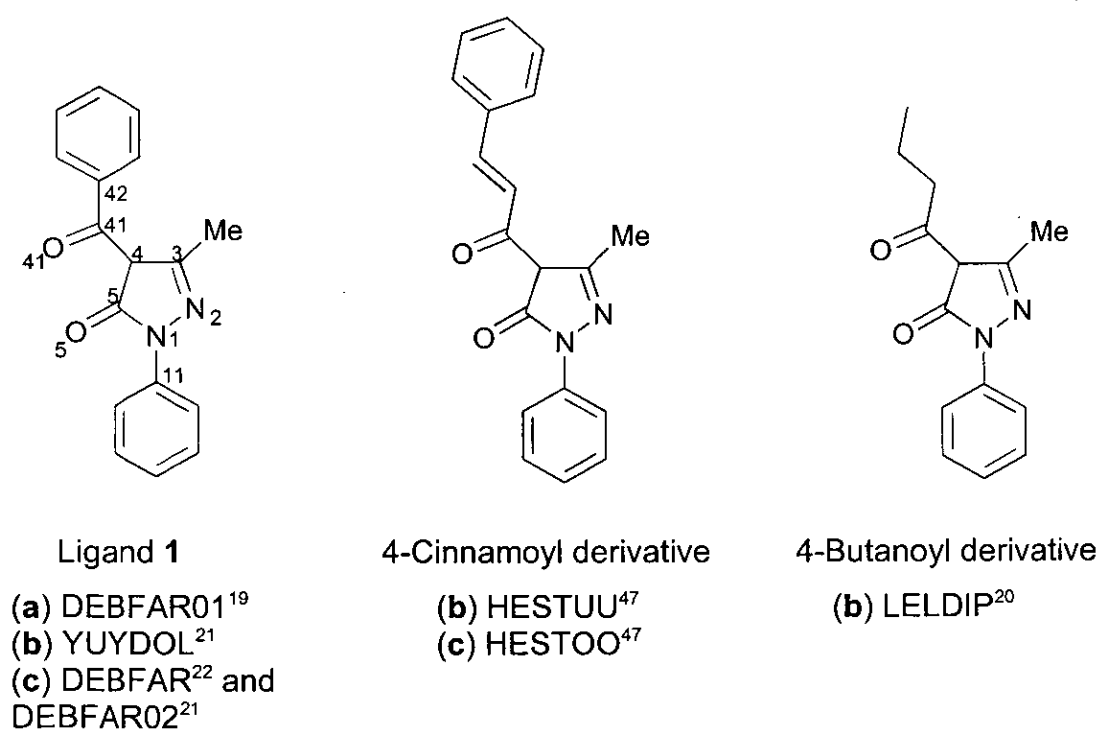


Figure 22 : Acyl pyrazolone free ligand structures, their tautomeric forms (refer to figure 34 and CCDC codes)

The bond lengths of interest in assessing the tautomerism in these ligands are presented in table 6. Bond labels refer to the diagram of ligand **1** in

figure 22. The majority of values for C41-C42, C41-C4 and N1-C11 are close to or greater than the average single C-C and C-N bond lengths, given in table 7 and indicate that the acyl group at the 4-position is a ketone not an enol. The C=O bond lengths of this keto group (C41-O41) vary quite considerably, with those of the diketone (a), DEBFAR01, and the keto/NH tautomer (c), DEBFAR02, closest to the expected C=O bond length of 1.21 Å (Table 7). Additionally, the C41-O41 bonds are longest in the 4-cinnamoyl and 4-butanoyl derivatives, which may reflect the effect of a non-aromatic group at the position α to the carbonyl functionality. The lengthening of this bond in the keto/enol tautomers is attributed to the presence of the intermolecular hydrogen-bond O41...H5-O5.

CCDC Code	DEBFAR01	YUYDOL ^a	DEBFAR02	DEBFAR	HESTUU	HESTOO	LELDIP
Tautomer	diketone (a)	keto/enol (b)	keto/NH (c)	keto/NH (c)	keto/enol (b)	keto/NH (c)	keto/enol (b)
R Factor / %	5.6	3.8	6.3	4.8	5.1	5.4	4.0
C41-C42	1.340(18)	1.490(3)	1.490(3)	1.494(9)	1.467(3)	1.474(3)	1.484(7)
C41-O41	1.233(11)	1.246(2)	1.226(3)	1.245(7)	1.274(3)	1.260(3)	1.256(6)
C41-C4	1.510(14)	1.436(4)	1.472(3)	1.462(9)	1.426(3)	1.472(4)	1.433(6)
C4-C5	1.37(2)	1.390(1)	1.435(4)	1.434(9)	1.408(3)	1.464(40)	1.386(6)
C5-O5	1.315(15)	1.323(3)	1.246(3)	1.233(8)	1.315(3)	1.255(3)	1.319(5)
C5-N1	1.484(15)	1.350(2)	1.391(3)	1.403(8)	1.329(3)	1.387(3)	1.347(5)
N1-N2	1.444(14)	1.389(2)	1.383(3)	1.377(7)	1.394(2)	1.383(3)	1.396(5)
N2-C3	1.282(17)	1.311(2)	1.334(3)	1.342(8)	1.327(3)	1.345(3)	1.327(6)
C3-C4	1.336(14)	1.433(1)	1.385(30)	1.398(8)	1.429(3)	1.402(3)	1.424(6)
N1-C11	1.358(19)	1.422(2)	1.418(3)	1.430(8)	1.454(3)	1.473(3)	1.426(6)
C4-H4	1.00	-	-	-	-	-	-
O5-H5	-	1.11(3)	-	-	0.95	-	0.89(5)
N2-H2	-	-	0.95	1.06	-	0.88	-
O41-O5	3.063(17)	2.663(2)	3.079(2)	3.076(6)	2.585(3)	4.477(3) ^b	2.583(5)

Table 6 : Bond lengths and bite distances (O41-O5) for the structures of acyl pyrazolones (in Å)

- a Bond lengths for YUYDOL are the averages of the two values for the two structural conformers of the keto/enol tautomer found in the unit cell
- b The configuration of HESTOO is such that the two carbonyl substituents point in opposite directions, hence the very large value of the distance O4...O5

In comparison with the standard⁵⁰ bond lengths reported in table 7, the C4-C5 bonds of the pyrazolone ring are intermediate in character, with those in the majority of diketone and keto/NH structures being longer (ca. 1.44 Å) than those in the keto/enol tautomers (ca. 1.40 Å) as expected. Similarly, the bond length values for C5-O5 in the keto/NH tautomers (c) are significantly shorter (ca. 1.25 Å) than those for the keto/enol tautomers (ca. 1.32 Å), which are very close to the standard⁵⁰ single C-O bond length of 1.33(2) Å (Table 7). The presence of an enolic group seems to shorten the bond C5-N1 most significantly in the structure HESTUU, resulting in a bond of intermediate character, while the equivalent bonds in the diketone and keto/NH tautomers are longer than the standard⁵⁰ C-N single bond length value of 1.36(1) Å (Table 7). Finally, the bond C3-C4 is again of intermediate character, being shorter in the keto/NH tautomers as would be expected, but the average value of ca. 1.40 Å in these keto/NH structures is still not indicative of a formal C=C double bond (1.32(2) Å⁵⁰).

Bond	C _{sp2} -O	C _{sp2} -C _{sp2}	C _{sp2} -N _{sp2}	N _{sp2} -N _{sp2}
Single	1.33(2)	1.46(2)	1.36(1)	1.40(3)
Double	1.21(1)	1.32(2)	1.28(1)	1.22(1)

Table 7 : Standard⁵⁰ single and double bond lengths (in Å)

In summary, although the *relative* bond lengths in these structures are as expected, the *actual* values in terms of formal single and double bond lengths are far from the accepted values. Tautomerism introduces a significant degree of intermediate character into the bonding in these free ligand structures, such that it might be better represented by some degree of

delocalisation rather than formal single double and single bonds as in the structures in figure 4. This is particularly true for the bonds of the chelating unit of the ligands, O41-C41-C4-C5-O5.

3.5.1.1.2 Hydrogen Bonding

In addition to evidence for the tautomerism of these ligands in the solid state, it is interesting to study the hydrogen bonding in these structures. The structures of the three keto/enol tautomers, YUYDOL, HESTUU and LELDIP, all have intramolecular hydrogen bonds between H5 and O41 of 1.69(4) Å, 1.70(2) Å and 1.81(5) Å respectively, as shown in figure 23.

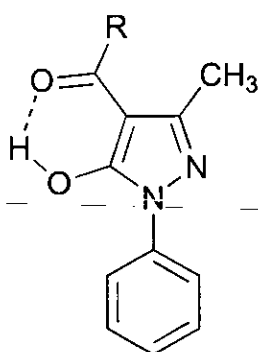


Figure 23 : Intramolecular hydrogen bonding as seen in the structures of the keto/enol (**b**) tautomers of YUYDOL (R = Ph), HESTUU (R = Ph(CH)₂) and LELDIP (R = C₃H₇)

Such strong intramolecular hydrogen bonds will stabilise this keto/enol tautomeric form and enhance the planarity of the ligand unit. In addition to the effects of the tautomerism of the ligand itself, such intramolecular hydrogen bonds may also shorten the bite distance (O41...O5; Table 5) of the ligand. The average bite distance of the keto/enol tautomers is found to be ca. 2.60 Å, which is significantly shorter than the equivalent distances in the diketone and keto/NH tautomers (Average value 3.07 Å). Lone pair - lone pair or dipole - dipole repulsive interactions between the two carbonyl oxygen atoms in these tautomers (**a** and **c**) are assumed to open up the O...O bite distances. There is no possibility of forming intramolecular hydrogen bonds in either the diketone (**a**) or keto/NH (**c**) tautomers of these ligands, however intermolecular hydrogen bonding between the ring NH and

the ring carbonyl oxygen atom on adjacent molecules is seen in the structures of the keto/NH tautomers. In DEBFAR the molecules are held in chains by such intermolecular hydrogen bonds ($O\cdots N$ 2.66 Å), forming a crystal packing motif frequently proposed for the NH tautomers of pyrazolones⁴⁷ (Figure 24). Additionally, a similar type of intermolecular hydrogen bond of 1.82 Å between the ring NH and the oxygen atom of a neighbouring lattice water molecule is observed in HESTOO.

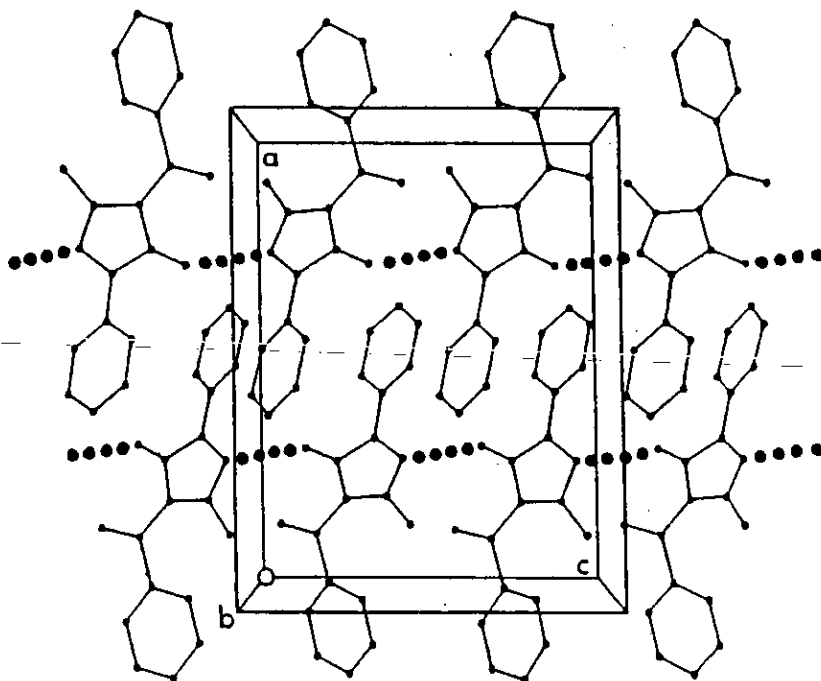
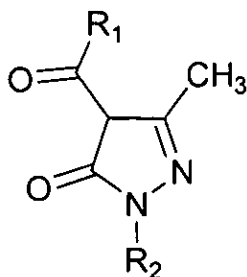


Figure 24 : Crystal packing in DEBFAR⁴⁷

3.5.1.2 Metal Complexes

In addition to the zinc(II) and copper(II) structures, **8** and **11**, reported here, there are seven other structures in the literature of particular relevance to discussing the coordination chemistry of acyl pyrazolones with reference to their solvent extraction properties. These structures are summarised in table 8. R_1 and R_2 refer to the diagram of an acyl pyrazolone ligand below.



Structure			Ligand, LH	
No. / CCDC Code	R Factor / %	Formula	R ₁	R ₂
Copper(II)				
11	3.89	[CuL ₂ (MeOH) ₂]	Ph	<i>t</i> -Bu
KUGBOD ¹⁹	7.0	[CuL ₂]	Ph	Ph
JEXXAL ⁵¹	8.0	[CuL ₂]	CF ₃	Ph
FEKQAN ⁵²	5.02	[CuL ₂ (H ₂ O)]	CH ₂ C(CH ₃) ₃	Ph
LIJVAB ^{53,a}	7.2	[CuL]	C ₈ H ₁₆ Bridge	Ph
Zinc(II)				
8	4.18	[ZnL ₂ (MeOH) ₂]	Ph	Ph
NOZSIE ⁵⁴	5.0	[ZnL ₂ (H ₂ O)]	<i>n</i> -C ₇ H ₁₅	Ph
Iron(III)				
LELDUB ²⁰	4.1	[FeL ₃]	CH ₃	Ph
LELDV ²⁰	7.6	[FeL ₃]	<i>n</i> -C ₃ H ₇	Ph

Table 8 : Metal complexes of acyl pyrazolones

^a This structure contains a bis-pyrazolone, tetradentate ligand, in which the two acylpyrazolone units are joined together by a C₈H₁₆ chain

It should be noted that although β-dicarbonyl compounds are very versatile and do exhibit a variety of coordination modes⁵⁵, a monoanionic, bidentate chelate is by far the most common and is the coordination mode observed in all the structures discussed here.

3.5.1.2.1 Mesomerism

As with the free ligand structures, it is interesting to study the nature of the bonding within the acyl pyrazolone metal complexes to assess the extent of delocalisation within the chelating unit of the coordinated ligand. The data presented in table 9 show that the bonds around the chelating unit of the ligands have lengths, which are intermediate between the accepted⁵⁰ values for single and double bonds. This suggests a large degree of π electron delocalisation within the bonding in the chelate unit as illustrated in figure 25.

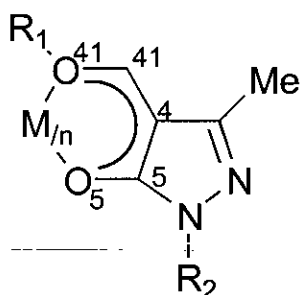


Figure 25 : Metal ion complexation involving acyl pyrazolones

It is interesting to note that these four bond lengths vary most greatly between chelate units in the two iron(III) structures, LELDUB and LELDOV. This is assumed to be a consequence of fitting three ligands around the central metal ion, which must result in a degree of steric strain within the structures.

Complex	Ligand ^a	O41-C41	C41-C4	C4-C5	C5-O5
Copper(II) Structures					
11	A	1.278(3)	1.398(3)	1.428(3)	1.281(3)
	B	1.276(3)	1.391(3)	1.430(3)	1.274(3)
KUGBOD	A and B ^{b,c}	1.26	1.39	1.34	1.32
JEXXAL	A and B ^b	1.254(7)	1.394(8)	1.447(9)	1.251(7)
FEKQAN	A	1.266(6)	1.394(7)	1.414(6)	1.279(5)
	B	1.262(5)	1.414(6)	1.414(6)	1.281(5)
LIJVAB ^d	A	1.280(12)	1.407(14)	1.420(14)	1.266(12)
	B	1.270(13)	1.385(15)	1.411(15)	1.280(13)
Zinc(II) Structures					
8	A and B ^b	1.252(3)	1.411(3)	1.427(3)	1.268(3)
NOZSIE	A	1.261(7)	1.417(8)	1.411(8)	1.282(7)
	B	1.260(7)	1.430(8)	1.404(8)	1.282(7)
Iron(III) Structures					
LELDUB ^e	A	1.262(7)	1.399(7)	1.429(8)	1.274(7)
	B	1.272(7)	1.390(7)	1.431(8)	1.278(7)
	C	1.268(7)	1.407(7)	1.426(7)	1.274(7)
LELDOV ^e	A	1.295(8)	1.404(9)	1.389(10)	1.289(8)
	B	1.252(9)	1.409(11)	1.409(9)	1.279(8)
	C	1.275(8)	1.389(9)	1.420(9)	1.286(8)
Overall Average		1.265(9)	1.401(10)	1.413(19)	1.279(9)
Accepted⁵⁰ Single and Double Bond Lengths					
Single	-	1.33(2)	1.46(2)	1.46(2)	1.33(2)
Double	-	1.21(1)	1.32(2)	1.32(2)	1.21(1)

Table 9 : Selected bond lengths for the metal complexes of acyl pyrazolones and accepted⁵⁰ single and double bond lengths (in Å)

- ^a The structures of the ligands are defined in table 8
- ^b The central metal atom is located on an inversion centre, hence ligands A and B are equivalent
- ^c Bond lengths for the structure KUGBOD were obtained using the Weblab Viewerlite p.c. crystallographic manipulation package⁵⁶
- ^d The ligand nomenclature A and B refer to the two pyrazolone units in the bis-pyrazolone structure
- ^e Bond lengths obtained using Platon multipurpose crystallographic tool⁵⁷

3.5.1.2.2 Metal to Donor Atom Bond Lengths

In almost all of the complexes discussed here, the M-O5 bond lengths are slightly shorter, ie: stronger, than the M-O41 bond lengths (Table 10), which may reflect a slightly greater σ -electron donation from this oxygen to the metal atom, or equally a greater degree of π -back donation by the metal atom to this oxygen atom resulting in shorter bonds. This observation was also made by Marchetti *et al.*⁵².

Bond	Metal - Donor Atom Bond Length / Å					
	M-O41		M-O5		M-OX	
	A	B	A	B	C	C
Copper(II)						
11^b	1.9310(19)	1.9759(18)	1.9308(17)	1.9243(19)	2.623(3)	2.363(3)
KUGBOD	1.91	1.91	1.89	1.89	-	-
JEXXAL	1.928(4)	1.928(4)	1.898(4)	1.898(4)	-	-
FEKQAN^c	1.938(2)	1.956(3)	1.911(3)	1.923(3)	2.248(4)	-
LIJVAB^d	1.911(1)	1.936(4)	1.925(11)	1.918(11)	-	-
Zinc(II)						
8^b	2.117(2)	2.117(2)	2.035(2)	2.035(2)	2.140(2)	2.140(2)
NOZSIE^c	2.061(4)	2.029(4)	1.979(4)	1.970(3)	2.001(4)	-
Iron(III)					O41	O5
LELDUB^e	2.029(4)	2.047(4)	2.014(4)	1.972(4)	2.017(4)	1.959(4)
LELDOV^e	2.003(5)	2.021(5)	1.985(5)	1.970(4)	2.024(5)	1.991(5)

Table 10 : Metal to donor atom bond lengths

- ^a The structures of the ligands are defined in table 8
- ^b Bond lengths M-OX in structures **11** and **8** refer to the bonds to coordinated methanol molecules : Cu1-O1M and Cu1-O2M in **11**; Zn1-O1M and Zn1-O1M' in **8**.
- ^c Bond lengths M-OX refer to the bonds between the central metal atom and the oxygen atom of the coordinated water molecule
- ^d Values quoted are the averages for the two conformers found in the unit cell

- ^e Bond lengths M-OX refer to the bonds Fe-O41 and Fe-O5 respectively of the third coordinated acyl pyrazolone ligand, C; Determined using Platon multipurpose crystallographic tool⁵⁷

The axially coordinated methanol molecules in structure **11** lie much further away from the central metal atom than the coordinated acyl pyrazolone ligands. This is a consequence of a tetragonal distortion along the z-axis in accordance with the Jahn-Teller theorem⁵⁸ and may also be due to the difference in interaction with a metal ion between charged and uncharged donor atoms. There is no electrostatic interaction between the methanolic oxygen atom and the copper(II) cation as methanol is a neutral donor. The Cu-O_{MeOH} bond lengths are 2.623(3) Å and 2.363(3) Å, which is unusual as Jahn Teller distortions are usually symmetrical and have bond lengths of approximately 2.4 Å¹⁸. A search for relevant structures in the CCDC¹⁸ revealed only two unsymmetrically distorted structures (CCDC Codes — FETDAJ and_PECMIT), the Cu-O bonds of which differed by ≤ 0.1 Å, whereas the difference in **11** is 0.26 Å, and may be a consequence of the mode of packing in this structure (Figure 27). The structure of **11** is presented in figure 26. It is interesting to note that the two ligands lie in a *cis* arrangement around the copper(II) ion, unlike the literature¹⁸ structures considered here, which are either *trans* or composed of symmetrical ligands, for which *cis* or *trans* configurations cannot be established.

The formation of intermolecular hydrogen bonds (*ca.* 0.98 Å) between OH and H of adjacent coordinated methanol molecules, and between methanolic protons and the carbonyl oxygen atom (O41) on adjacent molecules (*ca.* 2.20 Å) results in chains of molecules of **11** in the crystal (Figure 27).

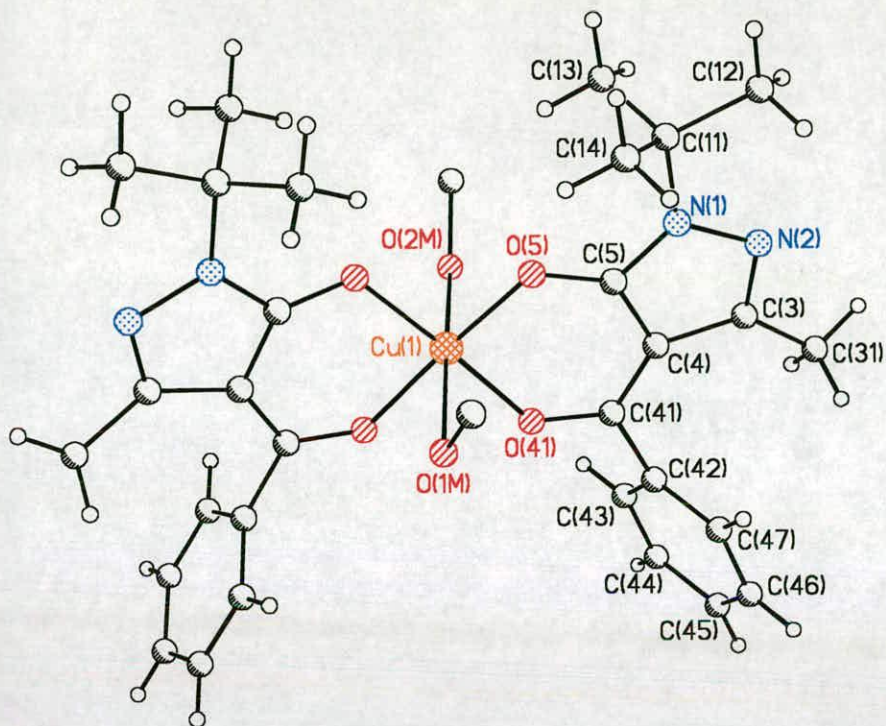


Figure 26 : Structure of $[\text{Cu}(4\text{-H})_2(\text{MeOH})_2]$: **11**. Hydrogen atoms on solvent molecules have been excluded for clarity.

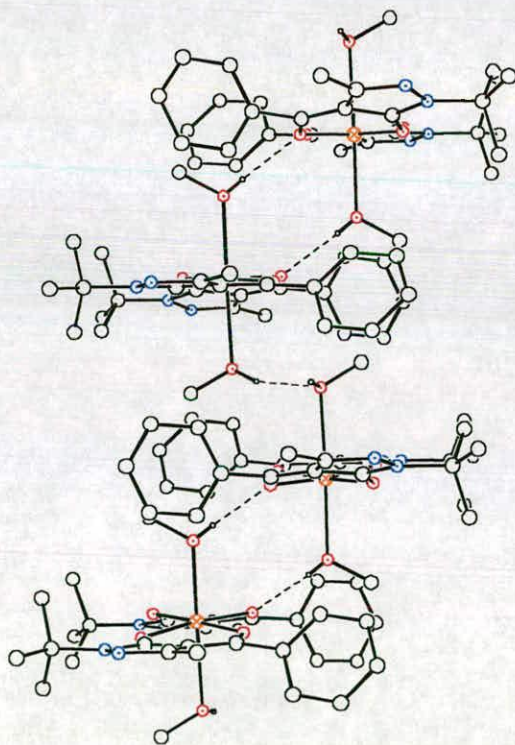


Figure 27 : Crystal packing of **11**

This type of intermolecular hydrogen bonding is not observed in the zinc(II) structure, **8**, and instead intermolecular hydrogen bonds between the OH of a methanol and the nitrogen atom at the 2-position of the pyrazolone ring are formed, again resulting in linear, polymeric, hydrogen-bonded chains of molecules of **8**, as illustrated in figure 28. The length of the intermolecular hydrogen bonds in this case is 2.03(3) Å.

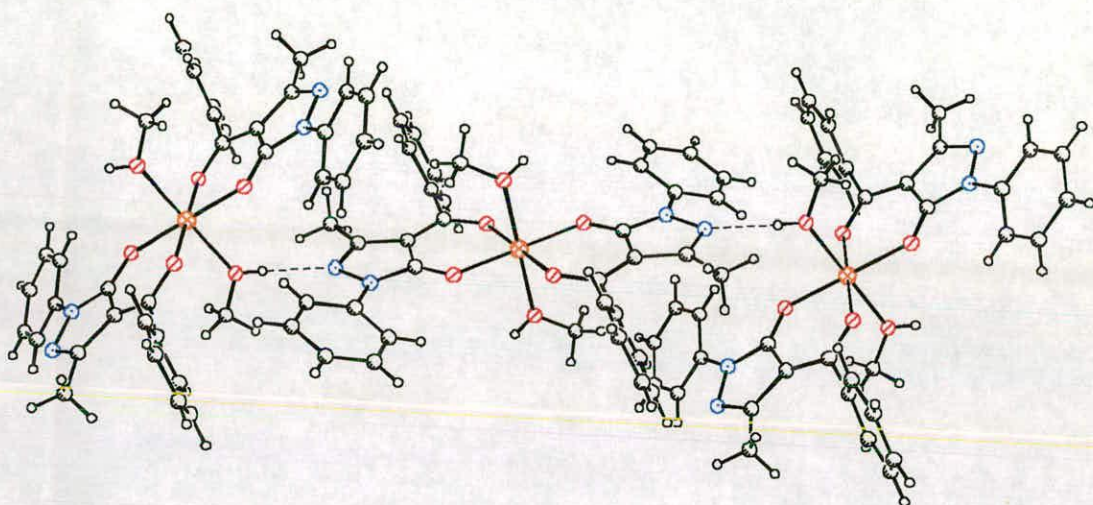


Figure 28 : Crystal packing of **8**

The apical water molecule in the square pyramidal structure of the copper(II) complex of 4-(2,2-dimethylpropanoyl)-3-methyl-1-phenyl-5-pyrazolone⁵², is also only weakly bound at a distance of 2.248(4) Å from the central metal atom. This represents an alternative Jahn-Teller type distortion relieving the degeneracy of the ground state electronic configuration of a planar complex, thus increasing its stability. In contrast, neither the apical water molecule in the zinc(II), square pyramidal structure, NOZSIE, nor the two axially coordinated methanol molecules in **8** are significantly removed from the central zinc atom, which illustrates the difference in behaviour between the copper(II) (d^9) and zinc(II) (d^{10}) cations due to their electron configurations. The average metal to donor atom distances in **8** and NOZSIE are 2.10(4) and 2.01(3) Å respectively, whereas it is 2.13(25) Å in the copper(II)

complex, 11. In general, the metal to pyrazolone donor atom bond lengths are shortest in the copper(II) complexes and are found to be approximately equal in the zinc(II) and iron(III) structures. The Cu-O41 and Cu-O5 bond lengths in LIJVAB, the copper(II) complex of the tetradentate ligand, do not differ significantly, which may be attributable to constraints introduced by the geometry of the tetradentate ligand. The solvent extraction properties of this type of bis-pyrazolone ligand linked by a C_n chain have been found to be highly dependent on the length of this linking chain. Ligands with links of $n \geq 8$ can form square planar copper species, as observed in the structure LIJVAB, and have been found to extract copper(II) quantitatively as CuL species. Ligands with links of $n < 8$ are unable to fold on to a copper(II) ion and instead have been found to extract copper as dimeric Cu_2L_2 species¹³. Slightly greater variation in the metal to donor atom bond lengths in the iron(III) structure, LELDOV, in comparison with the equivalent bonds in LELDUB is assumed to be due to the relative difficulty in accommodating three of the more bulky ligands ($R_1 = n-C_3H_7$ vs. $R_1 = CH_3$) around the iron(III) cation. It is noted that the iron(III) is high spin (d^5) octahedral in both structures and also that the ligands in LELDUB adopt a *fac* arrangement around the central iron atom, while those in LELDOV adopt a *mer* arrangement.

3.5.1.2.3 Bite Angles and Dihedral Angles between Coordination Planes

The bite angles in the complexes of acyl pyrazolones (Table 11) are approximately equal in the zinc(II) and iron(III) structures, which have average values of ca. 89° and 88° respectively, but are found to be much greater in the copper(II) complexes (average value = 93.5°). The majority of the copper(II) structures are square planar or tetragonally distorted octahedral, with the two chelating ligands lying in a plane containing the central copper atom. In the zinc complexes **8** and NOZSIE, the preferred, tetrahedral geometry of the zinc(II) ion is not adopted and the structures have distorted octahedral and square pyramidal geometries respectively. The two iron(III) structures have distorted octahedral geometries.

Structure ^a	Bite Angle / °			Dihedral Angle between Coordination Planes ^d / °
	A	B	C	
Copper(II)				
11	94.49(8)	94.12(8)	-	6.9
KUGBOD^b	93.6	93.6	-	0
JEXXAL	93.83(17)	93.83(17)	-	0
FEKQAN	92.95(13)	92.50(13)	-	12.4
LIJVAB^c	93.2(9)	92.9(5)	-	7.9
Zinc(II)				
8	89.23(6)	89.23(6)	-	33.4
NOZSIE	87.7(2)	89.68(15)	-	85.3
Iron(III)				
LELDUB	87.85(16)	88.40(17)	89.58(16)	85.3, 84.6, 84.4 ^e
LELDV	87.99(19)	88.54(18)	87.17(19)	83.8, 89.1, 87.6 ^e

Table 11 : Bite angles and dihedral angles between coordination planes in the acyl pyrazolone metal complexes

- ^a The structures of the ligands are defined in table 8
- ^b Values were obtained using the WebLab ViewerLite p.c. package⁵⁶
- ^c Values quoted are the averages for the two structural conformers found in the unit cell
- ^d The coordination planes are defined by O5-M-O41 for each ligand. The dihedral angles between these planes were determined using either SHELXTL⁵⁹ (Structures **8**, **11** and FEKQAN) or Cerius⁶⁰ (All other structures).
- ^e The dihedral angles for the iron structures are those between the coordination planes corresponding to ligands A & B, A & C and B & C respectively.

Deviations from perfect square planar or octahedral geometries, which would both have bite angles of 90°, arise due to a combination of constraints imposed upon the geometry of the complex by both the chelate ring size and, to a lesser extent, the steric effects of the ligand. Hancock⁶¹ has shown that from consideration of the minimal strain geometry of cyclohexane (in the chair conformation), the steric requirements of a six-membered metal chelate

ring with an aliphatic backbone are such that the bite angle is 109.5° , the metal to donor atom bond lengths (N in his work) are 1.6 \AA and the bite size is 2.5 \AA . This minimal strain geometry is retained as long as the chelated metal ion is of similar size to the tetrahedral carbon atom (Covalent radius 0.77 \AA ⁶²). In other words, very small metal ions are best coordinated in six-membered chelate rings with saturated carbon backbones, whilst larger cations destabilise this geometry and are better suited to forming five-membered chelate rings. The acyl pyrazolones discussed here all form six-membered chelate rings, but in this case have approximately planar structures, rather than the chair conformations analysed by Hancock⁶¹.

The steric constraints of bulky ligands will also cause geometric distortions. This is best illustrated by the values of the dihedral angles between the two coordination planes, although it should be noted that even though, for example, the two copper(II) complexes, KUGBOD and JEXXAL, have dihedral angles of 0° , there are likely to be significant distortions from planarity within the ligand unit, as is discussed in section 3.5.1.2.5.

It is interesting to compare the structure of the zinc complex **8** with that of the copper(II) complex (KUGBOD) of the same acyl pyrazolone ligand (**1**), which has perfectly planar geometry around the central copper(II) ion and shorter metal to donor bonds (by ca. 0.2 \AA) than **8**. While these shorter acyl pyrazolone-to-metal bonds in the copper complex are likely to result from the lower coordination number at the metal ion, they also suggest that **1** prefers to coordinate to copper(II) and thus might be expected to show good selectivity for copper(II) over zinc(II) in solvent extraction experiments. This was found to be the case, as the $\text{pH}_{1/2}$ value for the extraction of copper(II) into a kerosene phase containing ligand **1** is 2.0^8 , while zinc(II) is only extracted by **1** in the pH range $5.2\text{--}6.4^{11}$. It should be noted that the $\text{pH}_{1/2}$ value depends on the solvent system used as previously discussed¹¹, and in these extraction experiments no monodentate ligands were present to allow the zinc to be recovered as a bis-axially coordinated species analogous to **8**. The structure of **8** is presented in figure 29.

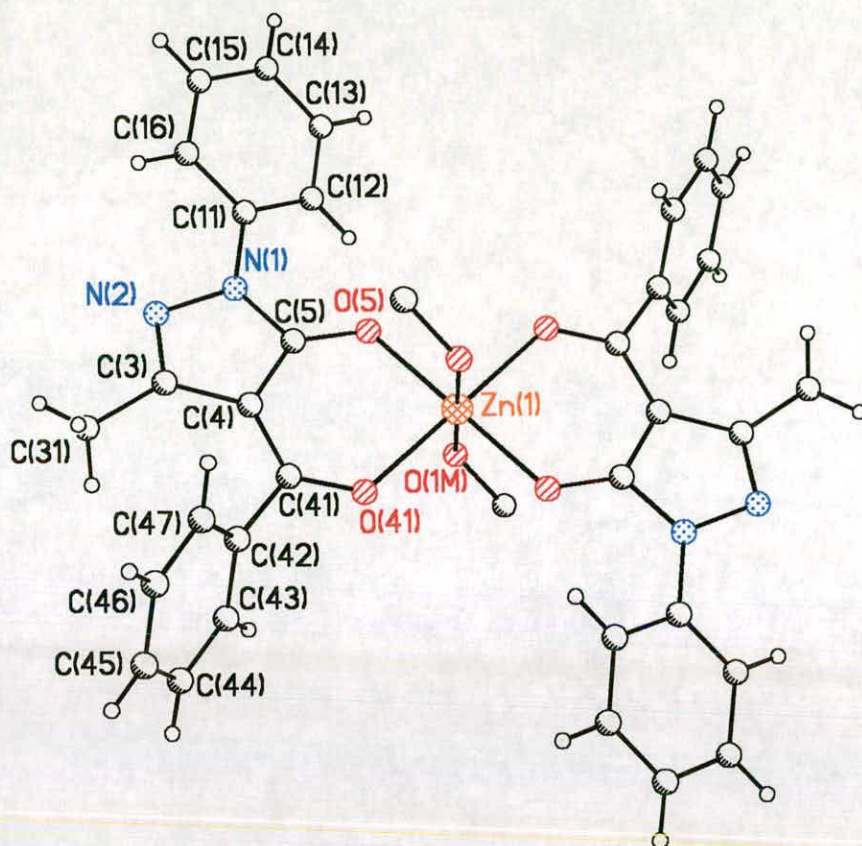


Figure 29 : Structure of $[Zn(1-H)_2(MeOH)_2]$: **8**. Hydrogen atoms on solvent molecules have been excluded for clarity.

3.5.1.2.4 Bite Distances

The bite distances in the structures of the free ligands in the keto/enol form, which most closely resembles the form of the chelated ligand in the metal complexes, have an average value of 2.60 Å. The bite distances observed in the metal complexes fall in the range 2.77 - 2.92 Å (Table 12) and indicate that in every case the ligand bite must expand to complex the metal ion. It is noted that all the bite distances quoted are much longer than the ideal bite distance for a puckered, six-membered chelate ring, which is 2.5 Å⁶¹.

Comparison of the copper(II) and zinc(II) structures shows that the formation of the copper complex is accompanied by a much smaller opening up of the ligand bite than the formation of the zinc complexes.

Structure ^a	Bite Distance / Å			
	Ligand A	Ligand B	Ligand C	Average
Copper(II)				
11^b	2.836(3)	2.855(3)	-	2.846(10)
KUGBOD^c	2.77	2.77	-	2.77
JEXXAL^b	2.764(6)	2.764(6)	-	2.764(6)
FEKQAN^c	2.79	2.80	-	2.795(5)
LIJVAB^{c,d}	2.775(10)	2.796(10)	-	2.786(11)
Zinc(II)				
8^b	2.917(3)	2.917(3)	-	2.917(3)
NOZSIE^b	2.800(6)	2.820(6)	-	2.810(10)
Iron(III)				
LELDUB^b	2.805(6)	2.802(6)	2.801(6)	2.803(2)
LELDV^b	2.771(7)	2.787(6)	2.768(6)	2.775(8)

Table 12 : Bite distances in the acyl pyrazolone metal complexes (in Å)

- ^a The structures of the ligands are defined in table 8
- ^b Values were determined using Platon multipurpose crystallographic tool⁵⁷
- ^c Values were obtained using the Weblab Viewerlite p.c. package⁵⁶
- ^d Values quoted for LIJVAB are the average of the values for the two structural conformers found in the unit cell

This is possibly because the “ideal” metal to oxygen bond length is significantly shorter for copper and can be accommodated to provide a near ideal O-Cu-O angle, with an opening of the bite from ca. 2.60 Å in the free ligand to an average value of 2.79 Å in the copper complexes, as illustrated below and shown in table 13. The ionic radii⁶³ of copper(II) ions with coordination numbers of 4-6 range from 0.57 - 0.73 Å, while those of zinc(II) ions with coordination numbers 5-6 are, in general, slightly longer, ranging from 0.68 - 0.74 Å.



Metal	l / Å	O-M-O (calc.) ^c / °	O-M-O (obs.) / °
Cu	1.927 ^a	84.9	93.5 ^a
Zn	2.043 ^b	79.0	89.0 ^b
Fe	2.003 ^b	80.9	88.3 ^b

Table 13 : "Natural" O-M-O bond angles based on the O-O bite distances in the free ligand, b (2.60 Å), and the observed M-O bond lengths

^a Average value of all copper(II) structures apart from KUGBOD

^b Average value of all structures

^c Calculated from $\sin \frac{\alpha}{2} = \frac{b}{2l}$, where α = O-M-O, b = bite distance in the free ligand and l = mean M-O bond length.

In contrast, the zinc complexes have a chelate bite distance (average 2.86 Å) significantly longer than in the free ligands but are still unable to achieve the ideal O-Zn-O angle of 109.5 °, presumably because the natural Zn-O bond is longer. The additional strain energy imposed on the ligand in opening up the bite for the zinc complex is in accordance with the observed selectivity of extraction (Cu(II) > Zn(II)) for these metals, as previously discussed.

The bite distances in the iron(III) structures are similar to those in the copper(II) complexes. A combination of factors is likely to account for this. The ionic radius⁶³ of high spin Fe(III) with coordination number 6 is slightly longer than a copper(II) complex with coordination number 4 (0.645 Å cf. 0.57 Å), and as the coordination number of the iron in the complexes is greater, it is expected that the "natural" Fe-O bond lengths in the pseudo-octahedral complexes will be longer. In order to accommodate the iron atom

with a reasonable O-Fe-O angle, the bite distance has to be increased more than for the copper complexes (Table 13).

A combination of significantly longer bite distances (by ca. 0.03 Å) and larger bite angles (by ca. 0.7 °) in LELDUB in comparison with the equivalent parameters in LELDOV, suggests that the ligands in LELDUB are trying to lie as far apart as possible and is perhaps surprising as the R₁ substituent in LELDUB (CH₃) is far less bulky than that in LELDOV (C₃H₇). This observation is likely to be a consequence of the *fac* arrangement of the ligands in LELDUB around the central iron atom in comparison with the *mer* arrangement in LELDOV, and, in turn, suggests that acyl pyrazolone ligands are flexible enough to distort to satisfy the requirements of the metal ion. Acyl pyrazolone ligands are not so flexible, however, that selectivity for copper(II) over iron(III), for example, is lost.

3.5.1.2.5 Dihedral Angles in the Coordinated Ligands

A final measure of the distortion in these metal complexes are the dihedral angles between the ring planes in the coordinated acyl pyrazolone ligands, which are presented in table 14. Study of the free ligand structures has shown that acyl pyrazolone ligands prefer to be as planar as possible in order to extend the π -electron delocalisation throughout their structure, and so such dihedral angles are a measure of how much the ligand must distort from its desired planarity on complexation to a metal ion. In the structures of the copper(II) and zinc(II) complexes of ligand **1**, it is clear that, as discussed previously, the overall distortion in the zinc(II) structure, **8**, is greater than that in the copper(II) structure, KUGBOD.

The structure of **11** merits more detailed analysis. The *cis* arrangement of the chelate units is different from that in all the other copper complexes and may be a consequence of the combination of bulky pyrazolone N-*t*-butyl and phenacyl groups. The phenyl groups of the phenacyl units in **11** are distorted further from the pyrazolone ring than those in the related N-phenyl structure, KUGBOD, and the CuO₄ unit is not planar (Table 11). The bulkiness of the substituents in **11** may also partially account for the copper

to oxygen bonds being significantly longer than in the other copper complexes (Table 10). From these results it can be predicted that ligand 4 might be a slightly weaker copper extractant than ligand 1, but in turn might show better selectivity for copper(II) over iron(III) due to the additional steric bulk of the N-*t*-butyl substituent.

Structure	Ligand ^a	Dihedral Angle between the pyrazolone ring planes ^b and the phenyl ring planes / °	
		N-Phenyl ^c	Phenacyl ^d
Copper(II)			
11 ^e	A, B	-	59.2, 85.9
KUGBOD ^f	A and B	16.6	50.3
JEXXAL ^f	A and B	6.5	-
FEKQAN ^f	A, B	9.8, 22.3	-
LIJVAB ^f	A, B	3.6, 8.0	-
Zinc(II)			
8 ^e	A and B	26.5	71.6
NOZSIE ^e	A, B	6.7, 13.9	-
Iron(III)			
LELDUB ^f	A, B, C	43.6, 35.4, 30.9	-
LELDV ^f	A, B, C	28.0, 4.5, 9.6	-

Table 14 : Dihedral angles between the pyrazolone ring plane and the phenyl ring planes (in °)

- ^a The structure of the ligands is defined in table 8
^b Pyrazolone ring plane defined by N1-N2-C3-C4-C5
^c N-phenyl ring plane defined by C11-C12-C13-C14-C15-C16
^d Phenacyl ring plane defined by C42-C43-C44-C45-C46-C47
^e Determined using SHELXTL⁵⁹
^f Determined using Cerius⁶⁰

The ligand units in both the structures JEXXAL and LIJVAB are the least distorted from total planarity, suggesting that these ligands allow copper(II) to adopt its preferred square planar geometry without having to bend

significantly out of the plane. The ligand distortions in the iron(III) complexes are significantly greater in LELDUB than LELDOV, which is again a consequence of the *fac* arrangement of the ligands around the central iron atom. In LELDOV only ligand A distorts significantly in order to accommodate all three ligands around the iron(III).

3.5.2 Pyrazolone Oximes

There are no known crystal structures of pyrazolone oxime free ligands or metal complexes in the literature¹⁸ (CCDC search performed October 1999), which is perhaps surprising as their synthesis and coordination chemistry have been previously studied²⁹⁻³³ and they are related to acyl pyrazolones, for which many structures have been determined¹⁸ (Section 3.5.1.1).

3.5.2.1 Free Ligands

As for acyl pyrazolones, pyrazolone oximes have four possible tautomeric forms (a-d), which are shown in figure 8. Previous studies³⁰⁻³³ have used solid state IR data to suggest that they adopt the enolic tautomeric form (b), and have a strong intramolecular hydrogen bond between the enolic proton and the nitrogen atom of the oxime group. In the absence of structural studies, however, these assignments cannot be confirmed. It is therefore of interest to examine the solid state structures of these ligands. Crystals of **12**, suitable for single crystal X-ray analysis and having the same morphology, were obtained from ethanol and toluene solutions. The structure of **12** is presented in figure 30. The form observed in the solid state is best represented by tautomer d (Figure 8) on the basis of both hydrogen positions and bond lengths. It should be noted that this tautomeric form has never been observed in structures of the closely related acyl pyrazolones.

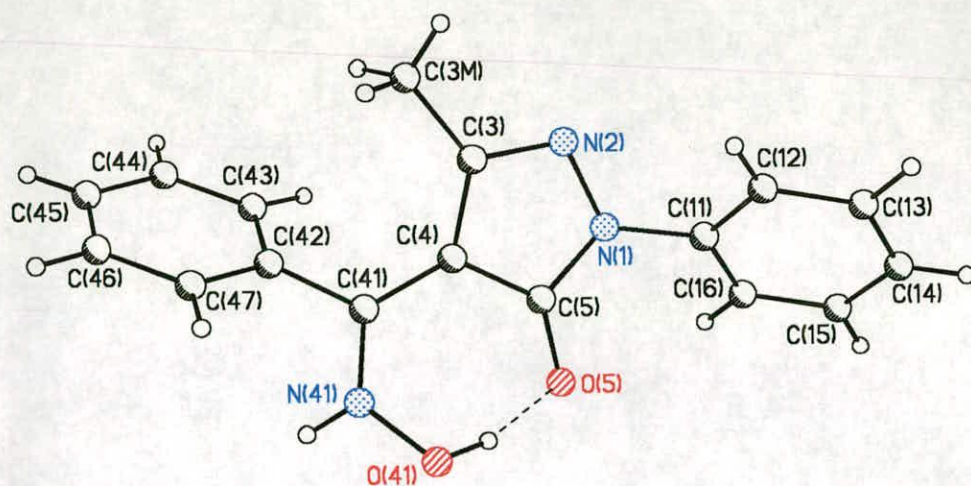


Figure 30 : Structure of pyrazolone oxime **12** showing the unusual Z configuration about the C41-N41 bond

Bond	O41-N41	N41-C41	C41-C4	C4-C5	C5-O5	N41-H _{N41}	O41-H _{O41}
Length	1.373(2)	1.310(2)	1.422(2)	1.429(2)	1.271(2)	0.863(19) ^a	0.94(3) ^a
Accepted Single and Double Bond Lengths⁵⁰							
Single	1.39(1) ^b	1.36(1)	1.46(2)	1.46(2)	1.33(2)	1.01(2)	0.97(1)
Double	1.22(1)	1.28(1)	1.32(2)	1.32(2)	1.21(1)	-	-

Table 15 : Bond lengths in the structure of **12** and relevant accepted bond lengths⁵⁰ (in Å)

^a Values determined using Platon 99⁵⁷

^b Specific value for oxime N-OH single bond lengths is 1.40(2) Å⁵⁰

It is clear that the tautomeric form of the ligand cannot be easily identified from the relevant bond lengths presented in table 15, and that the positions of the hydrogen atoms are essential in confirming the formal tautomer of the ligand. The structure is very delocalised with the bonds O41-N41, C41-C4 and C4-C5 possessing a large degree of single bond character, even though C41-C4 would be expected to be a double bond in tautomer **d**, while N41-C41 and C5-O5 are of intermediate character. This is assumed to be a consequence of the presence of the two hydrogen bonds found in this structure. The strong intramolecular hydrogen bond (1.54(3) Å) between O5 and H_{O41} will lengthen the formal double bond between C5 and O5, while

the intermolecular bond (2.022(19) Å) between H_N41 and N2 in adjacent molecules will directly effect N41-C41 and, to a lesser extent, O41-N41 and C41-C4. This intermolecular hydrogen bonding results in the formation of a linear, polymeric structure (Figure 31), illustrating the basicity of the nitrogen atom (N2) at the 2-position of the pyrazolone ring.

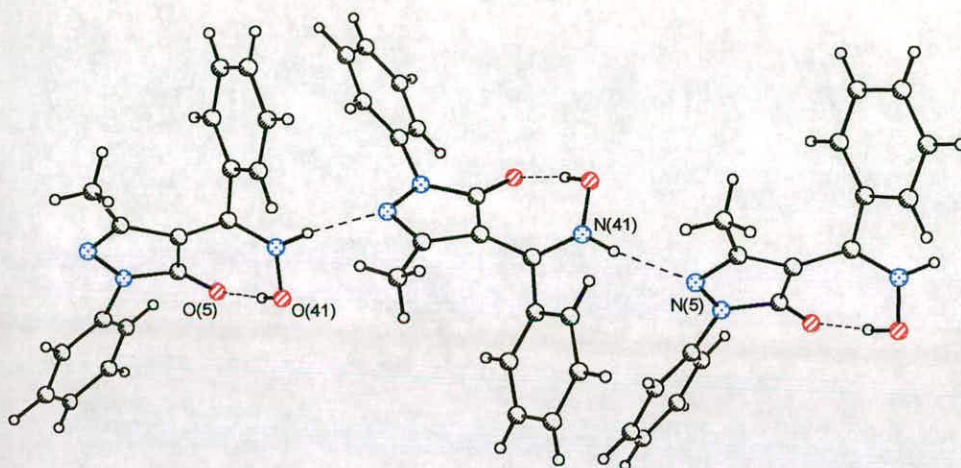


Figure 31 : Linear polymer of **12**

This N-H form of the oxime substituent (Figure 32) is very unusual¹⁸, the only other analogous, reported⁶⁴, X-ray structure being that of 2-(N-hydroxy)-aminomethylene-dimedone (Figure 33).

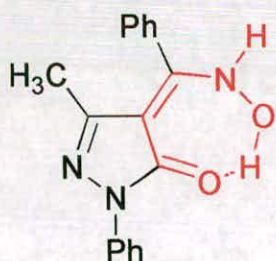


Figure 32 : NH form of oxime group (d)

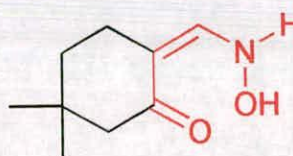


Figure 33 : Example of NH form

The results of calculations carried out by Dr. Michael Charlton (Avecia, Manchester) on the tautomeric forms of ligand **12** are presented in table 16. The structures of tautomers **a-d** were built and initially optimised using the SYBYL⁶⁵ modelling package and subsequently underwent further

optimisation using the MOPAC 93⁶⁶ program. The resulting gas phase structures were then used as input to the AMSOL⁶⁷ program, which calculates free energies of solvation. In addition to the tautomers shown in figure 8, similar calculations were performed for the structural conformers of tautomers **c** and **d**, in which the oxime OH substituent is hydrogen-bonded to the carbonyl oxygen atom at the 5-position of the pyrazolone ring.

Tautomer	Oxime OH Conformation	$\Delta H_f^{\text{gas}} / \text{kcal mol}^{-1}$	$\Delta H_f^{\text{H}_2\text{O}} / \text{kcal mol}^{-1}$	$\Delta H_f^{\text{Hexane}} / \text{kcal mol}^{-1}$
a : Ketone	non H-bonded	- 83.2	- 69.9	- 69.4
b : Enol	non H-bonded	- 88.9	- 76.9	- 73.1
c : Ring NH	non H-bonded	- 86.6	- 74.6	- 72.0
c : Ring NH	H-bonded	- 87.6	- 75.8	- 73.1
d : Oxime NH	non H-bonded	- 92.8	- 78.7	- 76.2
d : Oxime NH*	H-bonded	- 90.1	- 75.9	- 72.0

Table 16 : Theoretical heats of formation for tautomers **a-d** of ligand **12** in kcal/mol. The observed structure is denoted by *.

The structure observed in the solid state, **d**, was found to be the most stable of the four tautomers studied. It is surprising that the non hydrogen-bonded conformer was found to be more stable than its hydrogen-bonded analogue, however this may be due to the inability of such calculations to model hydrogen bonding accurately. The fact that the ΔH_f values in both water and hexane are similar suggests that, if borne out in practice, there might be equal partitioning of the ligand between the aqueous and hydrocarbon phases in a solvent extraction experiment.

3.5.2.2 Metal Complexes

The structures of four metal complexes of ligand **12** have been determined by X-ray crystallography and are listed in table 17.

Complex Number	Formula
17	[Cu(12-H) ₂ (DMF) ₂]
18	[Zn(12-H) ₂ (DMF) ₂]
19	[Ni(12-H) ₂ (DMF) ₂]
20	[Co(12) ₂ (MeOH) ₂](NO ₃) ₂

Table 17 : Metal complexes of the pyrazolone oxime ligand **12**

3.5.2.2.1 Mesomerism

The delocalisation of electrons in the deprotonated ligands of the metal complexes of **12** has been assessed by studying the lengths of the bonds in the chelate ring and these are presented in table 18.

Complex	N41-O41	C41-N41	C4-C41	C4-C5	C5-O5
17 Cu(II)	1.406(3)	1.291(3)	1.435(4)	1.408(3)	1.287(3)
18 Zn(II)	1.408(3)	1.292(4)	1.446(5)	1.407(4)	1.284(4)
19 Ni(II)	1.407(3)	1.290(4)	1.443(4)	1.408(4)	1.282(4)
20 Co(II)	1.409(3)	1.285(4)	1.473(4)	1.418(5)	1.270(4)
Average	1.408(1)	1.290(2)	1.449(12)	1.410(4)	1.281(5)
Accepted Single and Double Bond Lengths ⁵⁰ / Å					
Single	1.40(2) ^a	1.36(1)	1.46(2)	1.46(2)	1.33(2)
Double	1.22(1)	1.28(1)	1.32(2)	1.31(2)	1.21(1)

Table 18 : Bond lengths in the chelate ring of the coordinated ligands in complexes **17-20** (in Å). (^a Specific value for oxime N-OH⁵⁰)

It is clear that there is a much higher degree of electron localisation in the metal complexes than in the free ligand. From consideration of the relevant accepted bond lengths, it is also observed that the structures **17-20** are much less delocalised than the metal complexes of the acyl pyrazolones (Section 3.5.1.2.1). Bonds N41-O41 and N41-C41 can be classed as formal single and double bonds respectively, while C4-C41 has a very large degree of single bond character in **17-19** and is classed as a formal single bond in

20. The remaining bonds, C4-C5 and C5-O5 are both of intermediate character, as illustrated in figure 34. It is proposed that the electron densities in the bonds of the pyrazolone rings in **20** are likely to differ from those in the other complexes as a result of the protonation of N2.

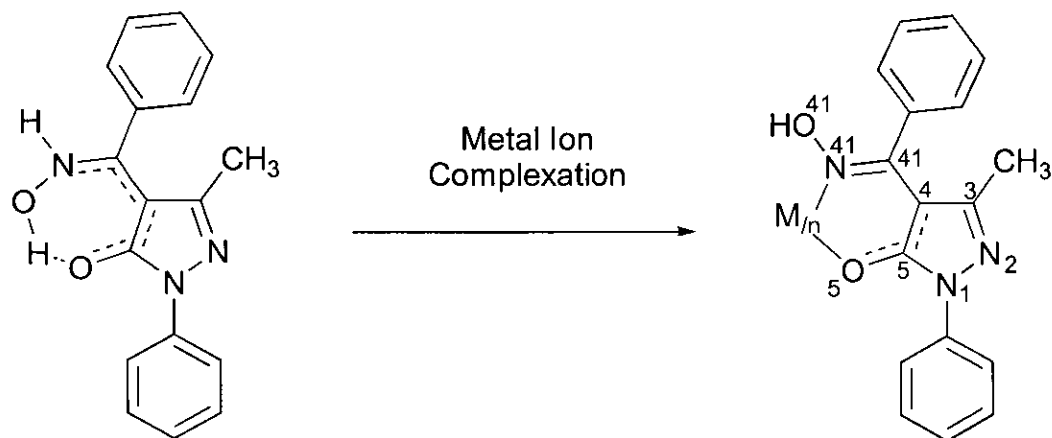


Figure 34 : Bonding changes within the chelate-ring of pyrazolone oximes on metal ion complexation

3.5.2.2.2 Hydrogen Bonding

As previously discussed in section 3.1.2, it is *theoretically* possible to form preorganised dimers of pyrazolone oxime free ligands, even though this was not observed in the solid state structure of **12**. It should also be remembered that this phenomenon was seen in the free ligand structures of only two P50-type oximes^{68,69}. It was still hoped, however, that on metal ion complexation the pyrazolone oxime ligands would form a pseudomacrocyclic arrangement around the metal atom *via* the formation of two inter-ligand hydrogen bonds. This structural motif has been seen in 14 published structures of metal complexes of P50-type oximes¹⁸, of which four are of copper(II)⁷⁰⁻⁷³, three of nickel(II)⁷⁴⁻⁷⁶, three of cobalt(III)^{77,78}, two of palladium(II)^{79,80} and one each of zinc(II)⁸¹ and gallium(III)⁸². This pseudomacrocyclic arrangement is thought to enhance the stability of such complexes thus promoting the solvent extraction of, in particular, metal ions which favour a square planar geometry

such as copper(II), nickel(II) and palladium(II). The structure of the copper(II) complex of 2-hydroxybenzaldehyde oxime⁷³ is shown in figure 35.

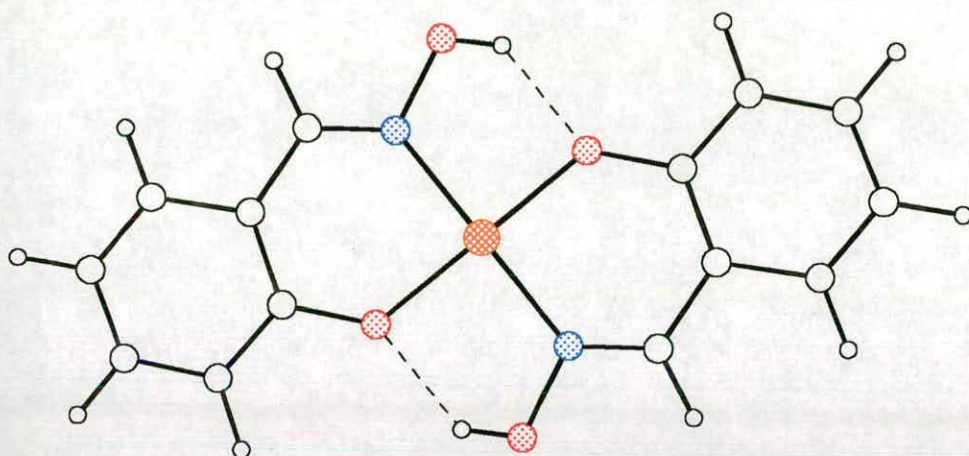


Figure 35 : Structure of the copper(II) complex of 2-hydroxybenzaldehyde oxime⁷³

All the complexes, **17-20**, reported here have distorted octahedra with the equatorial coordination plane made up of the metal ion plus the four donor atoms of the two coordinated oxime ligands. The two axial coordination sites are occupied by oxygen atoms from two types of solvent molecule, DMF in **17-19** and methanol in **20**. It should be noted that this geometry is not seen in the structures of complexes of P50-type oximes with the same metal ions. However in the P50-type structures there are intermolecular interactions, eg: between the oxime groups on adjacent molecules in the solid state. In all four structures, **17-20**, there are two strong inter-ligand hydrogen bonds between H_O41 and O5, the parameters of which are listed in table 19. These bonds define the desired, pseudomacrocyclic framework around the central metal atom thus promoting planarity of the MN₂O₂ coordination plane. The metal atoms lie on centres of inversion, hence the two coordinated oxime ligands and the two coordinated solvent molecules in each structure are equivalent.

Parameter	17 Cu(II)	18 Zn(II)	19 Ni(II)	20 Co(II)
Length H...O / Å	1.918(3)	2.005(3)	1.965(3)	1.93(4)
Length O...O / Å	2.855	2.921	2.900	2.940
Angle O-H...O / °	137.0(2)	140.2(3)	140.3(3)	151(4)
P50-type O...O / Å	2.59	2.77	2.53	2.50 ^a

Table 19 : Inter-ligand hydrogen bond parameters and average O...O distances in the structures of metal complexes of P50-type oximes^{70-78,81}

^a These complexes all contain cobalt(III)

It is clear from these data that the hydrogen bonds in the metal complexes of P50-type oximes are much shorter than those in 17-20, which suggests that pyrazolone oximes cannot fit as closely around the central metal ion as phenolic oximes. The reasons for this observation will be discussed in the following sections and summarised in 3.5.2.2.6. The structure of the copper(II) complex, 17, showing the inter-ligand hydrogen bonds is shown in figure 36.

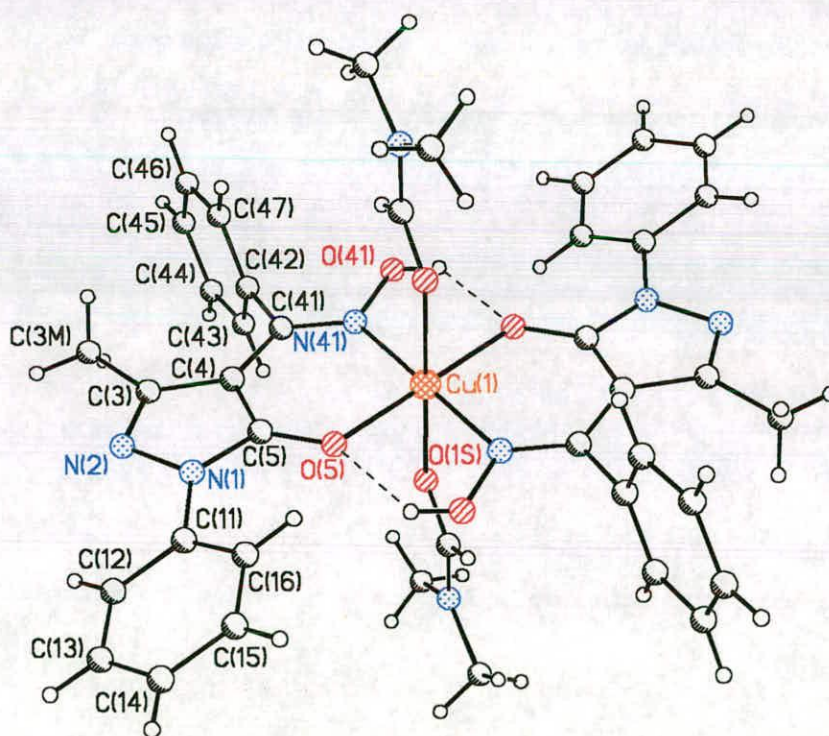


Figure 36 : Structure of $[\text{Cu}(\text{12-H})_2(\text{DMF})_2]$: 17

It should be noted that in **20**, the cobalt(II) has not been oxidised to the kinetically inert cobalt(III) on complexation. The pyrazolone rings are protonated at N2 and the 2+ charge on the metal ion is balanced by the presence of two nitrate anions, which are hydrogen-bonded to the two coordinated methanol molecules. This may have implications in the stripping section of a solvent extraction circuit, as this ligand could potentially transfer acid into the organic phase. The structure of **20** is shown in Figure 37.

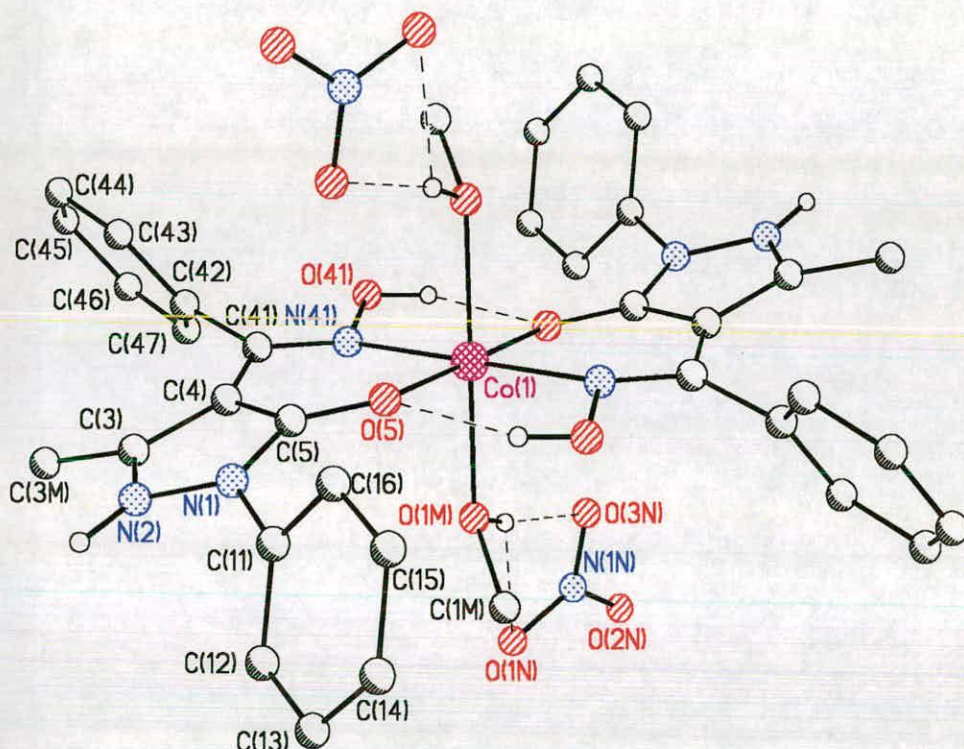


Figure 37 : Structure of $[\text{Co}(\mathbf{12})_2(\text{MeOH})_2](\text{NO}_3)_2$: **20**. All hydrogen atoms, apart from those involved in hydrogen bonding, have been omitted for clarity. There are no known cobalt(II) complexes for P50-type ligands¹⁸, which suggests that pyrazolone oxime ligands are able to stabilise the lower oxidation state. This may be due to the fact that these ligands are neutral, forming a dicationic $[\text{Co}(\text{LH})_2(\text{MeOH})_2]^{2+}$ complex, which is counterbalanced by the two nitrate anions, and the difficulty in oxidising this essentially dicationic complex to cobalt(III) thus forming a tricationic species. It is interesting to note that the C5-O5 bonds (1.270(4) Å) are much longer than a formal carbonyl bond (1.21(1) Å⁵⁰), while the Co-O bonds are somewhat

shorter than might be expected from complexation to a neutral donor. Both these observations are likely to be due to the effect of the pseudomacrocyclic motif on the delocalisation of the bonding in this structure. The formation of bifurcated intermolecular hydrogen bonds from the methanol OH and the NH at the 2-position in the pyrazolone ring to the nitrate anions results in the formation of chains in the crystal packing of **20**, as shown in figure 38.

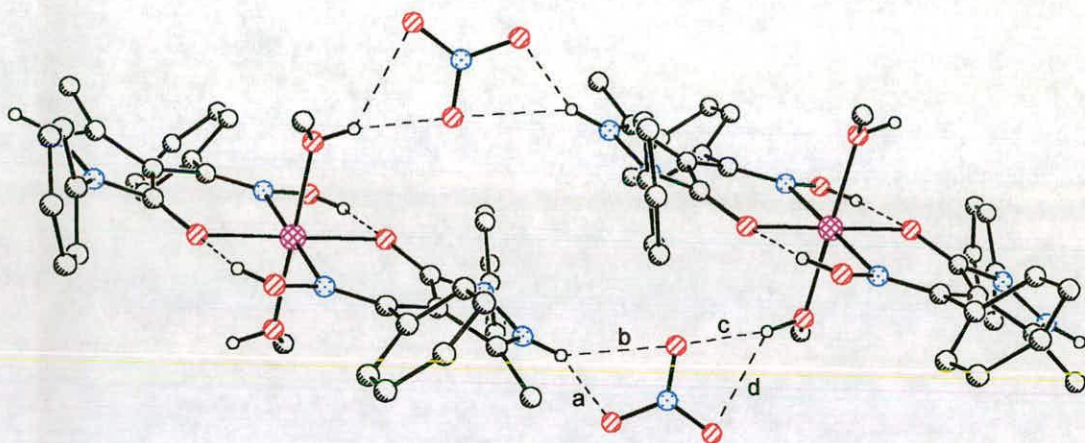


Figure 38 : Crystal packing of **20**

The lengths of the hydrogen bonds to the nitrate anions (a-d) are 1.85(2), 2.41(6) and 2.02(6) and 2.42(6) Å respectively.

3.5.2.2.3 Metal to Donor Atom Bond Lengths

The metal to donor atom distances in **17-20** are presented in table 20.

Bond	Ligand	17 Cu(II)	18 Zn(II)	19 Ni(II)	20 Co(II)
M-O5	A & B ^a	1.965(2)	2.053(2)	2.037	1.999(2)
M-N41	A & B ^a	1.973(2)	2.034(2)	2.008(2)	2.090(3)
M-O	Solvents (C)	2.454(3)	2.226(3)	2.120(2)	2.130(3)
P50-type Ligands		Cu(II)	Zn(II)^b	Ni(II)	Co(III)^c
M-O	Average	1.893	2.044	1.831	2.17
M-N	Average	1.955	2.041	1.875	2.16

Table 20 : Metal to donor atom bond lengths in the complexes **17-20** and in the complexes of P50-type oxime ligands (in Å)

- a An inversion centre coincident with the metal atom relates the two ligands A and B
- b This structure contains square pyramidal zinc(II)
- c These structures contain square pyramidal cobalt(III)

The metal to nitrogen and metal to oxygen bonds have very similar lengths in the pyrazolone oxime complexes **17-19**, in contrast with the planar copper(II) and nickel(II) complexes of the phenolic oximes, which have significantly shorter bonds to the phenolic oxygen atoms. This may be a consequence of the different bites defined by the two different ligand types (see later).

A comparison between the bond lengths in the coordination spheres of the complexes of pyrazolone oximes and phenolic oximes given in table 20 suggests that in general the pyrazolone oxime bonds to the given metal are longer. Interpretation of this difference needs to take into account the fact that the coordination numbers are also different. In particular, the nickel(II) pyrazolone oxime complex (**19**) is pseudo-octahedral, and is therefore expected to have longer metal to donor bond lengths than in the square planar nickel(II) complexes of phenolic oximes. Additionally, zinc(II) might be expected to adopt a tetrahedral geometry, but is also found to be pseudo-octahedral in **18** (Figure 39). The longest metal to donor atom bond lengths in **17-20** are those involving the oxygens of the coordinated solvent molecules. These distances are longest in the copper(II) complex, **17**, as expected, as the molecule shows a tetragonal distortion in accordance with the Jahn-Teller theorem, which results in Cu-O_{DMF} distances of 2.454(3) Å.

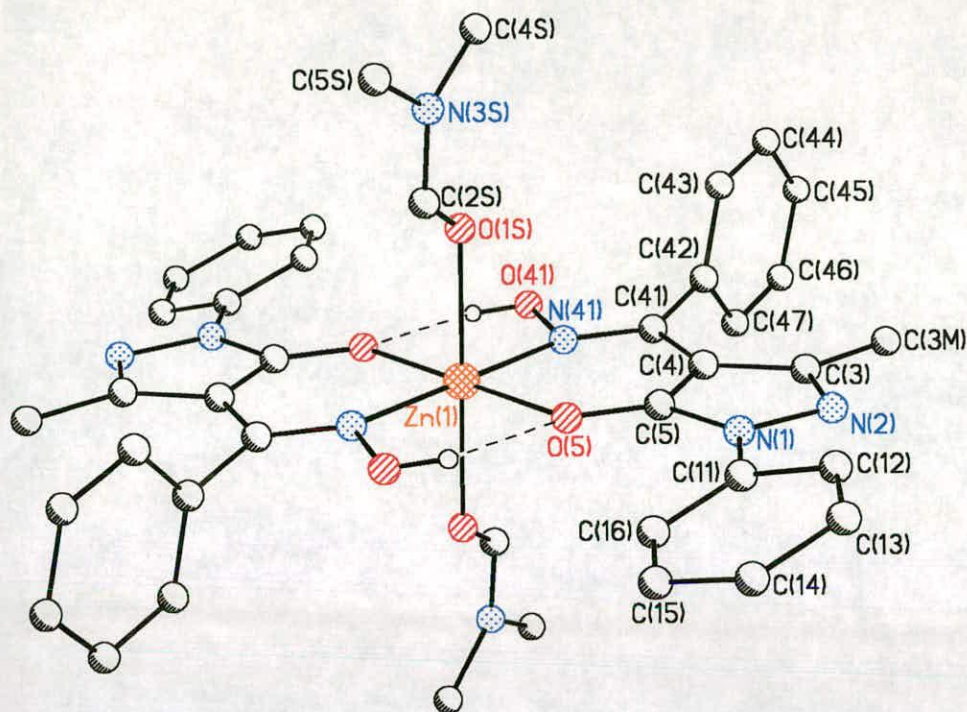


Figure 39 : Structure of $[\text{Zn}(\text{12-H})_2(\text{DMF})_2]$: **18**. Hydrogen atoms not involved in hydrogen bonding have been omitted for clarity.

3.5.2.2.4 Bite Angles and Bite Distances

The bite angles and bite distances in **17-20** are presented along with the average bite distances in the complexes of P50-type oximes^{70-78,81} for each type of metal cation in table 21.

Ligand	17 Cu(II)	18 Zn(II)	19 Ni(II)	20 Co(II)
Bite Angles (O5-M-N41) / °				
A & B	92.50(8)	91.21(10)	91.59(9)	91.90(10)
P50-type	91.2	87.5 ^a	92.6	91.9 ^b
Bite Distances (O5-N41) / Å				
A & B	2.844(3)	2.920(4)	2.900(3)	2.939(3)
P50-type	2.75	2.83 ^a	2.68	2.70 ^b

Table 21 : Bite angles (in °) and bite distances in the complexes **17-20** and bite distances in the metal complexes of P50-type oximes (in Å)

^a This structure contains square pyramidal zinc(II)

^b These complexes contain cobalt(III)

All the observed bite angles are close to 90° , matching the coordination requirements of the pseudo-octahedral metal ions, and are effectively provided by the six-membered chelate ring of the pyrazolone oxime ligands. The bite distances vary in a sequence $\text{Co(II)} > \text{Ni(II)} > \text{Cu(II)} < \text{Zn(II)}$, which correlates with the Irving-Williams order and reflects the variation of strength of bonding to the different metal ions. The much shorter bonds to copper in the N_2O_2 plane ensure that this metal can be readily accommodated in the pyrazolone oxime cavity with minimal opening up of the “natural” bite of the ligand. In the free ligand **12** the bite distance is longer (3.026 Å) than those observed in the metal complexes, however, this is not of great significance because the Z-configuration about the “imine” bond in the free ligand (Figure 30) has to be changed to an E-form to allow metal complex formation. The five-membered pyrazolone ring fused to the chelate ring will increase the “natural” bite distance of the ligand, in comparison with the fused six-membered ring in the P50-type complexes, as illustrated in figure 40.



Figure 40 : The effect of fused five- and six-membered rings on ligand bite size

The bite distances in the P50-type ligands do not follow the order predicted by the Irving-Williams rules, but instead show the smallest bite for nickel(II) ($\text{Co(III)} > \text{Ni(II)} < \text{Cu(II)} < \text{Zn(II)}$). This is a consequence of the square planar nickel(II) complex being in the low spin form, for which the metal-donor bonds are significantly shorter than in the other complexes (Table 20). It is important to remember, however, that these two sets of complexes cannot be directly compared in this way, as that the Irving-Williams rules relate specifically to divalent metal ions in pseudo-octahedral complexes.

3.5.2.2.5 Dihedral Angles

In order to assess how far the planarity extends away from the central coordination sphere (MN_2O_2) to the rest of the molecule in **17-20**, the dihedral angles between the chelate plane (defined as the best fit plane through M, O5, C5, N1, N2, C3, C4, N41, N42) and the two phenyl ring planes (defined as the best fit planes through C11-C16 and C42-C47) were determined and are presented along with the mean deviation from total planarity of the chelate plane in table 22.

Ring Plane	17 Cu(II)	18 Zn(II)	19 Ni(II)	20 Co(II)
N-phenyl ^a	20.6	18.8	18.6	60.4
Phenacyl ^b	91.9	91.6	90.9	63.0
Mean Deviation from Total Planarity of Chelate Plane^c / Å				
-	0.02	0.02	0.03	0.13

Table 22 : Dihedral angles (in °) between the phenyl ring planes and the chelate plane^c and mean deviations from total planarity of the chelate plane (in Å) in the complexes **17-20**

^a Best fit plane through C11, C12, C13, C14, C15, C16

^b Best fit plane through C43, C44, C45, C46, C47, C48

^c Best fit plane through M, O5, C5, N1, N2, C3, C4, N41, N42

The ligands in structures **17-19** show similar deviations from planarity, as would be expected, as they are isostructural containing only differing metal atoms as illustrated in figures 35, 38 and 40. The dihedral angles between the chelate plane and the N-phenyl plane are *ca.* 20 °, while those between the chelate plane and the phenacyl plane are *ca.* 90 °. Additionally, the pyrazoyl ring plane is almost totally coplanar with the chelate plane in **17-19**, the dihedral angle between these two planes being less than 1 ° in all three structures.

The equivalent angles in the cobalt(II) complex, **20**, are very different. The dihedral angles between the chelate plane and the N-phenyl and phenacyl ring planes are both approximately 60 °, while that between the chelate plane and the pyrazoyl ring plane is 8 °. These values reflect the very

different electronic structures in the ligands, which accompany the protonation of the pyrazolone nitrogen atom (N2). There is now very little conjugation between the N-phenyl group and the pyrazolone ring, or equally between the phenacyl oxime group and the pyrazolone ring, and the C4-C41 bond is close to the expected single bond value of 1.46(2) Å (Table 18).

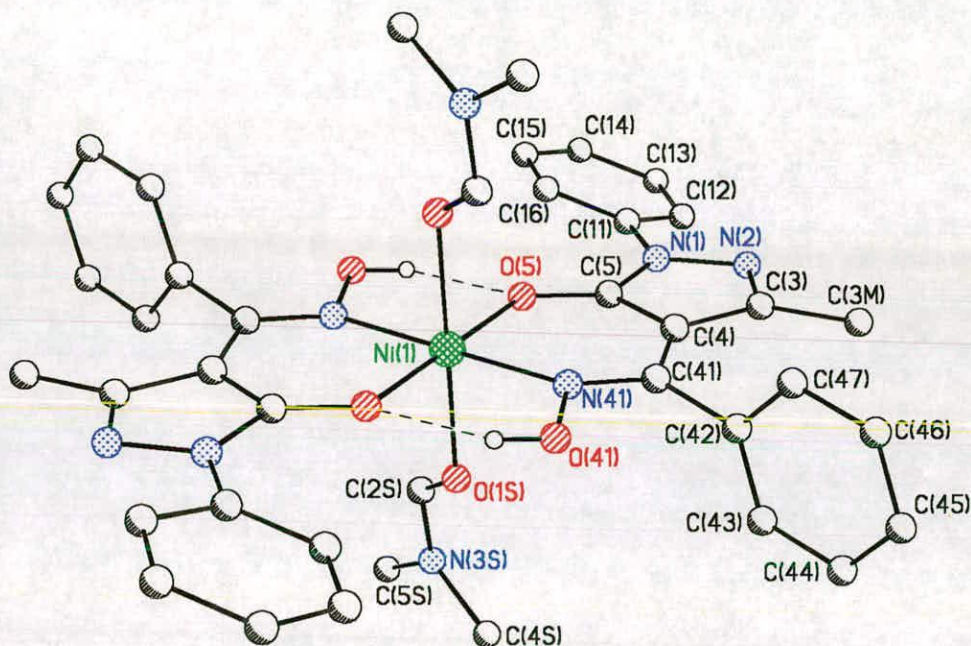


Figure 41 : Structure of $[\text{Ni}(\text{12-H})_2(\text{DMF})_2]$: **19**. Hydrogen atoms not involved in hydrogen bonding have been omitted for clarity.

3.5.2.2.6 Differences between the Structures of Metal Complexes of P50-type Oxime and Pyrazolone Oxime Ligands

A comparison of the observed bite distances (b in Figure 42) and the O...O hydrogen bond contacts (a in Figure 42) using the data given in Tables 19 and 21 initially suggests that the bonding cavities provided by the pyrazolone oximes are larger than those of the phenolic oximes. This observation does not accord with the observed greater "strength" of the pyrazolone ligands as extractants for copper(II) (Section 3.4.1) and probably

arises because the comparisons made in Tables 19 and 21 involve complexes with different coordination numbers.

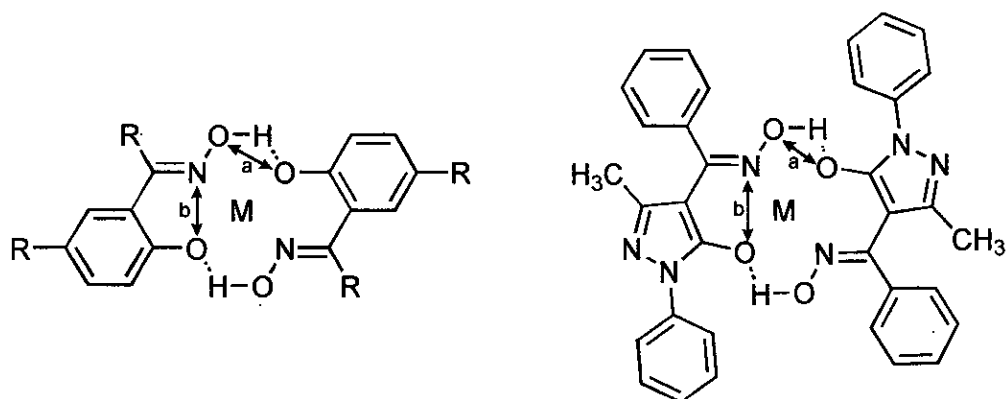


Figure 42 : Comparison of the observed cavity sizes in the pseudomacrocyclic pyrazolone oxime complexes 17-20 with those of the P50-type complexes

All the structures of the pyrazolone oxime complexes involve six-coordinate, pseudo-octahedra, for which the ionic or covalent radii of the complexed metals are greater than those of the four- or five-coordinate forms of the metals in the determined structures of the phenolic oximes complexes. It would therefore be useful to attempt to crystallise the copper and nickel complexes of ligand 12 in the absence of coordinating solvents to obtain four-coordinate planar complexes thus allowing direct comparison to be made with the literature structures of the phenolic oximes.

3.6 Conclusions

The work presented in this chapter set out to identify candidates as replacement solvent extractants for P50, which were not based on an alkyl phenol precursor. Pyrazolone oximes have been shown to mimic P50-type oximes in providing a pseudomacrocyclic motif based on inter-ligand hydrogen bonding, which imposes a planar geometry on the MN_2O_2 coordination sphere. In fact, the extractive strength of pyrazolone oximes for copper(II) was found to be too high for them to replace P50 in conventional circuits and additionally they showed surprisingly low selectivity for copper(II) over iron(III). It is possible that the strength of pyrazolone oximes

as copper extractants could be reduced *via* the use of modifiers, as discussed in section 1.5, however the selectivity issue could not be rationalised by studying structural data as no X-ray structures of iron(III) complexes of pyrazolone oximes exist in the literature or were determined during the course of this work. Additionally, the structure of the cobalt complex **20** suggests that problems might be encountered with the use of these ligands as solvent extractants, due to the ability of the basic pyrazolone ring nitrogen atoms to protonate forming a dicationic species, the charge of which must be counterbalanced to form a neutral species. This could potentially lead to acid transfer in the stripping section of a solvent extraction circuit, and it would therefore be important to determine the pK_a values of both the pyrazolone oxime free ligands and metal complexes to assess the probability of this occurring. The protonation is likely to be accompanied by a lowering of solubility of both the ligands and the complexes in the hydrocarbon phase, which could cause additional operational problems.

Acyl pyrazolones, which were initially predicted to be too weak to be used as solvent extractants for copper(II) in existing acid leach circuits, have been found to extract and strip copper(II) efficiently and selectively from sulphate media. Their good selectivity for copper(II) over iron(III) could be predicted on the basis that difficulties in fitting three ligands around the central metal ion to form a FeL_3 complex might be encountered, but an analysis of published structures of iron(III) complexes of acyl pyrazolones showed that the steric strain in these structures was not as great as initially predicted, and so this selectivity data is really quite surprising, but nonetheless very encouraging.

Development work incorporating studies on the stability, solubility, phase disengagement properties and extraction kinetics of both types of ligand is required to assess the real potential of acyl pyrazolones and pyrazolone oximes as solvent extractants, and such work will be carried out at Avecia.

3.7 Experimental

3.7.1 Instrumentation

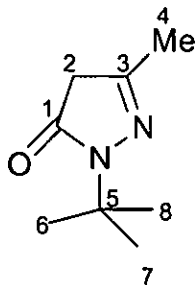
Melting points were determined with a Gallenkamp apparatus and are uncorrected. Elemental analysis was performed on a Perkin Elmer 2400 elemental analyser. IR spectra were obtained on a Perkin Elmer Paragon 1000 FT-IR spectrometer as potassium bromide discs or as liquid thin films. ^1H and ^{13}C NMR spectra were run on Bruker WP200, AC250 and DPX300 spectrometers. Chemical shifts (δ) are reported in parts per million (ppm) relative to residual solvent protons as internal standards. Electron impact (EI) mass spectra were obtained either on a Finnigan MAT4600 quadrupole spectrometer or on a Kratos MS50TC spectrometer. Fast atom bombardment (FAB) mass spectra were obtained on a Kratos MS50TC spectrometer in acetonitrile / 3-nitrobenzyl alcohol / thioglycerol matrices. Electrospray (ES) mass spectra were obtained on a Thermoquest LCQ spectrometer. Inductively coupled plasma atomic emission spectroscopy (ICP-AES) analysis was performed on a Thermo Jarrell Ash Iris ICP-AES spectrometer. Magnetic susceptibilities were measured for the paramagnetic complexes **7**, **9-11**, **17**, **19-22**, **24** and **25** using a Johnson Matthey magnetic susceptibility balance and molar susceptibilities were corrected for diamagnetism using Pascal's constants⁸³.

3.7.2 Solvent and Reagent Pretreatment

All reagents and solvents were commercially available (Acros or Aldrich) and were used as received, apart from the starting pyrazolone, 3-methyl-1-*tert*-butyl-5-pyrazolone, which was synthesised as described according to the literature method of Butler and DeWald⁸⁴. Solvents used for analytical purposes (NMR, MS) were of spectroscopic grade.

3.7.3 Synthesis of Starting Pyrazolones

3-Methyl-1-*tert*-butyl-5-pyrazolone⁸³



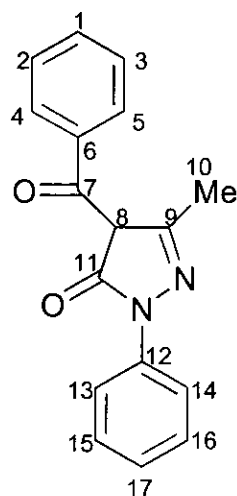
Triethylamine (41.8 ml, 0.3 mol) was added to a colourless solution of *tert*-butylhydrazine hydrochloride (27.41 g, 0.22 mol) in methanol (200 ml). The resulting colourless solution was cooled to 0 °C and ethylacetoacetate (25.5 ml, 0.2 mol) was added dropwise at such a rate as to maintain a temperature of 0 °C. Stirring at this temperature was continued for 4 h and the reaction medium was then heated under reflux for 72 h. The solvent was removed using a rotary evaporator to leave a pale yellow solid, which was washed with petroleum ether (40-65 °C) to give a cream-coloured powder (29.57 g, 87.13 %). mp 109 - 111 °C; (Found C, 57.02; H, 10.64; N, 14.03; C₈H₁₄N₂O.1¼CH₃OH requires C, 57.18; H, 9.88; N, 14.42 %); IR (cm⁻¹, KBr Disc): ν 2979.3s / 2943.6m (CH), 2677.4m (OH), 1594.1s (C=N), 1397.8s (C(CH₃)₃), 1036.7m (C-O); ¹H NMR (CDCl₃, 250 MHz): δ 1.34 (s, 9H, C(CH₃)₃), 1.91 (m, 3H, CH₃), 2.95 (s, 2H, CH₂); ¹³C NMR (CDCl₃, 63 MHz): δ 16.53 (C-4), 27.84 (C-6,7,8), 43.08 (C-2), 56.77 (C-5), 153.21 (C-3), 172.06 (C-1); EIMS 154 (39.5 %, LH), 139 (100.0 %, LH - CH₃), 98 (90.5 %, LH - C(CH₃)₃), 56 (81.5 %, C(CH₃)₃).

3.7.4 Acyl Pyrazolones

3.7.4.1 Synthesis of Ligands

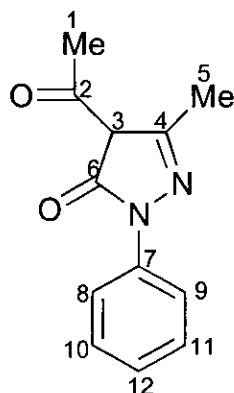
Ligands **1**, **5** and **6** were prepared as described for **1** by reaction of 3-methyl-1-phenyl-5-pyrazolone with the appropriate acyl chloride according to the method of Jensen³⁴.

4-Benzoyl-3-methyl-1-phenyl-5-pyrazolone (1)



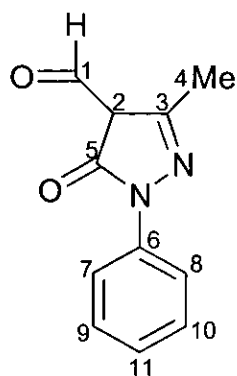
3-Methyl-1-phenyl-5-pyrazolone (15.0 g, 0.09 mol) was dissolved in hot dioxane (80 ml) with stirring. Calcium hydroxide (12.0 g, 0.16 mol) was added to the resulting yellow solution to give a pale yellow suspension, to which was added benzoyl chloride (9.9 ml, 0.09 mol) dropwise with stirring. The reaction mixture became darker in colour and more viscous and was subsequently heated under reflux for 30 min. After cooling to room temperature, the reaction medium was added portionwise with vigorous stirring to cold 2 M hydrochloric acid (200 ml). The resulting grainy beige precipitate was isolated by filtration and recrystallised from methanol / water (450 ml / 75 ml) to yield beige, feathery crystals of **1** (21.446 g, 86.67 %). mp 118-120 °C; (Found C, 73.67; H, 5.14; N, 10.24; C₁₇H₁₄N₂O₂ requires C, 73.36; H, 5.08; N, 10.07 %); IR (cm⁻¹, KBr Disc): ν 2579.8br s (OH & CH), 1645.4s (C=O), 1597.1m (C=N); ¹H NMR (CDCl₃, 200 MHz): δ 2.09 (s, 3H, CH₃), 7.25 - 7.34 (tt, J_{ortho} 7.47Hz, J_{meta} 2.44 Hz, 2H, *m*-ArH on N-Ph), 7.41 - 7.66 (m, 5H, ArH), 7.863 - 7.89 (dd, J_{ortho} 8.47Hz, 2H, *o*-ArH on N-Ph), 9.59 (br s, 1H, OH); ¹³C NMR (CDCl₃, 63 MHz): δ 15.73 (C-10), 103.46 (C-8), 120.68 / 126.58 / 127.75 / 128.30 / 131.77 (C 1-5, 13-17), 137.08 & 137.47 (C-6,12), 147.85 (C-9), 161.31 (C-11), 191.94 (C-7); EIMS *m/z* 278 (100.0 %, LH), 201 (26.4 %, LH-Ph), 105 (40.2 %, Ph-C=O), 77 (38.7 %, Ph).

4-Acetyl-3-methyl-1-phenyl-5-pyrazolone (2)^{35,36}



Sodium carbonate (6.36 g, 0.06 mol) was added with stirring to a yellow solution of 3-methyl-1-phenyl-5-pyrazolone (5.226 g, 0.03 mol) in THF (30 ml). Acetyl chloride (2.35 ml, 0.033 mol) was added dropwise to the yellow suspension and the reaction medium was subsequently heated under reflux for 24 h, during which time it became orange / brown in colour. The resulting suspension was cooled to room temperature and added portionwise to cold 2 M hydrochloric acid (200 ml). The resulting orange needles of **2** (1.448 g, 22.32 %) were filtered from the solution. mp 56 - 58 °C; (Found C, 66.01; H, 5.65; N, 12.70; C₁₂H₁₂N₂O₂·1/8H₂O requires C, 65.96; H, 5.66; N, 12.82 %); IR (cm⁻¹, KBr Disc): ν 3387.5w (OH), 1639.6s (C=O), 1591.5s (C=N), 1500.4s (C=C), 750.5s (Ar CH); ¹H NMR (CDCl₃, 200 MHz): δ 2.43 (s, 3H, CH₃), 2.45 (s, 3H, CH₃C=O), 7.21 - 7.30 (tt, 1H, *p*-ArH), 7.37 - 7.47 (tt, 2H, *m*-ArH), 7.77 - 7.84 (dd, 2H, *o*-ArH), 11.67 (br s, 1H, OH); ¹³C NMR (CDCl₃, 63 MHz): δ 15.36 (C-5), 26.47 (C-1), 104.04 (C-3), 120.45 (C-10,11), 126.42 (C-12), 128.93 (C-8,9), 136.98 (C-7), 147.52 (C-4), 160.22 (C-6), 194.19 (C-2); EIMS m/z 216 (86.5 %, LH), 201 (100.0 %, LH - CH₃), 91 (23.1 %, PhN), 77 (60.1 %, Ph).

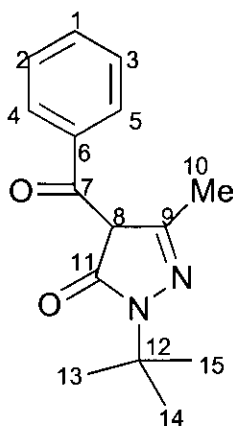
4-Formyl-3-methyl-1-phenyl-5-pyrazolone (**3**)³⁷



A pale yellow suspension of 3-methyl-1-phenyl-5-pyrazolone (8.71 g, 0.05 mol) in DMF (10.05 ml, 0.13 mol) was cooled to 0 °C in an ice bath. Phosphoryl chloride (5.59 ml, 0.06 mol) was added dropwise at such a rate that a temperature of 10-20 °C was maintained. The "gel-like", yellow reaction medium was heated on a steam bath for 1½ h, after which time the resulting orange / brown "syrup" was poured into ice water (40 ml) with vigorous stirring. The resulting yellow suspension was left to stand overnight and then filtered to give pale yellow, fibrous microcrystals of **3** (8.75 g, 86.60 %). NB : the product was not recrystallised due to previous difficulties encountered with the formation of an orange, dimeric by-product. mp 152 - 154 °C; (Found C, 65.56; H, 4.97; N, 13.97; C₁₁H₁₀N₂O₂ requires C, 65.33; H, 4.99; N, 13.86 %); IR (cm⁻¹, KBr Disc): ν 2715.7br m (CHO & OH), 1666.9m (C=O), 1636.0s (C=N), 1499.4m (C=C); ¹H NMR (DMSO-d₆, 200 MHz): δ 2.34 (s, 3H, CH₃), 7.24 - 7.33 (tt, J_{ortho} 7.43 Hz, J_{meta} 1.17 Hz, 1H, *p*-ArH), 7.42 - 7.52 (tt, J_{ortho} 7.42 Hz, 2H, *m*-ArH), 7.67 - 7.73 (dd, J_{ortho} 8.61 Hz, 2H, *o*-ArH), 9.59 (s, 1H, CH), 11.57 (br s, 1H, OH); ¹³C NMR (DMSO-d₆, 63 MHz): δ 14.06 (C-4), 105.50 (C-2), 121.32 (C-9,10), 126.31 (C-11), 129.16 (C-7,8), 137.35 (C-6), 149.12 (C-3), 158.98 (C-5), 181.58 (C-1); EIMS *m/z* 202 (100.0 %, LH), 185 (41.6 %, LH - OH), 91 (23.3 %, PhN), 77 (41.0 %, Ph).

4-Benzoyl-3-methyl-1-*tert*-butyl-5-pyrazolone (4)

The conventional method of ligand preparation³⁴ gave an impure product, which was subsequently purified *via* copper complexation (11) and stripping to yield 4.



Calcium hydroxide (2.134 g, 0.029 mol) was added with stirring to a yellow solution of 3-methyl-1-*tert*-butyl-5-pyrazolone (2.50 g, 0.0162 mol) in dioxane (20 ml). Benzoyl chloride (1.86 ml, 0.0162 mol) was added dropwise with vigorous stirring to the suspension, which was then heated under reflux for 2 h. Addition of the resulting dark brown suspension to cold 2 M hydrochloric acid (35 ml) gave a light brown oil. This was extracted into DCM (50 ml) to give an orange solution, which was separated, dried (anhydrous magnesium sulphate), filtered and reduced in volume using a rotary evaporator to leave a dark orange / brown oil. Attempts to isolate a pure product were unsuccessful, therefore the diketone was purified *via* complexation with copper(II).

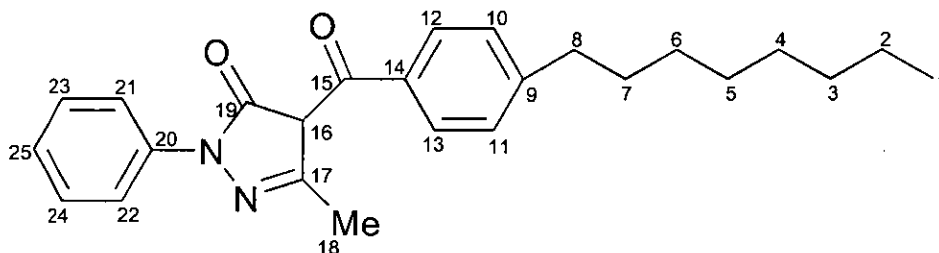
[Cu(4-H)₂(MeOH)₂] (11)

Copper(II) acetate monohydrate (1.617 g, 8.1 mmol) was added to a red / brown solution of the impure diketone (4.185 g, 0.0162 mol : taken as 100 % reaction) in methanol (70 ml). The resulting dark green suspension was stirred at room temperature for 15 min and then filtered to afford bottle green crystals, (1.270 g, 53.26 %). mp 196 - 198 °C; (Found C, 60.81; H, 5.86; N,

9.08; $C_{30}H_{34}N_4O_4Cu \cdot CH_3OH$ requires C, 61.01; H, 6.29; N, 9.18 %); IR (cm^{-1} , KBr Disc): ν 3490.5w (OH), 2977.3w & 2929.8w (CH), 1585.6s (C=N), 1441.0m & 1371.8m ($C(CH_3)_3$); FABMS m/z 898 (27.6 %, Cu_2L_3), 579 (81.5 %, CuL_2), 320 (80.8 %, CuL), 265 (100.0 %, $CuL - C(CH_3)_3$), 203 (59.8 %, $LH - C(CH_3)_3$), 77 (90.2 %, Ph); μ_{eff} 2.05 B.M

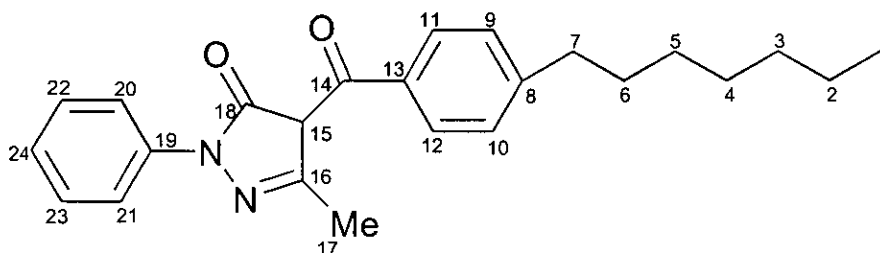
11 (1.270 g, 2.1 mmol), was dissolved in toluene (50 ml) and the resulting green solution contacted with 7 M sulphuric acid (70 ml). This gave a yellow organic phase and a pale blue aqueous phase. The two phases were separated and the organic phase was dried (anhydrous magnesium sulphate), filtered and reduced in volume using a rotary evaporator to afford yellow crystals of 4 (0.560 g, 53.97 %). mp 42 - 44 °C; (Found C, 67.24; H, 7.19; N, 10.08; $C_{15}H_{18}N_2O_2 \cdot \frac{1}{2}H_2O$ requires C, 67.38; H, 7.18; N, 10.48 %); IR (cm^{-1} , KBr Disc): ν 2984.4m (CH), 2671.7br m & 2554.7br m (OH & CH), 1602.7s (C=O), 1558.4s (C=N), 1420.1m & 1370.8m ($C(CH_3)_3$); 1H -NMR ($CDCl_3$, 200 MHz): δ 1.66 (s, 9H, $C(CH_3)_3$), 1.99 (s, 3H, CH_3), 7.16 - 7.66 (m, 5H, ArH), 11.91 (br s, 1H, OH); ^{13}C NMR ($CDCl_3$, 63 MHz): δ 15.49 (C-10), 28.38 (C-13,14,15), 58.86 (C-12), 102.97 (C-8), 127.43 (C-2,3), 128.10 (C-4,5), 131.16 (C-1), 138.69 (C-6), 145.12 (C-9), 160.56 (C-11), 193.51 (C-7); EIMS m/z 259 (37.6 %, LH), 243 (20.1 %, LH - O), 201 (100.0 %, LH - $C(CH_3)_3$), 105 (27.8 %, $PhC=O$), 77 (20.3 %, Ph).

3-Methyl-4-(4-n-octylbenzoyl)-1-phenyl-5-pyrazolone (5)



9.002 g, 46.10 %; yellow, feathery crystals (a); 4.703 g, 24.08 %; orange / brown powder (b); total yield 70.18 %; mp 54 - 55 °C (both products); (Found C, 75.38; H, 7.72; N, 7.09; $C_{25}H_{30}N_2O_2 \cdot \frac{1}{2}H_2O$ requires C, 75.14; H, 7.84; N, 7.01 %); IR (cm^{-1} , KBr Disc): ν 2919.1s / 2852.1m (CH), 1608.1s (C=N), 1556.2s (C=C), 759.5m (Ar CH); 1H NMR ($CDCl_3$, 200 MHz): δ (a) 0.85 - 0.90 (m, 3H, H1), 1.26 - 1.32 (m, 10H, H2-6), 1.62 - 1.68 (m, 2H, H7), 2.13 (s, 3H, H18), 2.65 - 2.71 (t, 2H, H8), 7.25 - 7.32 (m, 3H, H10,11,25), 7.42 - 7.49 (tq, 2H, H23,24), 7.55 - 7.59 (dt, 2H, H12,13), 7.84 - 7.90 (dq, 2H, H21,22); (b) as for (a) but 8.90 (br s, 1H, OH); ^{13}C NMR ($CDCl_3$, 63 MHz): δ - for (a) only : 13.97 (C-1), 15.87 (C-18), 22.53 (C-2), 29.10 (C-3), 29.13 (C-4), 29.29 (C-5), 31.02 (C-6), 31.72 (C-7), 35.89 (C-8), 103.45 (C-16), 120.55 (C-10,11), 126.41 (C-25), 128.05 (C-23,24), 128.28 (C-12,13), 128.96 (C-21,22), 134.66 (C-9), 137.23 (C-14), 147.53 (C-20), 147.77 (C-17), 161.71 (C-19), 191.38 (C-15); EIMS m/z (a) 390 (22.2 %, LH), 277 (12.6 %, LH - C_8H_{17}), 203 (44.0 %, LH - $C_8H_{17}Ph$), 91 (100.0 %, PhN), 77 (28.5 %, Ph); (b) 390 (42.9 %, LH), 277 (20.8 %, LH - C_8H_{17}), 200 (100.0 %, LH - $C_8H_{17}Ph$), 91 (39.9 %, PhN), 77 (19.8 %, Ph).

3-Methyl-4-(4-n-heptylbenzoyl)-1-phenyl-5-pyrazolone (6)



11.70 g, 62.20 %; beige, crystalline powder; mp 92 - 94 °C; (Found C, 76.82; H, 7.66; N, 7.35; $C_{24}H_{28}N_2O_2$ requires C, 76.55; H, 7.51; N, 7.44 %); IR (cm^{-1} , KBr Disc): ν 2926.9s + 2853.7m (CH), 2506.2 br s (OH), 1641.8s (C=O), 1500.3s (C=N), 782.3m + 755.6s (Ar CH); 1H NMR ($DMSO-d_6$, 200 MHz): δ 0.82 - 0.87 (m, 3H, H1), 1.24 - 1.28 (m, 8H, H2-5), 1.59 (br s, 2H, H6), 2.22 (s, 3H, H17), 2.60 - 2.66 (t, J_{vic} 7.26 Hz / plus J 15.01 Hz, 1H, H7), 7.27 - 7.33 (m, 3H, H9,10,24), 7.46 - 7.52 (t, J_{ortho} 7.49 / 8.03 Hz, 2H, H-22,23),

7.66 - 7.74 (m, 4H, H11,12,20,21), ca. 8.5 - 9.5 (br s, 0.5H, OH); ¹³C NMR (DMSO-d₆, 63 MHz): δ 14.04 (C1), 14.33 (C17), 22.19 (C2), 28.64 (C3), 28.75 (C4), 30.83 (C5), 31.35 (C6), 35.25 (C7), 104.51 (C15), 121.25 (C9,10), 126.24 (C24/C8?), 128.02 (C22,23), 129.10 (C11,12,20,21), 136.33 (C8/C24?), 137.12 (C13), 146.90 (C19), 150.0 (C16), 157.3 (C18), 189.24 (C14); EIMS *m/z* 376 (65.4 %, LH), 277 (28.8 %, LH - C₇H₁₅), 200 (100.0 %, LH - C₇H₁₅Ph).

ESMS : 3 x 10⁻⁴ M solution in MeOH; Spectrum tuned on 377.2. Parameters:

Flow Rate / μlmin ⁻¹	Sheath Gas, arb.	Aux. Gas, arb.	Spray Voltage / kV	Capillary Temp./°C	Capillary Volt. / V
10	50	0	5.5	170	17
Tube Lens off / V	Octapole 1 / V	Lens Voltage / V	Octapole 2 / V	Octapole RF / A	Spray Current / μA
55	-3	-16	-6	400	0.14

3.7.4.2 Synthesis of Metal Complexes³⁸

Complexes 7-10 were prepared as described for 7 via reaction of 2 equivalents of acyl pyrazolone 1 with one equivalent of the appropriate divalent metal acetate. Complex 11 was prepared as described in the synthesis of ligand 4 (Section 3.7.4.1).

[Cu(1-H)₂] (7)

Triethylamine (0.22 g, 2.2 mmol) and copper(II) acetate monohydrate (0.20 g, 1 mmol) were added to a yellow solution of 1 (0.56 g, 2 mmol) in methanol (25 ml). The resulting suspension was stirred at room temperature for 45 min, after which time the green precipitate was isolated by filtration. (0.578 g, 93.55 %); olive green powder; mp 274 - 276 °C; (Found C, 65.85; H, 4.34; N, 8.92 %; C₃₄H₂₆N₄O₄Cu requires C, 66.05; H, 4.25; N, 9.07 %); IR (cm⁻¹, KBr Disc): ν 1600.0m (C=O), 1592.0m (C=N), 1379.9m (C-O), 758.3m & 704.2m (Ar CH); FABMS *m/z* 618 (32.7 %, CuL₂), 279 (100.0 %, LH), 105 (55.5 %, PhNN); μ_{eff} 1.76 B.M.

[Zn(1-H)₂(MeOH)₂] (8)

0.561 g, 90.47 %; colourless crystals; mp 204 - 206 °C; (Found C, 62.75; H, 5.02; N, 7.97; C₃₄H₂₆N₄O₄Zn requires C, 62.73; H, 4.82; N, 8.36 %); IR (cm⁻¹, KBr Disc): ν 3450.3w (OH), 1611.8m (C=O), 1364.1m (C-O); ¹H NMR (CDCl₃, 200 MHz): δ 1.71 (s, 8H, CH₃ & H₂O), 3.42 (s, 5H, CH₃OH), 6.97 - 7.46 (m, 16H, ArH), 7.68 - 7.72 (d, 4H, *o*-ArH on N-Ph); FABMS *m/z* 963 (66.2 %, Zn₂L₃), 620 (100.0 %, ZnL₂), 276 (40.6 %, L).

[Co(1-H)₂.H₂O.MeOH] (9)

0.556 g, 83.80 %; salmon pink powder; mp 220 °C; (Found C, 62.99; H, 5.06; N, 8.20; C₃₄H₂₆N₄O₄Co.H₂O.CH₃OH requires C, 63.34; H, 4.87; N, 8.44 %); IR (cm⁻¹, KBr Disc): ν 3448.1w (OH), 1609.6s (C=O), 1367.9m (C-O), 768.2m (Ar CH); FABMS *m/z* 949 (17.8 %, Co₂L₃), 613 (100.0 %, CoL₂), 337 (81.0 %, CoL); μ_{eff} 4.25 B.M

[Ni(1-H)₂.H₂O.MeOH] (10)

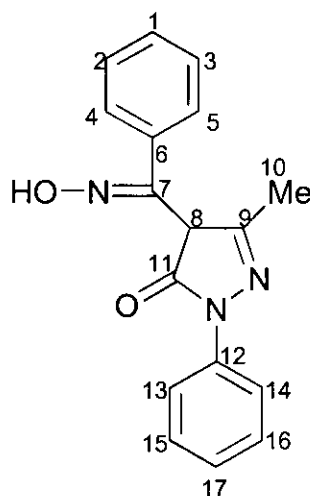
0.522 g, 78.68 %; pale green powder; mp 225 °C; (Found C, 63.33; H, 5.09; N, 8.17; C₃₄H₂₆N₄O₄Ni.H₂O.CH₃OH requires C, 63.36; H, 4.87; N, 8.45 %); IR (cm⁻¹, KBr Disc): ν 3245.6s (OH), 1610.8s (C=O), 1368.1m (C-O), 768.7m (Ar CH); FABMS *m/z* 613 (100.0 %, NiL₂), 336, (29.4 %, NiL); μ_{eff} 2.69 B.M

3.7.5 Pyrazolone Oximes

3.7.5.1 Synthesis of Ligands

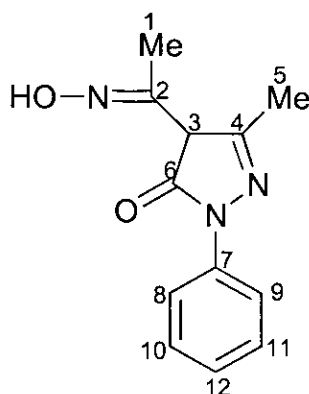
Compounds **12-14** were prepared as described for **12** by reaction of the appropriate acyl pyrazolone (**1-3**) with hydroxylamine hydrochloride³⁹. Compounds **15** and **16** were prepared as described for **6** via a similar reaction under anhydrous conditions according to the method of Tennant⁴⁵.

4-Benzoyl-3-methyl-1-phenyl-5-pyrazolone ketoxime (12)



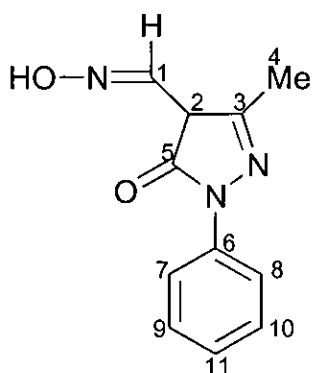
Hydroxylamine hydrochloride (0.516 g, 7.4 mmol) and potassium hydroxide (0.42 g, 7.5 mmol) were dissolved in hot ethanol (15 ml and 10 ml respectively) with stirring. The alkaline solution was added to the hydroxylamine hydrochloride solution with stirring to liberate the free hydroxylamine with the precipitation of potassium hydroxide. After standing at 0 °C for 10 min, the resulting colourless suspension was filtered into a yellow solution of **1** (2.068 g, 7.4 mmol) in ethanol (80 ml). The reaction was heated under reflux for 3½ h, during which time the solution became dark yellow. The solution was left to cool and reduced by half in volume on a rotary evaporator. Yellow crystals of **12** (1.687 g, 77.38 %) of X-ray quality were filtered from the solution. mp 171 -173 °C; (Found C, 69.69; H, 5.11; N, 14.21; C₁₇H₁₅N₃O₂ requires C, 69.60; H, 5.16; N, 14.33 %); IR (cm⁻¹, KBr Disc): ν 3447.9w (OH), 2723.2s (OH & CH); ¹H NMR (DMSO-d₆, 200 MHz): δ 1.59 (br s, 3H, CH₃), 7.17 - 7.90 (m, 11H, ArH & OH), 12.60 (br s, 1H, OH); ¹³C NMR (DMSO-d₆, 63 MHz): δ 14.64 (C-10), 95.89 (C-8), 119.59 & 125.01 & 128.13 & 128.76 (C-1-6, 12-17; the 2 quaternary carbons cannot be identified from the DEPT and are assumed to be masked by the two large signals at 128.13 and 128.76), 130.87 (C-9), 138.63 (C-7), 147.55 (C-11); EIMS *m/z* 293 (41.3 %, LH), 277 (100.0 %, LH - O(H)), 77 (54.8 %, Ph).

3-Methyl-4-methylketoximino-1-phenyl-5-pyrazolone (13)



Reflux 22 h; 0.283 g, 26.48 %; pale yellow microcrystals; mp 209 - 211 °C; (Found C, 61.05; H, 5.58; N, 17.85; $C_{12}H_{13}N_3O_2 \cdot \frac{1}{4}H_2O$ requires C, 61.12; H, 5.78; N, 17.83 %); IR (cm^{-1} , KBr Disc): ν 3018.6s (OH), 1646.4s & 1614.7s & 1593.7s (C=N, C=C), 710.9s (Ar CH); 1H NMR (DMSO- d_6 , 200 MHz): δ 2.04 (s, 3H, CH_3), 2.06 (s, 3H, CH_3CNOH), 7.18 - 7.25 (t, 1H, p -ArH), 7.40 - 7.48 (t, 2H, m -ArH), 7.69 - 7.80 (d, 2H, o -ArH), 9.36 (br s, 1H, NOH), 11.64 (br s, 1H, OH); ^{13}C NMR (DMSO- d_6 , 63 MHz): δ 12.05 (C-5), 22.51 (C-1), 101.75 (C-3), 120.31 (C-10,11), 125.25 (C-12), 129.08 (C-8,9), 138.43 (C-7), 145.83 (C-4), 169.83 (C-6), 173.13 (C-2); EIMS m/z 231 (40.1 %, LH), 189 (24.4 %, LH - NOH), 133 (24.9 %, LH - (C(Me)NOH)), 77 (43.2 %, Ph).

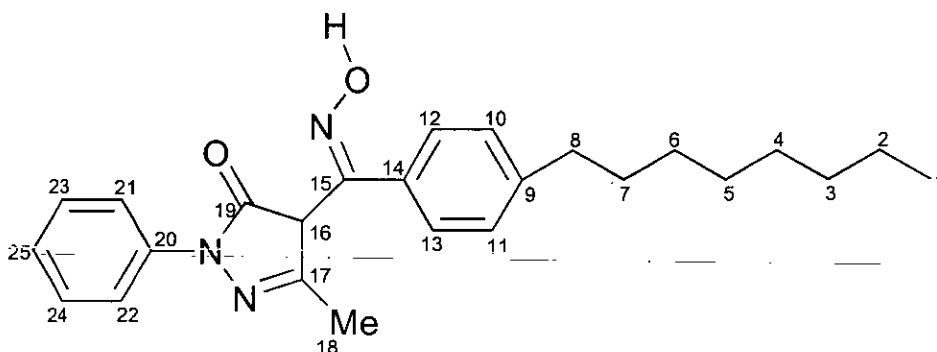
4-Aldoximino-3-methyl-1-phenyl-5-pyrazolone (14)



Reflux 5 h; 1.894 g, 87.17 %; yellow microcrystals; mp 155 - 158 °C; (Found C, 58.47; H, 5.06; N, 18.69; $C_{11}H_{11}N_3O_2 \cdot \frac{1}{2}H_2O$ requires C, 58.39; H, 5.36; N, 18.58 %); IR (cm^{-1} , KBr Disc): ν 3165.8w (OH), 2741.3m (CH), 1633.9s &

1598.2m & 1541.6s (C=N, C=C), 763.8m & 755.1m (Ar CH); ^1H NMR (DMSO- d_6 , 200 MHz): δ 2.16 (s, 3H, CH_3), 7.13 - 7.20 (tt, 1H, $p\text{-ArH}$), 7.22 - 7.52 (m, 2H, $m\text{-ArH}$), 7.76 (s, 1H, CH), 7.82 - 7.89 (dd, 2H, $o\text{-ArH}$); ^{13}C NMR (DMSO- d_6 , 63 MHz): δ 12.74 (C-4), 95.08 (C-2), 119.24 (C-9,10), 124.85 (C-11), 128.92 (C-7,8), 138.93 (C-6), 139.22 (C-3), 149.32 (C-1), 161.95 (C-5); EIMS m/z 217 (50.8 %, LH), 216 (55.2 %, L), 91 (100.0 %, PhN), 77 (99.4 %, Ph).

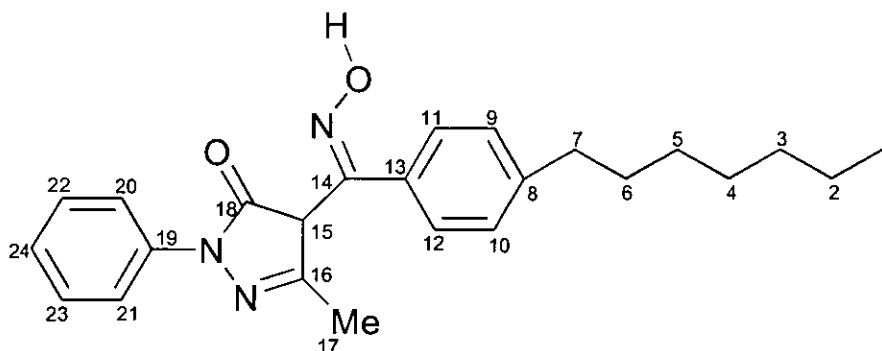
3-Methyl-4-(4-n-octylbenzoylketoximino)-1-phenyl-5-pyrazolone (15)



The synthesis was carried out in an inert atmosphere. A colourless suspension of hydroxylamine hydrochloride (6.95 g, 0.10 mol) in "superdry" ethanol (120 ml; dried using Mg / I_2 ⁸⁵) was treated with a pale yellow suspension of **5** (7.81 g, 0.02 mol) in "superdry" ethanol (80 ml) and freshly roasted anhydrous sodium carbonate (5.30 g, 0.05 mol) with vigorous stirring. The resulting mixture was stirred for 24 h at room temperature to give a yellow suspension, a TLC of which indicated the formation of a single product. The reaction medium was filtered, reduced in volume and filtered again to leave a viscous, yellow / brown residue, which solidified on standing to yield a grainy yellow / orange solid ((a) 5.13 g, 12.7 mmol), which was shown to be the desired product by NMR. The filtrate was left to stand and after ca. 3 weeks yielded yellow microcrystals ((b) 0.48 g, 1.2 mmol). Total yield of **15** = 5.62 g, 69.27 %. mp (a) 83 - 88 °C (wet); (b) 103 - 105 °C; (Found C, 73.30; H, 7.68; N, 10.25; $\text{C}_{25}\text{H}_{31}\text{N}_3\text{O}_2 \cdot \frac{1}{4}\text{H}_2\text{O}$ requires C, 73.21; H, 7.76; N, 10.25 %); IR (cm^{-1} , KBr Disc): ν (b) 3250w (OH), 2928.1s & 2854.5s

(CH), 1578.6m & 1542.2s & 1500.1s (C=N, C=C), 760.0m & 693.6m (CH); ^1H NMR (DMSO- d_6 , 200 MHz): (a) δ 0.83 - 0.90 (m, 3H, H1), 1.14 - 1.26 (m, 10H, H2-6), 1.57 (s, 5H, H7 & H18), 2.57 - 2.64 (t, 2H, H8), 7.18 - 7.47 (m, 7H, ArH), 7.82 - 7.87 (d, 2H, H21-22), 9.19 (br s, 2H, OH); ^1H NMR (DMSO- d_6 , 250 MHz): (b) δ 0.82 - 0.87 (m, 3H, H1), 1.23 - 1.27 (m, 10H, H2-6), 1.56 (s, 5H, H18, H7), 2.61 - 2.67 (t, 2H, H8), 7.17 - 7.23 (t, J_{meta} 6.93, 7.81 Hz, 1H, H25), 7.31 - 7.34 (d, J_{ortho} 13.45 Hz, 2H, H10-11), 7.40 - 7.47 (m, 4H, H12-13, H23-24), 7.91 - 7.94 (d, J_{ortho} 8.16 Hz, 2H, H21-22), 12.50 - 14.20 (br s, 1H, OH); ^{13}C NMR (DMSO- d_6 , 63 MHz): (b) δ 14.06 (C-1), 14.81 (C-18), 22.22 (C-2), 28.72 (C-3), 28.81 (C-4), 28.91 (C-5), 30.87 (C-6), 31.38 (C-7), 35.06 (C-8), 95.96 (C-16), 119.35 (C-10,11), 124.86 (C-25), 128.74 & 128.90 & 129.31 (C-23,24,12,13,21,22), 138.79 (C-9), 146.01 (C-14), 147.52 (C-20), 153.78 (C-17), 159.83 (C-19), 178.45 (C-15); FABMS (a) m/z 406 (100.0 %, LH), 390 (25.8 %, acyl precursor) plus a minor peak at 812 (1.4 %, (LH) $_2$); (b) m/z 406 (73.8 %, LH), 388 (100.0 %, LH - OH) plus a minor peak at 811 (4.6 %, (LH) $_2$).

3-Methyl-4-(4-n-heptylbenzoylketoximino)-1-phenyl-5-pyrazolone (16)



1.46 g, 67.66 %; pale yellow microcrystals; mp 137 - 139 °C; (Found C, 73.93; H, 7.42; N, 10.72; $\text{C}_{24}\text{H}_{29}\text{N}_3\text{O}_2$ requires C, 73.61; H, 7.48, N, 10.73 %); IR (cm^{-1} , KBr Disc): ν 3400w (OH), 2929.7s & 2855.7m (CH), 2506.2s (OH), 1499.0s (C=N / C=C), 761.1w (Ar CH); ^1H NMR (DMSO- d_6 , 200 MHz): δ 0.81 - 0.88 (m, 3H, H1), 1.24 - 1.27 (m, 8H, H2-5), 1.54 - 1.70 (m, 5H, H6,17), 2.60 - 2.68 (t, J_{vic} 7.23 / 7.37 Hz, 2H, H7), 7.14 - 7.22 (tt, J_{ortho} 7.34 / 7.37 Hz,

J_{meta} 2.28 / 3.45 / 2.30 Hz, 1H, H24), 7.30 - 7.34 (d, J_{ortho} 8.22 Hz, 2H, H9,10), 7.37 - 7.48 (m, 4H, H11,12,22,23), 7.89 - 7.94 (dd, J_{ortho} 8.67 Hz, 2H, H20,21), ca. 10.5 - 12.5 (br s, 1H, OH); ^{13}C NMR (DMSO- d_6 , 63 MHz): δ 14.01 (C1), 14.91 (C17), 22.20 (C2), 28.64 (C3), 28.68 (C4), 30.92 (C5), 31.38 (C6), 35.07 (C7), 96.02 (C15), 119.22 (C9,10), 124.62 (C24/C8?), 128.67 (C22,23), 128.88 (C11,12), 129.65 (C-20,21), 129.80 (C8/24?), 139.02 (C13), 145.58 (C-19), 147.37 (C16), 153.90 (C14), 160.20 (C18); FABMS m/z 392 (56.3 %, LH), 376 (100.0 %, LH - O).

ESMS : 3×10^{-4} M solution in MeOH; spectrum tuned on 392.2. Parameters:

Flow Rate / μmin^{-1}	Sheath Gas, arb.	Aux. Gas, arb.	Spray Voltage / kV	Capillary Temp./ $^{\circ}\text{C}$	Capillary Volt. / V
10	50	0	5.5	170	4
Tube Lens off / V	Octapole 1 / V	Lens Voltage / V	Octapole 2 / V	Octapole RF / A	Spray Current / μA
55	-2.5	-18	-7.5	400	0.19

ESMS : 1:1 mixture of nonyl phenol and **16**; Spectrum tuned on 392.2
Parameters:

Flow Rate / μmin^{-1}	Sheath Gas, arb.	Aux. Gas, arb.	Spray Voltage / kV	Capillary Temp./ $^{\circ}\text{C}$	Capillary Volt. / V
20	70	5	5.0	170	3
Tube Lens off / V	Octapole 1 / V	Lens Voltage / V	Octapole 2 / V	Octapole RF / A	Spray Current / μA
55	-2.25	-26	-8.0	400	0.34

3.7.5.2 Synthesis of Metal Complexes³⁸

Compounds **17-20** were prepared as described for **17** *via* reaction of ligand **12** with the appropriate divalent metal salt (**17** and **18** = acetate; **19** = chloride; **20** = nitrate). X-ray quality crystals of **17-19** were obtained *via* recrystallisation by diffusion of water into DMF solutions of the individual complexes. X-ray quality crystals of **20** were recovered from the reaction filtrate. Compounds **21-26** were prepared as described for **17** *via* reaction of one equivalent of the divalent metal acetate (0.25 mmol) and two equivalents (0.50 mmol) of the appropriate oxime ligand.

[Cu(12-H)₂(DMF)₂] (17)

Copper(II) acetate monohydrate (0.18 g, 0.9 mmol) was added with stirring to a yellow solution of the oxime **12** (0.53 g, 1.8 mmol) in methanol (25 ml). The resulting green suspension was stirred at room temperature for 45 min and the product recovered *via* filtration. (0.540 g, 75.58 %) green crystals; mp 245-247 °C; (Found C, 60.01; H, 4.88; N, 13.02; C₃₄H₂₈N₆O₄Cu.C₃H₇NO.H₂O requires C, 60.10; H, 5.05; N, 13.26 %); IR (cm⁻¹, KBr Disc): ν 3291.8m (OH), 1599.5m (C=N), 1016.5m (N-O); FABMS *m/z* 648 (66.4 %, CuL₂), 356 (32.5 %, CuL), 105 (100.0 %, PhNN), 77 (82.8 %, Ph); μ_{eff} 2.41 B.M

[Zn(12-H)₂(DMF)₂] (18)

(0.514 g, 71.75 %) colourless crystals; mp 214 - 216 °C; (Found C, 60.08; H, 5.15; N, 11.40; C₃₄H₂₈N₆O₄Zn.(CH₃OH)₂ requires C, 60.54; H, 5.09; N, 11.77 %); IR (cm⁻¹, KBr Disc): ν 3304.8m (OH), 2796.9m (CH), 1598.4m (C≡N), 1016.7m (N-O); FABMS *m/z* 651 (52.4 %, ZnL₂), 376 (51.9 %, ZnL₂.H₂O), 105 (100.0 %, PhNN).

[Ni(12-H)₂(DMF)₂] (19)

(0.482 g, 67.90 %) pale blue crystals; mp >300 °C; (Found C, 57.03; H, 4.32; N, 11.61; C₃₄H₂₈N₆O₄Ni.4H₂O requires C, 57.09; H, 5.08; N, 11.75 %); IR (cm⁻¹, KBr Disc): ν 3323.0s (OH), 2631.1s & 2539.1s (CH), 1635.0s & 1574.4s (C=N, C=C), 718.1s (Ar CH); FABMS *m/z* 643 (5.6 %, NiL₂), 278 (15.8 %, LH-NH), 215 (31.6 %, LH-Ph); μ_{eff} 2.83 B.M

[Co(12)₂(MeOH)₂](NO₃)₂ (20)

0.313 g, 46.51 %; yellow crystals; mp 155 - 157 °C; (Found C, 51.56; H, 4.55; N, 13.44; C₃₄H₃₀N₆O₄Co.(CH₃OH)₂.(NO₃)₂ requires C, 51.86; H, 4.60; N, 13.44 %); IR (cm⁻¹, KBr Disc): ν 3332.2m (OH & MeOH), 1600.4m (C=N), 1017.6m (N-O); ¹H NMR (DMSO-d₆, 200 MHz): δ 1.51 (s, 6H, CH₃), 3.11 (s, 6H, CH₃OH), 7.08 - 7.15 (t, 2H, ArH), 7.15 - 7.50 (m, 14H, ArH), 7.75 - 7.79

(m, 4H, ArH); FABMS m/z 644 (70.1 %, CoL_2), 351 (22.3 %, CoL), 105 (100.0 %, PhNN), 77 (91.7 %, Ph); μ_{eff} 4.03 B.M.

[Cu(13-H)₂] (21)

0.120 g, 29.35 % (based on CuL_2); brown powder (a); 0.013 g, 71.00 % - based on CuL_2); green powder from filtrate (b); mp (a) 278 - 280 °C, (b) 218 - 220 °C; IR (cm^{-1} , KBr Disc): ν (a) 3412.5w (OH), 1602.4s & 1592.6s (C=N), 1498.4s (C=C), 756.2m (Ar CH); FABMS m/z (a) 494 (21.0 %, $\text{CuL}_2 - 2 \text{CH}_3$), 216 (24.0 %, LH - CH_3), 77 (66.4 %, Ph); (b) 495 (5.4 %, $\text{CuL}_2 - 2 \text{CH}_3$), 216 (13.0 %, LH - CH_3), 77 (17.6 %, Ph); μ_{eff} 2.12 B.M.

[Cu(14-H)₂] (22)

0.096 g, 77.18 % (based on CuL_2); green/brown powder; mp 200 - 201 °C; IR (cm^{-1} , KBr Disc): ν 1623.2s & 1592.5s (C=N), 1007.6s (C-O), 754.4m (Ar CH); FABMS m/z 496 (22.1 %, CuL_2), 91 (37.4 %, PhN); μ_{eff} 1.42 B.M.

[Zn(14-H)₂]. $\frac{3}{4}\text{H}_2\text{O}$ (23)

0.104 g, 81.33 %; pale orange microcrystals; mp 225 - 227 °C; (Found C, 52.70; H, 4.22; N, 15.80; $\text{C}_{22}\text{H}_{20}\text{N}_6\text{O}_4\text{Zn}.\frac{3}{4}\text{H}_2\text{O}$ requires C, 52.35; H, 4.45; N, 16.11 %); IR (cm^{-1} , KBr Disc): ν 3370.1s (OH), 1637.6s & 1597.9m (C=N), 1530.0s (C=C), 754.0m (Ar CH); FABMS m/z 498 (6.8 %, ZnL_2), 77 (28.9 %, Ph).

[Co(14-H)₂]. $2\frac{1}{2}\text{H}_2\text{O}$ (24)

0.114 g, 84.91 %; pale green powder; mp 228 °C; (Found C, 49.52; H, 4.11; N, 14.91; $\text{C}_{22}\text{H}_{20}\text{N}_6\text{O}_4\text{Co}.\frac{2}{2}\text{H}_2\text{O}$ requires C, 49.25; H, 4.71; N, 15.67 %); IR (cm^{-1} , KBr Disc): ν 3402.9s (OH), 1641.7s & 1600.1m (C=N), 1529.3m & 1505.3m (C=C), 752.0m (Ar CH); FABMS m/z 492 (26.2 %, CoL_2), 91 (30.6 %, PhN); μ_{eff} 2.09 B.M.

[Ni(14-H)₂].2½H₂O (25)

0.116 g, 86.56 %; aquamarine microcrystals; mp 236 - 238 °C; (Found C, 47.43; H, 4.48; N, 15.41; C₂₂H₂₀N₆O₄Ni.2½H₂O requires C, 49.27; H, 4.71; N, 15.68 %); IR (cm⁻¹, KBr Disc): ν 3367.2s (OH), 1647.2s & 1600.6m (C=N), 1559.4s / 1534.5s / 1505.8s (C=C), 752.1m (Ar CH); FABMS *m/z* 580 (10.0 %, NiL₂.MeOH), 491 (23.4 %, NiL₂), 307 (11.5 %, NiL.MeOH), 278 (34.5 %, NiL), 217 (100.0 %, LH); μ_{eff} 2.73 B.M

[Cu(15-H)₂] (26)

0.31 g, 71.00 % (based on CuL₂); green / brown powder; mp : The product turned black at 175 °C, and decomposed fully at 195 - 198 °C; IR (cm⁻¹, KBr Disc): ν 3476.9s & 3375.3m & 3275.9m (OH), 2926.0m & 2853.8w (CH), 1602.8s (C=N), 1520.7s (C=C), 692.1m (CH); FABMS *m/z* 1344 (18.2 %, Cu₂L₃), 874 (78.5 %, CuL₂), 596 (17.7 %, Cu₃L), 530 (18.2 %, Cu₂L), 468 (68.8 %, CuL), 406 (5.7 %, LH).

3.7.6.1 Solvent Extraction Experiments from Sulphate Media

Solutions : 0.056 M CuSO₄.5H₂O in H₂O (pH 4.32 - 4.34)
0.1M LH in toluene
1M NaOH
1M H₂SO₄

Extraction Data

15 ml of the aqueous copper feed were contacted with 15 ml of the organic ligand solution in a tightly sealed, screw top, glass jar, equipped with a magnetic stirrer. The 2-phase system was stirred at 600 r.p.m. and at room temperature for ½ h, after which time the two phases were separated by filtration and the pH of the aqueous phase was measured. The number of moles of ligand, which had deprotonated to complex the copper, and, from this value, the number of moles of base required to achieve full deprotonation of the ligand were calculated and added in aliquots at ½ h

intervals to the extraction experiment. The pH of the aqueous phase was recorded and samples of the two phases were taken after each addition and equilibration, ie: stirring at 600 r.p.m. and at room temperature for ½ h, as before. The samples were diluted by a factor of 1:100 with water (aqueous samples) or white spirit (organic samples) and their copper content analysed by ICP-AES.

Strip Data

Aliquots of acid were added at intervals of ½ h to the fully loaded organic phase from the extraction experiment, and as in the extraction experiment, after each addition and equilibration period the pH of the aqueous phase was recorded and samples taken and diluted by 1:100 for analysis using ICP-AES.

The data collated in these experiments were plotted as a graph of pH versus % copper in the organic phase using Microsoft Excel.

Additional reagent screens were carried out at Avecia as described below.

Reagent Screen 1 : Copper Loading and Stripping Characteristics

0.05 M solutions of the ligand in dichloromethane were contacted in 1:1 organic : aqueous volumetric ratios with (a) an aqueous feed containing 5.00 gl^{-1} copper at pH 2 and (b) a strip acid feed containing 45.0 gl^{-1} copper and 125 gl^{-1} sulphuric acid at room temperature for 1 hour. The two phases were then separated and the copper content of the organic phase was determined by atomic absorption spectrometry (AAS) using a Perkin Elmer 3030AA spectrophotometer. The copper content of the aqueous phase was determined by titration against 0.1 M thiosulphate solution.

Reagent Screen 2 : Selectivity for Copper over Iron

0.05 M solutions of the ligand in dichloromethane were contacted in 1:1 organic :aqueous volumetric ratios with (a) a mixed aqueous feed containing 5 gpl copper and 5 gpl iron and (b) an aqueous feed containing 5 gpl iron at

room temperature for 1 hour. The metal content of the organic phase was determined by AAS as before. The results of both reagent screens for P50 in DCM are presented in table 23.

	Screen 1 : Copper Loading & Stripping		Screen 2 : Selectivity	
	Contact Solution	gl ⁻¹ Cu _{org}	Contact Solution	ppm Fe _{org}
Test (a)	5.00 gl ⁻¹ Cu	1.28	5.00 gl ⁻¹ Cu / 5.00 gl ⁻¹ Fe	<1 (1.42 gl ⁻¹ Cu)
Test (b)	45.0 gl ⁻¹ Cu / 125 gl ⁻¹ H ₂ SO ₄	0.18	5.00 gl ⁻¹ Fe	69

Table 23 : Results for loading, stripping and selectivity for P50

3.7.6.1 Acyl Pyrazolones

The results of solvent extraction experiments for ligand **6** are presented in table 24.

pH	% Cu _{org}
1.10	10.4
1.19	48.5
1.28	59.2
1.44	72.3
1.48	72.8
1.60	79.6
1.80	87.8
1.96	91.5
2.27	94.3
3.73	100

Table 24 : solvent extraction results for **6**

The results of the two reagent screens carried out for ligand **5** at Avecia are presented in table 25.

	Screen 1 : Copper Loading & Stripping		Screen 2 : Selectivity	
	Contact Solution	gpl Cu _{org}	Contact Solution	ppm Fe _{org}
Test (a)	5.00 gl ⁻¹ Cu	1.20	5.00 gl ⁻¹ Cu / 5.00 gl ⁻¹ Fe	12 (1.35 gl ⁻¹ Cu)
Test (b)	45.0 gl ⁻¹ Cu / 125 gl ⁻¹ H ₂ SO ₄	0.044	5.00 gl ⁻¹ Fe	87

Table 25 : Reagent screen results for 5

3.7.6.2 Pyrazolone Oximes

The results of solvent extraction experiments for ligand 15 are presented in table 26.

pH	% Cu _{org}
<0	3.0
0.00	16.3
0.03	42.9
0.05	48.6
0.10	54.5
0.34	69.3
1.64	76.3
1.64	84.3
1.70	90.3

Table 26 : Solvent extraction results for 15

The results of the two reagent screens carried out for ligand 16 at Avecia are presented in table 27.

	Screen 1 : Copper Loading & Stripping		Screen 2 : Selectivity	
	Contact Solution	gpl Cu _{org}	Contact Solution	ppm Fe _{org}
Test (a)	5.00 gl ⁻¹ Cu	1.60	5.00 gl ⁻¹ Cu / 5.00 gl ⁻¹ Fe	88 (1.67 gl ⁻¹ Cu)
Test (b)	45.0 gl ⁻¹ Cu / 125 gl ⁻¹ H ₂ SO ₄	1.65	5.00 gl ⁻¹ Fe	705

Table 27 : Reagent screen results for 16

Additional selectivity tests were carried out on 0.314 M solutions of the acylpyrazolone ligand **6** and the oxime ligand **15** in toluene using a mixed aqueous contact solution containing 10 gl^{-1} copper and 8.5 gl^{-1} iron. The organic phase was analysed after 20 min and 1 h and the results of the tests are presented in table 28.

Ligand	Contact Time / min	pH	% Cu _{org}	% Fe _{org}	Ratio of complexed Cu(II) : Fe(III)
6	20	0.95	84.1	6.81	12.4 : 1
	60	1.06	77.0	2.17	35.5 : 1
15	20	1.66	79.0	5.55	14.2 : 1
	60	1.42	87.8	10.4	8.4 : 1

Table 28 : Selectivity tests on **6** and **15**

3.7.7.7 X-Ray Crystallography

Structures were determined by Dr. Simon Parsons at the University of Edinburgh. In all cases data were collected at 220 K on a Stoe Stadi-4 diffractometer equipped with an Oxford Cryosystems low temperature device, using Cu-K α radiation for **8**, **11**, **18** and **19**, and Mo-K α radiation for **12**, **17** and **20**. Reflections were scanned in ω - θ mode. Structures **8**, **12**, and **17-20** were solved by direct methods (SHELXTL or SIR92^{59,86}) and **11** by Patterson methods (DIRDIF⁸⁷). All were completed by iterative cycles of least squares refinement against F^2 and difference Fourier synthesis (SHELXTL). H-atoms were idealised, being placed using geometric or difference maps and treated by riding or refall methods. In all cases non-H atoms were modelled with final anisotropic displacement parameters and final refinement statistics are presented in tables 29 (**8** and **11**) and 30 (**12**, **17-20**).

Structure	8	11
Formula	$C_{36}H_{34}N_4O_6Zn$	$C_{32}H_{42}N_4CuO_6$
M	684.04	642.24
Crystal system	monoclinic	triclinic
Space group	$P2_1/c$	P-1
a/Å	11.058(4)	9.840(4)
b/Å	15.861(9)	13.142(5)
c/Å	9.391(3)	14.241(6)
$\alpha/^\circ$	90	113.08(2)
$\beta/^\circ$	104.53(3)	99.47(3)
$\gamma/^\circ$	90	93.69(3)
$U/\text{Å}^3$	1594.4(12)	1654.3(11)
Crystal size/mm	0.54 x 0.35 x 0.23	0.54 x 0.27 x 0.16
$D_c/\text{g cm}^{-3}$	1.425	1.289
Z	2	2
μ/mm^{-1}	1.513	1.317
Transmission factors	$T_{\min} 0.190, T_{\max} 0.499$	$T_{\min} 0.731, T_{\max} 0.858$
θ Limits/ $^\circ$	4 - 70	3 - 70
No. of unique data	2842	5731
No. data with $[F > 4\sigma(F)]$	2607	4367
No. variables	220	397
R1	0.0389	0.0417
wR2	0.1131	0.1113
$\Delta\rho_{\max}, \Delta\rho_{\min}/e \text{ Å}^{-3}$	0.39, -0.64	0.39, -0.42

Table 29 : Crystallographic data for structures 8 and 11

Structure	12	17	18	19	20
Formula	C ₁₇ H ₁₅ N ₃ O ₂	C ₄₀ H ₄₂ N ₈ CuO ₆	C ₄₀ H ₄₂ N ₈ O ₂ Zn	C ₄₀ H ₄₂ N ₈ NiO ₆	C ₃₆ H ₃₈ N ₆ CoO ₆ .2NO ₃
M	293.52	794.36	796.19	789.53	833.67
Crystal system	monoclinic	monoclinic	monoclinic	monoclinic	monoclinic
Space group	Cc	P2 ₁ /n	P2 ₁ /n	P2 ₁ /n	P2 ₁ /n
a/Å	5.9081(3)	9.9660(13)	10.043(4)	10.0139(15)	10.9252(8)
b/Å	17.7457(11)	9.807(3)	9.563(3)	9.4693(15)	10.3713(10)
c/Å	14.0034(8)	19.771(5)	20.010(5)	20.056(2)	16.9298(12)
α/°	90	90	90	90	90
β/°	95.723(5)	90.72(3)	90.79(3)	90.546(11)	97.623(7)
γ/°	90	90	90	90	90
U/Å ³	1460.85(14)	1932.3(8)	1921.6(11)	1901.7(5)	1901.3(3)
Crystal size/mm	0.56 x 0.38 x 0.31	0.23 x 0.18 x 0.18	0.23 x 0.14 x 0.08	0.23 x 0.16 x 0.10	0.47 x 0.39 x 0.12
D _c /g cm ⁻³	1.334	1.365	1.376	1.379	1.456
Z	4	2	2	2	2
μ/mm ⁻¹	0.090	0.623	1.366	1.219	0.525
Transmission factors		T _{min} 0.588 T _{max} 0.605	T _{min} 0.225 T _{max} 0.689	T _{min} 0.396 T _{max} 0.523	T _{min} 0.462 T _{max} 0.542
θ Limits/°	2 - 33	2 - 28	4 - 60	4 - 70	2 - 25
No. of unique data	4784	4445	2823	3355	3345
No. data with [F>4σ(F)]	4009	2932	1823	2535	2473
No. variables	260	253	253	253	273
R1	0.0389	0.0504	0.0435	0.0499	0.0516
wR2	0.0906	0.1146	0.0912	0.1351	0.1190
Δρ _{max} , Δρ _{min} /e Å ⁻³	0.21, -0.20	0.27, -0.36	0.30, -0.25	0.22, -0.37	0.66, -0.52

Table 30 : Crystallographic data for structures 12 and 17-20

3.8 References for Chapter 3

- 1 E.C. Okafor, *Spectrochim. Acta*, 1981, **37A**(11), 939-944, 945-950
- 2 W. DeHorrocks and J.P. Sipe, *J. Am. Chem. Soc.*, 1971, 6800-6804
- 3 H. Samelson and A. Lempicki, *J. Chem. Phys.*, 1963, **39**(1), 110-112
- 4 Y.A. Zolotov and N.M. Kuzmin, "Extraction of Metals with Acylpyrazolones", Nauka, Moscow, 1977; *Chem. Abstr.* **89** : B81023X
- 5 K. Maruthi Prasad, N. Rama Rao, M.C. Garnorkar and C. Manohara Chary, *J. Organomet. Chem.*, 1989, **376**, 53-59
- 6 W. Mickler, A. Reich and E. Uhlemann, *Separation Science and Technology*, 1998, **33**(3), 425-435
- 7 K. Prochaska, R. Cierpiszewski, J. Szymanowski, E. Uhlemann and W. Mickler, *Solvent Extraction and Ion Exchange*, 1995, **13**(2), 215-227
- 8 Y. Akama, K. Sato, M. Ukaji, T. Kawata and M. Kajitani, *Polyhedron*, 1985, **4**(1), 59-63
- 9 M.O.C. Ogwuegbu and N.C. Oforka, *Hydrometallurgy*, 1994, **34**, 359-367
- 10 J.P. Brunette, M. Lakkis, G. Goetz-Grandmont and M.J.F. Leroy, *Polyhedron*, 1982, **1**(5), 461-466
- 11 S. Narayanan and G.N. Rao, *J. Radioanal. Chem.*, 1981, **67**(2), 285-297
- 12 S. Miyazaki, H. Mukai, S. Umetani, S. Kihara and M. Matsui, *Inorg. Chem.*, **28**, 3014-3017
- 13 I. Guiguemde, B.A. Diantouba, D. Lakkis, G.J. Goetz-Grandmont and J.P. Brunette, *Analisis*, 1996, **24**(8), 318-324
- 14 S. Umetani and M. Matsui, *Analytical Chemistry*, 1992, **64**(19), 2288-2292
- 15 B. Kuznik and D.M. Czakis-Sulikowska, *Monatshefte für Chemie*, 1988, **119**, 389-396

- 16 P. Thakur, K.C. Dash, M.P.L. Reddy, R. Luxmi Varma, T.R. Ramamohan and A.D. Damodaran, *Radiochimica Acta*, 1996, **75**(1), 11-16
- 17 S.A. Pai, K.V. Lohithakshan, P.D. Mithapar, S.K. Aggarwal and H.C. Jain, *Radiochimica Acta*, 1996, **73**(2), 83
- 18 D.A. Fletcher, R.F. McMeeking and D.F. Parkin, *J. Chem. Inf. Comput. Sci.*, 1996, **36**(4), 746-749. Cambridge Database Release 5.18 (1999)
- 19 F. Miao, X. Liu and Y. Li, *J. Inorg. Chem. (Wuji Huaxue Xuebao)*, 1991, **7**(2), 129.132; *Chem. Abstr.* **116** : 245603r
- 20 A.B. Uzoukwu, S.S. Al-Juaid, P.B. Hitchcock and J.D. Smith, *Polyhedron*, 1993, **12**(22), 2719-2724
- 21 Y. Akama, M. Shiro, T. Ueda and M. Kajitani, *Acta Cryst.*, 1995, **C51**, 1310-1314
- 22 M.J. O'Connell, C.G. Ramsay and P.J. Steel, *Aust. J. Chem.*, 1985, **38**, 401-409
- 23 E.C. Okafor, *Spectrochimica Acta*, 1984, **40A**(5), 397-401
- 24 T. Ueda and Y. Akama, *Chem. Phys. Lett.*, 1994, **222**, 559-562
- 25 Knorr, *Annalen*, 1887, **238**, 185-187
- 26 N.R. Shah and J.R. Shah, *J. Indian Chem. Soc.*, 1981, **58**, 851-854
- 27 N.R. Shah and J.R. Shah, *J. Inorg. Nucl. Chem.*, 1981, **43**, 1583-1590
- 28 N.R. Shah and J.R. Shah, *Indian J. Chem.*, 1982, **21A**, 176-177
- 29 E. Suenaga, *Yakugaku Zasshi*, 1959, **79**, 205-210
- 30 A.K. Rana and J.R. Shah, *Indian J. Chem.*, 1981, **20A**, 142-144
- 31 Y.M. Patel and J.R. Shah, *Indian J. Chem.*, 1985, **24A**, 800-802
- 32 Y.M. Patel and J.R. Shah, *Synth. React. Inorg. Met.-Org. Chem.*, 1986, **16**(1), 1-12
- 33 Y.M. Patel and J.R. Shah, *Synth. React. Inorg. Met.-Org. Chem.*, 1986, **16**(2), 145-154
- 34 B. S. Jensen, *Acta. Chem. Scand.*, 1959, **13**, 1668-1670
- 35 H. Li, C.H. Huang, Y.F. Zhou, X.S. Zhao, X.H. Xia, T.K. Li and J. Bai, *J. Mater. Chem.*, 1995, **5**(11), 1871-1878
- 36 Personal Communication : Mrs. S. Owens, Avecia

- 37 D.J. Wallace and J.M. Straley, *J. Org. Chem.*, 1961, **26**, 3825 - 3826
- 38 A.D. Garnovskii, *Koord. Khim.*, (Engl. Trans.), 1992, **18(7)**, 675 - 698
- 39 J. March, *Advanced Organic Chemistry*, Wiley, New York, 3rd Edition, 1985, pp. 805 - 806
- 40 P.Y. Sollenberger and R.B. Martin, *The Chemistry of the Amino Group*, Ed. S. Patai, Interscience, London, 1968, pp. 367-392
- 41 W.P. Jencks, *J. Am. Chem. Soc.*, 1959, **81**, 475-481
- 42 S. Dayagi and Y. Degani, *The Chemistry of the Carbon to Nitrogen Double Bond*, Ed. S. Patai, Interscience, London, 1970, pp. 69-71
- 43 A.F. Cockerill and R.G. Harrison, *The Chemistry of Functional Groups - Supplement A, Part 1*, Ed. S. Patai, Wiley, New York, 1977, pp. 288-299
- 44 R.L. Reeves, *The Chemistry of the Carbonyl Group*, Ed. S. Patai, Interscience, London, 1966, pp. 602-608
- 45 Personal Communication : Dr. G. Tennant, University of Edinburgh
- 46 D.H. Williams and I. Fleming, *Spectroscopic Methods in Organic Chemistry*, McGraw-Hill, London, 5th Edition, 1995
- 47 J.A.M. Guard and P.J. Steel, *Aust. J. Chem.*, 1994, **47**, 1453-1459
- 48 A.R. Katritsky, M. Karelson and P.A. Harris, *Heterocycles*, 1991, **32(2)**, 329-369
- 49 F. Bechtel, J. Gaultier and C. Hauw, *Cryst. Struct. Commun.*, 1973, **2**, 469-472
- 50 F.H. Allen, O. Kennard, D.G. Watson, L. Brammer, G. Orpen and R. Taylor, *J. Chem. Soc. Perkin Trans II*, 1987, S1-S19
- 51 B. Wang, J. Wu, P. Zheng, H. Zhang and H. Zhang, *Fud. Xue. Ziran Kex. (Fudan U)*, 1989, **28**, 24
- 52 F. Marchetti, C. Pettinari, A. Cingolani, D. Leonesi, A. Drozdov and S.I. Troyanov, *J. Chem. Soc. Dalton Trans.*, 1998, 3325-3333
- 53 G. Goetz-Grandmont, A. Tayeb, D. Matt, J.P. Brunette and L. Toupet, *Acta Cryst.*, 1995, **C51**, 53-57
- 54 W. Mickler, A. Reich, S. Sawusch, U. Schilde and E. Uhlemann, *Acta Cryst.*, 1998, **C54**, 776-779

- 55 S. Kawaguchi, *Coord. Chem. Rev.*, 1986, **70**, 51-84
- 56 Weblab ViewerLite 3.5, Molecular Simulations Inc., San Diego, C.A., 1999
- 57 PLATON multipurpose crystallographic tool: A.L. Spek, *Acta Cryst.*, 1990, **C34**, A46
- 58 M.J. Winter, *d-Block Chemistry*, Oxford University Press, Oxford, 1994
- 59 G.M. Sheldrick, SHELXTL version 5, Siemens Analytical X-ray Instrument, Madison, Wisc., USA, 1995
- 60 Cerius² Molecular Modelling System, Molecular Simulations Inc., San Diego, C.A.
- 61 R.D. Hancock, *Acc. Chem. Res.*, 1990, **23**, 253-257
- 62 D.F. Shriver, P.W. Atkins and C.H. Langford, *Inorganic Chemistry*, Oxford University Press, Oxford, 1991, pp. 333
- 63 R.D. Shannon, *Acta Cryst.*, 1976, **A32**, 751-767
- 64 Y.L. Slovkhotov, Y.T. Struchkov, E. Liepins, M.V. Petrova, M.V. Ablovatskaya, E. Gudriniece and Y.A. Strakov, *Latv. PSR Zinat. Akad. Vestis, Khim. Ser.*, 1989, **5**, 605-610
- 65 SYBYL Molecular Modelling Software, Tripos Inc., 1699 S. Hanley Rd., St. Louis, MO, U.S.A.
- 66 MOPAC 93 : QCPE Program 455. Quantum Chemistry Program Exchange, Dept. Of Chemistry, Indiana University, IN, U.S.A.
- 67 AMSOL Oxford Molecular Ltd., Oxford Science Park, The Medawae Centre, Oxford, U.K.
- 68 C.E. Pfluger and R.L. Harlow, *Acta Cryst.*, 1973, **B29**, 2608-2609
- 69 S.H. Simonsen, C.E. Pfluger and C.M. Thompson, *Acta Cryst.*, 1964, **14**, 269-272
- 70 P.L. Orioli, E.C. Lingafelter and B.W. Brown, *Acta Cryst.*, 1964, **17**, 1113-1118
- 71 K. Zhou, C. Zhou, X. Chen and C. Yuan, *Kexue Tongbao (Chin. Sci. Bull.)*, 1985, **30**, 1484-1489

- 72 M. Lalia-Kantouri, M. Uddin, C.C. Hadjikostas, H. Papanikolas, G. Palios, S. Anagostis and V. Anesti, *Z. Anorg. Allg. Chemie*, 1997, **623**(12), 1983-1990
- 73 M.A. Jarski and E.C. Lingafelter, *Acta Cryst.*, 1964, **17**, 1109-1112
- 74 R.C. Srivastava, E.C. Lingafelter and P.C. Jain, *Acta Cryst.*, 1967, **22**, 922-923
- 75 A.G. Hatzidimitriou, M. Iddin and M. Lalia-Kantouri, *Z. Anorg. Allg. Chemie*, 1997, **623**(4), 627-632
- 76 M. Lalia-Kantouri, M. Hartophylles, P.D. Jannakoudakis and G.P. Voutsas, *Z. Anorg. Allg. Chemie*, 1995, **621**(4), 645-653
- 77 L.F. Larkworthy and D.C. Povey, *J. Crystallogr. Spectrosc. Res.*, 1983, **13**(6), 413-420
- 78 M. Gallagher, M.F.C. Ladd, L.F. Larkworthy, D.C. Povey and K.A.R. Salib, *J. Crystallogr. Spectrosc. Res.*, 1986, **16**(16), 967-977
- 79 C.E. Pluger and R.L. Harlow, *Acta Cryst.*, 1970, **B26**, 1631-1633
- 80 G.P. Voutsas, K.G. Keramidas and M. Lalia-Kantouri, *Polyhedron*, 1996, **15**, 147-151
- 81 I. Potocnak, F.W. Heinemann, M. Rausch and D. Steinborn, *Acta Cryst.*, 1997, **C53**, 54-56
- 82 S.J. Rettig, A. Storr and J. Trotter, *Acta Cryst.*, 1992, **C48**, 1587-1590
- 83 E.A. Boudreaux and C.N. Mulay, *Theory and Applications of Molecular Paramagnetism*, Wiley, London, 1976
- 84 D.E. Butler and H.A. DeWald, *J. Org. Chem.*, 1971, **36**(17), 2542-2547
- 85 D.D. Perrin and W.L.F. Amarego, *Purification of Laboratory Chemicals*, Oxford University Press, Oxford, 3rd Edition, 1988, pp. 174
- 86 A. Altomare, G. Cascarano, C. Giacovazzi and A. Guagliardi, *J. Appl. Cryst.*, 1994, **27**, 1045-1050
- 87 P.T. Beurskens, G. Beurskens, W.P. Bosman, R. de Gelder, S. Garcia-Granda, R.O. Gould, R. Israël and J.M.M. Smits, DIRDIF, Crystallography Laboratory, University of Nijmegen, The Netherlands.

Chapter 4 : 3-(2-Hydroxyphenyl)-Pyrazoles

Contents	Page
4.1 Introduction	171
4.2 Synthesis of 3-(2-hydroxyphenyl)-pyrazoles and their Metal Complexes	172
4.2.1 Free Ligands	172
4.2.2 Metal Complexes	174
4.3 Characterisation	175
4.3.1 Free Ligands	175
4.3.2 Metal Complexes	177
4.4 Solvent Extraction from Sulphate Media	177
4.5 X-Ray Crystallography	179
4.5.1 Free Ligands	180
4.5.2 Metal Complexes	184
4.6 Conclusions	190
4.7 Experimental	191
4.7.1 Instrumentation	191
4.7.2 Solvent and Reagent Pretreatment	191
4.7.3 Synthesis of Precursors	192
4.7.4 Synthesis of 1-H-3-(2-Hydroxyphenyl)-pyrazole	194
4.7.5 Synthesis of Metal Complexes	195
4.7.6 Solvent Extraction Experiments	196
4.7.7 X-Ray Crystallography	196
4.8 References for Chapter 4	198

4.1 Introduction

3-(2-Hydroxyphenyl)-pyrazoles (Figure 1) have found various applications in chemistry, particularly due to their metal coordination properties¹. They have been used in biomimetic studies to try to model the active site of lactoferrin², and as small building blocks in the synthesis of polydentate, 3,5-diaryl-pyrazole ligands for the study of biomolecules containing two or more metal centres^{3,4}. Additionally, 3,5-diarylpyrazoles and their derivatives are known to have anti-bacterial activity⁵ and the simple 3-(2-hydroxy)-pyrazoles have also been trialled for use as UV-stabilisers⁶. The existence of an intramolecular hydrogen bond in these compounds (Figure 1) is thought to enhance their UV-stability⁶.

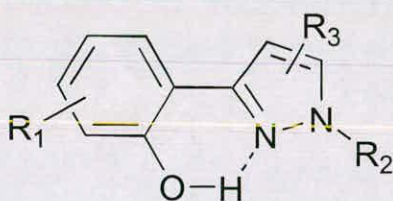


Figure 1 : 3-(2-Hydroxyphenyl)-pyrazoles. R_1 , R_2 , R_3 = alkyl, aryl, H

Derivatives of 3-(2-hydroxyphenyl)-pyrazoles, in which R_2 is a proton, have the ability not only to form intra- but also intermolecular hydrogen bonds, which could potentially result in the formation of preorganised, pseudomacrocyclic dimers (Figure 2) similar to those proposed for P50-type metal extractants. The formation of a pseudomacrocyclic dimer of 1-H-3-(2-hydroxyphenyl)-pyrazole (R_1 , R_2 , R_3 = H) in the solid state⁶ has been reported, and this structure will be discussed in detail in section 4.5.1. It was therefore hoped that these ligands might possess similar copper extraction properties to phenolic oximes, to which end the synthesis of 1-H-3-(2-hydroxyphenyl)-pyrazole and investigation of its metal extraction properties was undertaken. Additionally, other substituted 3-(2-hydroxy-phenyl)-pyrazole ligands have been synthesised and tested at Avecia, and these results will also be discussed in this chapter.

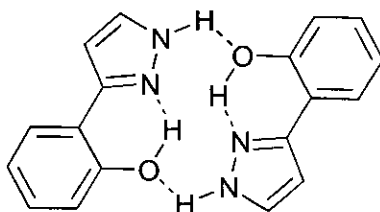


Figure 2 : Pseudomacrocyclic dimer of 1-H-3-(2-hydroxyphenyl)-pyrazole

4.2 Synthesis

4.2.1 Free Ligands

The synthesis of 1-H-3-(2-hydroxyphenyl)-pyrazole, **1**, was achieved by two different synthetic routes. The method of Maib and Jermanowska⁷ involves the initial formation of the precursor **2**, 3-(2-hydroxyphenyl)-1-thiocarbamyl-5-thiosemicarbazide-2-pyrazoline, *via* the reaction of chromone and thiosemicarbazide, and the subsequent acidification of **2** using aqueous formic acid solution (Figure 3).

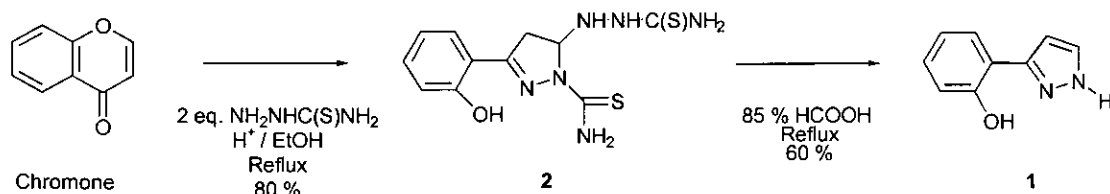


Figure 3 : Synthesis of **1** using method (a)

The main limitation of this synthetic pathway is that in order to increase the kerosene solubility of the ligand for example, substitution can only be introduced on the pyrazole ring and, additionally, the type of substituent would be dependent on the range of substituted chromones available, as illustrated in figure 4. Commercially available chromones have substituents X and Y, which are protons or methyl groups only, and the synthesis of suitable chromones with longer chain alkyl substituents was not considered to be commercially viable.

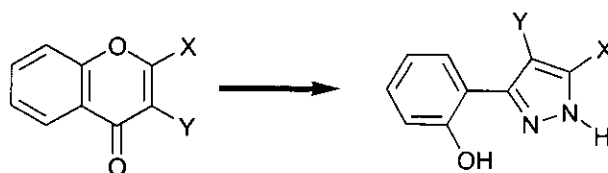


Figure 4 : The limitations of ligand synthesis using substituted chromones

The second method^{1,6,8} used to prepare **1** was based on the reaction of precursor **3**, 2-hydroxy- ω -formylacetophenone, and hydrazine monohydrate. **3** was prepared⁹⁻¹¹ by the reaction of ethyl formate with 2-hydroxyacetophenone in the presence of sodium hydride. The overall reaction scheme is presented in figure 5.

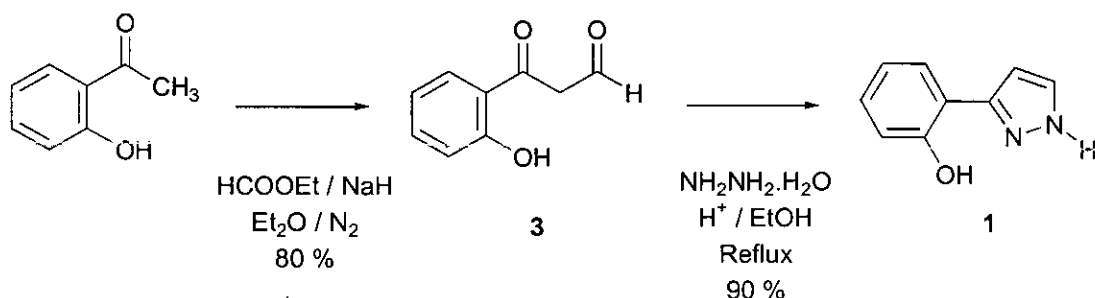


Figure 5 : Synthesis of **1** using method (b)

It should be noted that although this reaction pathway gave a better yield than the first method, the intermediate **3** was found to be prone to air oxidation, unless stored in an inert atmosphere, and decomposition was indicated by discoloration of the product. This method would, however, provide a much simpler route to the synthesis of more soluble ligands, as the substitution on the pyrazole and phenyl rings would be achieved through choice of alkyl ester and 2-hydroxyacetophenone respectively, as illustrated in figure 6.

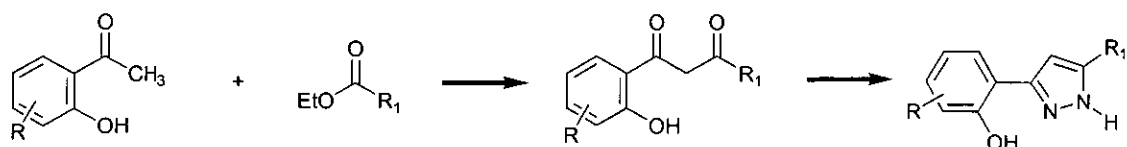


Figure 6 : Substitution possibilities using method (b)

This second synthetic pathway was the method used by Avecia to synthesise the 5- R_1 -3-(2-hydroxyphenyl)-pyrazoles discussed in section 4.4. A third method for the preparation of this type of ligand involving the reaction of substituted chromones directly with hydrazines has been reported⁸, but was not attempted in this study.

4.2.2 Metal Complexes

The copper(II) and nickel(II) complexes, **4** and **5**, were prepared by reaction of one equivalent of the appropriate metal acetate with two equivalents of ligand **1** in methanol at room temperature¹². The acetate in the reaction medium acts as a buffer binding the protons liberated from the ligands to form acetic acid. The reaction scheme is presented in figure 7.

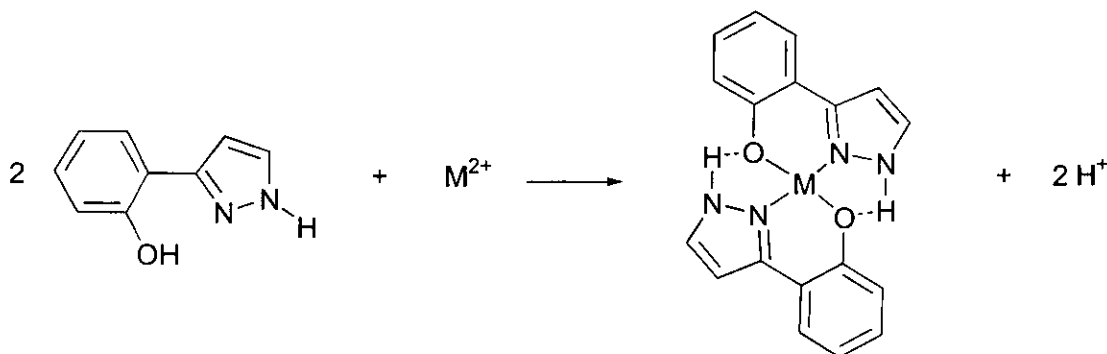


Figure 7 : Complexation of a metal(II) ion by **1** showing the desired, pseudomacrocyclic hydrogen bonding motif around the central metal ion

4.3 Characterisation

4.3.1 Free Ligand, 1

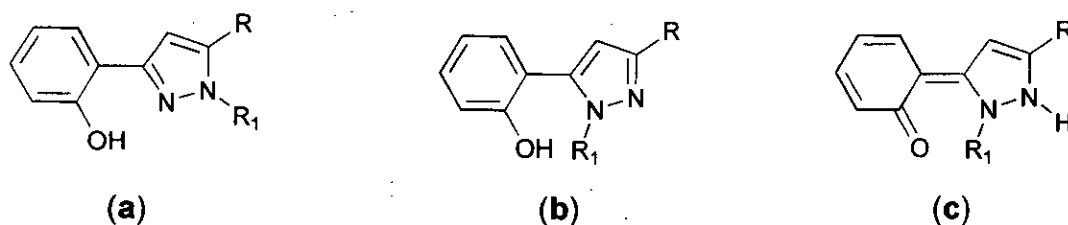


Figure 8 : Forms of N-substituted 3-(2-hydroxyphenyl)-pyrazoles

N-Substituted 3-(2-hydroxyphenyl)-pyrazoles have three possible forms, as shown in figure 8. Evidence for the quinonoid⁶ type form, c, has never been recorded in the literature, and additionally all spectroscopic data on this type of molecule gives strong evidence for their existence in an aryl pyrazole form (either a or b). Both of the isomers, a and b, of the derivative, in which R is a proton and R₁ a phenyl group, have been identified on the basis of ¹H NMR evidence by Singh *et al.*⁸. Isomer b is the minor isomer in this case, due to the steric crowding caused by the proximity of the N-phenyl ring to the hydroxyl group. This also causes a disruption of the co-planarity of the phenyl ring and the pyrazole ring due to twisting around the carbon - carbon bond linking the two rings. Addison and Burke¹ synthesised the derivative, in which R is a methyl group and R₁ a phenyl group and concluded that the isomer formed in this case must also be b, since it was impossible to form a copper(II) chelate from the ligand. However, it is likely that it would be difficult to form a metal chelate from *either* isomer due to the steric bulk of the substituents. X-ray crystallography gives evidence for the existence of both isomeric forms of this ligand⁶, however solution state evidence is less well defined, with literature IR and ¹H NMR data unable to be unambiguously assigned to either isomer a or b⁶⁻⁸. ¹³C NMR has, however, been shown to provide more conclusive evidence on the structures of pyrazoles¹³. This is

particularly true for the study of the tautomeric forms of the ligand (**1**) of interest in this project, which does not have an N-alkyl or N-aryl substituent. Ligand **1** could show two tautomeric forms, which are both able to form intramolecular hydrogen bonds (Figure 9), leaving one proton available to form intermolecular hydrogen bonds with other molecules of **1** or solvent molecules. The formation of intermolecularly hydrogen bonded dimers of tautomer **a** has been observed in the solid state⁶.

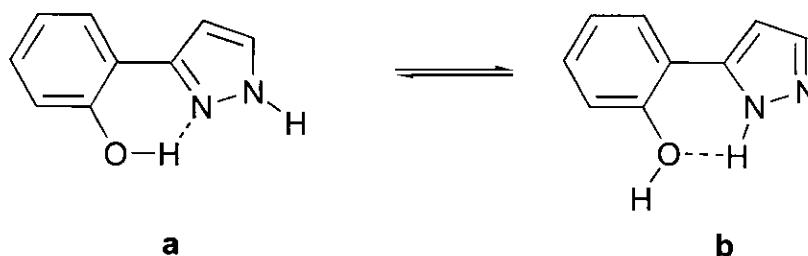


Figure 9 : Tautomeric forms of ligand **1**

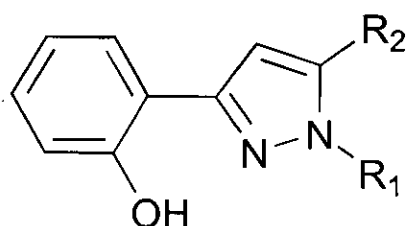
The solid state IR spectrum of **1** shows the expected absorptions for OH, NH, C=N, C-O and aromatic C-H stretches. The OH and NH absorptions overlap at ca. 3300 cm^{-1} , which is low for hydroxyl absorptions and indicates that this group is intramolecularly hydrogen-bonded¹⁴. The products obtained from both synthetic routes to **1** have identical ¹H NMR spectra. It is interesting to note that the amino and hydroxyl protons occur at approximately 11 and 13 ppm respectively. These δ -values suggest a large degree of deshielding of both protons presumably caused by hydrogen bonding¹⁴ to either other molecules of **1** or, more likely, solvent molecules of DMSO. The EI mass spectra of **1** were as expected, with peaks assignable to the parent molecules and to the expected fragments of the free ligand. In an attempted to gain evidence for ligand association in solution, electrospray mass spectrometry was run on a 10^{-5} M sample of **1** in methanol. The low mass range (50-200 a.m.u.) spectrum showed a peak for the free ligand at 161 a.m.u., however peaks assignable to higher oligomers were not seen in the normal mass range (200-2000 a.m.u.).

4.3.2 Metal Complexes

The IR spectrum of the copper(II) complex, **4**, shows a bathochromic shift of ca. 50 cm^{-1} of the absorption of the phenolic C-O stretch on complexation, indicating that it is likely to be occurring *via* the hydroxyl oxygen atom. This cannot be confirmed by the absence of the hydroxyl O-H stretch in the spectrum of **4**, however, as a broad absorption at ca. 3470 cm^{-1} presumably due to solvent or water is observed. An absorption at ca. 3300 cm^{-1} attributable to the N-H stretch indicates that this structural feature has not been lost on complexation. The FAB mass spectrum of **4** shows peaks assignable to CuL_2 and CuL , while that of **5** is considerably more complicated, showing peaks assignable to fragments Ni_xL_y ($x,y = 1-4$). These species are assumed to have been formed in the mass spectrometer.

4.4 Solvent Extraction from Sulphate Media

The results of reagent screens carried out to assess the copper loading and stripping capacities and the selectivity for copper(II) over iron(III) of a variety of 3-(2-hydroxyphenyl)-pyrazoles are presented in table 1. The tests were carried out by Mr. John Campbell of Avecia (Manchester) using 0.05 M solutions of the ligands in dichloromethane as described in section 3.7.6.1. The substituent nomenclature, R_1 and R_2 , refers to the diagram below.



Aqueous Contact Solution		5.00 gl ⁻¹ Cu Feed	Strip Acid ^a	5.00 gl ⁻¹ Cu/ 5.00 gl ⁻¹ Fe Feed		5.00 gl ⁻¹ Fe Feed
R ₁	R ₂	gl ⁻¹ Cu	gl ⁻¹ Cu	gl ⁻¹ Cu	ppm Fe	ppm Fe
H ^b	H	1.02	0.003	1.0	- ^c	- ^c
CH ₃	H	0.10	0.000	- ^d	- ^d	- ^d
H	<i>tert</i> -Bu	1.10	0.005	1.1	5	320
H	n-C ₈ H ₁₇	1.30	0.005	1.4	1	420
H	C ₂ H ₅ OC(O)	1.10	0.003	- ^e	- ^e	- ^e
P50		1.44	0.196	1.4	< 1	69

Table 1 : Solvent extraction data for 3-(2-hydroxyphenyl)-pyrazoles and P50 : Metal loadings in the organic phase

- ^a Strip acid contains 5.00 gl⁻¹ copper(II) and 125 gl⁻¹ sulphuric acid
^b Ligand 1; All other ligands were synthesised by Mr. J. Campbell at Avecia
^c The results of these tests are unreliable due to precipitation of the iron(III) complex
^d These tests were not carried out due to lack of copper loading ability
^e Data not available

It is clear that all the ligands tested, apart from the N-methyl derivative, possess copper loading characteristics comparable to those of P50 and are stripped of copper much more efficiently. The N-methyl derivative only loaded copper to ca. 6 % (based on the formation of CuL₂ from a 0.05 M ligand solution) as might be expected due to the steric bulk of the methyl substituent blocking access to the chelating unit of the ligand. The n-octyl derivative loads copper to a slightly higher capacity than the *tert*-butyl derivative. This may result from more favourable solvation of this more lipophilic derivative in the solvent, dichloromethane. These ligands also showed good selectivity for copper(II) over iron(III) despite loading iron(III) to approximately 40 % (based on the formation of FeL₃ from a 0.05 M ligand solution) on contact with a pure 5 gl⁻¹ iron(III) feed.

On contact with increasingly strong strip acid, however, these ligands became protonated until, at a concentration of 200 gl⁻¹ sulphuric acid, they

were 100 % protonated. This result suggests that if used in a solvent extraction circuit these reagents may facilitate the transfer of acid into the organic phase, which would cause major operational problems. In an attempt to circumvent this problem, the ester-substituted derivative (Figure 10) was synthesised and tested. Electron-withdrawing groups, such as esters and nitro substituents, decrease the basicity of a molecule by spreading the charge out such that the system becomes stabilised¹⁵. Thus the acidity (and therefore pK_a value) of the system increases. This methodology proved successful and no evidence for protonation was seen on prolonged contact of this ligand (Figure 10) with strip acid.

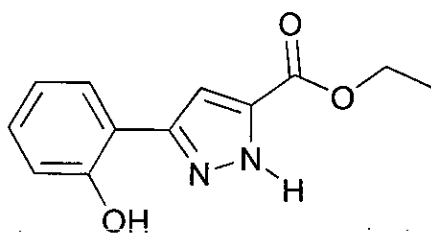


Figure 10 : 3-(2-Hydroxyphenyl)-pyrazole-5-carboxylic acid ethyl ester

4.5 X-Ray Crystallography

There are eighteen structures containing the fragment illustrated in figure 11 in version 5.18 of the Cambridge Crystallographic Database¹⁶, of which only four are relevant to this work. These structures are summarised in table 2.

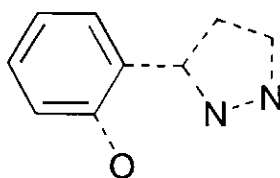


Figure 11 : Fragment used in CCDC search
Note : - - - denotes "any" type of bond

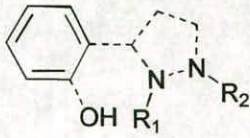
Ligand	R ₁	R ₂	CCDC Code	Notes
	-	H	KUFVAI ⁶	Ligand 1
	-	CH ₃	MEPZFE ²	[FeL ₂ (MeOH) ₂]NO ₃ .MeOH
	-	CH ₃	KUFVEM ⁶	-
	CH ₃	-	KUFVOW ⁶	-

Table 2 : CCDC search results

4.5.1 Free Ligands

The structure of the free ligand 1 was determined by Catalán *et al.*⁶ and is presented in figure 12.

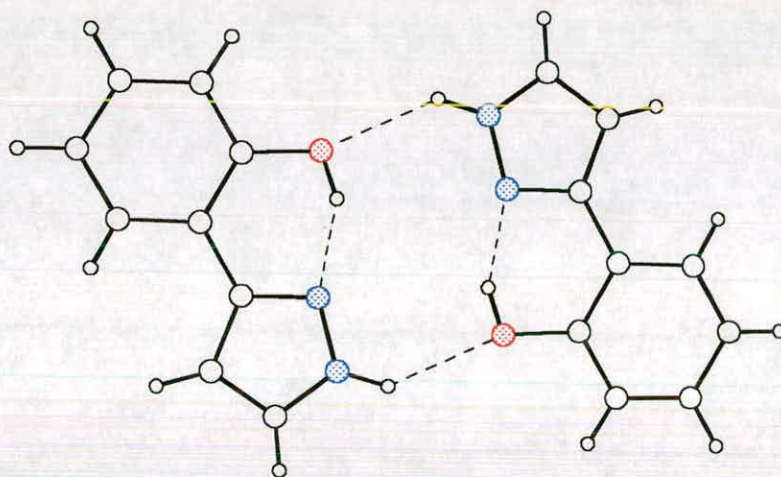
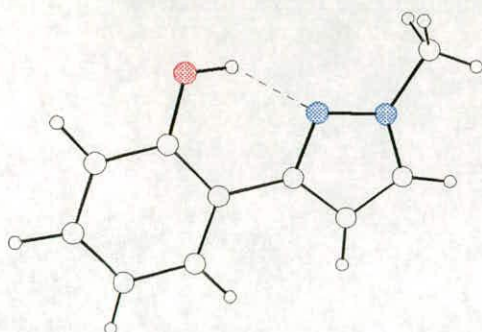
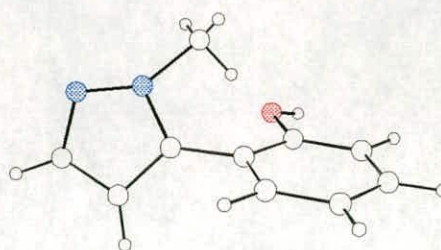


Figure 12 : Structure of 1-H-3-(2-hydroxyphenyl)-pyrazole, **1**⁶.
CCDC code KUFVAI

The molecule exists as independent, hydrogen bonded dimers, as shown in figure 12, two of which are found in the unit cell. Additionally, the structures of the two N-methylated derivatives of 3-(2-hydroxyphenyl)-pyrazole have been determined⁶ and are shown in figure 13.



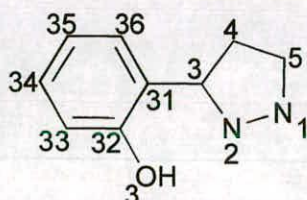
1-Methyl derivative
CCDC code : KUFVEM



2-Methyl derivative
CCDC code : KUFVOW

Figure 13 : The structures of methylated derivatives of **1**

These three structures can be compared to assess the effect of the methyl substituent and its position on the preorganisation of the ligands, in terms hydrogen bonding interactions, planarity and extent of delocalisation of the bonding in these structures. The hydrogen bonding parameters in all three structures are presented in table 3. Atom numbering is defined below.



Structure	H-Bond	D-H...A	D...A / Å	H...A / Å	D-H...A / °
Ligand 3 KUFVAI	Intra	O3-H...N2	2.595(3)	1.78(4)	151(4)
	Inter	N1-H...O3'	2.986(3)	2.22(4)	138(3)
1-methyl KUFVEM	Intra	O3-H...N2	2.596(3)	1.84(5)	145(4)
2-methyl KUFVOW	Inter	O3-H...N2'	2.715(3)	1.88(3)	173(3)
P50-type^a	Intra	O-H...N	2.626	1.834	147.4
	Inter	O-H...O'	2.816	1.988	159.8

Table 3 : Hydrogen bonding parameters⁶ for **1** (KUFVAI) and its 1-methyl (KUFVEM) and 2-methyl (KUFVOW) derivatives

^a These parameters are taken from the dimeric structure of 2-hydroxybenzaldehyde oxime^{17,18}; CCDC code : SALOXM.

The intramolecular hydrogen bonding in **1** is very similar to that in the 1-methyl derivative (KUFVEM), but the intramolecular hydrogen bond is shorter than that found in the P50-type oxime. Conversely, the intermolecular hydrogen bond is longer. No intramolecular hydrogen bond exists in the 2-methyl derivative (KUFVOW), due to the presence of the methyl substituent on N2. The methyl substituents in KUFVEM and KUFVOW are assumed to prevent the formation of dimers as seen for **1**, and instead molecular networks are formed *via* additional, weak interactions ($H\cdots A \geq 2.55 \text{ \AA}$) between aryl hydrogen atoms and phenolic oxygen atoms on adjacent molecules⁶.

The planarity of the ligands can be assessed in terms of both torsion angle around the C31-C3 bond, which links the two rings or the dihedral angle between the phenyl ring plane (defined by C31-36) and the pyrazole ring (defined by N1, N2, C3-C5) plane in each ligand. These parameters are presented in table 4.

Structure	Torsion Angle C32-C31-C3-N2 / °	Dihedral Angle / °
1	2.7(4)	3.1
1-methyl	4.7(5)	4.2
2-methyl	61.7(4)	59.3

Table 4 : Torsion angles and dihedral angles in **1** (KUFVAI) and its 1-methyl (KUFVEM) and 2-methyl (KUFVOW) derivatives⁶

Ligand **1** and its 1-methyl derivative are almost planar, but the methyl substituent on N2 in KUFVOW leads to significant distortions, resulting in a dihedral angle between the two ring planes of ca. 60 °.

While the equivalent bonds in the phenyl rings in all three structures are of comparable length, falling within the range 1.36 - 1.41 Å, the bonds in the pyrazole rings differ slightly, as shown in table 5. From comparison with the standard bond lengths¹⁹ recorded in table 6, the bonds in the structure of ligand **1** can all be described as being of "intermediate character", ie: the

pyrazole system is delocalised. The majority of bonds in KUFVEM and KUFVOW are also of intermediate character, apart from N1-C5 in the 1-methyl derivative (KUFVEM) and N2-C3 in the 2-methyl derivative (KUFVOW), which can be classed as single bonds. This is due to the presence of the methyl derivatives on N1 and N2 respectively. Additionally, C3-C4 is comparatively shorter whilst C4-C5 is comparatively longer in the 2-methyl derivative, suggesting a much greater overall degree of localisation in this ligand than in the other two. This is likely to be a reflection of the lack of planarity in this structure, which precludes the possibility for hydrogen bonding. Interestingly, the bonds C32-O3 are not significantly different in the methylated derivatives, while that in **1** is longer, indicating that the intramolecular hydrogen bond in this structure may be stronger than that found in its 1-methyl derivative (KUFVEM).

Bond	1	1-methyl	2-methyl
N2-C3	1.336(3)	1.335(4)	1.357(3)
C3-C4	1.410(3)	1.401(5)	1.377(4)
C4-C5	1.369(4)	1.359(5)	1.390(4)
C5-N2	1.331(4)	1.432(5)	1.334(2)
N1-N2	1.345(3)	1.354(4)	1.358(3)
C3-C31	1.466(3)	1.463(5)	1.468(4)
C32-O3	1.369(3)	1.359(5)	1.358(3)
O3-H3	0.90(4)	0.87(5)	0.84(3)
N1-H1	0.93(5)	-	-
N1-C1	-	1.451(6)	-
N2-C2	-	-	1.457(4)

Table 5 : Bond lengths⁶ (in Å) in **1** (KUFVAI) and its 1-methyl (KUFVEM) and 2-methyl (KUFVOW) derivatives

Note : Nomenclature refers to diagram with table 3

Bond	C _{sp2} - O	C _{sp2} - C _{sp2}	C _{sp2} - N _{sp2}	N _{sp2} - N _{sp2}
Single	1.33(2)	1.46(2)	1.36(1)	1.40(3)
Double	1.21(1)	1.32(2)	1.28(1)	1.22(1)

Table 6 : Standard single and double bond lengths (in Å)¹⁹

4.5.2 Metal Complexes

The structure of the copper(II) complex (4) of ligand 1 was determined and is shown in figure 14. It can be seen that this ligand mimics the metal complexing behaviour of P50-type oximes by forming inter-ligand (N-H...O) hydrogen bonds of 2.23(4) Å. The only structure in the literature¹⁶, which can be directly compared with that of 4, is that of the iron(III) complex of 3-(2-hydroxyphenyl)-5-methyl-pyrazole² (Figure 15), in which the equivalent distance (H_{N1}...O') is 2.77 Å.

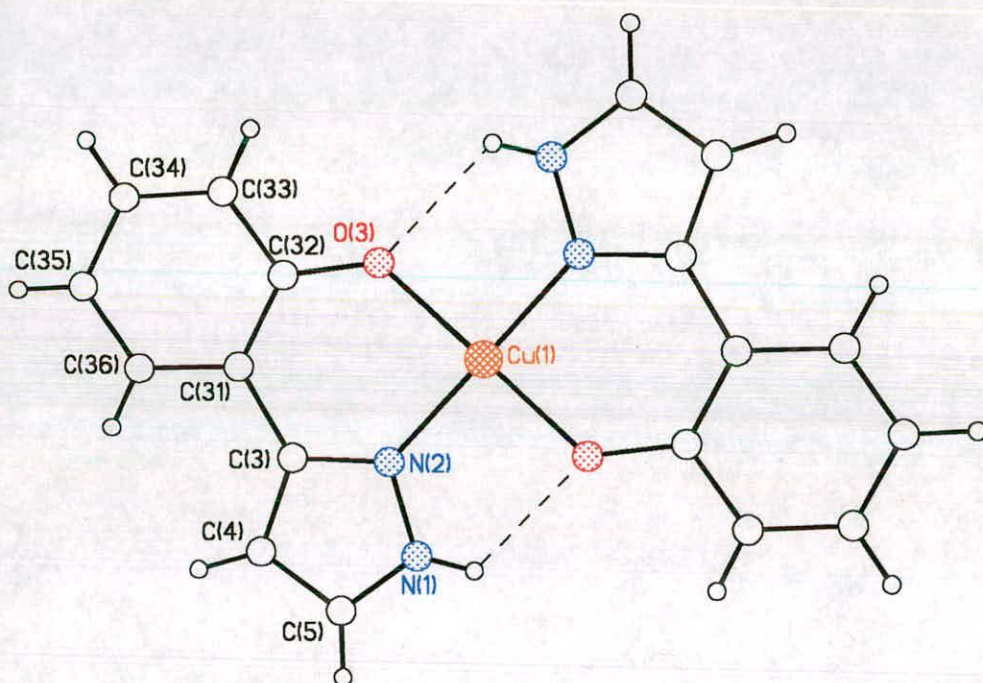


Figure 14 : Structure of [Cu(1-H)₂] : 4

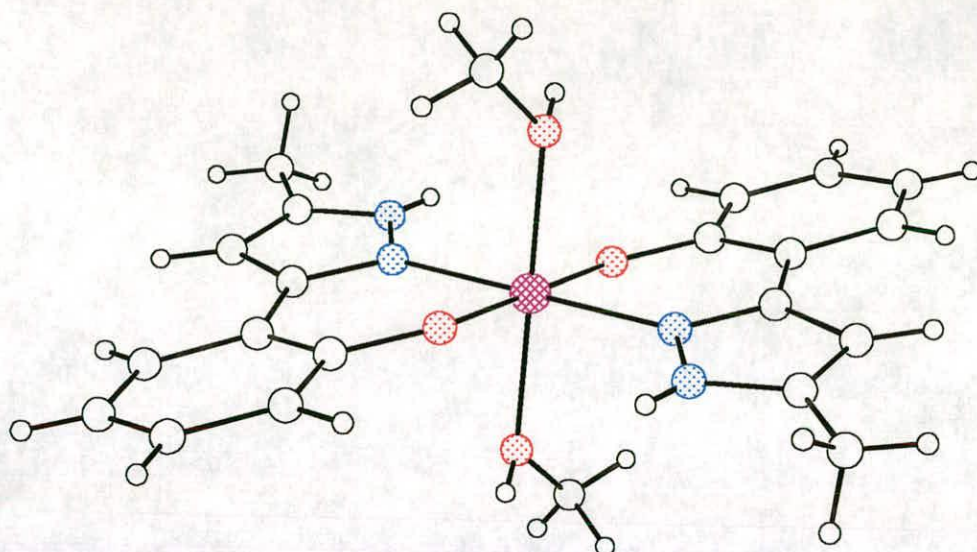


Figure 15 : Central coordination sphere of the iron(III) complex of 3-(2-hydroxyphenyl)-5-methyl-pyrazole², [FeL₂(MeOH)₂]NO₃.MeOH (CCDC code : MEPZFE). The nitrate anion and additional lattice methanol molecule have been excluded for clarity.

Whilst this is considered²⁰ to be relatively long for an effective hydrogen bond, the donor atom to acceptor atom distance (N1...O3'; 3.079 Å) is only slightly longer than in many comparable complexes (see, for example, table 19 in chapter 3). The positioning of the hydrogen atom in these systems is discussed later (see table 10).

It is also interesting to note that whilst the iron(III) structure is octahedral, the axial coordination sites are occupied by methanol molecules and not by another pyrazole ligand. This may arise from steric crowding preventing three pyrazole ligands from fitting round the iron(III) cation to form a neutral complex. Also, any arrangement of three bidentate ligands (1) about an octahedral metal ion will prevent the formation of the apparently favoured pseudomacrocyclic planar units with "head-to-tail" hydrogen bonding. Instead the 1+ charge on the resulting [FeL₂(MeOH)₂] complex is counterbalanced by a lattice nitrate anion. It is interesting to note that there are no known, comparable, mononuclear iron complexes of P50-type oxime ligands, although several multinuclear structures have been reported¹⁶.

The coordination plane of the central copper atom in structure **4** is very nearly square, suggesting that this ligand provides ideal geometry for a copper(II) ion to form a square planar complex. The metal to donor atom distances in **4**, the iron(III) structure MEPZFE (Figure 15) and the copper(II) complexes of phenolic oximes¹⁶ are presented in table 7.

Structure	M	M-O	M-N
4	Cu(II)	1.9148(14)	1.919(2)
P50-type	Cu(II)	1.893	1.955
MEPZFE	Fe(III)	1.888(3)	2.068(3)

Table 7 : Metal to donor atom distances in **4** and MEPZFE² along with the average values for five copper(II) complexes of P50-type oximes¹⁶ (in Å)

The Cu-O and Cu-N distances in **4** are very similar, whilst in P50-type complexes the Cu-O bonds are significantly shorter than the Cu-N bonds. The phenolic oxygens also appear to be more strongly bonded in the iron(III) pyrazole complex, MEPZFE (Figure 15). It is to be expected, however, that the relatively hard iron(III) cation will interact more strongly with the phenolic donor. In the copper(II) pyrazole complex, **4**, the two ligands are assumed to provide a rigid framework for the metal ion, such that this variation becomes insignificant.

Structure	M	O-M-N / °	O...N / Å
4	Cu(II)	90.89(7)	2.732(2)
P50-type	Cu(II)	91.2(4)	2.75(3)
MEPZFE	Fe(III)	86.9(1)	2.723

Table 8 : Bite angles and bite distances in **4** and MEPZFE² along with the average values for five copper(II) complexes of P50-type oximes¹⁶

It is interesting to note that the bite distances in both pyrazole complexes, **4** and MEPZFE, are very similar and, in turn, are slightly shorter than those in

the phenolic oxime complexes. The bite distance in the free ligand structures of **1** (KUFVAI⁶) is shorter (2.594 Å) than those in the pyrazole complexes suggesting that, on complexation of either copper(II) or iron(III), the ligand must distort to accommodate the metal ion. The mean deviations from planarity of the whole chelate unit (defined by M, O3, C32, C31, C3, N2, N1, H1, O3A, C32A, C31A, C3A, N2A, N1A, H1A) in **4** and the iron(III) complex, MEPZFE, are 0.01 and 0.10 Å²². The planarity of the chelating unit about its central C31-C3 bond can be compared by determining the torsion angle C32-C31-C3-N2, which is 0.3 ° in the copper complex **4**, whilst in the iron complex it is 7.2 °. The dihedral angles between the pyrazole ring plane (defined by N1, N2, C3, C4, C5) and the phenyl ring plane (defined by C31-C36) in the coordinated ligands are found to be 1.7 ° and 7.3 ° respectively, indicating that whilst the copper complex is almost totally planar, there are significant distortions from planarity in the iron complex. Interestingly, the only significant difference between the bond lengths in the ligand **1** (KUFVAI⁶) and the two metal complexes, which are presented in table 9, is that of C32-O3, which is longer in the free ligand possibly due to the effect of the intramolecular hydrogen bond (Table 7). On complexation, the phenol group is deprotonated and complexation occurs *via* O3, thus the stronger bond is probably a reflection of the π back donation by the metal ions.

Bond	Ligand 1	Cu(II) Complex 4	Fe(III) Complex ²
N2-C3	1.336(3)	1.343(3)	1.339(4)
C3-C4	1.410(3)	1.405(3)	1.406(6)
C4-C5	1.369(4)	1.372(3)	1.367(6)
C5-N2	1.331(4)	1.330(3)	1.330(5)
N1-N2	1.345(3)	1.345(3)	1.356(5)
C3-C31	1.466(3)	1.459(3)	1.464(5)
C32-O3	1.369(3)	1.323(3)	1.332(4)
N1-H1	0.93(5)	0.806	0.67

Table 9 : Bond lengths in **4** and MEPZFE compared with those in **1**⁶
 Note : Nomenclature refers to diagram with table 3

The parameters illustrated in figure 16 indicate that the cavity in the free ligand dimer of **1** is significantly larger than that in the complex **4**, despite the inter-ligand hydrogen bonds being essentially the same length.

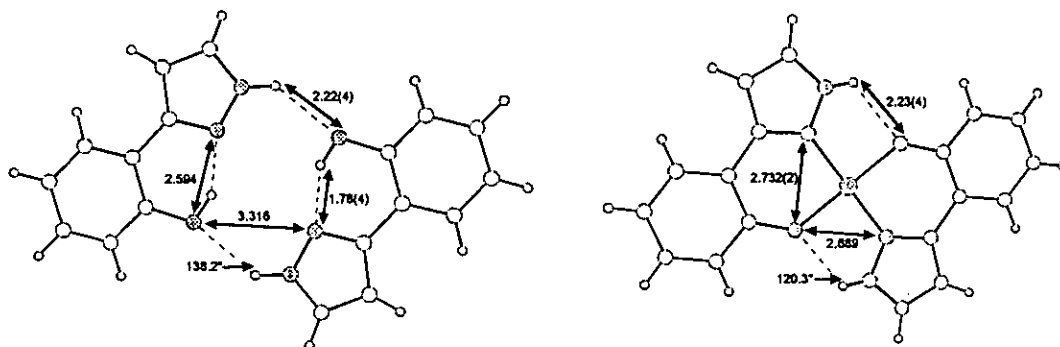


Figure 16 : A comparison of the geometry in the free pyrazole ligand **1** (KUFVAI⁶) vs. that in the copper complex **4**. (Lengths in Å)

Not only are the two coordinated ligands in **4** held much more closely together but the bite distance also increases in length by more than 0.1 Å, indicating that the pyrazole ligand must significantly reorganise on complexation to copper(II). In comparison, the geometries of the free ligand dimer of a phenolic oxime ligand¹⁷ and that of its copper(II) complex²¹ are very similar, as shown in figure 17. Rearrangement of the free phenolic oxime ligand on complexation to copper(II) is minimal, the main difference in the geometries being the much closer approach of the two coordinated ligands in SALCOP. This is most clearly illustrated by the O...N' distance of 2.763 Å in comparison with that of 3.060 Å in the free ligand dimer.

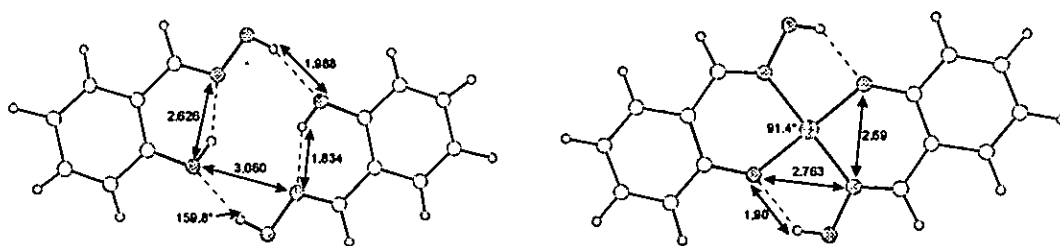


Figure 17 : A comparison of the geometry in the phenolic oxime free ligand (SALOXM¹⁷) vs. that in its copper complex (SALCOP²¹). (Lengths in Å)

From comparison of the two copper(II) complexes, **4** and SALCOP²¹ (Figures 16 and 17 respectively), it is clear that the coordination geometries of the two systems are very similar, the main difference being in the length of the inter-ligand hydrogen bond, which is 1.90 Å in SALCOP and 2.23 Å in **4**. These values are, however, dependent on the positioning of the hydrogen atoms and a more reliable measure of the hydrogen bonding within a molecule is the donor (D) atom to acceptor (A) atom distance, which is presented in table 10, together with the lengths and angles hydrogen atoms and "standard" parameters²⁰ for this type of hydrogen bond and the equivalent parameters for the two free ligand dimers, SALCOP¹⁷ and **1** (KUFVAI⁶), and the iron(III) structure, MEPZFE².

Parameter	Standard Values	SALOXM	SALCOP	1 (KUFVAI)	4	MEPZFE
H...A / Å	1.5-2.2	1.988	1.90	2.22(4)	2.23(4)	2.772
D...A / Å	2.5-3.2	2.816	2.577	2.596(3)	2.720	3.079
D-H...A / °	130-180	159.8	135.9	138(4)	120.3	111.0

Table 10 : Hydrogen bonding parameters and standard values²⁰

This type of hydrogen bond is classed as a medium strength hydrogen bond, in which the D-H distance is greater than the H...A distance and the attraction is mainly electrostatic²⁰. It is clear from these data that, as previously mentioned, although the H...A distance in the iron(III) structure (MEPZFE) is judged too long for this type of hydrogen bond, the D...A distance falls within the stated range. This is likely to be due to the angle formed at the hydrogen atom, which is relatively small. The equivalent distances in the two copper complexes also fall within the stated ranges. Both the H...A and D...A distances in **4** are longer than those in SALCOP, while the angle at the hydrogen atom is significantly smaller.

Interestingly, the donor set geometry (N_2O_2) is much more nearly “square” in **4** than in SALCOP, which may be due to the fact that not only a six-membered ring but also a five-membered ring is fused to the chelate ring. Even though the bite distance ($N\cdots O$) in **4** is longer than that in SALCOP, the inter-ligand $N\cdots O$ distance is significantly shorter, such that the N_2O_2 donor set in SALCOP can be described as rectangular rather than square. The bite angle in **4** is also significantly smaller than that of SALCOP, and the deviations from overall planarity of the chelate planes are found to be 0.01 Å and 0.03 Å respectively, which again show that the pyrazole ligand results in the more planar system. Finally, the metal to donor atom bond lengths in **4** and SALCOP are copper to nitrogen, 1.919(2) and 1.94(1) Å, and copper to oxygen, 1.9148(14) and 1.92(1) Å, respectively, which again indicate that the geometry adopted on complexation of both types of ligand is very similar. It can therefore be concluded that the very similar copper extraction characteristics of these two types of ligand could be predicted on the basis of the geometries of their solid state complex structures. This discussion is particularly valid in this case, as the solid state structures described are very likely to be very similar to those of the species, $[CuL_2]$, extracted into the non-polar, hydrocarbon phase.

4.6 Conclusions

Ligands based on 3-(2-hydroxyphenyl)-pyrazole have been found to extract and strip copper(II) comparably to P50-type oximes. This is thought to be due, in part, to their ability to provide copper(II) with an extremely square planar coordination geometry on formation of a CuL_2 complex, which is structurally very similar to that of the phenolic oxime complexes. The pyrazole-based free ligands also show a similar propensity to self-association to the phenolic oximes. Development work on, for example, the solubility and solvent extraction kinetics of this class of ligand is being undertaken at Avecia.

4.7 Experimental

4.7.1 Instrumentation

Melting points were determined with a Gallenkamp apparatus and are uncorrected. Elemental analysis was performed on a Perkin Elmer 2400 elemental analyser. IR spectra were obtained on a Perkin Elmer Paragon 1000 FT-IR spectrometer as potassium bromide discs. ^1H and ^{13}C NMR spectra were run on Bruker WP200 and AC250 spectrometers. Chemical shifts (δ) are reported in parts per million (ppm) relative to residual solvent protons as internal standards. Electron impact (EI) mass spectra were obtained either on a Finnigan MAT4600 quadrupole spectrometer or on a Kratos MS50TC spectrometer. Fast atom bombardment (FAB) mass spectra were obtained on a Kratos MS50TC spectrometer in 3-nitrobenzyl alcohol / thioglycerol matrices. Electrospray (ES) mass spectra were obtained on a Thermoquest LCQ spectrometer.

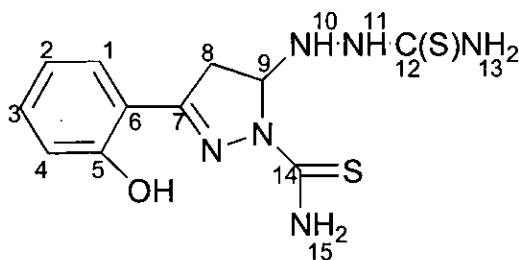
4.7.2 Solvent and Reagent Pretreatment

All reagents and solvents were commercially available (Acros or Aldrich) and were used as received, apart from the precursors 3-(2-hydroxyphenyl)-1-thiocarbonyl-5-thiosemicarbazide-2-pyrazoline (**2**) and 2-hydroxy- ω -formylacetophenone (**3**), which were synthesised as described according to the literature methods^{7,9-11}. Solvents used for analytical purposes (NMR, MS) were of spectroscopic grade.

4.7.3 Synthesis of Precursors

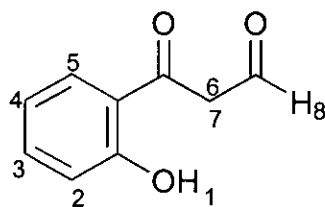
3-(2-Hydroxyphenyl)-1-thiocarbamyl-5-thiosemicarbazide-2-pyrazoline⁷

(2)



Concentrated hydrochloric acid (14 drops) was added dropwise with vigorous stirring to a suspension of chromone (2.0 g, 14 mmol) and thiosemicarbazide (2.5 g, 27 mmol) in ethanol (100 ml). The reaction was heated under reflux for 4 h and the resulting colourless precipitate of **2** filtered off and dried (3.42 g, 78.76 %). mp 208 - 209 °C; (Found C, 42.52; H, 4.66; N, 27.06; C₁₁H₁₄N₆S₂O requires C, 42.56; H, 4.55; N, 27.08 %); IR (cm⁻¹, KBr Disc): ν 3417.6m & 3288.0m & 3225.5s (NH), 3151.7m (OH), 1607.3s & 1593.5s (C=N), 1494.3s (N-C=S), 1372.2m & 1341.7m (C=S), 823.9m & 756.2m (Ar CH); ¹H NMR (DMSO-d₆, 200 MHz): δ 3.33 - 3.37 (m, 2H, H8), 5.58 - 5.63 (d, J_{vic} 8.57 Hz, 1H, H9), 5.94 (br s, 1H, H10), 6.92 - 6.96 (d, J_{ortho} 7.52 Hz, 2H, H1,3), 7.29 - 7.37 (td, J_{ortho} 7.12 / 6.87 / 8.31 Hz, J_{meta} 1.45 Hz, 1H, H2), 7.57 - 7.61 (d, J_{ortho} 8.09 Hz, 1H, H4), 7.66 & 7.90 (2 br s, 2H, H13), 8.20 (br s, 2H, H15), 8.85 (br s, 1H, H11), 9.65 (s, 1H, H5); ¹³C NMR (DMSO-d₆, 63 MHz): δ 38.07 (C8), 73.44 (C9), 116.14 (C6), 117.00 + 119.62 (C1,3), 129.54 (C2), 132.16 (C4), 156.28 (C7), 156.59 (C5), 175.59 (C12), 182.71 (C14); EIMS *m/z* 219 (As in the literature⁷, there is no peak for the parent ion) 17.6 %, M⁺ - NH₂NHC(S)NH₂ = fragment "A", 161 (100.0 %, A - HNCS), 131 (72.6 %, A - {HNCS+N₂+H}), 91 (65.4 %, NH₂NHC(S)NH₂).

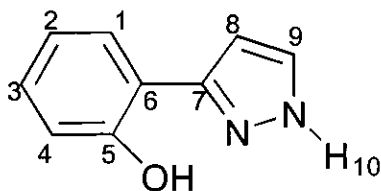
2-Hydroxy- ω -formylacetophenone⁹⁻¹¹ (**3**)



The synthesis was carried out in an inert (nitrogen) atmosphere. Ethyl formate (36.5 ml, 0.452 mol; 98 %) was added with stirring to a grey suspension of sodium hydride (8.34 g, 0.208 mol; 60 % dispersion in mineral oil) in diethyl ether (80 ml; distilled). 2-hydroxyacetophenone (6.2 ml, 0.051 mol) was added slowly with cooling (ice bath) to the reaction medium. When the resulting reaction had subsided, the pale yellow reaction medium was heated under reflux for 10 min, cooled and stirred at room temperature overnight. Ice / water (300 ml) was carefully added to the thick, yellow suspension under cooling (ice bath) and the solution washed with diethyl ether (2 x 200 ml). The diethyl ether layer was removed *via* rotary evaporation and the remaining aqueous layer containing the sodium salt of the desired product was acidified (glacial acetic acid) to give a colourless, microcrystalline precipitate, **3** (6.559 g, 77.71 %). NB: The product was found to turn orange when left for *ca.* three weeks in air. mp 82 °C; ¹H NMR (DMSO-*d*₆, 200 MHz): δ [2.69 - 2.71 (dd, J_{gem} 4.10 Hz, 1H) & 3.00 - 3.02 (dd, J_{gem} 3.32 Hz, 1H) J 61.61 Hz, H6,7], 6.95 - 7.10 (m, 2H, H3,5), 7.52 - 7.61 (t, J_{ortho} 7.76 Hz, J_{meta} 1.80 Hz, 1H, H4), 7.69 - 7.74 (dd, J_{ortho} 7.78 Hz, J_{meta} 1.47 Hz, 1H H2), 8.30 (br s, $\frac{1}{4}$ H, H8 ?), 9.49 (br d, J 8.80 Hz, $\frac{1}{4}$ H, H1); EIMS m/z 164 (73.4 %, M^+), 147 (51.1 %, $M^+ - \text{OH}$), 136 (35.4 %, $M^+ - \text{CO}$), 121 (100.0 %, $M^+ - \text{CHO}$).

4.7.4 Synthesis of 1-H-3-(2-hydroxyphenyl)-pyrazole (1)

Two methods were employed in the synthesis of **1**, as described below.



Method a⁷

Precursor **2** (2.0 g, 6.4 mmol) was added to an aqueous solution of formic acid (40 ml of 85 % solution) and the reaction heated under reflux for 2 hour. The resulting pale yellow solution was cooled to RT and neutralised using aqueous sodium carbonate solution (53 g, 0.5 mol, in 200 ml H₂O) to yield a pale pink precipitate. The crude product (0.77 g) was recrystallised from ethanol / water (10:1) to give a pale beige, microcrystalline solid, **1** (0.51 g, 59.92 %). mp 93 - 95 °C; (Found C, 67.05; H, 4.67; N, 17.35; C₉H₈N₂O requires C, 67.48; H, 5.04; N, 17.49 %); IR (cm⁻¹, KBr Disc): ν 3272.6 br s (NH, OH), 1589.2s (C=N), 1257.7s (C-O), 778.9s & 746.0s (Ar CH); ¹H NMR (DMSO-d₆, 200 MHz): δ 6.84 - 6.94 (m, 3H, H1,3,8), 7.13 - 7.21 (t, J_{ortho} 7.45 Hz, J_{meta} 1.66 Hz, 1H, H2), 7.70 - 7.75 (dd, J_{ortho} 7.60 Hz, J_{meta} 1.44 Hz, 1H, H4), 7.87 (s, 1H, H9), 10.98 (br s, 1H, H10), 13.23 (br s, 1H, H5); ¹³C NMR (DMSO-d₆, 63 MHz): δ 102.36 (C1), 116.50 (C3), 117.17 (C8), 119.32 (C2), 126.95 (C9), 128.83 (C4), 131.24 (C6), 148.94 (C7), 155.18 (C5); EIMS *m/z* 160 (100.0 %, LH), 131 (34.2 %, LH - NNH), 77 (12.1 %, Ph).

Method b^{1,6,8}

A mixture of hydrazine monohydrate (1.50 ml, 0.031 mol), precursor **3** (5.0 g, 0.03 mol) and glacial acetic acid (5 drops) in ethanol (100 ml; dried²³) was heated under reflux for 4 h. The resulting yellow solution was reduced in volume to yield a colourless, microcrystalline product, **1** (4.449 g, 92.60 %). ¹H NMR (DMSO-d₆, 200 MHz): δ 6.83 - 6.85 (m, 3H, H1,3,8), 7.12 - 7.20 (t, J_{ortho} 7.68 Hz, J_{meta} 1.70 Hz, 1H H2), 7.70 - 7.74 (dd, J_{ortho} 7.71 Hz, J_{meta} 1.66 Hz, 1H, H4), 7.84 - 7.85 (d, J_{vic} 2.35 Hz, 1H, H9), 10.0 - 13.0 (br s, 0.8 H,

OH₅ / NH₁₀); EIMS *m/z* 160 (100.0 %, LH), 131 (64.7 %, LH - NNH), 77 (17.9 %, Ph).

Electrospray mass spectrometry acquisition parameters for a 10⁻⁵ M sample of **1** in HPLC grade methanol are presented in table 8. A peak for the free ligand was observed at 161 a.m.u. in the low mass range (50-200 a.m.u.), however no peaks for oligomeric species were observed in the normal mass range (200-2000 a.m.u.).

Flow Rate / μLmin^{-1}	Sheath Gas, arb.	Aux. Gas, arb.	Spray Voltage / kV	Capillary Temp./ $^{\circ}\text{C}$	Capillary Volt. / V
10	50	0	5.5	200	25
Tube Lens off / V	Octapole 1 / V	Lens Voltage / V	Octapole 2 / V	Octapole RF / A	Spray Current / μA
45	-3	-24	-5.5	-	0.83

Table 11 : ESMS parameters for **1**

4.7.5 Synthesis of the Metal Complexes¹²

[Cu(3-H)₂] : **4**

Copper acetate monohydrate (0.19 g, 0.9 mmol) was added to a solution of **1** (0.30 g, 1.9 mmol) in methanol (10 ml). Instantly a dark olive green precipitate of **4** was formed, which was isolated by filtration and dried *in vacuo* (0.34 g, 93.68 %). X-ray quality crystals were obtained by layered liquid / liquid diffusion of hexane into a DCM solution of **4**. dec. 253 - 255 $^{\circ}\text{C}$; (Found C, 56.4; H, 3.7; N, 14.4; C₁₈H₁₄N₄O₂Cu requires C, 56.6; H, 3.7; N, 14.7 %); IR (cm⁻¹, KBr Disc): ν 3468.2 br m (OH from solvent (MeOH)), 3323.8s (NH), 1599.7s (C=N), 1318.2s (C-O), 746.4s (Ar CH); FABMS *m/z* 383 (68.9 %, CuL₂), 222 (57.6 %, CuL).

It should be noted that a similar reaction to try to prepare the equivalent zinc(II) complex was carried out, but that no evidence for zinc complexation could be gained from mass spectroscopy experiments.

[Ni(3-H)₂] : **5**

A nickel(II) complex of **1** was prepared as for **4**, using nickel(II) acetate tetrahydrate as the source of nickel (II). 0.097 g, 82.37 %; green powder;

dec. 260 °C; FABMS m/z 1039 (1.9 %, Ni₄L₅), 872 (1.0 %, Ni₄L₄), 808 (9.8 %, Ni₃L₄), 753 (1.6 %, Ni₂L₄), 650 (4.4 %, Ni₃L₃), 593 (3.5 %, Ni₂L₃), 433 (6.1 %, Ni₂L₂), 377 (100.0 %, NiL₂), 217 (20.5 %, NiL), 161 (13.2 %, LH).

4.7.6 Solvent Extraction Experiments

Reagent screens to assess the load and strip characteristics (Screen 1 : Tests a and b) and the selectivity for copper(II) over iron(III) (Screen 2 : Tests a and b) of a range of 3-(2-hydroxyphenyl)-pyrazoles, were carried out as described in section 3.7.6.1. The experiments were performed by Mr. John Campbell at Avecia (Manchester) using 0.05 M solutions of the ligands in DCM.

4.7.7 X-Ray Crystallography

The structure of **4** was determined by Dr. Simon Parsons at the University of Edinburgh. The data were collected at 220 K on a Stoe Stadi-4 diffractometer equipped with an Oxford Cryosystems low temperature device, using Cu-K α radiation. Reflections were scanned in ω - θ mode. The structure was solved by Patterson methods (DIRDIF²⁴) and completed by iterative cycles of least squares refinement against F^2 and difference Fourier synthesis (SHELXTL¹⁹). H-atoms were idealised, being placed using geometric or difference (H1) maps and treated by riding or refall (H1) methods. In all cases non-H atoms were modelled with final anisotropic displacement parameters and final refinement statistics are presented in tables 12.

Structure	4	Crystal size/mm	0.50 x 0.16 x 0.16
Formula	C ₁₈ H ₁₄ N ₄ O ₂ Cu	D_c/g cm⁻¹	1.666
M	381.87	Z	2
Crystal system	monoclinic	μ/mm⁻¹	2.207
Space group	P2 ₁ /n	Transmission factors	T _{min} 0.333, T _{max} 0.433
a/Å	5.1667(2)	θ Limits/°	5-70
b/Å	12.1668(7)	No. of unique data	3475
c/Å	12.2541(7)	No. data with [F>4σ(F)]	1260
α/°	90	No. variables	120
β/°	98.906(4)	R1	0.0319
γ/°	90	wR2	0.0918
U/Å³	761.03(7)	Δρ_{max}, Δρ_{min}/e Å⁻³	0.262, -0.385

Table 12 : Crystallographic data for structure 4

4.8 References for Chapter 4

- 1 A.W. Addison and P.J. Burke, *J. Hetero. Chem.*, 1981, **18**, 803-805
- 2 E.W. Ainscough, A.M. Brodie, J.E. Plowman, K.L. Brown, A.W. Addison and A.R. Gainsford, *Inorg. Chem.*, 1980, **19**, 3655-3663
- 3 A.M.S. Silva, L.M.P.M. Almeida, J.A.S. Cavaleiro, C. Foces-Foces, A.L. Lamas-Saiz, C. Fontenas, N. Jagerovic and J. Elguero, *Tetrahedron*, 1997, **53**(34), 11645-11658
- 4 S.K. Dutta, K.K. Nanda, U. Flörke, M. Bhadbhade and K. Nag, *J. Chem. Soc. Dalton Trans.*, 1996, 2371-2379
- 5 R.B. Palkar and H.E. Master, *Indian Journal of Heterocyclic Chemistry*, 1999, **8**, 315-318
- 6 J. Catalán, F. Fabero, R.M. Claramunt, M.D. Santa Maria, M. C. Foces-Foces, F.H. Cano, M. Martinez-Ripoll, J. Elguero and R. Sastre, *J. Am. Chem. Soc.*, 1992, **114**, 5039-5048
- 7 P. Maib and Z. Jermanowska, *Pol. J. Chem.*, 1987, **61**, 111-122
- 8 S.P. Singh, D Kumar and D. Kumar, *Synth. Comm.*, 1996, **26**(17), 3193-3200
- 9 R. Mozingo, *Organic Syntheses Collective Volume III*, Wiley, New York, 1955, pp. 387-390
- 10 A. Schönberg and A. Sina, *J. Am. Chem. Soc.*, 1950, **72**, 3396-3399
- 11 R.S. Becker, S. Chakravorti, C.A. Gartner and M. de Graca Miguel, *J. Chem. Soc. Faraday Trans.*, 1993, **89**(7), 1007-1019
- 12 A.D. Garnovskii, *Koord. Khim.*, (*Engl. Trans.*), 1992, **18**(7), 675 - 698
- 13 C. Lopez, R.M. Claramunt, S. Trofimenko and J. Elguero, *Canadian J. Chem.*, 1993, **71**(5), 678-684
- 14 D.H. Williams and I. Fleming, *Spectroscopic Methods in Organic Chemistry*, McGraw-Hill, London, 5th Edition, 1995
- 15 J. March, *Advanced Organic Chemistry*, Wiley Interscience, New York, 4th Edition, 1992, pp. 263-265
- 16 D.A. Fletcher, R.F. McMeeking and D.F. Parkin, *J. Chem. Inf. Comput. Sci.*, 1996, **36**(4), 746-749. Cambridge Database Release 5.18 (1999)

- 17 C.E. Pfluger and R.L. Harlow, *Acta Cryst.*, 1973, **B29**, 2608-2609
- 18 PLATON multipurpose crystallographic tool: A.L. Spek, *Acta Cryst.*, 1990, **C34**, A46
- 19 F.H. Allen, O. Kennard, D.G. Watson, L. Brammer, G. Orpen and R. Taylor, *J. Chem. Soc. Perkin Trans II*, 1987, S1-S19
- 20 G.A. Jeffrey, *An Introduction to Hydrogen Bonding*, Oxford University Press, New York, 1997
- 21 M.A. Jarski and E.C. Lingafelter, *Acta Cryst.*, 1964, **17**, 1109-1112
- 22 G.M. Sheldrick, SHELXTL version 5, Siemens Analytical X-ray Instrument, Madison, Wisc., USA, 1995
- 23 D.D. Perrin and W.L.F. Amarego, *Purification of Laboratory Chemicals*, Oxford University Press, Oxford, 3rd Edition, 1988, pp. 174
- 24 P.T. Beurskens, G. Beurskens, W.P. Bosman, R. de Gelder, S. García-Granda, R.O. Gould, R. Israël and J.M.M. Smits, DIRDIF, Crystallography Laboratory, University of Nijmegen, The Netherlands.

Chapter 5 : Diazopyrazolones

Contents	Page
5.1 Introduction	203
5.1.1 The Escondida Process	203
5.1.1.1 Background to the Process	203
5.1.1.2 The Process	204
5.1.1.3 Advantages of an Ammoniacal Leach over an Acid Leach	205
5.1.1.4 Current Reagents	206
5.1.1.5 The Requirements of a Solvent Extractant	208
5.1.1.6 Diazopyrazolones	208
5.2 Synthesis of Diazopyrazolones and their Metal Complexes	209
5.2.1 Ligands	209
5.2.2 Metal Complexes	210
5.2.3 Stability of Diazopyrazolone Ligands	211
5.3 Characterisation of Diazopyrazolones and their Metal Complexes	211
5.3.1 IR Spectroscopy	211
5.3.2 NMR Spectroscopy	212
5.3.2.1 Free Ligands	212
5.3.2.2 Metal Complexes	216
5.3.3 Mass Spectrometry	218
5.3.4 Electrochemistry	219
5.4 Solvent Extraction using Diazopyrazolones	220
5.4.1 From Sulphate Media	220
5.4.2 From Ammoniacal Media	226
5.5 X-ray Crystallography of Diazopyrazolones and their Metal Complexes	229
5.5.1 Bonding	230
5.5.1.1 In the Free Ligands : Tautomerism	230
5.5.1.2 In the Metal Complexes : Mesomerism	232
5.5.2 General Trends in the Structures of the Metal Complexes; 8-12	234
5.5.2.1 Metal to Donor Atom Bond Lengths	234

5.5.2.2	Bite Angles and Bite Distances	235
5.5.2.3	Torsion Angles and Dihedral Angles	237
5.5.3	Comparison of the two Copper(II) Structures, 8 and 12	238
5.5.4	The Zinc(II) Complex, 9	242
5.5.5	The Cobalt(III) Complex, 10	243
5.5.6	The Nickel(II) Complex, 11	245
5.6	Conclusions	246
5.7	Experimental	247
5.7.1	Instrumentation	247
5.7.2	Solvent Reagent and Pretreatment	247
5.7.3	Synthesis of Starting Pyrazolones	248
5.7.4	Synthesis of the Ligands	248
5.7.5	Synthesis of the Metal Complexes	253
5.7.6	Solvent Extraction Experiments	256
5.7.6.1	From Sulphate Media	256
5.7.6.2	From Ammoniacal Media	259
5.7.6.3	Stability Tests on Diazopyrazolone Ligands	261
5.7.7	X-ray Crystallography	262
5.8	References for Chapter 5	264

5.1 Introduction

Acid leach solvent extraction systems, such as the one described in section 1.3.2, are best suited to the treatment of high grade, oxidic, copper ores¹. However, the majority of copper ores are sulphidic, such as bornite (Cu_5FeS_4 / Cu_3FeS_3), chalcocite (Cu_2S) and chalcopyrite (CuFeS_2), and are still treated using extractive pyrometallurgy. The economic and environmental benefits of hydrometallurgical processing are well known and so a considerable amount of work has been directed at the treatment of sulphidic copper ores using ammoniacal (NH_3 / NH_4^+) leach solutions².

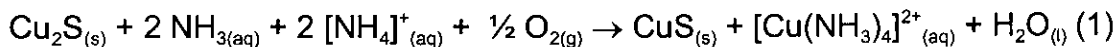
5.1.1 The Escondida Process

5.1.1.1 Background to the Process

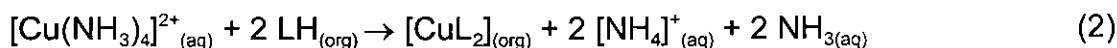
The leaching of sulphidic copper ores using ammonia was first proposed by Balzac³ in 1903, however it remained undeveloped until the 1970s when a considerable amount of work was carried out in this area⁴. The chemistry behind what is now called "The Escondida Process", named after the largest copper mine in the world, La Escondida in Chile⁵, was first patented by General Mills Chemicals Inc.^{6,7} (later Henkel Corporation) in the late 1970s. Since that time, a lot of development work has been carried out to try to optimise the process and make it commercially viable⁸⁻¹¹. In fact it was the wish of BHP, which owns La Escondida, to process some of the copper concentrate produced on site instead of transporting it to other refining facilities around the world, that ultimately resulted in the development of the Escondida process¹². In November 1994 a 80 000 tonnes *per annum* facility to process chalcocite-based ores using ammoniacal leach technology was opened near Antofagasta in Chile. The process has, however, encountered problems, which are for the most part related to the choice of solvent extractant. These problems will be described in section 5.1.1.4.

5.1.1.2 The Process

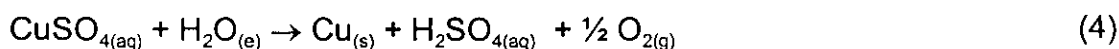
The ammoniacal leaching of chalcocite under mildly oxidative conditions only dissolves 50% of the total copper present in the ore, leading to the generation of two streams, as described in equation 1. The leaching of chalcocite is believed to proceed through the formation of $[\text{Cu}(\text{NH}_3)_2]^+$, which is then rapidly oxidised to $[\text{Cu}(\text{NH}_3)_4]^{2+}$.



An enriched copper ore, covellite (CuS), is subsequently treated in a smelter, while the aqueous solution containing copper(II) ammine complexes is treated by solvent extraction, stripping and electrowinning in the conventional manner. This solution has a pH value of *ca.* 5, which means that only a weakly acidic solvent extractant ($\text{pH}_{1/2} \leq 5$) is required to transfer the copper(II) ions into an organic phase in the solvent extraction stage of the process (Equation 2).



The regenerated ammoniacal leachant is recycled to the leaching step with only minimal addition of fresh ammonia required. Stripping of the copper from the loaded organic solution (Equation 3) followed by electrowinning (Equation 4) regenerates the extractant without overall consumption of acid.



The recycling of reagents between each of the stages of the overall process leads to a materials balance represented by equation 5. Chalcopyrite produces copper and covellite, with the consumption of power and production of minimal residues as in a conventional acid leach circuit. In total, more than 97 % of the total copper present in the ore is recovered by

the combination of hydrometallurgical and smelting processes as described, with less than 3 % lost to tailings².



5.1.1.3 The Advantages of an Ammoniacal Leach over a Conventional Acid Leach¹²

The advantages of using an ammoniacal leach solution rather than an acid leach solution to treat sulphidic copper ores are summarised below.

1. The rate of partial dissolution (ie: ca. 50 %) of the total copper present in the ore is much faster than the rate of total dissolution would be. Additionally, partial dissolution avoids the problems caused by sulphur oxidation products, for example ammonium sulphate, as sulphur oxidation is slow and cannot occur on this leaching timescale.
2. Ammoniacal leach solutions have been shown to dissolve copper to a much higher concentration than acid leach solutions, thus fewer solvent extraction steps are required to transfer maximum copper into the stripping stage of the process.
3. The pH of the leachant is ca. 8.5 - 10.0, which is maintained by buffering with ammonium sulphate. At this pH only $[\text{Cu}(\text{NH}_3)_4]^{2+}$ is significantly stable in solution in comparison with, for example, the equivalent zinc, nickel and cobalt ammine species, and so only copper is significantly solubilised. For this reason the solvent extraction stage of the process is more of a lixiviant regeneration step than one of purification, unlike that in an acid leach circuit, in which the extractant is required to show high selectivity for copper over iron and other metals. The presence of only minimal impurities in the ammoniacal leach solution leads to the production of copper of extremely high purity (99.9995 %).
4. The pH (ca. 0.3-0.5) of the acid required to strip the copper back into the aqueous phase of this system is higher than that required in a conventional acid leach system (pH 0). This may lead to lower anode corrosion rates and lower levels of sulphate in the cathode product have also been observed¹².

In summary, the use of ammoniacal leaching in a solvent extraction circuit for the treatment of sulphidic copper ores results in fast and efficient load and strip kinetics at ambient temperature and pressure, an extremely high purity copper product and, as a result, good process economics.

5.1.1.4 Current Reagents

To date, β -diketones have been the most successful solvent extractants trialled for use in the Escondida process. Henkel's LIX54 reagent, 1-phenyl-3-*iso*-heptyl-1,3-propane dione (Figure 1), was found to be the most suitable β -diketone as its extractive strength was well suited to the requirements of the Escondida circuit.

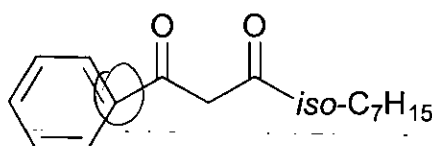


Figure 1 : Structure of LIX54

However, during repetitive use of LIX54 it was found that it became increasingly difficult to strip¹¹. This was attributed to the formation of a ketimine from the reaction of the β -diketone with excess ammonia in the system (Figure 2).

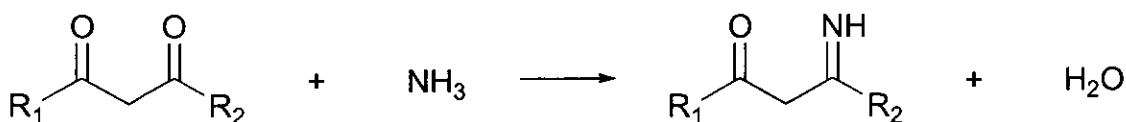


Figure 2 : Formation of the ketimine

Additionally it was suspected that the ketimine might be an intermediate in a degradation pathway resulting in surfactant-type by-products, which might contribute to entrainment of aqueous species in the loaded organic phase. A number of solutions to this problem have been proposed¹¹, including the application of highly sterically hindered β -diketones to prevent ketimine

formation, and the use of combined extraction systems of, for example, hydroxyphenyl oximes and β -diketones to speed up the kinetics of both loading and stripping^{11,13}. It should be noted, however, that hydroxyphenyl oximes facilitate the transfer of ammonia into the organic phase and that this is therefore not a viable solution to the problem. Another approach would be to reduce the ammonia concentration in the lixiviant, as high $[\text{NH}_3]$ increases $[\text{LH}]$ thus depressing copper extraction, as is clear on consideration of the extraction equilibrium (Equation 2). This effect is obviously dependent on the extraction equilibrium constant and significantly decreases when this constant is high, ie: for strong extractants such as hydroxyphenyl oximes. For weaker extractants, such as β -diketones, however, it is significant and reducing the concentration of ammonia could present a partial solution to the problem¹³.

The inherent instability of LIX-type β -diketones to basic conditions is an unavoidable problem, however, and as such other compounds have been investigated as possible replacements for LIX54 in Escondida-type copper recovery processes. Following the fundamental work of Zolotov¹⁴ on the application of acyl pyrazolones (Figure 3) as solvent extractants, a large number of papers on the extraction of a range of metals from acidic aqueous solutions into organic solvents using acyl pyrazolones have been published¹⁵⁻¹⁹.

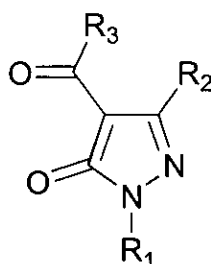


Figure 3 : Acyl pyrazolones; $\text{R}_1 = \text{R}_3 =$ alkyl, aryl; $\text{R}_2 =$ alkyl

Mickler and Uhlemann²⁰ found that the acyl pyrazolone, 4-*iso*-octanoyl-3-methyl-1-phenyl-5-pyrazolone (Figure 3 : $\text{R}_1 = \text{Ph}$; $\text{R}_2 = \text{Me}$; $\text{R}_3 = \textit{iso}\text{-C}_7\text{H}_{15}$) compared most favourably with LIX54 in the recovery of copper from

ammoniacal media in terms of extractive strength and efficiency, but the low solubility of its copper complex limited its application in this area.

5.1.1.5 The Requirements of an Ammoniacal Leach Solvent Extractant

It is clear that the key requirements of a solvent extractant suitable for use in an Escondida-type process are directly related to the characteristics of the leach solution. These requirements are summarised as follows.

1. The leach solution has a high copper concentration, therefore the solvent extractant is required to have a high copper loading capacity in order to transfer the maximum copper possible into the organic phase.
2. There are minimal impurities, for example iron and other metals, in the leach solution, therefore the solvent extractant does not require high selectivity for copper over, in particular iron, as is paramount in a conventional acid leach circuit. The main impurity in the copper ore is pyrite (FeS_2), however this is not solubilised by the leachant and is removed from the system with the covellite *via* a flotation step².
3. As a consequence of the high pH of the leach solution (*ca.* pH 5), the solvent extractant only requires a $\text{pH}_{1/2}$ value of ≤ 5 but, more importantly, must be extremely stable to base and ammonia.

Additionally, the solvent extractant and its copper complex need to be soluble in the kerosene solvents employed in solvent extraction circuits and, as with an acid leach extractant, need to have good phase disengagement and separation properties to avoid the problem of entrainment into the aqueous phase.

5.1.1.6 Diazopyrazolones

Diazopyrazolones (Figure 4) are structurally related to acyl pyrazolones (Figure 3) but have not been previously investigated as copper extractants. They possess very well-defined synthetic chemistry²¹ due to their extensive use, as both ligands and metal complexes, in the dyestuffs industry^{22,23}, and have been shown to form neutral 2:1 ligand:copper complexes^{24,25} with a

$[\text{N}_2\text{O}_2]^{2-}$ donor set analogous to that found in the hydroxyphenyl oxime extractants used to recover copper from acid leach solutions²⁶.

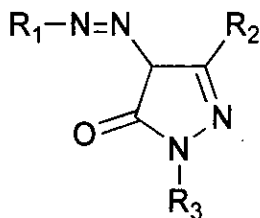


Figure 4 : Diazopyrazolones; R_1, R_3 = alkyl, aryl; R_2 = alkyl

The use of pyrazolone derivatives in medicinal chemistry, usually as their antipyrene tautomers, is extensive²⁷ and consequently the antimicrobial activity of nickel and copper chelates of diazopyrazolones has also been successfully trialled²⁸, again illustrating the diversity of applications of this class of compound.

5.2 Synthesis of Diazopyrazolones and their Metal Complexes

5.2.1 Synthesis of the Free Ligands

The free ligands, 1 - 7, which are listed in Table 1, were prepared in good yield by the standard method²¹ of coupling the appropriate pyrazolone with the diazonium salt derived from the appropriate *para*-substituted aniline. The retrosynthetic pathway for the synthesis of the ligands is presented in Figure 5.

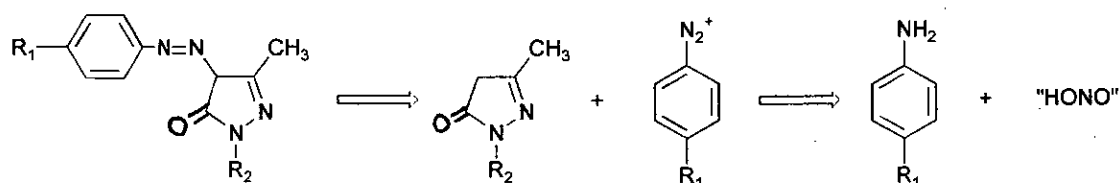


Figure 5 : Retrosynthesis of diazopyrazolones; R_1 = alkyl, R_2 = alkyl, aryl

The reactivity of the 4-position of the pyrazolone ring towards electrophiles of this type is well-known and is indicative of the lability of the protons at this position, which is easily monitored using ^1H NMR spectroscopy²⁹. All the free ligands prepared are highly coloured (orange), which is expected as this type of compound is used extensively in the dyestuffs industry²². As already discussed, the solubility of both the free ligands and their metal complexes is of paramount importance if the ligand is to be used as a solvent extractant. Although the solubilities of the crystalline free ligands, **1** - **4**, in toluene were adequate for solvent extraction studies, the solubilities of their metal complexes were not and led to the synthesis of the more soluble ligands, **5** - **7**, which were viscous oils. The solubilities of ligands **1** and **5** in toluene were found, using ^1H NMR techniques, to be 1.2 M and 2.4 M respectively.

Ligands	R ₁	R ₂	Complexes	
1	t-Bu	Ph	8	[Cu(1-H) ₂]
2	H	Ph	9	[Zn(1-H) ₂]
3	t-Bu	H	10	[Co(1-H) ₃].3MeOH
4	t-Bu	Me	11	[Ni(1-H) ₂ .(MeOH) ₂].2MeOH
5	t-Bu	t-Bu	12	[Cu(2-H) ₂]
6	s-Bu	t-Bu	13	[Cu(5-H) ₂]
7	nonyl	t-Bu	14	[Cu(6-H) ₂]
			15	[Cu(7-H) ₂]

Table 1 : Diazopyrazolone ligands and metal complexes, **1** - **15**

5.2.2 Synthesis of the Metal Complexes

The metal complexes, **8** - **15**, listed in Table 1, were prepared in good yield by reaction of the free ligand with the appropriate divalent metal salt. The reaction scheme is presented in Figure 6.

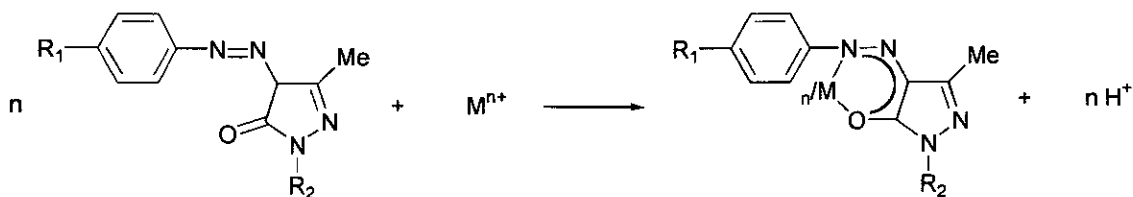


Figure 6 : Synthesis of the metal complexes of diazopyrazolones

5.2.3 Stability of Diazopyrazolone Ligands

The stability of the solvent extractant to the basic conditions of the Escondida process is of paramount importance, as already discussed. The stability of ligand **5** was assessed by contacting separate samples of a 0.056 M solution of **5** in toluene with equal volumes of 34 $g\ l^{-1}$ (19 x excess of copper) and 3.4 $g\ l^{-1}$ (1 x excess of copper) ammoniacal copper feeds at room temperature over a period of 552 h (23 days). Analysis of both the aqueous and organic phases using ICP-AES showed that, within experimental error, the amount of copper extracted did not decrease over this time period, hence it was concluded that the ligand was not undergoing chemical degradation and was stable to prolonged contact with ammoniacal feeds.

5.3 Characterisation of Diazopyrazolones and their Metal Complexes

5.3.1 IR Spectroscopy

There are three possible tautomeric forms of diazopyrazolones, which are illustrated in Figure 7. The solid state IR spectra of ligands **1-7** show three definitive absorptions, which are characteristic of their hydrazone tautomers (Figure 7 : **b**). These are the N-H stretch at approximately $3400\ cm^{-1}$, the C=O stretch at approximately $1650\ cm^{-1}$, and the C=N stretch at approximately $1550\ cm^{-1}$. The carbonyl stretch is low suggesting the presence of intramolecular hydrogen-bonding to it from the NH group²⁹. On metal ion complexation, the N-H and C=O stretches are no longer observed in the IR, confirming that complexation occurs through the carbonyl oxygen (now in the enol form) and the hydrazone nitrogen (now in the diazo form)

c)²⁸. On complexation, the C=O absorption of the free ligand is replaced by the C-O absorption at ca. 1096 cm⁻¹.

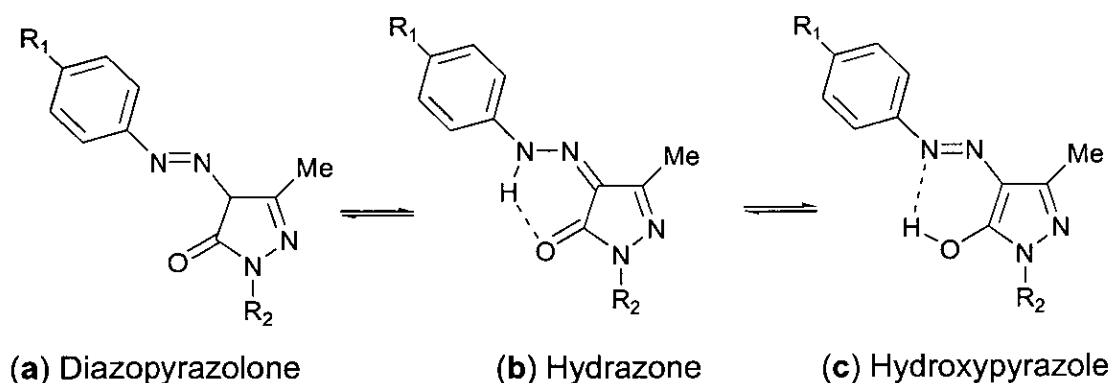


Figure 7 : Tautomeric forms of diazopyrazolones

5.3.2 NMR Spectroscopy

5.3.2.1 Free Ligands

The ¹H and ¹³C NMR spectra are consistent with the expected structures for ligands 1-7. Crystallographic studies on related diazopyrazolones have shown that they also adopt the hydrazone tautomeric form (Figure 7 : b) in the solid state³⁰⁻³⁷. In contradiction to these results, Whitaker³⁸ proposes an enol tautomer (Figure 7 : c) on the basis of powder X-ray data. Full X-ray analysis would be required to confirm this, however, as powder X-ray data cannot be used to confirm or disprove the presence of specific tautomeric forms. On consideration of all other X-ray structures available³⁰⁻³⁷, it is assumed that Whitaker's conclusion is incorrect in this case.

The fact that diazopyrazolones seem to exist exclusively in the hydrazone form in comparison with the structurally similar 1-aryl-2-azonaphthols^{39,40}, which exist in a tautomeric equilibrium between their keto and enol forms (Figure 8), is indicative of a much smaller resonance stabilisation of the enol form of diazopyrazolones²⁹. Additionally, the acidity of the proton at the 4-position of the pyrazolone ring will mean the formal diazopyrazolone tautomer (Figure 7 : a) will preferentially rearrange to form the hydrazone tautomer. It is interesting to note that no such tautomeric equilibrium has

been elucidated for the structurally similar 1-arylo-2-phenols, which exist exclusively in their azo-phenol form⁴¹.

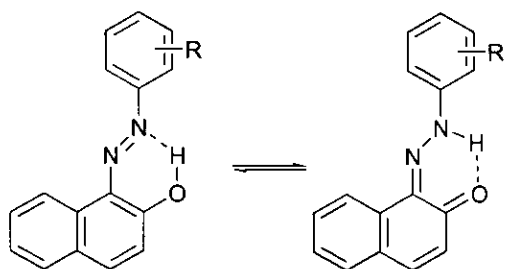


Figure 8 : Tautomerism of 1-aryl-2-azonaphthols

In order to further investigate the tautomerism of these ligands in solution nuclear Overhauser effect spectroscopy (NOESY) was carried out on solutions of **1** in both deuterated chloroform and deuterated dimethyl sulphoxide. ¹⁵N NMR experiments carried out by Connor *et al.*³⁰ previously showed positive NOESY results indicating the presence of these ligands as hydrazone tautomers.

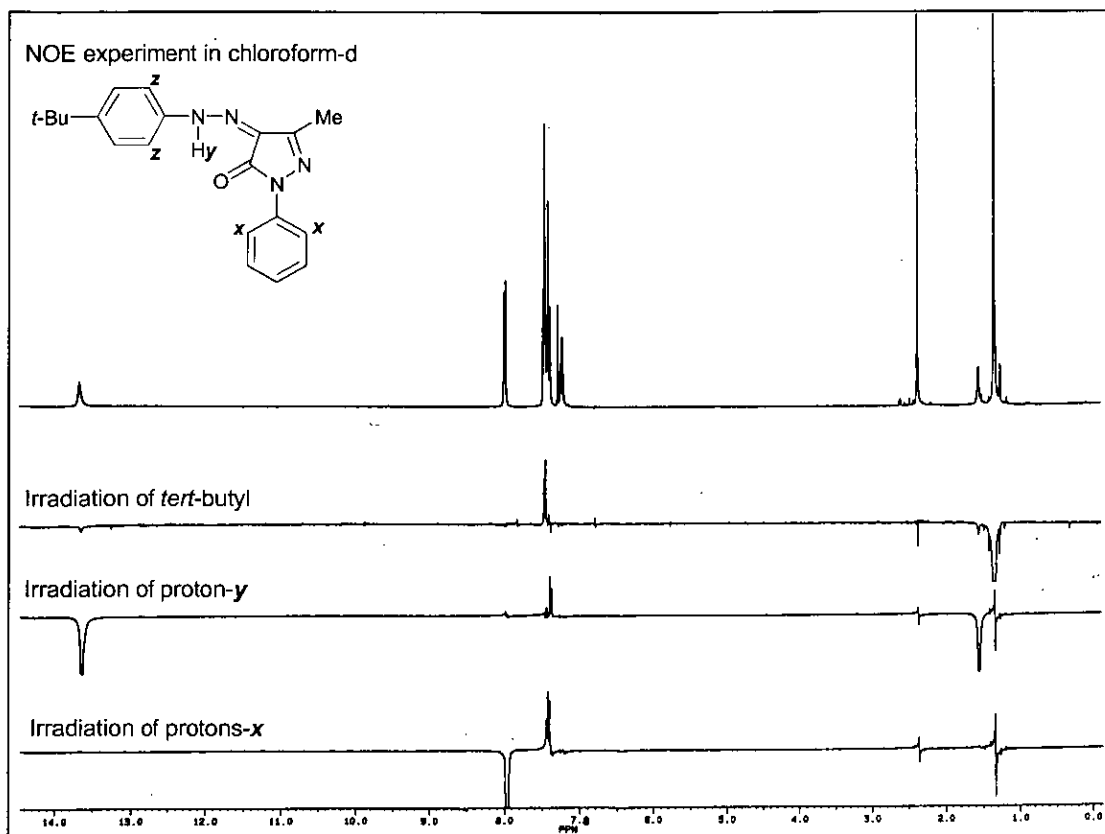


Figure 9 : NOE spectra of **1**

NOESY results for **1** (Figure 9) indicate that proton-*y* is found nearer to the nitrogen in the azo group than to the oxygen atom on the pyrazolone ring, i.e. the structure adopted by **1** is the hydrazone tautomer as shown in figure 9. In deuterated chloroform, irradiation of the doublet due to protons-*x* gave no visible enhancement of the signal of proton-*y* (singlet at 13.6 ppm). If **1** was in the enol form (Figure 7 : **c**), an effect on this singlet would be expected, as it would be assignable to the enolic proton at the 5-position on the pyrazolone ring. The only enhancement in this case, however, was of the doublet due to the *meta* protons on the same phenyl ring. In both deuterated chloroform and deuterated dimethyl sulphoxide, irradiation of the singlet due to proton-*y* induced a substantial enhancement of the doublet due to protons-*z*, which would indeed be expected if the diazo group was in fact in the hydrazone form. The broad singlet due to water in the deuterated dimethyl sulphoxide was also suppressed in this final experiment indicating that proton-*y* is exchanging with the water on the NMR time scale. These

results support the existing evidence that the hydrazone tautomer of diazopyrazolones predominates not only in the solid state but also in solution.

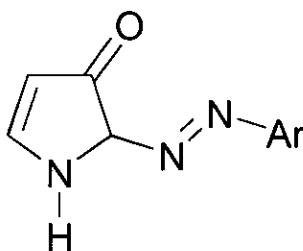


Figure 10 : 2-Arylazo-3-pyrrolones

McNab *et al.*⁴² found that in their study of the structurally similar 2-arylazo-3-pyrrolones (Figure 10), the assignment of tautomeric forms based solely on ^1H NMR evidence was unsatisfactory and that ^{13}C NMR evidence was much more reliable in this case. Although this was not found to be the case for ligands **1 - 7**, it is still interesting to look at the ^{13}C NMR data of **1 - 7**, and the δ -values of carbon atoms of interest (in ppm) in **1 - 7** and in the starting pyrazolones (average values) are presented in table 2.

From these data, it is clear that carbon A is the least effected by changes in R_1 and R_2 and carbon B is the most effected, which suggests that R_2 has a more pronounced effect on chemical shift than R_1 due to its closer proximity to carbon B. This is found not to be the case, however, as the variation in the chemical shift of carbon B in the series of ligands, in which R_2 remains constant and R_1 varies (ie: comparison of ligands **1** and **2**, or ligands **5**, **6** and **7**; Average δ -values for carbon B are 144.72 (± 3.74) and 143.57 (± 2.13) respectively) is much greater than in the series of ligands, in which R_1 remains constant and R_2 varies (Ligands **1**, **3**, **4** and **5**; Average δ -value for carbon B is 146.69 (± 0.94)). In ligands **5**, **6** and **7**, the δ -value of carbon B moves to higher field with increasing size of the alkyl group at R_1 . This is assumed to be due to the increased electron-donating effect of R_1 and the consequential shielding of carbon B.

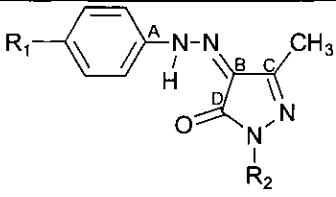
Ligand					Solvent
	Carbon A	Carbon B	Carbon C	Carbon D	
1	137.97	148.46	149.19	157.75	CDCl ₃
2	137.89	140.98	148.44	157.62	CDCl ₃
3	139.11	146.80	147.90	160.39	DMSO-d ₆
4	139.00	145.96	148.12	157.66	DMSO-d ₆
5	138.93	145.53	148.35	159.14	CDCl ₃
6	139.24	144.80	145.37	159.08	CDCl ₃
7	139.13	140.37	145.56	159.13	CDCl ₃
Average	138.75	144.70	147.56	158.68	-
E.S.D.	± 0.47	± 2.30	± 0.91	± 0.86	-
Starting Pyrazolone	---	42	154	172	CDCl ₃

Table 2 : ¹³C NMR data (in ppm)

Finally, the value of carbon D in the starting pyrazolone is 172 ppm, which is in the range expected for this lactam-type of carbon atom. Its average value in the ligands 1-7 is significantly lower (159 ppm), which is surprising as it might be expected that carbon D would be deshielded in 1-7 due to the electron-withdrawing nature of the hydrogen bond and so resonate at a higher frequency (lower field). The reason for this observation is unclear. Finally it is also interesting to note that “external parameters”, such as variation in solvent, have little effect on the δ -values of the carbon atoms, which agrees with a similar observation made by McNab *et al.*⁴².

5.3.2.2 Metal Complexes

¹H NMR spectra were obtained for the diamagnetic complexes **9** and **11**. The spectrum of the tetrahedral zinc(II) complex, **9**, (Figure 11) shows

resonances that can be assigned to a single ligand indicating that both coordinating ligands are in chemically and magnetically equivalent environments. This suggests that the molecule retains its 2-fold symmetry in solution. Interestingly, this does not agree with the distorted tetrahedral X-ray structure of **9** (Section 5.5.4), reiterating the point that solution studies are unreliable in predicting what is present in the solid state and *vice versa*.

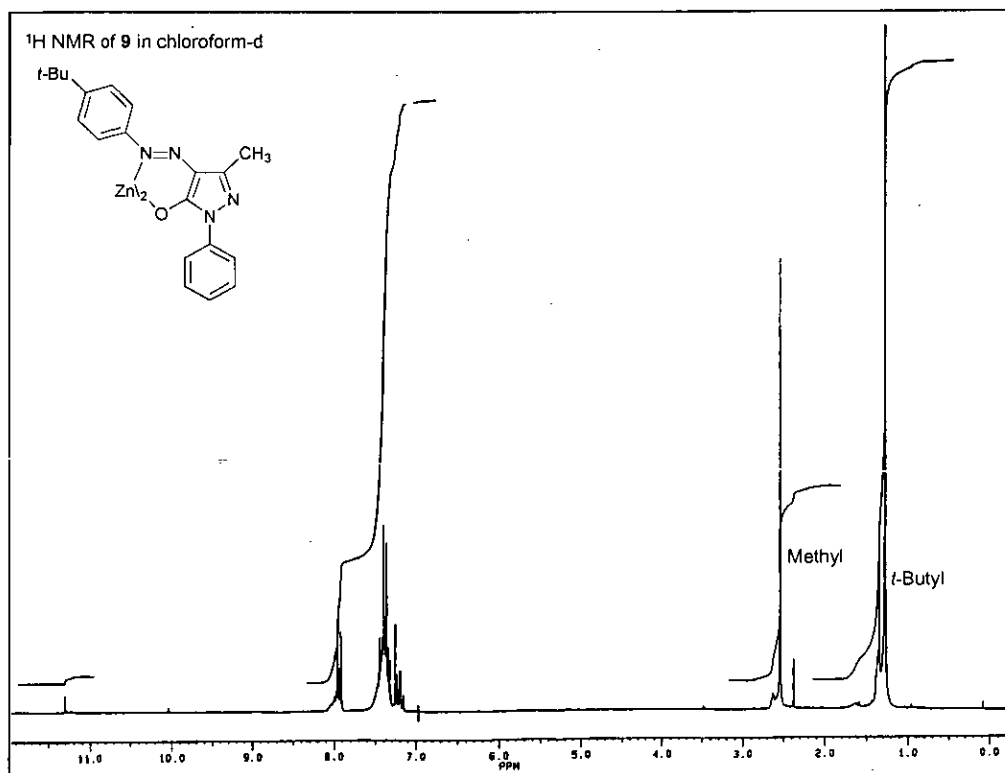


Figure 11 : ¹H NMR spectrum of the zinc complex, **9**

The spectrum for the low spin, octahedral cobalt(III) complex, **11**, (Figure 12) is considerably more complicated. It shows six singlets for the three *tert*-butyl groups and three methyl groups indicating that the molecule does not possess 3-fold symmetry and that the three coordinating ligands are found in very different chemical and magnetic environments. Six distinct signals are observed in the aromatic region of the spectrum. Two doublets, a singlet and a triplet are assigned to just one of the three coordinating ligands. The aromatic protons on the remaining two ligands resonate to give two distinct multiplets, suggesting that these two ligands are found in similar chemical

and magnetic environments, which are different to that of the third ligand. This agrees with solid state observations (Section 5.5.5).

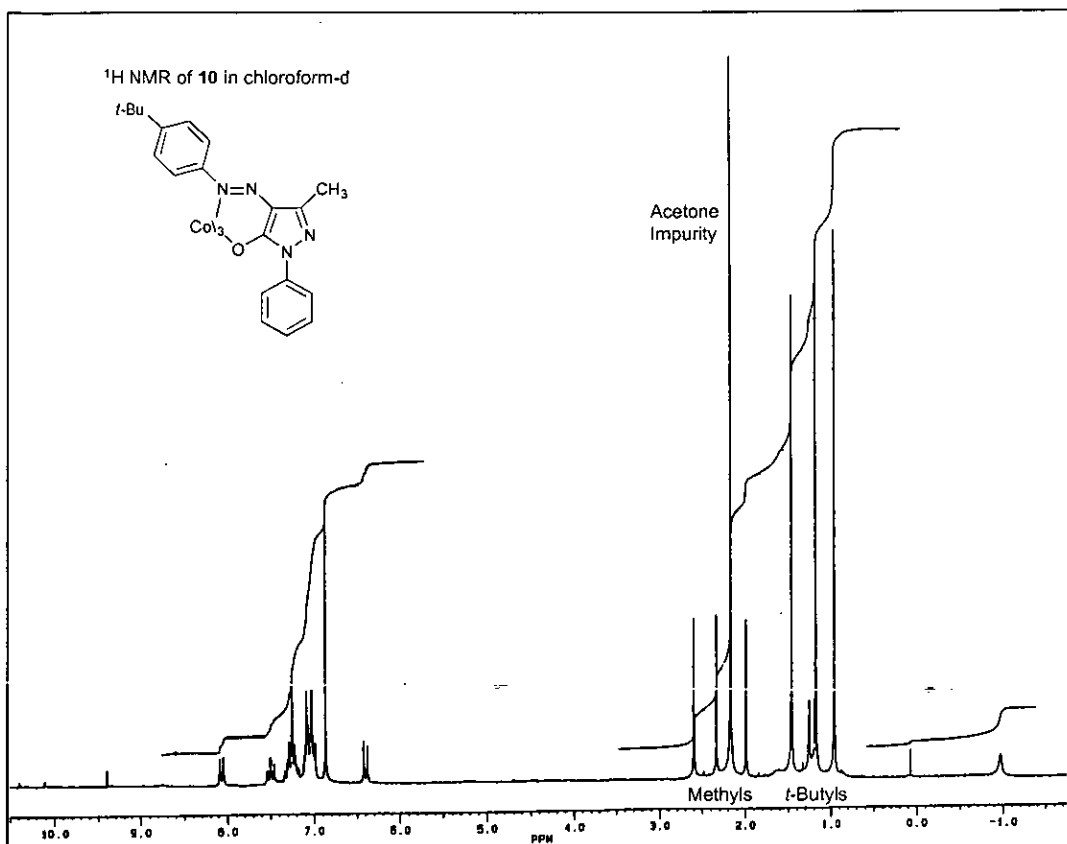


Figure 12 : ¹H NMR spectrum of the cobalt complex, **10**

5.3.3 Mass Spectrometry

The EI mass spectra for ligands **1** - **7** all display fragmentation patterns, which would be expected for this type of compound. For example, there are peaks in the spectra consistent with the losses of methyl, phenyl and *tert*-butyl substituents. The FAB mass spectra for complexes **8** - **14** all show the expected ML_2 or ML_3 peaks. However, the FAB mass spectra of **8** and **12** show additional peaks which are attributable to oligomeric species assigned as M_2L_3 and M_2L_2 for **8** and M_3L_4 , M_3L_3 , M_3L_2 and M_2L_2 for **12**. In both cases the metal ion present is copper(II), however for other copper(II) complexes characterised, **13** and **14**, there are no such peaks in the mass spectra. These peaks assignable to oligomers are assumed to be due to species

formed in the mass spectrometer as C/H/N analysis data of **8** and **12** give no indication of their presence in the recrystallised products.

5.3.4 Electrochemistry⁴³

Cyclic voltammetry (CV) was carried out on solutions of the copper(II) and cobalt (III) complexes, **8** and **10**, in dichloromethane containing a 0.1 M *tert*-butyl ammonium *tetra*-fluoro borate ($t\text{Bu}_4\text{N}(\text{BF}_4)$) electrolyte. The concentrations of the sample solutions were approximately 4×10^{-3} M with respect to the metal complexes. The cyclic voltammogram of **8** is presented in Figure 13. The Cu(II)/Cu(I) redox couple was found to be fully reversible with a potential, E , of -0.71 V relative to the standard ferrocene/ferrocenium couple.

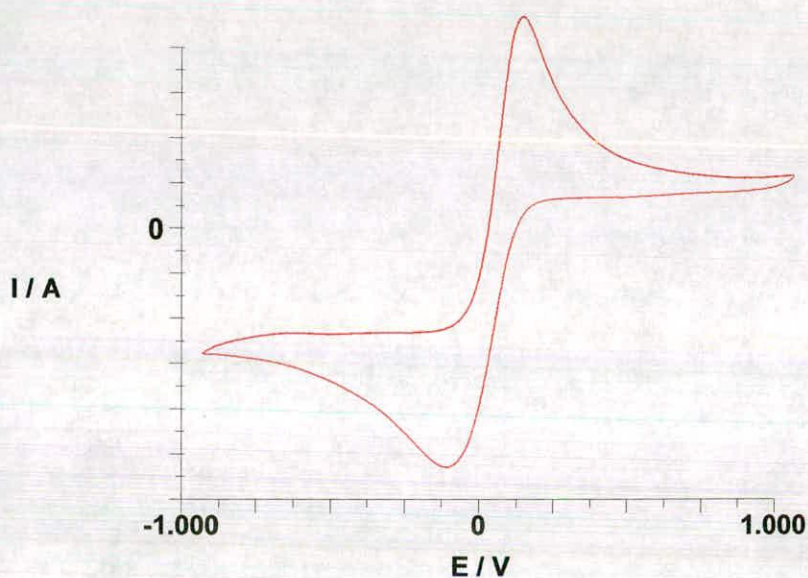


Figure 13 : Cyclic voltammogram of **8**; Scan rate 0.1V/s

The cyclic voltammogram of **10** is presented in Figure 14. The Co(III) to Co(II) reduction is non-reversible with an E_p^{RED} of -0.55 V at a scan rate of 0.1V/s, which lowers to -0.66 V at a scan rate of 0.3 V/s. This means that the initial reduction of cobalt(III) to cobalt(II) is followed by an oxidative electrochemical reaction of the cobalt(II) species, which results in new products and not the starting cobalt(III) complex. This is unsurprising as it is

known from X-ray crystallography (section 5.5.5) that the pseudo-octahedral cobalt(III) complex is highly distorted due to steric crowding within the molecule, therefore other less-strained species will preferentially form in the electrochemical experiment. Lowering the temperature of the experiment in order to slow down the rate of following chemical reactions, did not have any effect on the cyclic voltammogram in this case.

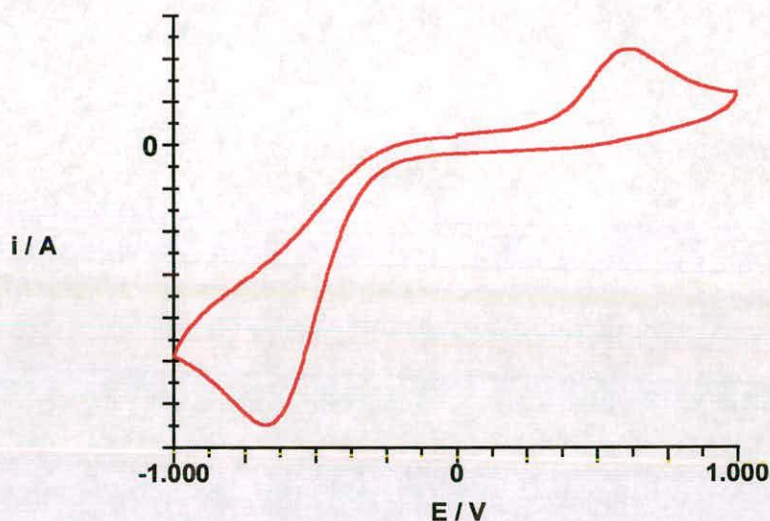


Figure 14 : Cyclic voltammogram of **10**; Scan rate 0.3 V/s

5.4 Solvent Extraction using Diazopyrazolones

5.4.1 From Sulphate Media

Initial solvent extraction experiments using diazopyrazolones were carried out under standard metal sulfate leach conditions to determine the extractive strength of these ligands in toluene in terms of $\text{pH}_{1/2}$ -values. These values could then be directly compared with those of current commercial extractants, which are ca. 1.6 in similar solvent systems, for example xylene²⁶. It should be recalled at this stage that in the extraction step of the Escondida process addition of sulphuric acid is controlled such that the pH is held at approximately 5 (Section 5.1.1.5), and a ligand with an acid leach $\text{pH}_{1/2}$ -value of ≤ 5 would therefore be suitable for use in this type of extraction process². The variations in the shapes of the S-curves presented in figures

16-19 are assumed to be due to errors introduced in the collation of extraction data. For example, errors due to inaccuracies in the weighing and dilution of materials, the pipetting of solutions and the standardisation and measurement of ICP-AES data may result in total errors as great as 10 %, and it is clear from consideration of figure 15, for example, that just one incorrect data point could have a significant effect on the appearance of the S-curve. Additionally, use of the Microcal Origin[®] programme to fit the extraction data to Boltzmann distribution curves may also result in somewhat inaccurate S-curves.

The S-curves for the extraction of copper(II), zinc(II) and nickel(II) using **1** in toluene are presented in figure 15.

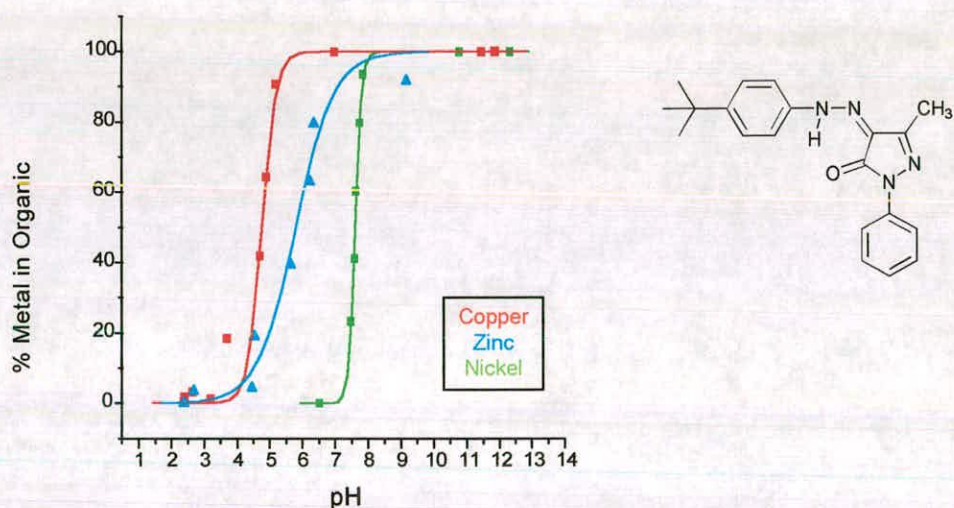


Figure 15 : S-curves for **1** with copper(II), zinc(II) and nickel(II)

The $\text{pH}_{1/2}$ -values for the extraction of copper(II), zinc(II) and nickel(II) are 4.7, 5.8 and ca. 7 respectively. It can be seen that **1** possesses the ability to selectively extract a given metal depending on the pH of the system. However the separation of copper and zinc is not nearly as good as that observed for hydroxyphenyl oximes (Chapter 1; Figure 5), which suggests that this type of ligand might in fact be more suited to the extraction of zinc than of copper. This observation is further discussed in section 5.5.4 with respect to the crystal structures of the relevant metal complexes. It should be noted that reproducibility of the extraction of cobalt(II) was poor. The

results obtained were indicative of extraction accompanied by oxidation of cobalt(II) to cobalt(III) and are therefore not reported here. The potential poisoning of the solvent extractant by cobalt(III) is unlikely to be a problem in practice, however, as Escondida ores do not contain significant levels of cobalt and, if present, it will be converted to kinetically inert and thermodynamically stable cobalt(III) ammine complexes by the leachant. The $\text{pH}_{1/2}$ -value of 1 for copper(II), 4.7, would be ideal for an Escondida-type extractant, however a limiting factor to the solvent extraction properties of **1** were the solubilities of the metal complexes formed. In all cases some precipitation of the metal complexes from the organic phase was seen, although it was minimal for nickel(II). Mass balances were therefore unobtainable for **1**. This insolubility was thought to be due to π -stacking of the planar N-phenyl units in adjacent molecules (Figure 25) and so in an attempt to improve the solubility of the ligands, and therefore the metal complexes, the N-phenyl group (R_2) was replaced firstly with a methyl group (**4**) and then with a *tert*-butyl substituent (**5**). The solubility of **5** in toluene (2.4 M) was found to be twice that of **1** using ^1H NMR techniques. The results of solvent extraction experiments for copper(II) with **4** and **5** are presented with those for copper(II) with **1** in figure 16.

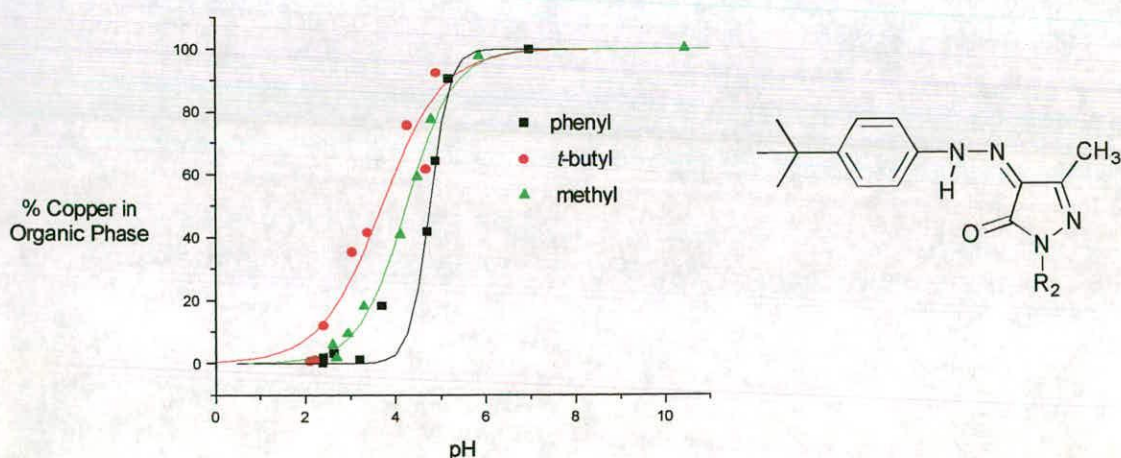


Figure 16 : S-curves for **1**, **4** and **5** with copper(II)

It is shown that replacement of the phenyl group firstly by a methyl group and subsequently a *tert*-butyl group reduces the $\text{pH}_{1/2}$ -value of the solvent extractant significantly from 4.76 to 4.23 and 3.69 respectively. Again slight precipitation of the copper complex was observed for **4**, but for **5** it was negligible, showing that replacement of the phenyl ring with a *tert*-butyl group not only increases the “strength” of the extractant but also the solubility of its metal complexes.

In order to investigate the effect of a change in substituent at the 4-position on the phenyl ring attached to the azo group (R_1) on the extractive properties of this type of ligand, a further set of solvent extraction experiments was carried out using ligands, in which the *tert*-butyl group at this position was replaced firstly by a *sec*-butyl group (**6**) and subsequently by a nonyl group (**7**). The solubilities of **6** and **7** in toluene were greater than that of **5**, with the solubility of **6** being measured as 3.7 M by ^1H NMR. The results of this set of solvent extraction experiments are presented with those of **5** for copper(II) in figure 17.

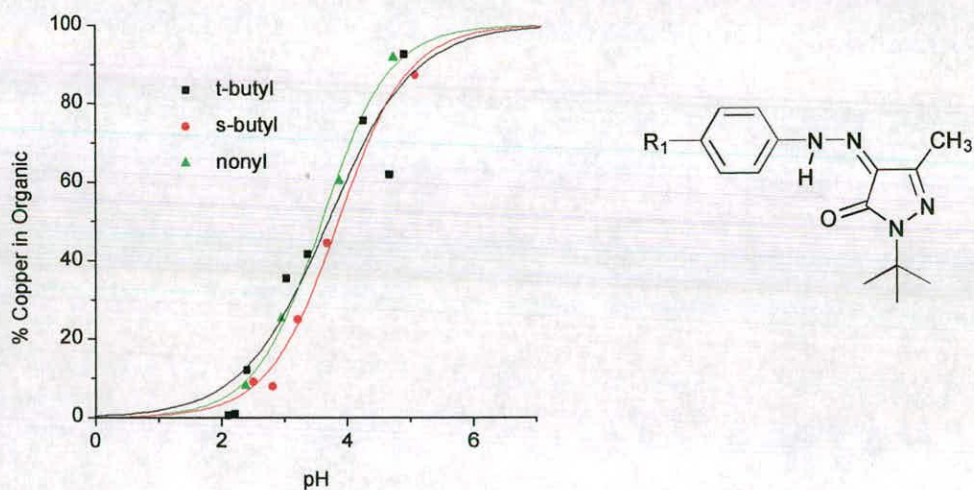


Figure 17 : S-curves for **5**, **6** and **7** with copper(II)

The $\text{pH}_{1/2}$ -values of **5** and **6** are very similar (3.69 and 3.74) which suggests that the relative strengths of these extractants are unaffected by the branching pattern of the 4-butyl substituent. The nonyl derivative, **7**, is the

strongest solvent extractant of this series of diazopyrazolones with a $\text{pH}_{1/2}$ -value 3.52, however the overall errors in the technique are such that these differences are essentially insignificant. This set of extraction experiments does show, however, that changing this alkyl group has a greater effect on the solubility of the ligand than on its extraction capability, which would be expected due to the distance between the alkyl group and the chelating unit of the ligand.

Finally, the selectivity of this class of more soluble diazopyrazolone ligands was studied, in order to assess the effect of substituent changes on the selectivity of this type of ligand for copper over other transition metal ions. The results of solvent extraction experiments carried out for copper(II), zinc(II), cobalt(II) and nickel(II) with ligand **5** are presented in Figure 18.

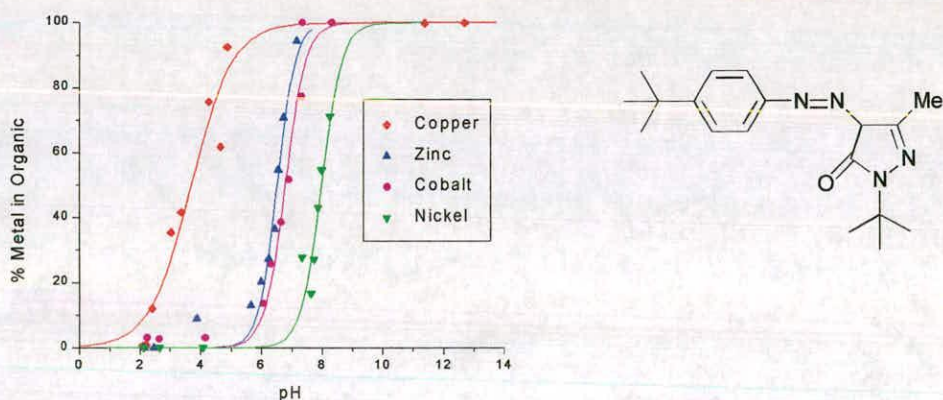


Figure 18 : S-curves for **5** with copper(II), zinc(II), cobalt(II) and nickel(II)

It is interesting to note that in this case, the results of the cobalt(II) extraction do not indicate that oxidation from cobalt(II) to cobalt(III) has occurred, and suggests that this ligand is able to stabilise the lower oxidation state. This observation could be explained by the fact that it is assumed that only two of these sterically much more demanding ligands (c.f. **1**) can fit around a central cobalt ion thus forming $(\text{Co}(\mathbf{5}\text{-H})_2]$. This reasoning does not explain why the selectivity for copper over other transition metals is much better than that of ligand **1** as it would be expected that both copper(II) and nickel(II) would be destabilised by complexation to **5** in comparison with **1**, ie: the $\text{pH}_{1/2}$ values

would increase, while the zinc(II) $\text{pH}_{1/2}$ value would remain relatively unchanged. The $\text{pH}_{1/2}$ values for the four metals, copper, zinc, cobalt and nickel, are 3.6, 6.4, 6.7 and 7.9 respectively, however, showing that while the $\text{pH}_{1/2}$ value for copper(II) has decreased significantly (from 4.7), the values for both zinc and nickel have increased (from 5.8 and 7.0 respectively). This indicates that not only does this ligand bind copper much more comfortably, but that it also binds much less well to zinc and nickel, which is a rather unexpected result.

In summary, solvent extraction experiments carried out under standard acid leach conditions have shown that :

1. Diazopyrazolones do not possess sufficient extractive strength to be of use in existing acid leach copper extraction circuits, however they may be applicable to an Escondida-type circuit, having an optimum $\text{pH}_{1/2}$ -value of ca. 4.
2. The replacement of aromatic with alkyl substituents at R_2 significantly increases not only the solubility but also the extractive strength of this class of potential solvent extractant. The solubility enhancement is assumed to be due to the loss of ligand planarity, while the improved extractive strength is due to the electron donation of the alkyl group, which will increase the acidity of the proton *via* resonance stabilisation. Amides are themselves relatively non-basic due to the lone pair on the nitrogen being delocalised *via* orbital overlap with the neighbouring carbonyl group π -orbital. Their conjugate bases are therefore extremely stable as they are a hybrid of two resonance forms (Figure 19)²¹.

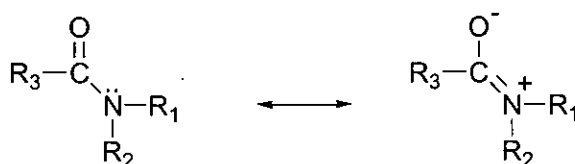


Figure 19 : Resonance stabilisation of amides

3. Varying the branching pattern or increasing the size of the alkyl substituent, R_1 , does not significantly effect the extractive strength of the ligand, which might be predicted as R_1 is a long way away from the chelating unit of the ligand and so any effect it has on the extraction capability of the ligand will be greatly diminished. The solubility of the ligand is, however, significantly effected by variation in R_1 .
4. The more soluble diazopyrazolone ligands (**5**) seems to possess much higher selectivity than ligand **1** for copper(II) over other transition metal ions.

5.4.2 From Ammoniacal Media

The extraction capabilities of **6** and **7** for copper(II) from ammoniacal media were investigated, the results of which are presented in the form of extraction isotherms in figure 20. Extraction and strip isotherms vary most significantly in shape in the region of low metal concentration, with a steeper slope indicating a stronger extractant or, in the case of a strip isotherm, more efficient stripping. The extraction capacity (ie: the maximum amount of metal which is loaded into the organic phase) as well as the stoichiometry of the species extracted into the organic phase can be determined from an extraction isotherm, while the amount of copper reclaimed by stripping is easily obtained from a strip isotherm²⁶.

The extraction isotherms for **6** and **7** show that the maximum copper loading of **6** (19.2 gl^{-1} ; 64 %) is much lower than that of **7** (25.6 gl^{-1} ; 85 %) even though the initial gradient of the extraction isotherm of **6** is greater than that of **7** indicating that it is the stronger extractant. Stripping of the loaded organic phase of **7** using simulated spent tankhouse electrolyte (30.0 gl^{-1} copper; 180 gl^{-1} sulphuric acid) was found to be virtually quantitative indicating that this ligand is not only a good extractant but also undergoes efficient stripping under these conditions.

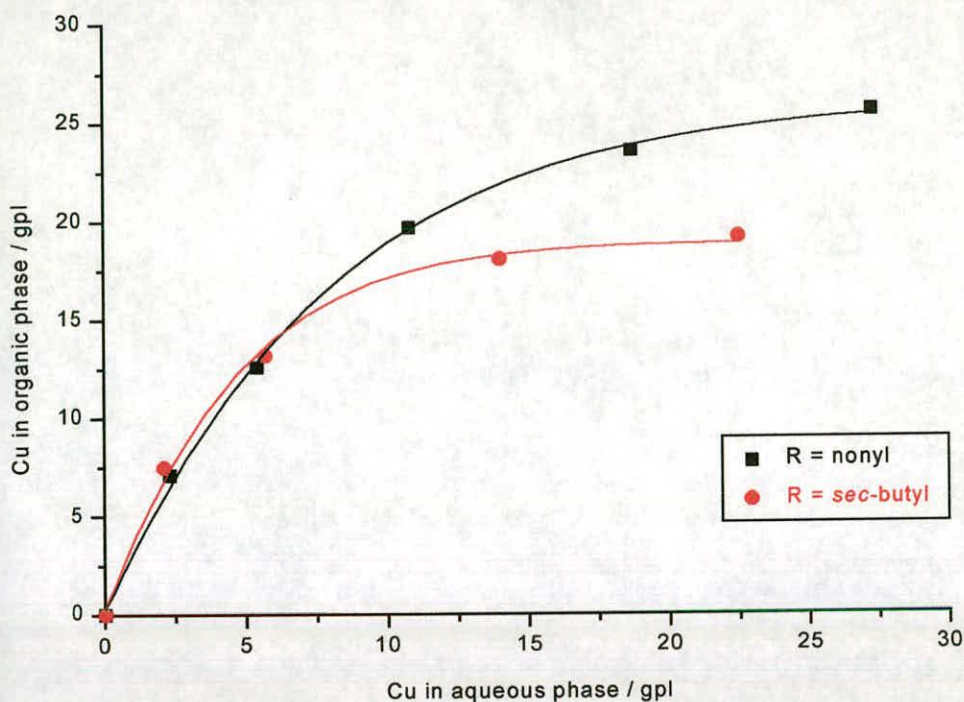


Figure 20 : Extraction isotherms of **6** and **7** for copper(II) from ammoniacal feed. (All scales gl^{-1})

In practice, more than one extract and one strip stage is incorporated into a solvent extraction plant to form what is known as a “countercurrent process”. This is so called because the aqueous and organic streams flow in opposite directions such that fresh extractant is contacted with an aqueous phase of very low copper concentration, and a heavily loaded organic phase is contact with fresh feed solution. Such a process ensures maximum copper transfer into the organic phase using manageable volumes of organic extractant solution³. The optimum number of extract and strip stages for a given extractant can be estimated by constructing McCabe-Thiele⁴⁴ diagrams, such as figure 21, from experimental data.

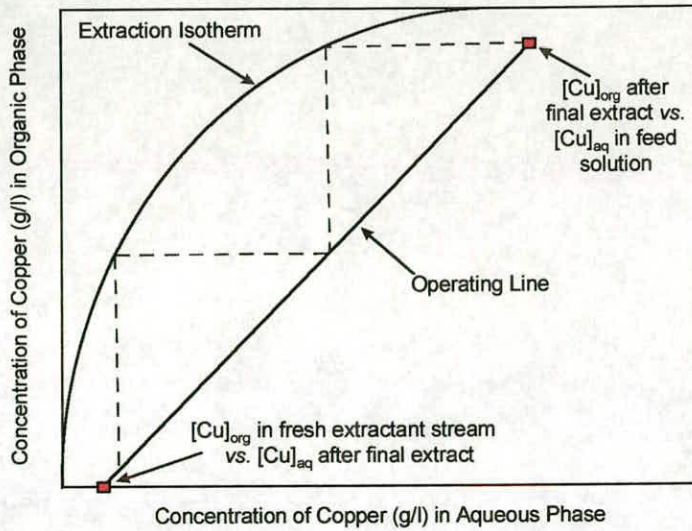


Figure 21 : A McCabe-Thiele construction for the extraction section of a solvent extraction circuit, containing two extraction stages (All scales g l^{-1})

McCabe-Thiele diagrams for copper extraction and stripping using 7 were constructed and modelled⁴⁵ by Dr. D.C. Cupertino, Avecia, and are presented in figure 22. The data were modelled for a process based on 2 extract and two strip stages and assumed 90 % and 95 % efficiencies in extraction and stripping.

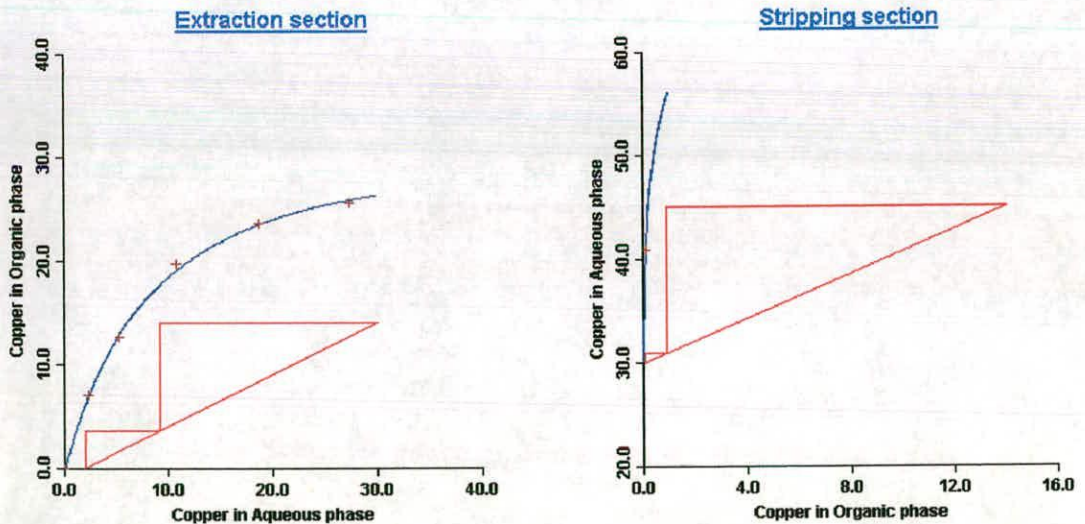
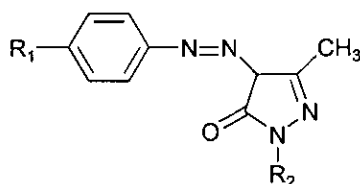


Figure 22 : McCabe-Thiele constructions for the recovery of copper using 7. (All scales g l^{-1})

The computer model indicates that copper recoveries in excess of 93 % may be expected. Additionally, a regenerated electrolyte containing 45 gl⁻¹ copper will be produced in the stripping stage, from which the copper metal value may then be recovered in a conventional electrowinning process (Section 1.3.2.4).

5.5 X-Ray Crystallography

The Cambridge Crystallographic Database (CCDC)⁴⁶ (Search performed August, 1999) contains the crystal structures of only two metal complexes of diazopyrazolone ligands, the chromium(III) bischelate of 1-(4-bromophenyl)-4-(2-carboxylato-5-methylphenylazo)-3-methyl-5-pyrazolone reported by Jaggi in 1968⁴⁷ and the tin(IV) bischelate of 4-(2-hydroxyphenylazo)-3-methyl-1-phenyl-5-pyrazolone reported by Banße *et al.* in 1997⁴⁸. The reported structures differ fundamentally from those reported here and summarised in table 3, however, in that the diazopyrazolone ligands have additional functionality that makes them tridentate rather than bidentate.



Complex	Formula	Chelating Ligand		
		No.	R ₁	R ₂
8	[Cu(1-H) ₂]	1	<i>t</i> -Bu	Ph
9	[Zn(1-H) ₂]	1	<i>t</i> -Bu	Ph
10	[Co(1-H) ₃].3MeOH	1	<i>t</i> -Bu	Ph
11	[Ni(1-H) ₂ .(MeOH) ₂].2MeOH	1	<i>t</i> -Bu	Ph
12	[Cu(2-H) ₂]	1	<i>t</i> -Bu	Ph
13	[Cu(5-H) ₂]	5	<i>t</i> -Bu	<i>t</i> -Bu
14	[Cu(6-H) ₂]	6	<i>s</i> -Bu	<i>t</i> -Bu
15	[Cu(7-H) ₂]	7	nonyl	<i>t</i> -Bu

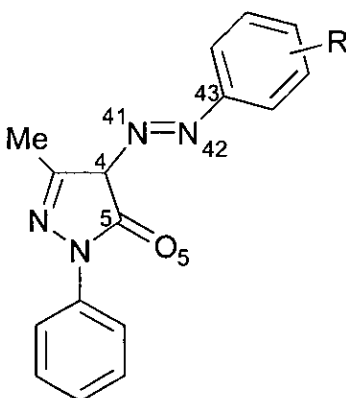
Table 3 : Descriptions of complexes 8-12

5.5.1 Bonding

5.5.1.1 Bonding in the Free Ligands : Tautomerism

Eight structures of six related diazopyrazolone ligands have been reported³⁰⁻³⁷. It is interesting first of all to assess the tautomeric forms of these ligands as observed in the solid state. There are three possible tautomers of diazopyrazolones, as already discussed (Figure 7). Tables 4, 5 and 6 give values for the five bonds lengths of interest, C5-O5, C4-C5, C4-N41, N41-N42 and N42-C43, in assessing the delocalisation in both the structures of the free ligands and metal complexes. The bond nomenclature refers to the diagram below.

Of the five bonds considered, C5-O5, C4-N41 and N41-N42 do not agree with the average single and double bond lengths given in table 4. C5-O5 is found to have significant double bond character in all but one structure³⁷, with the slight lengthening of this bond presumably due to the intramolecular hydrogen bond between O5 and H42. In the majority of free ligand structures (ca. 65 %), the C4-N41 bond is shorter than the N41-N42 bond and is also much closer to the accepted value for C=N (1.28(1) Å). The remaining bonds, C4-C5 and N42-C43, are single bonds. These observations indicate that the hydrazone tautomers (Figure 1 : **b**) of these ligands are predominant, which is in agreement with the evidence acquired by spectroscopic techniques previously described (Sections 5.3.1 and 5.3.2).



Ligand R	C5-O5	C4-C5	C4-N41	N41-N42	N42-C43
<i>p</i> -Cl	1.240(17)	1.544(21)	1.397(19)	1.358(19)	1.438(19)
<i>o</i> -Br	1.234(4)	1.461(5)	1.312(4)	1.317(4)	1.405(5)
<i>o</i> -Cl	1.230(3)	1.468(4)	1.307(3)	1.318(3)	1.397(3)
<i>p</i> -NO ₂	1.227(3)	1.457(3)	1.305(3)	1.320(4)	1.396(4)
<i>o,m'</i> -Cl	1.231(2)	1.474(3)	1.298(2)	1.327(2)	1.388(2)
α - <i>o,p</i> -Me ^a	1.233(4)	1.455(5)	1.311(4)	1.311(4)	1.405(4)
β - <i>o,p</i> -Me ^a	1.230(8)	1.454(10)	1.313(9)	1.307(7)	1.406(9)
<i>o,p</i> -Me ^b	1.27	1.45	1.29	1.33	1.39
Average ^c	1.231(2)	1.462(7)	1.308(4)	1.317(5)	1.400(6)
Accepted Bond Lengths	C_{sp2}-O	C_{sp2}-C_{sp2}	C_{sp2}-N_{sp2}	N_{sp2}-N_{sp2}	C_{sp2}-N_{sp2}
Single	1.33(2)	1.46(2)	1.36(1)	1.40(3)	1.36(1)
Double	1.21(1)	1.32(2)	1.28(1)	1.22(1)	1.28(1)

Table 4 : Bond lengths of C5-O5, C4-C5, C4-N41, N41-N42 and N42-C43 in the free ligand structures³⁰⁻³⁷ and relevant accepted bond lengths³⁸

- ^a α & β refer to the different packing modes of the single crystal in the bulk material. α = packed in layers parallel to the b-axis; β = packed in columns parallel to the b-axis.
- ^b Lengths obtained from CCDC⁴⁶ / Cerius⁴⁹
- ^c Golinski³¹ (R=13.5%) and Struchkov³⁷ structures not included

The hydrogen bond parameters and bite distances for the free ligands are presented in table 4. Although an intramolecular hydrogen bond between O5 and H42 is observed in every structure, the proton is statistically closer to N42 (The N42-H42 distance is approximately half that of O5...H42). This hydrogen bond will of course assist in the stabilisation of the diazo-enolate form of the ligand. It should be noted that in all but two^{31,37} free ligand structures, the hydrogen atoms were found and not placed. Additionally, extremely weak intramolecular hydrogen bonds (ca. 3 Å) are observed between O5 and a CH of the *ortho* methyl group in two of the structures^{35,36} of 4-(2,2'-dimethylphenylazo)-3-methyl-5-pyrazolone. Such a hydrogen bond

will hinder rotation around the N42-C43 bond and may, as a result, enhance the planarity of that part of the molecule.

Ligand	R Factor / %	N42-H42 / Å	O5-H42 / Å H-Bond	O5-N42 / Å Bite Distance
<i>p</i> -Cl	13.7	1.00	2.20	2.94
<i>o</i> -Br	3.75	0.836(35)	2.01	2.714(4)
<i>o</i> -Cl	8.2	1.05	1.92	2.746(3)
<i>p</i> -NO ₂	4.5	0.90(2)	2.06(2)	2.783(3)
<i>o,m'</i> -Cl	6.5	1.05	1.94	2.755(2)
α - <i>o,p</i> -Me	8.5	0.97(4)	1.99	2.807(4)
β - <i>o,p</i> -Me	9.2	0.92(6)	2.04	2.755(8)
<i>o,p</i> -Me	7.5	0.85	2.14	2.77
Average	-	0.95	2.04	2.76

Table 5 : Lengths of N42-H42, the intramolecular hydrogen bond, O5...42 and the bite distance, O5-N42, in the free ligand structures³⁰⁻³⁷ with the R factors of these structures. Note: Values without ESDs are obtained from CCDC⁴⁶ / Cerius⁴⁹

5.5.1.2 Bonding in the Metal Complexes : Mesomerism

The bonding in the metal complexes is summarised in table 6. On complexation, the ligand adopts a formal diazo-enolate tautomeric form (Figure 7 : c), however the situation is significantly more complicated than in the free ligand structures. Whereas the average value of C4-N41 (1.344(6) Å) is much closer to the accepted C_{sp²} - N_{sp²} single bond value of 1.36(1) Å, the N41-N42 bond lengths are significantly affected by complexation of N42 to the metal and vary between 1.27 - 1.31 Å, indicating that this bond is now of intermediate character. The lengths of the C5-O5 bonds are also affected by complexation of O5 to the metal and becomes significantly longer than the equivalent bonds in the free ligands. Again this bond is now intermediate in character. The lengths of the C4-C5 bonds in the complexes are slightly

shorter than in the free ligands but are still considered to be single bonds. It is concluded that a stable, delocalised system, illustrated in figure 23, is the best model of the bonding in the chelate rings of these complexes.

Complex	Ligand	C5-O5	C4-C5	N41-C4	N41-N42	N42-C43
Cr(III) ⁵³	A	1.28(5)	1.40(5)	1.38(5)	1.31(5)	1.39(5)
	B	1.18(5)	1.44(5)	1.36(5)	1.27(5)	1.42(5)
Sn(IV) ⁵⁴	A & B ^a	1.304(4)	1.415(5)	1.329(4)	1.298(4)	1.412(5)
8	A	1.273(4)	1.414(5)	1.344(5)	1.294(4)	1.429(5)
	B	1.269(5)	1.425(6)	1.337(5)	1.311(5)	1.419(5)
9	A	1.278(2)	1.425(3)	1.340(2)	1.297(2)	1.427(2)
	B	1.291(2)	1.420(3)	1.347(3)	1.293(2)	1.425(2)
10	A	1.283(6)	1.412(7)	1.335(7)	1.269(6)	1.446(7)
	B	1.276(6)	1.395(8)	1.342(7)	1.301(6)	1.453(7)
	C	1.287(6)	1.405(7)	1.345(7)	1.285(6)	1.419(7)
11	A	1.268(2)	1.417(3)	1.359(2)	1.283(2)	1.434(2)
	B	1.263(2)	1.425(3)	1.358(2)	1.284(2)	1.443(7)
12	A	1.281(5)	1.425(7)	1.339(6)	1.296(5)	1.437(6)
	B	1.273(5)	1.422(7)	1.343(6)	1.288(5)	1.437(6)
Average ^b	-	1.277(7)	1.417(7)	1.344(6)	1.291(8)	1.434(9)

Table 6 : Lengths (in Å) of the bonds C5-O5, C4-C5, C4-N41, N41-N42 and N42-C43 in the complexes, **8-12**

^a The tin atom is located on an inversion centre, hence the two ligands are equivalent.

^b Averages of the bonds found in the complexes **8 - 12** only

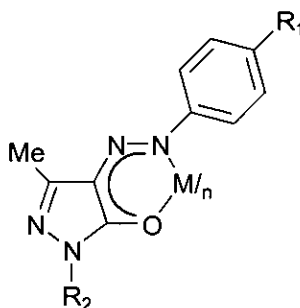


Figure 23 : Diazopyrazolone complexes

5.5.2 General Trends in the Structures of the Metal Complexes, 8-12

5.5.2.1 Metal to Donor Atom Bond Lengths

In all of the structures reported here, **8-12**, the metal to nitrogen donor atom bond lengths are longer than the metal to oxygen donor atom distances, reflecting the slight variation in electrostatic attraction between these donor atoms (Table 7). Additionally, the Pauling covalent radii⁵⁰ for nitrogen and oxygen are 0.70Å and 0.66Å respectively, which means that with similar metal ions the metal to oxygen donor bond is likely to be the shorter one.

Distance	10	11	8	9	12
A M-O	1.909(4)	2.0126(13)	1.930(3)	1.9394(14)	1.920(3)
B M-O	1.898(4)	2.0164(13)	1.928(3)	1.9483(14)	1.935(3)
A M-N	1.962(4)	2.0877(17)	1.972(3)	2.028(2)	1.994(4)
B M-N	1.954(5)	2.0824(17)	1.974(3)	2.009(2)	2.000(4)
C M-X	1.959(4) ^a	2.1017(15) ^c	-	-	-
C M-X	1.980(5) ^b	2.1269(14) ^d	-	-	-

Table 7 : Metal to donor atom bond lengths in the complexes **8-12** (in Å)

^{a,b} X = O, N of ligand C respectively

^{c,d} X = O of coordinated methanols, M and N respectively

The Pauling covalent radii for the transition metal ions in **8-12**, along with their geometries and spin states are presented in table 8. The covalent radii increase in the order Co(III) < Cu(II) < Zn(II) < Ni(II), which mirrors the order of increasing metal to donor atom bond lengths in complexes **8-12**. The cobalt(III) complex, **10**, has the shortest metal to donor atom bond lengths, which is expected as in the low spin, d^6 , octahedral configuration all electrons are in the t_{2g} level giving a CFSE of $2.4 \Delta_o$. Conversely the octahedral, nickel(II) complex, **11**, has two unpaired electrons in the e_g level therefore increasing its radius (cf. Pauling covalent radius for Ni(II)), square planar

($n=0$) = 1.20Å) and resulting in a CFSE of $1.2 \Delta_o$. This structure has the longest metal to donor atom bond lengths in this series of complexes.

Complex	8 & 12	9	10	11
TM Ion	Cu(II)	Zn(II)	Co(III)	Ni(II)
Geometry	D _{4h}	T _d	O _h	O _h
Spin State	d ⁹	d ¹⁰	L.S. d ⁶	d ⁸
n	1	0	0	2
Pauling Covalent Radius / Å	1.28	1.31	1.22	1.39

Table 8 : Transition metal ion parameters

Note: TM = transition metal; n = number of unpaired electrons; L.S. = low spin

The copper to oxygen bond lengths in **8** and **12** are slightly shorter than the equivalent bonds in the zinc complex, **9**. The copper to nitrogen donor atom bonds lengths in **8** are significantly shorter than the equivalent bonds in **9**, however, illustrating the importance of π -bonding in the planar copper complex.

5.5.2.2 Bite Angles and Bite Distances

Bite angles in the complexes **8-12** increase in the order Ni < Cu < Co < Zn (Table 9). The five-membered pyrazolone ring fused to the chelate ring will restrict the N-O bite distances available to the four different metal ions under consideration. Further constraints are introduced by the high degree of delocalisation within the chelate ring itself (Tables 4 and 6) and such effects on bite distance will also obviously effect the bite angles of the metal complexes. It is expected that the pseudo-tetrahedral zinc structure, **9**, will have the largest bite angles and that those for structures **8**, **10**, **11** and **12** will be close to 90°.

Bite Angles / °					
	10	11	8	9	12
A	94.3(2)	92.20(6)	92.86(12)	97.21(7)	92.9(2)
B	95.2(2)	91.55(6)	93.72(13)	97.33(6)	92.83(15)
C	92.3(2)	-	-	-	-
Average	93.9(11)	91.88(33)	93.29(43)	97.27(6)	92.87(4)
Bite Distances⁵¹ / Å					
A	2.837(6)	2.955(2)	2.827(4)	2.977(3)	2.837(6)
B	2.845(6)	2.938(2)	2.848(4)	2.971(3)	2.852(6)
C	2.841(6)	-	-	-	-
Average	2.841(3)	2.947(9)	2.838(11)	2.974(4)	2.845(8)

Table 9 : Bite angles and distances in the complexes, **8-12**

The average bite angle for the zinc complex, **9**, is 97.3°, which fits neither that of a perfect tetrahedron (109.5°) nor that of orthogonal geometry (90°) particularly well and is likely to be due to constraints introduced by the ligand bite distance, resulting in a compromise between the available bite distance and the ideal metal to donor atom distances. The average free ligand bite distance is 2.76 Å (Table 5), so in every case the ligand must distort to accommodate the metal ion. The variation in bite angle in the cobalt complex, **10**, (92.3 - 95.2 °) is assumed to be due to the steric constraints of fitting three ligands around the central cobalt(III) ion, resulting in a distorted octahedral geometry. Bite distances increase in the order Co ≈ Cu < Ni < Zn. This is perhaps unexpected as one might expect this distance to increase with increasing bite angle. However, these values reflect both the variation in bite angle and the variation in metal to donor atom bond length as already discussed.

5.5.2.3 Torsion Angles and Dihedral Angles

The torsion angles around the diazo bond and the dihedral angles of each of the planes of the two phenyl rings in the ligands to the chelate plane are presented in table 10.

Torsion Angles / °	10	11	8	9	12
C4A-N41A-N42A-C43A	-176	176	-173	178	176
C4B-N41B-N42B-C43B	176	174	-178	180	177
C4C-N41C-N42C-C43C	171	-	-	-	-
Dihedral Angles to chelate plane ^a / °					
phenyl A (azo) ^b	92.6	57.2	51.9	18.7	37.2
phenyl B (azo)	57.3	100.5	38.0	24.0	40.6
phenyl C (azo)	64.5	-	-	-	-
phenyl A (pyr) ^c	143.4	29.9	16.7	13.6	17.7
phenyl B (pyr)	178.1	38.7	32.0	23.6	13.4
phenyl C (pyr)	4.7	-	-	-	-

Table 10 : Torsion angles and dihedral angles in the complexes, **8-12**

- ^a Best fit plane through M, O5, C5, N1, N2, C3, C4, N41, N42
^b Best fit plane through C43, C44, C45, C46, C47, C48
^c Best fit plane through C11, C12, C13, C14, C15, C16

Both parameters give a good indication of geometrical distortions in the complexes, **8-12**, which are attributed to inter-ligand repulsion. The torsion angles around the diazo bonds are closest to 180° (ie: planar) in the zinc complex, **9**, which is expected as the two ligands lie well apart due to the pseudo-tetrahedral geometry of the complex. This is further illustrated by the dihedral angles to the chelate plane in **9**, which are also closest to planar. Although the configurations around the diazo bonds in all the complexes are approximately planar arising from stabilisation of the six-membered chelate rings, the patterns of distortion defined by the dihedral angles in the copper(II), nickel(II) and cobalt(III) complexes, **8**, **12**, **11** and **10**, are much more complicated. In the copper(II) complexes, **8** and **12**, the phenyl ring

attached to the diazo unit is significantly more removed from the plane of the chelate ring than that attached to the pyrazolone unit. These distortions are additionally more pronounced in **8**, which suggests that the *tert*-butyl substituents are forcing the phenyl rings out of the plane defined by the chelate ring. The large dihedral angles in both the cobalt(II) complex, **10**, and the nickel(II) complex, **11**, are attributed to crowding of the ligands around the central metal ion. In **10** such large distortions are to be expected due to the presence of three bulky ligands around the central metal. In **11**, the nickel(II) has been forced to adopt a less favourable octahedral geometry, due to the bulk of the ligands, and the two vacant coordination sites are occupied by oxygen atoms from two methanol molecules. This can be explained in terms of CFSE values. Nickel(II) will preferentially form D_{4h} complexes (CFSE $1.56 \Delta_{sp}$), but if this is not possible it will distort to form a tetrahedral complex with CFSE $0.8 \Delta_T$. However, the CFSE of the equivalent octahedral complex is $1.2 \Delta_O$, therefore nothing is gained by the complex adopting a tetrahedral geometry and so it adopts an octahedral geometry *via* the coordination of two methanol molecules.

It can be concluded from these general comparisons that the bulky diazopyrazolone ligands seem to be most well suited to the pseudo-tetrahedral geometry preferred by zinc(II). Inter-ligand repulsion terms play a significant role in destabilising the copper(II) complexes, **8** and **12**, and this is clearly illustrated by the relatively good solvent extraction of zinc(II) by 3-methyl-1-phenyl-4-(4-*tert*-butylphenylazo)-5-pyrazolone, **1**, in comparison with that of copper(II), as described in section 5.4.1.

5.5.3 Comparison of the Copper(II) Structures, **8** and **12**.

In the copper(II) complexes **8** and **12** the geometry around the central metal atoms approximates closely to square planar, with a mean deviation from the plane of the inner ring (defined by Cu, O5A, C5A, C4A, N41A, N42A, O5B, C5B, C4B, N41B AND N42B) of $\pm 0.31 \text{ \AA}$ and $\pm 0.25 \text{ \AA}$ respectively. The very small difference between these values may be attributed to the steric bulk of the *tert*-butyl substituents in **8**.

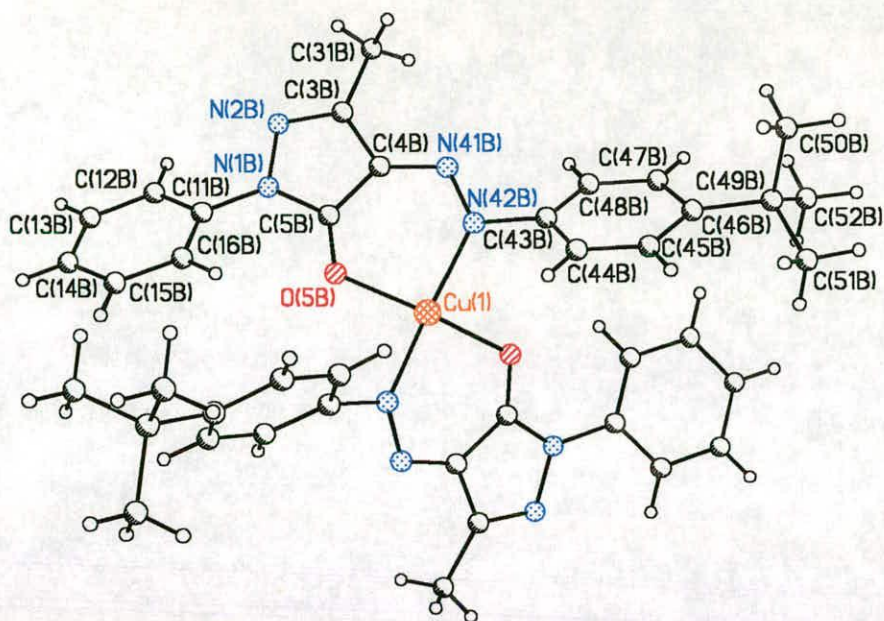


Figure 24 : Structure of $[\text{Cu}(1\text{-H})_2] : 8$

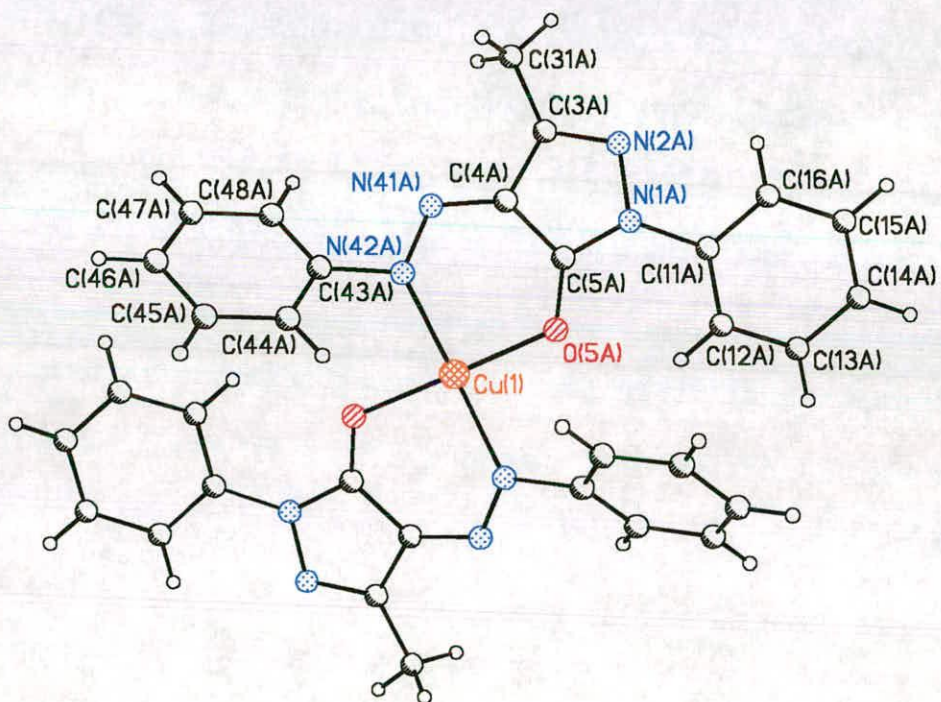


Figure 25 : Structure of $[\text{Cu}(2\text{-H})_2] : 12$

The dihedral angles between the two coordination planes (defined by Cu, O, N) in **8** and **12** are 22.7° and 18.4° respectively, again providing evidence for significant deviations from planarity in both structures. The two ligands around each central copper(II) cannot lie flat due to interligand repulsions. The shortest interligand contact distances in **8** and **12** are presented in table 11. These contact distances are found to be significant and certainly indicate that steric repulsion contribute to the geometric distortions in the two copper(II) structures. The inability of the diazopyrazolone ligands to lie completely flat on coordination to copper(II) must contribute also to the relative weakness of these ligands as copper solvent extractants. The electrons involved in the conjugated system of the coordinated ligand cannot fully delocalise to stabilise the complex.

Complex	Inter-ligand Distance / Å			
	<i>tert</i> -butyl → phenyl ring		phenyl ring → phenyl ring	
8	C50A-C15B	4.148(8)	C47A-C15B	3.884(7)
	C52B-C15A	4.145(7)	C15A-C46B	4.125(6)
	H50A-H15B	2.782 ^a	C16A-C43B	4.054(7)
	-	-	C48A-H16B	3.201 ^a
	-	-	C43A-H16B	3.337 ^a
12	-	-	C45A-C12B	3.662(9)
	-	-	C47A-C13B	3.849(9)
	-	-	C13A-C47B	3.736(11)
	-	-	C12A-C46B	3.839(11)
	-	-	H48A-H13B	2.774 ^a

Table 11 : Inter-ligand contact distances in **8** and **12**

^a ESDs could not be determined for bonds involving protons, as the positions of the protons were calculated not found.

It is interesting to note, however, that the planarity of the ligands is not so disrupted that stacking between adjacent molecules in the crystal packing cannot occur. The shortest distance between pyrazoyl rings in adjacent

molecules of **8** is 3.24 Å, which is typical for π - stacking⁵² and as such they form dimeric units (Figure 26).

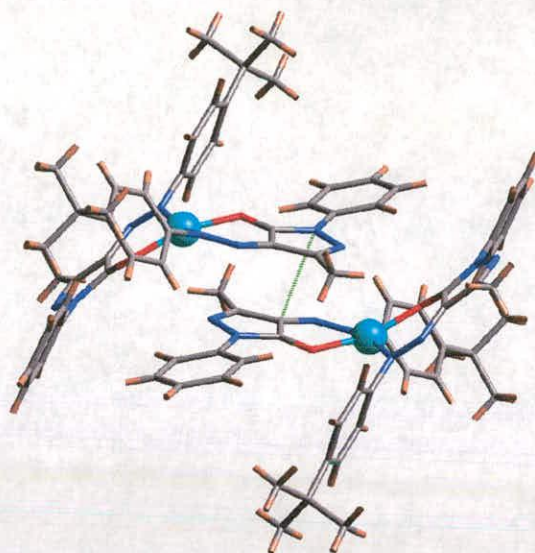


Figure 26 : The dimeric unit formed by π - π stacking in **8**. The shortest distance between the two molecules is shown in green.

The two complexes in the dimer are slightly offset from one another so the pyrazoyl rings do not lie directly on top of one another. This agrees with the observation made by Hunter and Saunders⁵² that although face to face stacking is favoured by Van der Waals interactions, it is disfavoured by π - π repulsion. The presence of a strongly polarising atom, such as a heteroatom, positively influences the electrostatic interaction between two molecules. In **8**, however, this face to face stacking is not sufficiently stabilised by such polarisation effects and an offset stacking is preferred. Interestingly, a dimeric unit is also observed in the crystal structure of the free ligand, 3-methyl-1-phenyl-4-(4-nitrophenylazo)-5-pyrazolone³³, but the stacking in this structure is heavily influenced by the polarisation effect of the *para*-nitro substituent, and so in this case the stacking is anti-parallel.

2.5.4 The Zinc(II) Complex, 9

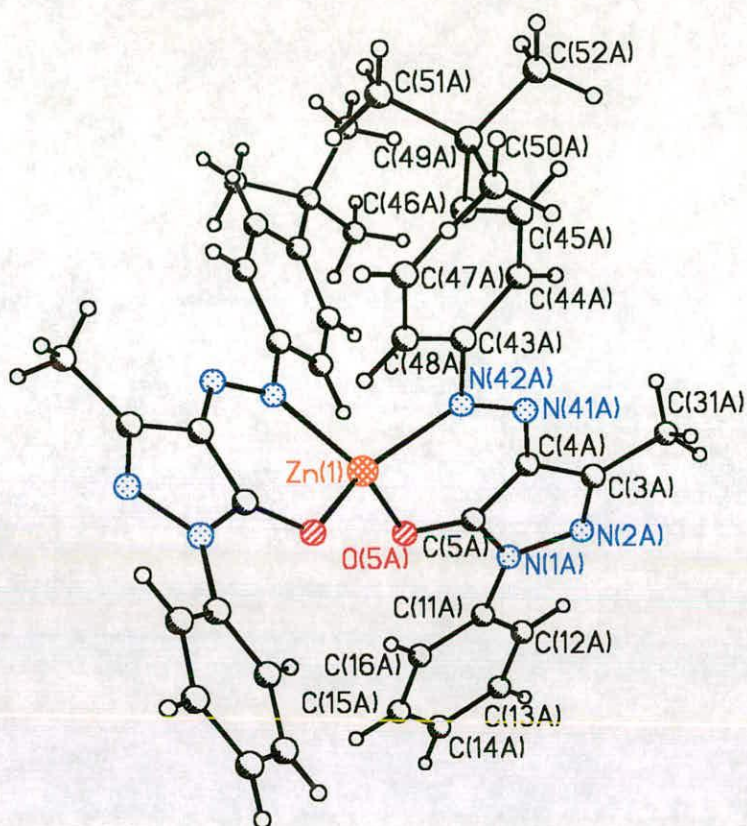


Figure 27 : Structure of $[\text{Zn}(\mathbf{1-H})_2] : \mathbf{9}$

Initial inspection of the structure of the zinc(II) complex, **9**, suggests it possesses nearly perfect tetrahedral geometry as the sum of the angles around the central metal ion is 658.29° (A perfect tetrahedron would have a sum of angles of $657^\circ : 6 \times 109.5^\circ$). However the individual angles at the central metal ion vary between 97.21 - 123.16° , suggesting much less perfect tetrahedral symmetry than initially indicated. Indeed for a four-coordinated complex the sum of angles around the central metal would be 660° ($2 \times 90^\circ$ & $4 \times 120^\circ$), which shows that this is an unsatisfactory test for tetrahedrality. A more reliable indicator for tetrahedrality in a molecule is the dihedral angle between the two coordination planes (defined by the metal and two donor atoms, Zn, O and N here), which is 80.7° for **9**. For a perfect tetrahedron,

this angle would be 90° , therefore this dihedral angle does still represent a degree of steric strain. **9** can be described as pseudo-tetrahedral and, despite this deviation from perfect tetrahedral geometry, is the least sterically strained of all the structures, **8-12**, which indicates why this diazopyrazolone ligand is a good solvent extractant for zinc(II) in comparison with copper(II). This favourable geometry is further illustrated by the fact that the torsion angles around the diazo bonds (C4-N41-N42-C43) in **9** are closest to planar (178° and 180°) of those in all the metal complexes, **8 - 12**.

2.5.5 The Cobalt(III) Complex, **10**

During the formation of complex **10**, the cobalt(II) starting material is oxidised to the cobalt(III) state and adopts a low spin, d^6 , octahedral geometry, with the angles in the three orthogonal planes adding up to 360.4° and 359.5° and 360.0° . Mean deviations from planarity of these three planes are ± 0.02 , 0.04 and 0.07 \AA and the angles between each of these planes with respect to the others are 90.0° , 91.9° and 87.9° . Although both these parameters suggest slight deviations from perfect octahedral geometry, variations in metal to donor atom bond lengths are a clearer indication of this ranging from $1.91 - 1.98 \text{ \AA}$. The structure is therefore pseudo-octahedral with the three coordinated ligands arranging themselves in a *mer* configuration around the central metal with respect to their three oxygen and three nitrogen donor atoms.

The dihedral angles between the plane of the phenyl ring (defined by C11 - C16) and the chelate plane (defined by Co, O5, C5, C4, N41, N42) for ligands A, B and C are 143.4° , 178.1° and 4.7° respectively, while the dihedral angles between the planes of the phenyl (defined by C43 - C48) and the chelate plane are 92.6° , 57.3° and 64.5° . Torsion angles around the azo N=N bonds (C4-N41-N42-C43) are -176° , 176° and 171° respectively. These results indicate that of the three coordinated ligands, A is the most distorted from planarity, while planarity of the pyrazoyl ring plus N-phenyl ring unit is the best preserved in B and C of all the five structures, **8 - 12**.

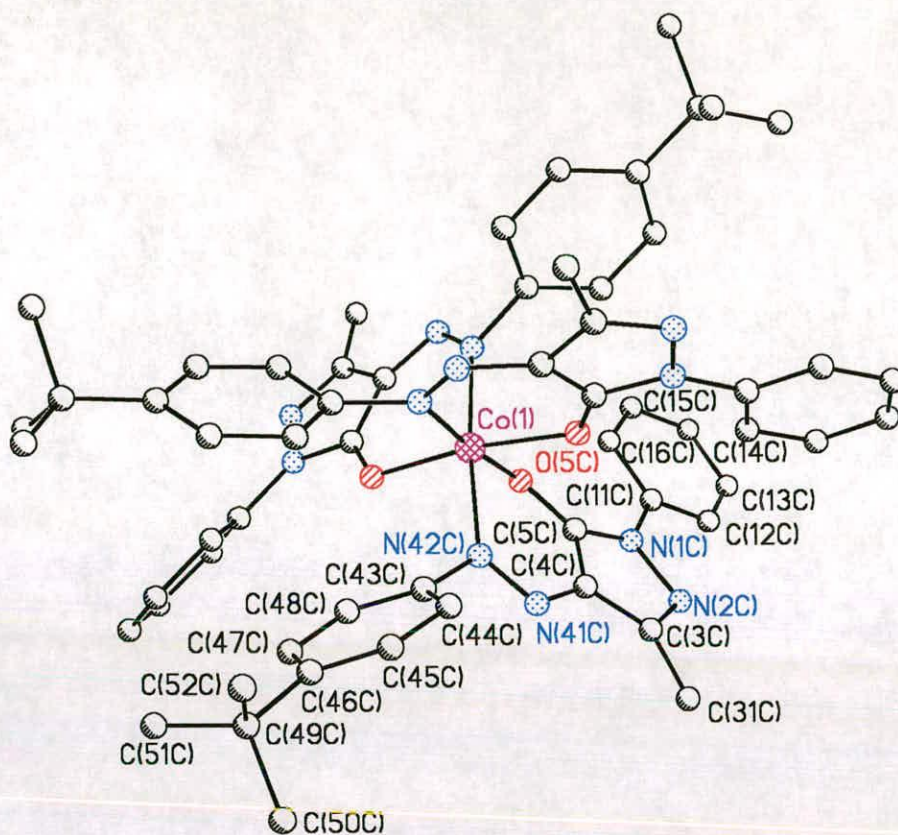


Figure 28 : Structure of $[\text{Co}(\mathbf{1-H})_3] \cdot 3\text{MeOH}$: **10**; Non-coordinated methanol molecules and hydrogen atoms have been excluded for clarity.

Again it is reasonable to assume that distortions occur due to steric strain within this crowded molecule. The *mer* octahedral geometry means that the relative lengths of the metal to donor atom bond lengths may be predicted on the basis that nitrogen should show a greater trans effect than oxygen. As such we can predict that the nitrogens trans to one another will have longer metal to donor atom bond lengths (N42A : 1.962(2) Å; N42C : 1.980(2) Å) than the nitrogen trans to the oxygen (N42B : 1.898(4) Å). The oxygen trans to the nitrogen will have a longer (weaker) bond length (O5C : 1.959(4) Å) than those of the oxygen atoms trans to one another (O5A : 1.909(4) Å; O5B : 1.898(4) Å). This is indeed found to be the case.

5.5.6 The Nickel Complex, 11

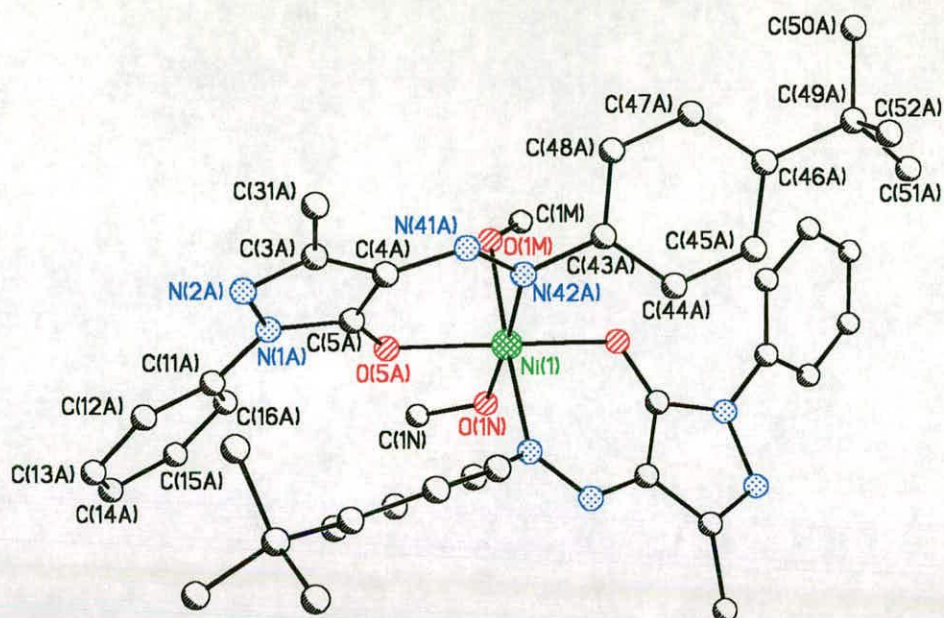


Figure 29 : Structure of $[\text{Ni}(\text{1-H})_2(\text{MeOH})_2] \cdot 2\text{MeOH}$: **11**; Non-coordinated methanol molecules and hydrogen atoms have been excluded for clarity.

In the structure of complex **11** nickel(II) might have been expected to adopt a stable low spin d^8 square planar configuration, but the bulk of the ligands mean that the two diazopyrazolone units cannot lie in the square plane and instead octahedral symmetry at the metal is observed, with the inner coordination sphere being completed by two oxygen atoms donated by two solvent molecules. The solvent donor atoms are found furthest from the central metal ion at an average distance of 2.114 Å and, as in **10**, this is presumably in part due to these oxygen atoms being trans to nitrogens. Additionally, the methanol oxygen atoms are uncharged donors, whereas each of the four pyrazolone donor atoms have a formal charge of $-\frac{1}{2}$. Electrostatic interactions will therefore also occur between these four atoms and the nickel(II) cation, which will result in stronger (shorter) metal to donor atom bonds. The deviation from perfect octahedral geometry is not evident from the sums of the angles of the three orthogonal planes passing through the central nickel(II) ion, which are 359.66 °, 360.41 ° and 360.08°.

However, the three angles along the x, y and z axes (ie: N42A-Ni-O5N; N42B-Ni-O1M; O5A-Ni-O5B) vary between 167.61 - 177.06° indicating that the octahedral symmetry in this structure is far from perfect. The mean deviations from planarity of the three chelate planes (defined by the nickel plus the four donor atoms only) are ± 0.10 , 0.03 and 0.03 Å.

5.6 Conclusions

The work presented in this chapter has shown that while diazopyrazolone ligands are unsuitable for use as copper extractants in a conventional acid leach circuit, their extraction and stripping characteristics are well suited to copper recovery from ammonical media such as in the Escondida process. Additionally, diazopyrazolones are cheap and easy to synthesise.

Spectroscopic techniques such as IR and NMR have provided useful information on the tautomerism of diazopyrazolones both in solution and in the solid state, while X-ray crystallographic structural studies have been used to try and elucidate the reasons for the relative weakness of this type of ligand as copper extractants. The steric bulk of the diazopyrazolone ligand, **1**, has caused interesting geometric distortions in its transition metal complexes, which ultimately favour a tetrahedral geometry such as that of conventional zinc(II) complexes, as opposed to a square planar geometry of conventional copper(II) complexes.

The only perceived drawback to the use of diazopyrazolones as copper extractants is their intense colour, which would require extremely careful handling on a plant to prevent staining.

5.7 Experimental

5.7.1 Instrumentation

Melting points were determined with a Gallenkamp apparatus and are uncorrected. Elemental analysis was performed on a Perkin Elmer 2400 elemental analyser. IR spectra were obtained on a Perkin Elmer Paragon 1000 FT-IR spectrometer as potassium bromide discs or as liquid thin films. ^1H and ^{13}C NMR spectra were run on Bruker WP200, AC250 and DPX300 spectrometers. NOE experiments were run on a Bruker WH360 spectrometer. Chemical shifts (δ) are reported in parts per million (ppm) relative to residual solvent protons as internal standards. Electron impact (EI) mass spectra were obtained either on a Finnigan MAT4600 quadrupole spectrometer or on a Kratos MS50TC spectrometer. Fast atom bombardment (FAB) mass spectra were obtained on a Kratos MS50TC spectrometer in acetonitrile / 3-nitrobenzyl alcohol matrices. Electrochemistry was carried out under nitrogen using a 0.5 mm platinum working electrode, an Ag^+/AgCl reference electrode, a platinum counter electrode and a 0.1 M *tert*-butyl ammonium tetra-fluoroborate electrolyte. Inductively coupled plasma atomic emission spectroscopy (ICP-AES) analysis was performed on a Thermo Jarrell Ash ICP-AES spectrometer. Magnetic susceptibilities were measured for the paramagnetic complexes **8**, **11**, **12**, **13**, and **14** using the Evans NMR method^{53,54} or a Johnson Matthey magnetic susceptibility balance and molar susceptibilities were corrected for diamagnetism using Pascal's constants⁵⁵.

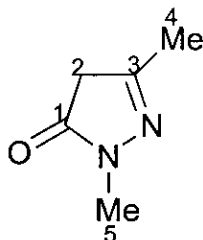
5.7.2 Solvent and Reagent Pretreatment

Substituted anilines and pyrazolones were commercially available (Acros or Aldrich) with the exception of 1,3-dimethyl-5-pyrazolone and 3-methyl-1-*t*-butyl-5-pyrazolone, which were prepared by the method of Butler *et al.*⁵⁶. Solvents used for analytical purposes (NMR, MS) were of spectroscopic grade. Deuterated dimethylsulphoxide for use in NOE experiments was

dried over 4Å molecular sieves under nitrogen. All other reagents and solvents were used as received.

5.7.3 Synthesis of Starting Pyrazolones

1,3-Dimethyl-5-pyrazolone



A solution of methylhydrazine (5.85 ml, 0.11 mol) in methanol (90 ml) was cooled to 0 °C and ethylacetoacetate (12.75 ml, 0.1 mol) was added dropwise to it with stirring. The reaction medium was stirred at 0 °C for 4 h and then heated under reflux for 1 h. The solvent was removed from the resulting pale yellow solution using a rotary evaporator to leave a yellow, oily residue, which was left to stand overnight during which time a colourless, crystalline solid had formed. The crude product was recrystallised from petroleum ether (40-65 °C) / toluene (100 ml / 50 ml) to yield a colourless, microcrystalline powder (8.846 g, 78.90 %).

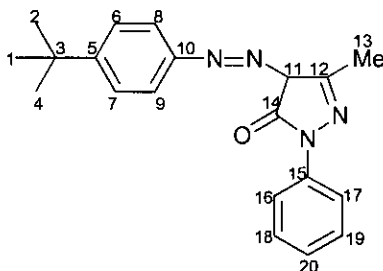
mp 143 - 144 °C; IR (cm⁻¹, KBr Disc): ν 2923.7s (CH), 1578.1s-broad (C=O, C=N), 1303.9m (CH); ¹H NMR (CDCl₃, 200 MHz): δ 2.07 (s, 3H, C-CH₃), 3.16 (s, 2H, CH₂), 3.25 (s, 3H, N-CH₃); ¹³C NMR (CDCl₃, 63 MHz): δ 16.76 (C-4), 30.89 (C-5), 41.29 (C-2), 155.38 (C-3), 172.12 (C-1); EIMS *m/z* 112 (33.9 %, LH), 69 (39.1 %, LH - 2CH₃ - O), 41 (100.0 %, CH₃NN).

3-Methyl-1-tert-butyl-5-pyrazolone - The synthesis for this starting pyrazolone is described in section 3.7.3.

5.7.4 Synthesis of the Ligands

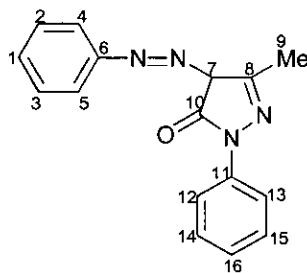
Compounds 1-7 were prepared as described for 1 by diazotisation of the reagent grade anilines and coupling²¹ with the appropriate pyrazolones.

3-Methyl-1-phenyl-4-(4-*t*-butylphenylazo)-5-pyrazolone (1)



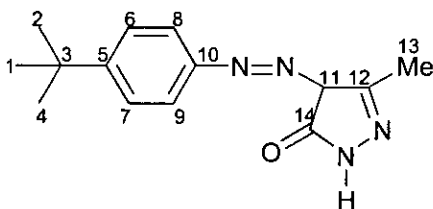
Aqueous sodium nitrite (2 M, 10 ml) was added to a stirred solution of 4-*t*-butylaniline (2.98 g, 20 mmol) in water (20 ml) containing concentrated hydrochloric acid (4 ml, 40 mmol) at 0–5 °C. After 1 h this was added to a solution of 3-methyl-1-phenyl-5-pyrazolone (3.48 g, 20 mmol) in acetone (40 ml) and water (40 ml) at 0-5 °C. Addition of sodium acetate (10 g, 120 mmol) yielded a bright orange suspension, which was stirred for 2 h at 0-5°C, collected by filtration, washed with water and recrystallised (methanol : water, 20:1) to yield **1** (5.34 g, 66.4 %) as orange needles; mp 138-139 °C (Found C, 71.8; H, 6.75; N, 17.0; C₂₀H₂₂N₄O requires C, 71.8; H, 6.6; N, 16.8 %); IR (cm⁻¹, KBr disc) : ν 3430m (NH), 1654s (C=O), 1551s (C=N); ¹H NMR (CDCl₃, 200 MHz): δ 1.32 (s, 9H, C(CH₃)₃), 2.36 (s, 3H, CH₃), 7.15-7.24 (tt, J_{ortho} 7.41 Hz, J_{meta} 1.87 Hz, 1H, *p*-ArH-ring), 7.34-7.47 (m, J_{ortho} 6.34 Hz : 4H (ArH-N=N) and 2H (*m*-ArH-ring)), 7.91-7.98 (dd, J_{ortho} 7.58 Hz, J_{meta} 2.11 Hz, 2H, *o*-ArH-ring), 13.62 (br s, 1H, NH); ¹³C NMR (CDCl₃, 63 MHz): δ 11.71 (C-13), 31.20 (C-1,2,3), 34.52 (C-3), 115.51 (C-8,9), 118.48 (C-16,17), 125.00 (C-20), 126.47 (C-6,7), 127.88 (C-5), 128.81 (C-18,19), 137.97 (C-10), 138.59 (C-15), 148.46 (C-11), 149.19 (C-12), 157.75 (C-14); EIMS *m/z* 334 (70.0 %, M⁺), 319 (100.0 %, M - CH₃), 132 (14.1 %, (CH₃)₃CPh), 91 (20.0 %, PhN), 77 (34.9 %, Ph).

3-Methyl-1-phenyl-4-phenylazo-5-pyrazolone (2)



79.2 %; orange needles; mp 153-155 °C (Found C, 69.1; H, 5.0; N, 20.1; C₁₆H₁₄N₄O requires C, 69.0; H, 5.1; N, 20.1 %); IR (cm⁻¹, KBr disc) : ν 3436m (NH), 1657s (C=O), 1551s (C=N); ¹H NMR (CDCl₃, 200 MHz): δ 2.35 (s, 3H, CH₃), 7.14-7.25 (m, 2H, *p*-ArH), 7.35-7.47 (m, 6H: 4H *m*-ArH plus 2H *o*-ArH-N=N), 7.91-7.98 (dd, J_{ortho} 7.56 Hz, J_{meta} 1.23 Hz, 2H, *o*-ArH), 13.56 (br s, 1H, NH); ¹³C NMR (CDCl₃, 63 MHz): δ 11.67 (C-9), 115.66 (C-4,5), 118.39 (C-12,13), 125.00 (C-1), 125.66 (C-16), 128.34 (C-11), 128.79 (C-2,3), 129.52 (C-14,15), 137.89 (C-6), 140.98 (C-7), 148.44 (C-8), 157.62 (C-10); EIMS m/z 278 (100.0 %, M⁺), 202 (33.1 %, M - Ph), 93 (22.5 %, Ph - NH₂), 77 (62.3 %, Ph).

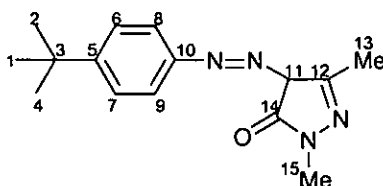
1-Hydro-3-methyl-4-(4-*t*-butylphenylazo)-5-pyrazolone (3)



22.35 %; orange/brown microcrystalline powder; mp 133-136 °C (Found C, 64.6; H, 7.3; N, 21.4; C₁₄H₁₈N₄O requires C, 65.1; H, 7.0; N, 21.7 %); IR (cm⁻¹, KBr disc) : ν 3424s & 3156s (NH), 1664s (C=O), 1551s (C=N); ¹H NMR (DMSO-d₆, 200 MHz): δ 1.26 (s, 9H, C(CH₃)₃), 2.14 (s, 3H, CH₃), 3.17 (s, 1H, NH), 7.42 (s, 4H, ArH), 11.54 (s, 1H, NH-Ar); ¹³C NMR (DMSO-d₆, 63 MHz): δ 11.70 (C-13), 31.20 (C-1,2,4), 34.34 (C-3), 115.51 (C-8,9), 126.39 (C-6,7),

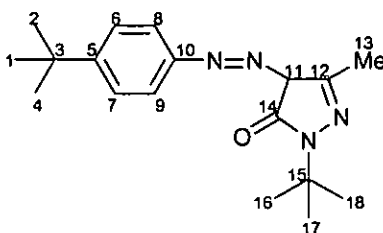
127.78 (C-5), 139.11 (C-10), 146.80 (C-11), 147.90 (C-12), 160.39 (C-14); EIMS m/z 258 (73.7 %, M^+), 243 (100.0 %, $M - CH_3$), 133 (34.2 %, $(CH_3)_3CPh$), 77 (9.7 %, Ph).

1,3-Dimethyl-4-(4-*t*-butylphenylazo)-5-pyrazolone (4)



93.2 %; orange microcrystals; mp 81-83 °C (Found C, 66.0; H, 7.5; N, 20.2; $C_{15}H_{20}N_4O$ requires C, 66.1; H, 7.4; N, 20.6 %); IR (cm^{-1} , KBr disc) : ν 3452s (NH), 1661s (C=O), 1560s (C=N), 838m (ArH); 1H NMR ($CDCl_3$, 200 MHz): δ 1.31 (s, 9H, $C(CH_3)_3$), 2.25 (s, 3H, C- CH_3), 3.38 (s, 3H, CH_3), 7.30-7.47 (m, J_{ortho} 9.00 Hz, 4H, ArH), 13.43 (br s, 1H, NH); ^{13}C NMR ($DMSO-d_6$, 63 MHz): δ 11.45 (C-13), 30.75 (C-15), 31.17 (C-1,2,4), 34.35 (C-3), 115.65 (C-8,9), 126.40 (C-6,7), 127.52 (C-5), 139.00 (C-10), 145.96 (C-11), 148.12 (C-12), 157.66 (C-14); EIMS m/z 272 (74.5 %, M^+), 257 (100.0 %, $M - CH_3$), 133 (30.5 %, $(CH_3)_3CPh$), 43 (17.3 %, H_3C-N_{ring}).

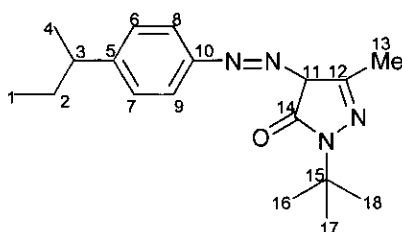
3-Methyl-1-*t*-butyl-4-(4-*t*-butylphenylazo)-5-pyrazolone (5)



60.4 %; orange oil (Found C, 69.0; H, 8.5; N, 17.1; $C_{18}H_{26}N_4O$ requires C, 68.7; H, 8.35; N, 17.8 %); IR (cm^{-1} , liquid thin film) : ν 1650s (C=O), 1556s (C=N), 1395s & 1365s ($C(CH_3)_3$); 1H NMR ($CDCl_3$, 300 MHz): δ 1.32 (s, 9H, Ar- $C(CH_3)_3$), 1.58 (s, 9H, N- $C(CH_3)_3$), 2.23 (s, 3H, CH_3), 7.30-7.40 (dd, 4H,

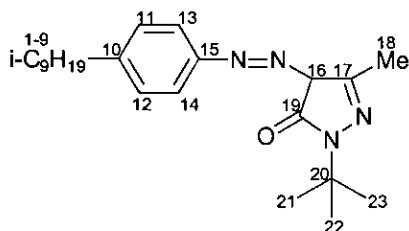
ArH), 13.71 (br s, 1H, NH); ^{13}C NMR (CDCl_3 , 63 MHz): δ 11.52 (C-13), 28.26 (C-1,2,3), 31.19 (C-16,17,18), 34.40 (C-3), 57.48 (C-15), 115.15 (C-8,9), 126.29 (C-6,7), 128.79 (C-5), 138.93 (C-10), 145.53 (C-11), 148.35 (C-12), 159.14 (C-14); EIMS m/z 314 (64.2 %, M^+), 299 (50.8 %, $\text{M} - \text{CH}_3$), 258 (19.28 %, $\text{M} - \text{C}(\text{CH}_3)_3$), 243 (100.0 %, $\text{M} - (\text{CH}_3 + \text{C}(\text{CH}_3)_3)$), 133 (27.4 %, $(\text{CH}_3)_3\text{CPh}$), 57 (26.8 %, $\text{C}(\text{CH}_3)_3$).

3-Methyl-4-(4-s-butylphenylazo)-1-t-butyl-5-pyrazolone (6)



75.2 %; orange oil; (Found C, 66.3; H, 8.1; N, 16.6; $\text{C}_{18}\text{H}_{26}\text{N}_4\text{O} \cdot \frac{3}{4}\text{H}_2\text{O}$ requires C, 65.9; H, 8.5; N, 17.1 %); IR (cm^{-1} , liquid thin film) : ν 1649s (C=O), 1560s (C=N), 1395m & 1367s $\text{C}(\text{CH}_3)_3$; ^1H NMR (CDCl_3 , 300 MHz): δ 0.79-0.85 (t, 3H, $\text{CH}_{3(\text{chain})}$), 1.22-1.28 (d, 3H, CHCH_3), 1.53-1.67 (m, 11H, $\text{C}(\text{CH}_3)_3$ and CH_2), 2.23 (s, 3H, CH_3), 2.55-2.65 (q, 1H, -CH), 7.16-7.34 (dd, 4H, ArH), 13.71 (br s, 1H, NH); ^{13}C NMR (CDCl_3 , 63 MHz): δ 11.45 (C-13), 11.98 (C-1), 21.58 (C-4), 28.19 (C-16,17,18), 30.96 (C-2), 41.02 (C-3), 57.38 (C-15), 115.33 (C-8,9), 127.91 (C-6,7), 128.65 (C-5), 139.24 (C-10), 144.80 (C-11), 145.37 (C-12), 159.08 (C-14); EIMS m/z 314 (57.34 %, M^+), 299 (27.07 %, $\text{M} - \text{CH}_3$), 285 (26.34 %, $\text{M} - \text{CH}_3\text{CH}_2$), 258 (13.41 %, $\text{M} - \text{C}(\text{CH}_3)_3$), 229 (100.0 %, $\text{M} - \text{C}(\text{CH}_3)_3\text{CNN}$), 91 (31.52 %, PhN), 57 (25.35 %, s-Bu/t-Bu).

3-Methyl-4-(4-nonylphenylazo)-1-*t*-butyl-5-pyrazolone (7)



52.5 %; orange oil; ^1H NMR (CDCl_3 , 300 MHz): δ [0.78-0.93 (m) plus 0.93-1.03 (d) plus 1.03-1.10 (d) plus 1.10-1.14 (d) plus 1.22-1.37 (m) plus 1.50-1.55 (d)] (17H, *nonyl H*), 1.55 (s, 9H, $\text{C}(\text{CH}_3)_3$), 2.5-2.7 (m, 2H, $-\text{CH}_2\text{-Ar}$), 7.18-7.32 (dd, 4H, *ArH*), 13.71 (br s, 1H, *NH*); ^{13}C NMR (CDCl_3 , 63 MHz): δ 11.53 (C-18), 28.25 (C-21,22,23), *nonyl substituent* : [22.42 (CH_3 or CH), 22.51 (quaternary), 27.95 (CH_3 or CH), 28.87 (CH_3 or CH), 29.89 (CH_3 or CH), 30.99 (quaternary), 33.02 (CH_2), 41.20 (CH_2), 51.04 (CH_2)], 57.48 (C-20), 115.41 (C-13,14), 128.67 (C-10), 129.29 (C-11,12), 139.13 (C-15), 140.37 (C-16), 145.56 (C-17), 159.13 (C-19).

5.7.5 Synthesis of the Metal Complexes

[Cu(1-H) $_2$]: (8)

Copper(II) nitrate trihydrate (0.242 g, 1 mmol) in methanol (15 ml) was added to 1 (0.668 g, 2 mmol) in methanol (40 ml) containing potassium hydroxide (0.112 g, 2.00 mmol). The resulting dark brown solution was stirred for 0.5 h at room temperature to afford a dark black / brown precipitate, which was recrystallised (methanol : acetone, 3:1) to yield dark red crystals of $\text{Cu}(\text{1-H})_2$ (0.528 g, 72.3 %); mp 238-240 °C (Found C, 65.5; H, 5.9; N, 15.4; $\text{C}_{40}\text{H}_{42}\text{N}_8\text{CuO}_2$ requires C, 65.8; H, 5.8; N, 15.3 %); IR (cm^{-1} , KBr disc): ν 1561s (C=N), 1414m & 1367m ($\text{C}(\text{CH}_3)_3$); FABMS m/z 858 (28.9 %, Cu_2L_3), 794 (29.2 %, Cu_2L_2), 730 (13.2 %, CuL_2), 461 (32.0 %, Cu_2L), 397 (41.1 %, CuL), 334 (38.5 %, L), 133 (100.0 %, $(\text{CH}_3)_3\text{CPh}$), 63 (89.9 %, Cu); $\mu_{\text{eff}} = 1.88$ B. M. (Evans).

[Zn(1-H)₂] : (9)

Zinc(II) acetate dihydrate (0.079 g, 0.36 mmol) was added to **1** (0.701 g, 2.1 mmol) in methanol (20 ml) containing triethylamine (1 ml, 7.17 mmol). The resulting pale yellow solution was stirred for 0.5 h at room temperature to yield pale yellow crystals of Zn(1-H)₂ (0.193 g, 75.3 %); mp 233-235 °C (Found C, 64.1; H, 5.9; N, 15.2; C₄₀H₄₂N₈O₂Zn.H₂O requires C, 64.0; H, 5.9; N, 14.9 %); IR (cm⁻¹, KBr disc): ν 1549s (C=N), 1413s & 1365m (C(CH₃)₃); ¹H NMR (CDCl₃, 200 MHz): δ 1.27 (s, 18H, 2 C(CH₃)₃), 2.54 (s, 6H, 2 CH₃), 7.15-7.47 (m, 14H, N=NArH), 7.47-7.99 (m, 4H, o-ArH_{ring}); FABMS *m/z* 731 (100.0 %, ZnL₂), 334 (42.7 %, L).

[Co(1-H)₃](MeOH)₃ : (10)

Cobalt(II) acetate tetrahydrate (0.087 g, 0.35 mmol) was added to **1** (0.701 g, 2.10 mmol) in methanol (20 ml). The resulting dark orange solution was stirred for 0.5 h at room temperature to yield red crystals of Co(1-H)₃.3MeOH (0.241 g, 59.6 %); mp 212-213 °C (Found C, 67.7; H, 6.1; N, 15.4; C₆₀H₄₂N₁₂CoO₃ requires C, 68.0; H, 6.0; N, 15.9 %); IR (cm⁻¹, KBr disc): ν 1556s (C=N), 756s (ArH); ¹H NMR (CDCl₃, 200 MHz): 0.95 (s, 9H, C(CH₃)₃), 1.17 (s, 9H, C(CH₃)₃), 1.45 (s, 9H, C(CH₃)₃), 1.99 (s, 3H, CH₃), 2.33 (s, 3H, CH₃), 2.59 (s, 3H, CH₃), [6.37-6.42 (d, 2H), 6.86 (s, 4H), 6.98-7.33 (m, 18H), 7.45-7.53 (t, 2H), 8.04-8.09 (d, 1H)]: 27 ArH; FABMS *m/z* 1059 (17.5 %, CoL₃), 725 (100.0 %, CoL₂), 525 (8.6 %, CoL + (CH₃)₃CPh), 133 (9.0 %, (CH₃)₃CPh).

[Ni(1-H)₂](MeOH)₂ : (11)

Nickel(II) acetate tetrahydrate (0.087 g, 0.35 mmol) was added to **1** (0.701 g, 2.10 mmol) in methanol (20 ml). The resulting dark orange solution was stirred for 0.5 h at room temperature to yield red crystals of Ni(1-H)₂(MeOH)₂.2MeOH (0.168 g, 60.8 %); mp 245-247 °C (Found C, 64.4; H, 6.2; N, 14.7; C₄₀H₄₂N₈NiO₂.H₂O requires C, 64.6; H, 6.0; N, 15.1 %); IR (cm⁻¹, KBr disc): ν 1581s (C=N), 755s (ArH); FABMS *m/z* 725 (100.0 %, NiL₂), 393 (16.9 %, L).

NiL), 334 (74.2 %, L), 257 (8.1 %, L - Ph), 133 (66.2 %, (CH₃)₃CPh), 91 (71.1 %, PhN), 57 (85.9 %, C(CH₃)₃); $\mu_{\text{eff}} = 2.67$ B. M. (Evans).

[Cu(2-H)₂]: (12)

Copper(II) acetate monohydrate (0.100 g, 0.5 mmol) was added to **2** (0.278 g, 1 mmol) in methanol (25 ml). The resulting red solution afforded a red / brown powder, Cu(L₂)₂.2MeOH (0.277 g, 89.6 %); FABMS *m/z* 682 (Cu(2-H)₂. 2MeOH). The red/brown powder was recrystallised by diffusion of water into a DMF solution of the complex to yield red crystals, Cu(2-H)₂, mp 220-222 °C (Found C, 61.8; H, 4.1; N, 18.1; C₃₂H₂₆N₈CuO₂ requires C, 62.2; H, 4.25; N, 18.1 %); IR (cm⁻¹, KBr disc): ν 1564s (C=N), 1394w & 1364m (C(CH₃)₃); FABMS *m/z* 1300 (7.0 %, Cu₃L₄), 1022 (4.0 %, Cu₃L₃), 745 (13.8 %, Cu₃L₂), 681 (14.8 %, Cu₂L₂), 618 (55.6 %, CuL₂), 340 (17.9 %, CuL), 77 (40.5 %, Ph); $\mu_{\text{eff}} = 1.80$ B. M. (Balance).

[Cu(5-H)₂]: (13)

Copper(II) acetate monohydrate (0.299 g, 1.5 mmol) was added to **5** (0.943 g, 3 mmol) in methanol (20 ml). The resulting dark brown solution was stirred for 0.5 h at room temperature to afford a brown, microcrystalline powder, Cu(5-H)₂ (0.710 g, 68.6 %); mp 197-199 °C (Found C, 62.4; H, 7.3; N, 16.0; C₃₆H₅₀N₈CuO₂ requires C, 62.6; H, 7.3; N, 16.2 %); IR (cm⁻¹, KBr disc): ν 1562 (C=N), 1393w & 1367s (C(CH₃)₃); FABMS *m/z* 691 (100.0 %, M⁺), 509 (24.6 %, M - (2 C(CH₃)₃ + 2 CH₃)), 376 (50.4 %, CuL), 314 (58.8 %, L), 243 (36.8 %, L - (C(CH₃)₃ + CH₃)), 133 (74.3 %, (CH₃)₃CPh), 91 (30.7 %, (CH₃)₃CN), 57 (89.2 %, C(CH₃)₃); $\mu_{\text{eff}} = 1.57$ B. M. (Balance).

[Cu(6-H)₂]: (14)

Copper(II) acetate monohydrate (0.299 g, 1.50 mmol) was added to **6** (0.943 g, 3 mmol) in methanol (20 ml). The resulting dark brown solution was stirred for 0.5 h at room temperature to yield a black / brown, microcrystalline powder, Cu(6-H)₂ (0.890 g, 85.9 %); mp 196-198 °C (Found C, 62.7; H, 7.2; N, 16.0; C₃₆H₅₀N₈CuO₂ requires C, 62.6; H, 7.3; N, 16.2 %); IR (cm⁻¹, KBr

disc): ν 1556 (C=N), 752s & 698/688m (ArH); FABMS m/z 691 (78.8 %, M^+), 376 (16.0 %, CuL), 314 (100.0 %, L), 229 (26.5 %, L - $(C(CH_3)_3N=N)$), 91 (10.1 %, $C(CH_3)_3N$); $\mu_{\text{eff}} = 1.61$ B. M. (Balance).

[Cu(7-H)₂] : (15)

Copper(II) acetate monohydrate (0.299 g, 1.50 mmol) was added to **7** (1.154 g, 3 mmol) in methanol (20 ml). The resulting dark brown solution was stirred for 0.5 h at room temperature and then left to stand. After ca. 6 months a dark brown / black microcrystalline powder had formed, Cu(7-H)₂.H₂O (0.539 g, 42.3 %); mp 93 - 95 °C (Found C, 64.8; H, 8.2; N, 14.0; C₄₆H₇₀N₈O₂Cu.H₂O requires C, 65.1; H, 8.6; N, 13.2 %); IR (cm⁻¹, KBr disc): ν 3440.0m (OH from H₂O), 2954.4s (alkyl CH), 1565.7s (C=N), 1468.0 + 1440.0s (CH), 1366.1m ($C(CH_3)_3$), 1095.6s (C-O); FABMS m/z 830 (41.0 %, CuL₂), 447 (19.1 %, CuL), 384 (26.3 %, LH), 329 (11.8 %, LH - $C(CH_3)_3$), 57 (98.4 %, $C(CH_3)_3$).

5.7.6 Solvent Extraction Experiments

5.7.6.1 From Sulphate Media

Solutions : 0.085 M MSO₄.xH₂O in H₂O
0.1M LH (0.15 M LH for cobalt curve) in toluene
1M NaOH
1M H₂SO₄

Ten 20 ml screw-top glass jars each containing 5 ml LH solution, 2.5 ml MSO₄ solution (which corresponds to 85 % of the theoretical amount of metal needed for 100 % ML₂ complexation) and (2.5 - x) ml H₂O, where x was the amount of base or acid required to raise/lower the pH of the solution, were set up. Sample 1 contained no acid or base, ie: there was no pH correction. In order to determine the exact amount of acid/base required to be added to samples 2-10, sample 1 was stirred at ca. 600 r.p.m. for 2 hours at ambient temperature. The organic and aqueous layer were then separated by filtration and the pH-value of the aqueous layers measured. By knowing the

pH of the initial 0.085 M MSO_4 solution, the number of moles of LH which had been deprotonated could be calculated and hence the amount of base/acid required for full deprotonation (and also full "re-protonation") was calculated and added cumulatively to each of the samples 2-10, such that the pH increased gradually typically within the range of 2-12 pH units. A 110 % theoretical excess of acid/base required was added to the most acidic and most basic samples respectively. The solvent extraction on samples 2-10 was carried out in the same way as for sample 1. Finally all 10 aqueous and 10 organic solutions were diluted by a factor of 1:100 using water or white spirit respectively, and the metal content determined by ICP-AES. $\text{pH}_{1/2}$ curves were then drawn using the Microcal[®] Origin 5.0 curve fitting programme.

The results for the extraction of copper(II), zinc(II) and nickel(II) from sulphate media using ligand 1 in toluene are presented in table 12.

Copper(II)		Zinc(II)		Nickel(II)	
pH	% $\text{Cu}_{\text{org}}^{\text{a}}$	pH	% $\text{Zn}_{\text{org}}^{\text{a}}$	pH	% $\text{Ni}_{\text{org}}^{\text{a}}$
2.38	0.10	2.38	0.00	6.52	0.00
2.40	1.70	2.67	3.47	7.47	23.25
2.63	3.20	4.45	4.43	7.60	41.17
3.20	1.20	4.52	18.9	7.63	60.35
3.70	18.30	5.62	39.44	7.75	79.72
4.70	41.90	6.21	63.07	7.85	93.54
4.89	64.30	6.34	79.52	10.77	99.93
5.18	90.56	9.16	91.58	12.32	99.93
6.98	99.86				
11.44	99.96				
11.87	99.93				

Table 12 : Solvent extraction data for copper(II), zinc(II) and nickel(II) from sulphate media using ligand 1

^a % $\text{Metal}_{\text{org}}$ were calculated from $[\text{Metal}_{\text{aq}}]$ due to precipitation of metal complexes

The results for solvent extraction experiments for copper(II), zinc(II), nickel(II) and cobalt(II) from sulphate media using ligand 5 are presented in table 13.

Copper(II)		Zinc(II)		Cobalt(II)		Nickel(II)	
pH	% Cu _{org}	pH	% Zn _{org}	pH	% Co _{org}	pH	% Ni _{org}
2.10	0.61	2.13	0.00	2.25	2.96	2.13	0.00
2.21	0.90	2.46	0.00	2.64	2.74	2.66	0.00
2.40	11.99	3.88	9.00	4.16	3.06	4.08	0.11
3.03	35.41	5.66	13.10	6.08	13.59	7.35	16.67
3.37	41.65	6.00	20.30	6.32	25.72	7.65	27.75
4.26	61.85	6.25	27.30	6.66	38.55	7.74	27.28
4.67	75.63	6.45	36.50	6.91	51.67	7.87	43.01
4.90	92.54	6.57	54.70	7.32	77.27	7.99	54.86
11.40	99.83	6.73	70.80	7.36	100.00	8.26	71.22
12.71	99.96	7.17	94.36	8.33	100.00		

Table 13 : Solvent extraction data for copper(II), zinc(II), nickel(II) and cobalt(II) from sulphate media using ligand 5. % Zn_{org} and % Ni_{org} were calculated from [Metal_{aq}] due to precipitation of the metal complexes. % Cu_{org} and % Co_{org} reported are real data

The results for solvent extraction experiments for copper(II) from sulphate media using ligands 3, 6 and 7 are presented in table 14.

Ligand 3		Ligand 6		Ligand 7	
pH	% Cu _{org}	pH	% Cu _{org}	pH	% Cu _{org}
2.60	4.85	2.50	9.07	2.38	8.04
2.69	1.70	2.81	7.89	2.95	25.33
2.94	9.33	3.21	25.00	3.87	60.30
3.29	18.07	3.68	44.48	4.73	91.82
4.10	40.85	5.08	87.29	9.06	99.29
4.48	59.30	12.29	99.92		
4.80	77.70				
5.85	97.67				
10.45	99.95				
11.99	99.96				

Table 14 : Solvent extraction data for copper(II) from sulphate media using ligands 3, 6 and 7. % Cu_{org} for ligand 3 was calculated from [Cu_{aq}] due to precipitation of the metal complex

5.7.6.2 From Ammoniacal Media

The determination of load (6 and 7) and strip (7) isotherms for copper(II) from ammoniacal media was carried out by Mrs. Sue Owens (Avecia) as described below. The solutions used in the experiments were :

(1) Extraction Isotherms

The ammoniacal feed solution (the aqueous phase), containing 30.0 gl^{-1} copper, 45.0 gl^{-1} NH_3 and 75.0 gl^{-1} H_2SO_4 , was made up using 471.2 g of copper(II) sulphate pentahydrate, 164 g of ammonium sulphate and 974 ml of 8.4 M ammonia solution. A total volume of 4 l was achieved *via* dilution with water.

The organic phase consisted of a 1.0 M ligand solution in Philips Orfom[®] SX7 (20 % aromatic / 80 % aliphatic kerosene).

(2) Strip Isotherms

The aqueous phase in consisted of aqueous strip acid containing 30.0 gl^{-1} copper and 180 gl^{-1} H_2SO_4 . The organic phase was the loaded organic phase from the extraction isotherm determination. 0.1 M aqueous standard thiosulphate solution was used in the titrations to determine copper content of the aqueous phase.

Extraction Isotherms

Six glass screw top bottles containing varying organic : aqueous volume ratios were set to stir for 1 hour at 1000 r.p.m. and RT using paddle stirrers. The screw tops were pre-drilled to accommodate the stirrers. The phases were separated, the aqueous phase filtered using Whatman No. 1 filter paper and titrated against a standard 0.1 M thiosulphate solution to determine the amount of copper remaining in the aqueous phase. The amount of copper, which had transferred into the organic phase was subsequently found by difference, having previously determined the exact amount of copper in the feed solution by titration as before.

Strip Isotherms

The loaded organic solutions from the extraction isotherm were combined and contacted with a volume of copper feed in an organic : aqueous ratio of 1 : 1.5 for ½ hour to ensure maximum copper loading. The phases were then separated and the loaded organic phase filtered using Whatman phase separation paper. Three glass screw top bottles were then charged with varying organic : aqueous volumetric ratios of the loaded organic phase and aqueous strip acid and set to stir for 1 hour at 1000 r.p.m. at RT using paddle stirrers. The phases were separated and the aqueous phase filtered, before being titrated against standard thiosulphate solution (0.1 M) to determine the amount of copper present. The amount of copper in the organic phase was found by difference as before.

The results of loading experiments for 6 and 7 are presented in table 15.

Ligand 6				
O:A Ratio / ml		Aqueous Cu		Organic Cu
Organic	Aqueous	0.1 M S ₂ O ₃ / ml	Cu / gl ⁻¹	gl ⁻¹
20	5	0.65	2.1	7.5
20	10	2.7	5.7	13.2
10	10	2.2	14.0	18.1
10	20	3.55	22.5	19.2
10	40	8.7	27.6	18.0
Ligand 7				
32	8	1.8	2.3	7.1
20	10	2.55	5.4	12.6
10	10	5.1	10.8	19.7
10	20	5.9	18.7	23.6
5	40	8.6	27.3	25.6

Table 15 : Load data for ligands 6 and 7

The results of the strip experiment carried out for 7 are presented in table 16.

O:A Ratio / ml		Aqueous Cu		Organic Cu
Organic	Aqueous	0.1 M S ₂ O ₃ / ml	Cu / gl ⁻¹	gl ⁻¹
20	5	13.4	85.1	13.3
10	10	9.7	61.6	0
5	20	6.4	40.6	0

Table 17 : Strip data for ligand 7

5.7.6.3 Stability Tests on Diazopyrazolone Ligands

Three glass screw top bottles containing aqueous : organic contacts, as described below, were set up.

1. 100 ml 0.056 M solution of **5** in toluene and 100 ml 3.40 gl⁻¹ ammoniacal copper feed.
2. Repeat of 1.
3. 50 ml 0.056 M solution of **5** in toluene and 50 ml 34.0 gl⁻¹ ammoniacal copper feed.

The samples were stirred continuously at room temperature for a total of 552 h (23 days), during which time samples of each phase were taken, filtered, diluted and analysed for copper content using ICP-AES. The results of these tests are shown in table 18.

Time / h	Contact 1 / ppm Cu		Contact 2 / ppm Cu		Contact 3 / ppm Cu	
	Organic	Aqueous	Organic	Aqueous	Organic	Aqueous ^a
1	20.34	12.83	19.37	14.46	19.98	12.67
24	20.12	12.95	19.58	16.14	20.88	15.48
216	19.78	8.793	19.77	9.812	20.26	10.80
384	21.84	8.501	22.38	8.586	23.49	8.626
552	21.58	9.121	20.07	9.323	20.38	9.187

Table 18 : Feed stability test data for ligand 5

Note : All samples were diluted by a factor of 1:100, apart from ^a, which was diluted by a factor of 1:1000. The theoretical maximum copper content (assuming CuL₂ formation) for each diluted organic sample is 17.8 ppm, and for each diluted aqueous sample is 34.3 ppm. The variation in the mass balances for each sample was deemed to be within experimental error.

5.7.7 X-ray Crystallography

The structures of **8-12** were determined by either Dr. Simon Parsons or Mr. Steven Harris at the University of Edinburgh. In all cases data were collected at 220K on a Stoe Stadi-4 diffractometer equipped with an Oxford Cryosystems low-temperature device, using Cu-K α radiation for **8, 9, 11** and **12**, and Mo-K α radiation for **10**. Reflections were scanned in ω - θ mode. Structures **8** and **12** were solved by direct methods (SHELXTL or SIR92)^{57,58}, and **9 - 11** by Patterson methods (DIRDIF)⁵⁹. All were completed by iterative cycles of least-squares refinement against F^2 and difference Fourier syntheses (SHELXTL). H-atoms were idealised, those belonging to CH₃ groups being first located in a difference synthesis. In all cases all non-H atoms were modelled with anisotropic displacement parameters and final refinement statistics are presented in table 19.

Crystals of **12** grew as aggregates of blocks, and none of the crystals studied were single. In the case of the sample from which data are reported here a random reflection search located 25 reflections, and this pattern was completely indexed on the basis of two orientation matrices⁵⁹. Some reflections in the search list gave integral indices with only one of these matrices, others could be satisfactorily indexed with both. Data were collected as described above using one of these matrices; no absorption correction was applied. Routine refinement converged to $R1 = 6.75\%$ with a difference synthesis extrema of 1.13 and -0.74 eÅ⁻³.

The relationship between the two orientation matrices identified after the initial reflection search can be expressed by the matrix⁶⁰

$$\begin{pmatrix} 0.01 & -0.414 & 0.50 \\ 0 & -1 & 0 \\ 2.03 & -0.815 & 0.01 \end{pmatrix}$$

Several twinning models were considered, including splitting reflections with $k=5n$ and $l=2n$, but with only slight improvement. In all cases the twin scale factor was less than 10%. It is possible that the off-diagonal terms in this matrix are far enough from rational numbers that scan path taken during data collection meant that the twinning did not affect the intensity measurements in a consistent manner, and the best agreement indices were obtained when all reflections whose transformed indices differed from integral values by less than 0.15 were omitted (603 data in all). R1 under these conditions was 5.04%. Other refinement details are given in table 19.

Structure	8	9	10 *	11	12
Formula	C ₄₀ H ₄₂ N ₈ Cu ₂ O ₂	C ₄₀ H ₄₂ N ₈ O ₂ Zn	C ₆₀ H ₆₃ N ₁₂ CoO ₃ .3MeOH	C ₄₂ H ₅₀ N ₈ NiO ₄ .2MeOH	C ₃₂ H ₂₆ N ₈ CuO ₂
M	730.36	732.19	115.28	853.69	618.15
Crystal system	monoclinic	triclinic	triclinic	triclinic	triclinic twin
Space group	P2 ₁ /n	P-1	P-1	P-1	P-1
a/Å	11.603(3)	12.280(5)	12.965(6)	10.5849(12)	8.307(4)
b/Å	23.586(4)	13.615(5)	15.604(6)	14.8955(17)	11.311(6)
c/Å	13.649(2)	14.172(5)	15.584(6)	15.1532(17)	16.415(8)
α/°	90	113.74(2)	75.83(3)	76.735(6)	75.87(4)
β/°	97.24(2)	95.13(2)	85.67(3)	79.025(6)	75.79(4)
γ/°	90	113.635(14)	86.50(4)	77.539(7)	71.58(4)
U/Å ³	3705.5(13)	1896.2(12)	3045(2)	2245.6(4)	1395.1(12)
Crystal size/mm	0.39x0.39x0.31	0.31x0.31x0.19	0.48x0.36x0.32	0.48x0.31x0.27	0.32x0.16x0.16
D _c /g cm ⁻³	1.309	1.282	1.260	1.263	1.472
Z	4	2	2	2	2
μ/mm ⁻¹	1.197	1.256	0.342	1.065	1.485
Transmission factors	T _{min} 0.275, T _{max} 0.587	T _{min} 0.703, T _{max} 0.895	T _{min} 0.528, T _{max} 0.580	T _{min} 0.494, T _{max} 0.584	T _{min} 0.364, T _{max} 0.706
θ Limits/°	3-60	3-70	2-25	3-70	2-70
No. of unique data	5435	6746	10736	7969	3946
No. data with [F>4σ(F)]	4000	5713	5472	6601	3098
No. variables	462	469	739	567	390
R1	0.0614	0.0342	0.0846	0.0389	0.0504
wR2	0.1732	0.1002	0.2201	0.1042	0.1753
Δρ _{max} , Δρ _{min} /e Å ⁻³	0.75, -0.59	0.26, -0.29	0.69, -0.79	0.44, -0.31	0.43, -0.48

Table 19 : Crystal data for structures 8 - 12

Note : * This unit cell may be transformed into a pseudo C-centred monoclinic cell by the matrix (011/01-1/-100), but R_{int} for 2/m Laue symmetry was 64 %

5.8 References for Chapter 5

- 1 *Handbook of Extractive Metallurgy*, ed. F. Habashi, Wiley-VCH, Weinheim (Germany), 1997, Volumes II and III
- 2 *Proceedings of "The Paul Queneau International Symposium on Extractive Hydrometallurgy of Copper, Nickel and Cobalt"*, Vol. 1 : Fundamental Aspects, eds. R.G. Reddy and R.N. Weizenbach, The Minerals, Metals and Materials Society, Warrendale (U.S.A.), 1993
- 3 F. Habashi, *A Textbook of Hydrometallurgy*, Imprimerie D'Édition Marquis Limité, Quebec, 1993, **ch. 21**, pp. 408-497
- 4 IBM Intellectual Property Network; www.patents.ibm.com
- 5 www.chileinfo.com
- 6 US Patent 4065502, 1977, General Mills Chemicals Inc.
- 7 US Patent 4175012, 1979, Henkel Corporation
- 8 US Patent 5176802, 1991, BHP
- 9 WO Patent 93/04208, 1993, Henkel Corporation
- 10 WO Patent 97/09453, 1997, Henkel Corporation
- 11 WO Patent 97/29215, 1997, Henkel Corporation
- 12 W.P.C. Duvesteyn, *Australian Institute of Mining and Metallurgy Publication Series*, 1995, **95**, Ch. 13(3), pp. 29-42
- 13 G. Kyuchoukov, M.B. Bogacki and J. Szymanowski, *Industrial and Engineering Chemistry Research*, 1998, **37**, 4084-4089
- 14 Y.A. Zolotov and N.M. Kuzmin, "Extraction of Metals with Acylpyrazolones", Nauka, Moscow, 1977; *Chem. Abstr.* **89** : B81023X
- 15 S. Miyazaki, H. Mukai, S. Umetani, S. Kihara and M. Matsui, *Inorg. Chem.*, 1989, **28**(15), 3014-3017
- 16 I. Guiguemde, B.A. Diantouba, D. Lakkis, G.J. Goetz-Grandmont and J.P. Brunette, *Analisis*, 1996, **24**(8), 318-324
- 17 S.A. Pai, K.V. Lohithakshan, P.D. Mithapara, S.K. Aggarwal and H.C. Jain, *Radiochimica Acta*, 1996, **73**(2), 83-87
- 18 S. Umetani and M. Matsui, *Analytical Chemistry*, 1992, **64**(19), 2288-2292

- 19 P. Thakur, K.C. Dash, M.L.P. Reddy, R. Luxmi Varma, T.R. Ramamohan and A.D. Damodaran, *Radiochimica Acta*, 1996, **75**(1), 11-16
- 20 W. Mickler and E. Uhlemann, *Separation Science and Technology*, 1993, **28**(10), 1913-1921
- 21 J. March, "*Advanced Organic Chemistry*", Wiley, New York, 3rd Edition, 1985
- 22 *Kirk-Othmer Encyclopædia of Chemical Technology*, eds. M. Grayson and D. Eckroth, Wiley, New York, 3rd Edition, 1978, Volume 6, pp. 819-868
- 23 M. Idelson, I.R. Karady, B.H. Mark, D.O. Rickter and V.H. Hooper, *Inorg. Chem.*, 1967, **6**, 450-458
- 24 F.A. Snavely, W.C. Fernelius and B.P. Block, *J. Am. Chem. Soc.*, 1957, **79**, 1028-1030
- 25 F.A. Snavely, B.D. Kreckler and C.G. Clark, *J. Am. Chem. Soc.*, 1959, **81**, 2337-2338
- 26 J. Szymanowski, "*Hydroxyoximes and Copper Hydrometallurgy*", CRC Press, London, 1993
- 27 R. Brogden, *Drugs* 32, 1986, Supplement 4, 60-70
- 28 S.A. Ibrahim, M.A. El-Gahami, Z.A. Khafagi and S.A. El-Gyar, *J. Inorg. Biochem.*, 1991, **43**, 1-7
- 29 R. Jones, A.J. Ryan, S. Sternhell and S.E. Wright, *Tetrahedron*, 1963, **19**, 1497-1507
- 30 J.A. Connor, R.J. Kennedy, H.M. Dawes, M.B. Hursthouse and N.P.C. Walker, *J. Chem. Soc. Perkin Trans 2*, 1990, 203-207
- 31 B. Golinski, G. Reck and L. Kutschabsky, *Zeitschrift für Kristallographie*, 1982, **158**, 271-278
- 32 A. Whitaker, *Acta Cryst.*, 1988, **C44**, 1587-1590
- 33 V. Bertolasi, P. Gilli, V. Ferretti and G. Gilli, *Acta Cryst.*, 1994, **B50**, 617-625
- 34 A. Whitaker, *Acta Cryst.*, 1988, **C44**(10), 1767-1770

- 35 A. Whitaker, *Journal of Crystallographic and Spectroscopic Research*, 1991, **21**(4), 463-469
- 36 A. Whitaker, *Journal of Crystallographic and Spectroscopic Research*, 1992, **22**(4), 385-390
- 37 L.G. Kuzmina, L.P. Grigoryeva, Y.T. Struchkov, Z.I. Yezhkova, B.Y. Zaitsev, V.A. Zaitseva and P.P. Pronkin, *Khimiya Geterotsiklicheskikh Soedinenii*, 1985, **6**, 816-821
- 38 A. Whitaker, *Journal of the Society of Dyers and Colourists*, 1989, **105**, 267-268
- 39 K.J. Morgan, *J. Chem. Soc.*, 1961, 2151-2159
- 40 A. Lycka and V. Machacek, *Dyes & Pigments*, 1986, **7**(3), 171-185
- 41 A. Burawoy and J.T. Chamberlain, *J. Chem. Soc.*, 1952, 3734-3740
- 42 A.J. Blake, H. McNab and L.C. Monahan, *J. Chem. Soc. Perkin Trans. 1*, 1991, 701-704
- 43 A.C. Fisher, *Electrode Dynamics*, Oxford University Press, Oxford, 1996
- 44 W. McCabe and E. Thiele, *Ind. Eng. Chem.*, 1925, **17**, 605
- 45 J. Morrison and B. Townson, *Mathematical Modelling Systems using the MINCHEM II Computer Program, Proceedings of Extractive Metallurgy*, The Institute of Mining and Metallurgy, London, 1989
- 46 D.A. Fletcher, R.F. McMeeking and D.F. Parkin, *J. Chem. Inf. Comput. Sci.*, 1996, **36**(4), 746-749
- 47 H. Jaggi, *Helvetica Chimica Acta*, 1968, **51**(3), 580-592
- 48 W. Banße, N. Jäger, E. Ludwig, U. Schilde, E. Uhlemann, A. Lehmann and H. Mehner, *Zeitschrift für Naturforschung B*, 1997, **52**(2), 237-242
- 49 Weblab Viewerlite 3.5, Molecular Simulations Inc., San Diego, C.A., 1999
- 50 L. Pauling, *The Nature of the Chemical Bond*, 3rd Edition, Cornell University Press, New York, 1960
- 51 PLATON multi-purpose crystallographic tool: A.L. Spek, *Acta Cryst.*, 1990, **C34**, A46
- 52 C.A. Hunter and J.K.M. Saunders, *J. Am. Chem. Soc.*, 1990, **112**, 5525-5534

- 53 D.F. Evans, *J. Chem. Soc.*, 1959, 2003-2005
- 54 K. D. Bartle, D. W. Jones and S. Maricic, *Croatica Chem. Acta*, 1968, **40**, 227-240
- 55 E.A. Boudreaux and C.N. Mulay, *Theory and Applications of Molecular Paramagnetism*, Wiley, London, 1976
- 56 D.E. Butler and H.A. DeWald, *J. Org. Chem.*, 1971, **36**(17), 2542-2547
- 57 G.M. Sheldrick, SHELXTL version 5, Siemens Analytical X-ray Instrument, Madison, Wisc., USA, 1995
- 58 A. Altomare, G. Cascarano, C. Giacovazzi and A. Guagliardi, *J. Appl. Cryst.*, 1994, **27**, 1045-1050
- 59 P.T. Beurskens, G. Beurskens, W.P. Bosman, R. de Gelder, S. García-Granda, R.O. Gould, R. Israël and J.M.M. Smits, DIRDIF, Crystallography Laboratory, University of Nijmegen, The Netherlands.
- 60 A.J.M. Duisenberg, *J. Appl. Cryst.*, 1992, **25**, 92-96

Chapter 6 : Conclusions and Future Work

Conclusions and Future Work

The main objective of the work presented for this thesis was to identify alternative ligand types, which could be used to replace the phenolic ("P50-type") oximes used commercially in copper recovery. Because these are derived from 4-alkyl phenols, which are potential endocrine disruptors, it is probable that the use or manufacture of the phenolic oxime extractants may be restricted on the grounds of safety or for environmental reasons. From this work, three good candidates have emerged as direct replacements for P50-type oximes in conventional acid leach solvent extraction circuits, the acyl pyrazolones, the pyrazolone oximes and the 3-(2-hydroxyphenyl)-pyrazoles. A fourth ligand type, the diazopyrazolones, is much weaker in terms of extractive strength, but has been shown to be suitable for use in an "Escondida-type" process to recover copper from ammoniacal leach solutions.

The design of the candidate extractants was based on the assumption that hydrogen bonding between chelating units in a planar copper(II) complex would enhance the "strength" and selectivity of extraction. Such a situation is well documented in the structures of complexes of P50-type oximes. For these ligands, it has also been assumed that preorganisation of the donor set by intermolecular hydrogen bonding contributes to their efficacy as extractants. A review of the literature provides no clear evidence for formation of pseudomacrocyclic dimers being the norm in high polarity or aromatic solvents, but in non-polar, hydrocarbon solvents, P50-type oximes can not only form dimeric species, but also higher oligomers. Spectroscopic methods such as IR and NMR have been successfully used to provide *qualitative* evidence for the self-association of P50-type oximes in solution. However, it is concluded that only colligative techniques such as cryoscopy and osmometry can provide reliable, *quantitative* evidence for the formation of hydrogen-bonded oligomers. Additionally, ESMS has been utilised for the first time to provide evidence for oxime association in the gas phase, and it will be interesting to see if more reliable, solution data on this and related

systems can be recovered in the future with the development of this technique.

The three ligand systems, the acyl pyrazolones, the pyrazolone oximes and the 3-(2-hydroxyphenyl)-pyrazoles, all fit the essential requirement of a replacement for P50, in that they are not based on 4-alkyl phenol precursors. The pyrazolone oximes and 3-(2-hydroxyphenyl)-pyrazoles are true P50 mimics in that they provide an $N_2O_2^{2-}$ donor set and form inter-ligand hydrogen bonds on complexation, which will enhance the stability of the metal complex. The acyl pyrazolones provide the copper with an O_4^{2-} donor set and are unable to form stabilising inter-ligand hydrogen bonds. Acyl pyrazolones and 3-(2-hydroxyphenyl)-pyrazoles have been shown to extract and strip copper(II) comparably to P50, however, the pyrazolone oximes extract copper(II) very strongly from both feed solutions and strip acid and are therefore too strong to be used as a replacement for P50. It is possible that their extractive strength could be favourably adjusted *via* the addition of modifiers, such as long chain alcohols or esters, or the substitution of electron-donating groups into the ligand system to decrease its acidity. The inter-ligand hydrogen bonds formed on metal ion complexation with both pyrazolone oximes and 3-(2-hydroxyphenyl)-pyrazoles have been shown to impose an essentially planar geometry even on metals such as zinc(II), and in fact the coordination sphere in the copper(II) complex of 1-H-3-(2-hydroxyphenyl)-pyrazole has been found to be almost totally square. Additionally, all three types of ligand possess good selectivity for copper(II) over iron(III), the main contaminant in an acid leach solvent extraction circuit. This is perhaps surprising in the case of the acyl pyrazolones, as it was originally thought that their all oxygen donor set would favourably complex ferric iron.

Potential problems for the practical application of the pyrazolone and pyrazole-based ligands in an acidic sulphate circuit have been identified. The basicity of the ring nitrogens suggests that these types of ligand might facilitate the transfer of acid into the organic phase in the stripping section of a solvent extraction circuit. Such a problem would lead to major operational

difficulties, however, the basicity of the ring nitrogen in 3-(2-hydroxyphenyl)-pyrazoles has been successfully reduced *via* the introduction of an electron-withdrawing ester substituent into the ligand system. Development work on the stability, solubility, phase disengagement properties and extraction kinetics of these three types of ligand will be carried out at Avecia.

The diazopyrazolones, while being too weak to be considered as replacements for P50, have been shown to be well suited to use in an "Escondida-type" process to recover copper from ammoniacal leach solutions. Structural studies suggest that the relative "weakness" of diazopyrazolones as copper extractants is due to the steric constraints of the ligands preventing copper(II) from adopting a favourable planar geometry. Importantly, the diazopyrazolones were found to be stable to prolonged contact with ammoniacal feed, which has been a major stumbling block in the past development of this solvent extraction system using extractants based on the LIX range of reagents.

In summary, this work has illustrated the potential and diversity of relatively simple ligands based on pyrazole and pyrazolone structures and has shown how modifications to, for example, the solubility and extractive strength of these ligands can be easily achieved *via* simple synthetic steps. Both the ligands and metal complexes discussed have provided interesting and varied structural chemistry, which has been used, in part, to try to rationalise the differences in behaviour of these ligands as solvent extractants for a range of transition metals. The importance of ligand-ligand interactions in tuning the "strength" and selectivity of complex formation has been underlined by these studies and has great consequences for the development of relatively simple (inexpensive) metal extractants, which have some of the characteristics of much more elaborate, polydentate, macrocyclic systems.